Futoshi Kurisu
AL. Ramanathan
Absar Ahmad Kazmi
Manish Kumar *Editors*

Trends in Asian Water Environmental Science and Technology

Springer

Trends in Asian Water Environmental Science and Technology

Futoshi Kurisu • AL. Ramanathan
Absar Ahmad Kazmi • Manish Kumar
Editors

Trends in Asian Water Environmental Science and Technology

Springer

Editors
Futoshi Kurisu
Research Center for Water Environment
University of Tokyo
Tokyo, Japan

AL. Ramanathan
School of Environmental Sciences
Jawaharlal Nehru University
New Delhi, India

Absar Ahmad Kazmi
Department of Civil Engineering
Indian Institute of Technology
Roorkee, India

Manish Kumar
Department of Environmental Science
Tezpur University
Tezpur, Assam
India

Co-published by Springer International Publishing, Cham, Switzerland, with Capital Publishing Company, New Delhi, India.

Sold and distributed in North, Central and South America by Springer, 233 Spring Street, New York 10013, USA.

In all other countries, except SAARC countries—Afghanistan, Bangladesh, Bhutan, India, Maldives, Nepal, Pakistan and Sri Lanka—sold and distributed by Springer, Haberstrasse 7, D-69126 Heidelberg, Germany.

In SAARC countries—Afghanistan, Bangladesh, Bhutan, India, Maldives, Nepal, Pakistan and Sri Lanka—printed book sold and distributed by Capital Publishing Company, 7/28, Mahaveer Street, Ansari Road, Daryaganj, New Delhi 110 002, India.

ISBN 978-3-319-39257-8 ISBN 978-3-319-39259-2 (eBook)
DOI 10.1007/978-3-319-39259-2

Library of Congress Control Number: 2016953346

Printed on acid-free paper

This Springer imprint is published by Springer Nature
The registered company is Springer International Publishing AG Switzerland

Foreword

Climate change, population growth, and urbanization create new challenges that professionals must address to reduce negative impacts on water resources. Over the past several decades, humans concerned with the environment have embraced the notion that one of the most important indicators of the health of natural resources is the quality of the water. It follows that when the quality of rivers, lakes, streams, ponds, and wetlands is improved and protected, there will be more healthy lands, wildlife, and overall environment. The integration, coordination, and management of human activities within the natural boundaries of a watershed to protect or improve water quality include a number of activities, such as river basin management, water quality monitoring and assessment, water withdrawal, hydropower production, wastewater discharge permit, control of nonpoint source pollution, critical-area protection, and wetland restoration and protection.

Water recycling technologies can significantly reduce net water abstraction from the environment, but many of those technologies require an increase in the consumption of other resources, especially energy. In our resource-constrained world, increasing the consumption of any resource, even for necessary functions such as water management, must be carefully considered. However, with the growing water demand, the rate of using reclaimed water is gaining pace in the Asian markets. Water recycling involves a combination of technologies to treat the wastewater and make it reusable or attain a safe standard for discharge. Technologies such as nanotechnology and membrane technology have been widely used for water and wastewater treatment depending upon the required quantity and quality and the applicable cost as per the specific use.

The scientists and practitioners should develop the following environmental skills and competencies for proper management of the environment such as analyzing or interpreting environmental samples and data; liaising and partnering with stakeholders; presenting expert information on environmental matters; developing sustainable development indicators, plans, or strategies; implementing or monitoring sustainable development strategies or programs; conducting environmental

assessments; and developing or implementing environmental communications and awareness programs.

The chapters in this book provide a platform for scientists and practitioners to discuss issues ranging from cutting-edge to practical levels on water environment technologies in Asian context. The scientists and practitioners exchange their knowledge on water environment technology, both in terms of local, region-specific, and general aspects. This volume tries to address the various contemporary issues such as wastewater treatment and monitoring, water quality problems, and groundwater contamination, with particular emphasis on integrated scientific strategies for management of these issues.

I would like to congratulate the great efforts of the editorial team of this volume which will serve as a scientific information base for addressing the different water quality issues in Asian context among the scientists, water quality practitioners, researchers, and engineers for the effective dissemination of knowledge in the field of water environment technology.

Research Center for Water Environment Technology
Graduate School of Engineering
The University of Tokyo
Tokyo, Japan

Hiroaki Furumai

Preface

Asia, as a whole region, faces severe stress on water availability, primarily due to high population density. Many regions of the continent suffer from severe problems of water pollution on local as well as regional scale. Water, environment, and pollution together constitute a three axial problem that all concerned people in the region would like to focus on. This book will attract a number of researchers, policy makers, and graduate students who will get an invaluable knowledge concerning environmental issues on water in Asia. This book aims to liven up the discussion by scientists and practitioners to discuss issues ranging from cutting-edge to practical levels on water environment technologies in Asian context.

It is a multidisciplinary book focused on global human health consequences of exposure to water pollution in natural environment. The book provides a unique platform for scientists from various fields including engineering, biogeochemical sciences, hydrogeochemistry, social sciences, and public policy to exchange ideas and share information on research for the possible solutions to water pollution.

Water, being the most important factor required for life, needs proper attention in terms of uses as well as treatments. The scientists and engineers working in the field of water have to encounter new challenges, where the effective use of new techniques, such as tracers and modeling simulation, is becoming inevitable. The purpose of this book is to define the emerging water problems and to provide possible technical solutions to the arising problems. The research works included in this book explore the various water research domains with relevant techniques and the subject matter that deals with the concurrent "Emerging Water Quality Issues." This book gives emphasis on topics like (i) emerging water problems in Asian countries, (ii) pollution dynamics in water environment, (iii) water quality and risk, (iv) water and wastewater treatment and monitoring, (v) sociological approach, and so forth.

The chapters included in this book comprise topics dealing with the subject mentioned above and are intended for the students, professionals, researchers, and engineers working on various aspects of water quality issues. The book seeks its impact from its diverse topic coverage revealing situations of different

contemporary issues, such as water quality problems, drinking water and wastewater treatment, metal contamination in water using isotope tracers, biological treatment techniques, and sociological approach.

It is worth mentioning that all the chapters have been prepared by individuals who are experts in their field. Honest effort has been made to check the scientific validity, depth of study, and justification of each chapter through several iterations. The editors, and hardworking water professionals, have put together a comprehensive reference work with a belief that this book will be of immense use for present and future colleagues who teach, study, research, and/or practice in this particular field.

Tokyo, Japan — Futoshi Kurisu
New Delhi, India — AL. Ramanathan
Roorkee, India — Absar Ahmad Kazmi
Tezpur, Assam, India — Manish Kumar

Contents

About the Editors

Futoshi Kurisu is an associate professor at the Research Center for Water Environment Technology (RECWET), the University of Tokyo. He has received awards for the excellent paper for young scientists from the Japan Society of Civil Engineers in 2001. He has also won the Takeda Techno-Entrepreneurship Award and Kurita Excellent Research Award for Water and Environmental Studies, in 2002 and 2010, respectively. He has more than 70 papers in peer-reviewed journals. He is member of the Japan Society on Water Environment, Japan Society of Microbial Ecology, Japan Society of Civil Engineers, Japan Society for Environmental Biotechnology, Japan Society of Water Treatment Biology, International Water Association, and International Society of Microbial Ecology. His current research interests are microbial enhancement of soil/groundwater bioremediation, microbial analysis of biological water/wastewater treatment processes, and water quality evaluation of water resources for reuse.

AL. Ramanathan a PhD in sedimentary geochemistry, is currently a professor in the School of Environmental Sciences, Jawaharlal Nehru University, New Delhi, India. He is engaged in coastal research in different parts of the world, such as nutrient dynamics, paleoenvironment, source identification, etc., with a number of universities and research organizations in India, Australia, Russia, the USA, etc. He has guided several PhDs in the above subject and published more than 60 papers in referred reputed journals. He has also published 5 books and several chapters in many books. He has got three times IFS Sweden (Project) Awards for his work on mangrove biogeochemistry besides working in national and international projects from Indo-Australian, Indo-Russian, DST, MoEF, MoWR, etc. He was a postdoctoral fellow under the STA Japan program, UGC-Russian Academy of Science program, CSIR, INSA, DST, etc. He is chief editor of the *Journal of Climate Change* and a member of the editorial board in the *Indian Journal of Marine Sciences* and served as referee for many national and international journals as well.

Absar Ahmad Kazmi is a professor of environmental engineering in the Department of Civil Engineering, IIT Roorkee. He obtained his doctorate of engineering from the University of Tokyo in 1999. After working as a project engineer in Nishihara Environment Technology, Tokyo, during 1999–2004, he is actively involved in teaching, research, consultancy, and continuing education programs in IIT Roorkee. He has received many awards and published more than 150 papers in peer-reviewed journals, book chapters, and conferences. He is a member and chairman of several committees of national and state governments most notable are the Ministry of Urban Development on the preparation of design and O&M manuals of sewage treatment, Research Advisory Committee of the Ministry of Environment and Forests, and National Green Tribunal. He chaired several conferences, delivered expert lectures, did several sponsored research projects, and was involved with various consultancy projects from various companies and organizations.

Manish Kumar a PhD in environmental engineering from the University of Tokyo, Japan, is a faculty member at Tezpur Central University, Assam, India. He has four book publications to his credit. A well-proven publication record (>50) with 12 years of experience in hydrology and water management and working experience at prestigious institutes like the University of Tokyo, Japan Kunsan National University, S. Korea Uppsala University, Sweden and Jawaharlal Nehru University (JNU), Delhi, is credited to his name. He is the recipient of the research grant award from the Kurita Water Environment Foundation (KWEF), Japan (ID P:14009) major research project grant from the University Grants Commission (UGC), India (2012–2015) uranium research grant by the Bhabha Atomic Research Centre (BARC), Mumbai (2015) Water Advanced Research and Innovation (WARI) Fellowship, USA (2016–2017) two best poster awards as coauthor of the paper Best Research Award 2013 at the 4th Asia-Pacific Water Young Professionals (APWYP) conference at Tokyo by the International Water Association (IWA) initiative DST Young Scientist Award (2012–2015) JSPS Foreign Researcher Fellowship (2010–2012) COE Young Researcher Fund (2007) and Linnaeus-Palme stipend from SIDA, Sweden (2005). He is on the editorial board of the *Journal of Groundwater for Sustainable Development* (Elsevier Journal) and *International Journal of Earth Sciences and Engineering*.

Part I
Wastewater Treatment and Monitoring: Physico-Chemical Treatment

Chapter 1
RSM and ANN-GA Experimental Design Optimization for Electrocoagulation Removal of Chromium

Manpreet S. Bhatti, Ashwani K. Thukral, Akepati S. Reddy, and Rajeev K. Kalia

1 Introduction

Heavy metal removal from industrial wastewater is affected using conventional treatment technologies such as chemical precipitation, ion-exchange, reverse osmosis and biological treatment etc. (Adhoum et al. 2004). Electrocoagulation removal of heavy metals is a fast process on account of quick start up, compact treatment facility, reduced sludge formation and better removal efficiencies, thus becoming a more common technology. Chromium is widely used in electroplating, metallurgical and refractory industries for chrome plating, chrome alloys, tanning, pigment production and as corrosion inhibitor etc. CPCB (2001) prescribed wastewater discharge standards of 2 mg/L for total chromium and 0.05 mg/L for hexavalent chromium. Untreated effluents of electroplating, leather and textile industries have high chromium concentration of 140 mg/L, 10–50 mg/L and 5–20 mg/L respectively (Abassi et al. 1997). Wastewaters containing chromium, designated as a priority pollutant by USEPA, have to be treated before being discharged into the environment (Metcalf and Eddy 2003). Chromium speciation in effluent mainly depends upon pH, redox potential and its kinetics along with presence/absence of reducing agents (WHO 1996). A two-step chemical precipitation (reduction at pH <3 followed by precipitation at pH ~8) of chromium is most widely used treatment technology at industrial scale with precipitants of hydroxide, carbonates and sulfide

M.S. Bhatti (✉) • A.K. Thukral
Department of Botanical and Environmental Sciences, Guru Nanak Dev University, Amritsar, Punjab, India
e-mail: mbhatti73@gmail.com

A.S. Reddy
School of Energy and Environment, Thapar University, Patiala, Punjab, India

R.K. Kalia
GGS Super Thermal Power Plant, Ropar, Punjab, India

F. Kurisu et al. (eds.), *Trends in Asian Water Environmental Science and Technology*, DOI 10.1007/978-3-319-39259-2_1

(Eckenfelder 2000). This technique produces huge quantity of hazardous sludge with poor process control. Whereas, electrocoagulation removal of chromium was studied by various researchers in the recent past (Akbal and Camci 2011, 2012; Al Anbari et al. 2012; Arroyo et al. 2009; Beyazit 2014; Bhagawan et al. 2014; Cataldo et al. 2012; Dermentzis et al. 2011; Espinoza-Quiñones et al. 2012; Liu et al. 2014; Hamdan and El-Naas 2014; Heidmann and Calmano 2008; Odongo and McFarland 2014; Sarahney et al. 2012; Shahriari et al. 2014; Vasudevan et al. 2012; Verma et al. 2013 and Zongo et al. 2009). Response surface methodology (RSM) based optimization for electrocoagulation was studied by Bhatti et al. 2009, 2011a; Espinoza-Quiñones et al. 2012; Liu et al. 2014; Olmez 2009; Xu et al. 2014; Zaroual et al. 2009 and artificial neural network (ANN) approach by Aber et al. 2009 and Bhatti et al. 2011a, b. The present work aims at multiple response optimization for maximizing chromium removal efficiency while minimizing energy consumption for iron electrodes under different process conditions viz., chromium concentration, pH, current density and treatment time. Experimental results were analyzed using RSM and artificial neural network-genetic algorithm to optimized electrocoagulation of Cr(VI) from $K_2Cr_2O_7$ solution.

2 Materials and Methods

A stock solution of $K_2Cr_2O_7$ (Spectrochem, India) containing 500 mg/L of Cr (VI) was prepared in deionized water. The stock solution was diluted to obtain desired concentration. The pH was set using 0.01 M H_2SO_4 or 0.01 M NaOH. Conductivity of the solution was maintained around 2000 ± 100 μS/cm using KCl. AR grade reagents and chemicals were used in the present study.

2.1 Experimental Setup and Procedure

Experimental setup for electrocoagulation is given in Fig. 1.1. Cr(VI) solution (32.5 mg/L to 72.5 mg/L) was used in the present study using iron-iron pair of electrodes at 15 mm electrode spacing. EDX (Quanta F-200 FEI, Netherland) spectrum of the iron electrode gave its composition as 93.55 % iron with C (4.25 %) and minor impurities (<1 %) for Mg and Si. Regulated DC power supply (specifications 0–32 V and 0–10 A) was procured from Aplab, Mumbai (L-3210). Current intensity was recorded using digital panel meter, and the energy consumed was recorded and average of amperage at the start and at the end of the experiment. A 540 ml of desired strength of Cr(VI) solution was taken in the electrocoagulation reactor. The electrodes were submerged up to a depth of 20 cm in the solution, to give 100 cm^2 of effective electrode area. Treated wastewater was allowed to settle for 2 h, and the supernatant analyzed for Cr(VI) and total chromium concentration. Chromium removal efficiency and energy consumption were determined as follows:

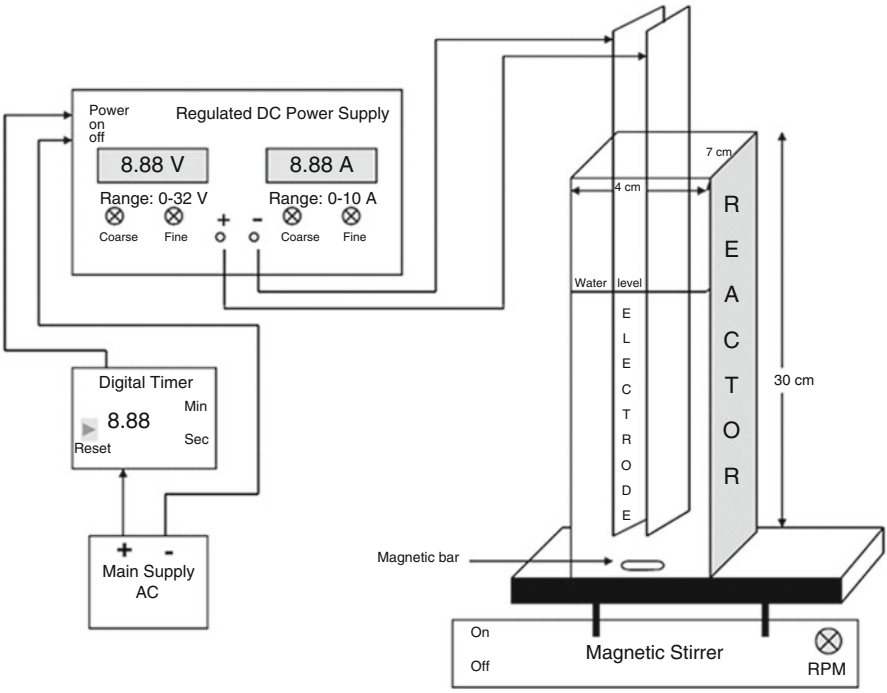

Fig. 1.1 Electrocoagulation experimental setup (Reprinted with permission from ref. Bhatti et al. (2009). Copyright 2009 Elsevier)

$$\begin{aligned}
\text{Cr(VI) removal efficiency } (\%) &= (C_\mathrm{i} - C_\mathrm{f})/C_\mathrm{i} \times 100 \\
\text{Energy consumption (Wh)} &= V \times I \times h \\
\text{Energy consumption (kWh m}^{-3}) &= \text{Wh} \times 1000/\text{Vol.} \\
\text{Energy consumption (kWh/kg)} &= [V\,I\,h \times 1000]/\left[(C_\mathrm{i} - C_\mathrm{f}) \times \text{Vol.}\right.
\end{aligned}$$

where C_i and C_f represent the initial and final concentrations of Cr(VI) in mg/L, V (voltage), I (amperage) and h (electrolysis time in hours) and Vol. (volume of solution in litres).

2.2 *Analytical Techniques*

Cr(VI) and total chromium was determined colorimetrically as per method no. 3500-Cr (APHA 1998). 1,5-diphenylcarbazide, MW 242.28 procured from Central Drug House, Mumbai was used as complexometric reagent for Cr (VI) estimation at 540 nm. Total chromium was determined after oxidizing Cr (III) to Cr(VI) using $KMNO_4$ under acidic conditions. The difference in Cr(VI) and

total chromium was negligible (<0.1 mg/L) in many of the random samples. Thus, chromium removal efficiency is reported instead of Cr(VI) removal efficiency.

2.3 Electrocoagulation Process

The process of electrocoagulation involves a sequence of several chemical and physical phenomena. The in situ production of ions involves formation of coagulants by electrolytic oxidation of sacrificial electrodes, destabilization of colloidal contaminants, breaking of emulsion and flocculation. Generally, aluminum and iron electrodes are employed for in situ generation of coagulating agents. A potential difference is maintained across the electrodes with the help of external power supply. In this process, the anode is sacrificed for the dissolution of electrolytic coagulating ions as follows:On anode

$$\mathrm{Fe(s)} \rightarrow \mathrm{Fe(II)} + 2\,\mathrm{e}^{-}$$

On cathode

$$2\mathrm{H_2O} + 2\,\mathrm{e}^{-} \rightarrow 2\mathrm{OH}^{-}{}_{(\mathrm{aq})} + \mathrm{H}_{2(\mathrm{g})}$$

Overall reaction in bulk solution (pH between 6 and 8) is as follows:

$$\mathrm{CrO_4}^{-2}{}_{(\mathrm{aq})} + 8\mathrm{H}^{+}{}_{(\mathrm{aq})} + 6\mathrm{Fe(II)}_{(\mathrm{aq})} \rightarrow \mathrm{Cr(III)}_{(\mathrm{aq})} + 6\mathrm{Fe(III)}_{(\mathrm{aq})} + 4\mathrm{H_2O}$$

$$\mathrm{Cr_2O_7}^{-2}{}_{(\mathrm{aq})} + 14\,\mathrm{H}^{+}{}_{(\mathrm{aq})} + 6\mathrm{Fe(II)}_{(\mathrm{aq})} \rightarrow 2\mathrm{Cr(III)}_{(\mathrm{aq})} + 6\,\mathrm{Fe(III)}_{(\mathrm{aq})} + 7\mathrm{H_2O}$$

$$\mathrm{Cr(III)}_{(\mathrm{aq})} + 3\mathrm{OH}^{-}{}_{(\mathrm{aq})} \rightarrow \mathrm{Cr(OH)}_{3(\mathrm{s})}$$

2.4 Experimental Design

Preliminary screening was done to determine significant process variables and treatments were selected on the basis of significant differences in Cr(VI) removal efficiency (>20 %) for further studies. Working standards of each selected parameters were decided on the basis of preliminary experimentation. Factorial design (2^4) was used for screening and determining the relative importance of the independent process variables. The design was augmented to centre composite design (CCD). The process variables were initial Cr(VI) concentration, pH, current density and treatment time.

2.4.1 Response Surface Methodology

RSM employs polynomial models for data fitting. CCD, the most widely used experimental, is given as follows:

$$Y = b_o + \sum_{n=1}^{v} b_n X_n + \sum_{n=1}^{v} b_{nm} X_n^2 + \sum_{n<m}^{v} b_{nm} X_n X_m,$$

where b_o is fixed response at the central point of the experiment; b_n, b_m and b_{nm} are linear, quadratic and cross product coefficients, respectively, and v is number of variables.

Each variable was defined at five different levels ($-\alpha$, -1, 0, $+1$ and $+\alpha$) for developing second order models (Anderson and Whitcomb 2004). ANOVA was performed to determine the significance differences ($p \leq 0.05$) in responses under different conditions. Cr(VI) removal efficiency (%) was used as a response. To guard against systematic bias, the experimental runs were conducted in a randomized manner. The experiments were performed at optimum conditions to validate and confirm the model. Generally, the experimental data was fit into second order quadratic model with the help of multiple regression technique. Model fitting and graphical analyses were carried out using Design-Expert 8.0.7.1 software (Stat-Ease Inc., Minneapolis, MN, USA). Sequential model sum of squares table gives cumulative improvement in the model fit with addition of model terms. ANOVA table was generated for fitted model and model *lack of fit* was checked to compare the residual error with the pure error obtained from the replicated runs. Non-significant *lack of fit* was assessed from the tabulated F-values. Significant model terms were identified at $p = 0.95$ and model reduction was done by eliminating non-significant model terms, thereby improving predicted R^2. Model goodness of fit was evaluated from coefficient of determination (R^2) and coefficient of variation (CV) to check the variability explained and robustness of the fitted model. Signal to noise (S/N) was estimated from adequacy precision ratio, with S/N ratio >4 being satisfactory for the model. Model selection and model building are depicted in Fig. 1.2. Before moving to graphical analysis, diagnostic plots like normal probability plots and actual vs. predicted plot were observed to eliminate any outlier in the data. Regression equations for chromium removal efficiency and energy consumption are simultaneously optimized for energy efficient chromium removal using desirability function (Bhatti et al. 2011b).

2.4.2 Artificial Neural Network-Genetic Algorithm

ANN modelling is a non-linear technique for data fitting. ANN model (three layers) was generated from the experimental data and the fitted model was integrated with GA toolbox using MATLAB software (The Mathworks, Inc. v7.6). Pareto front was generated for two conflicting goals (maximizing Cr(VI) removal efficiency and

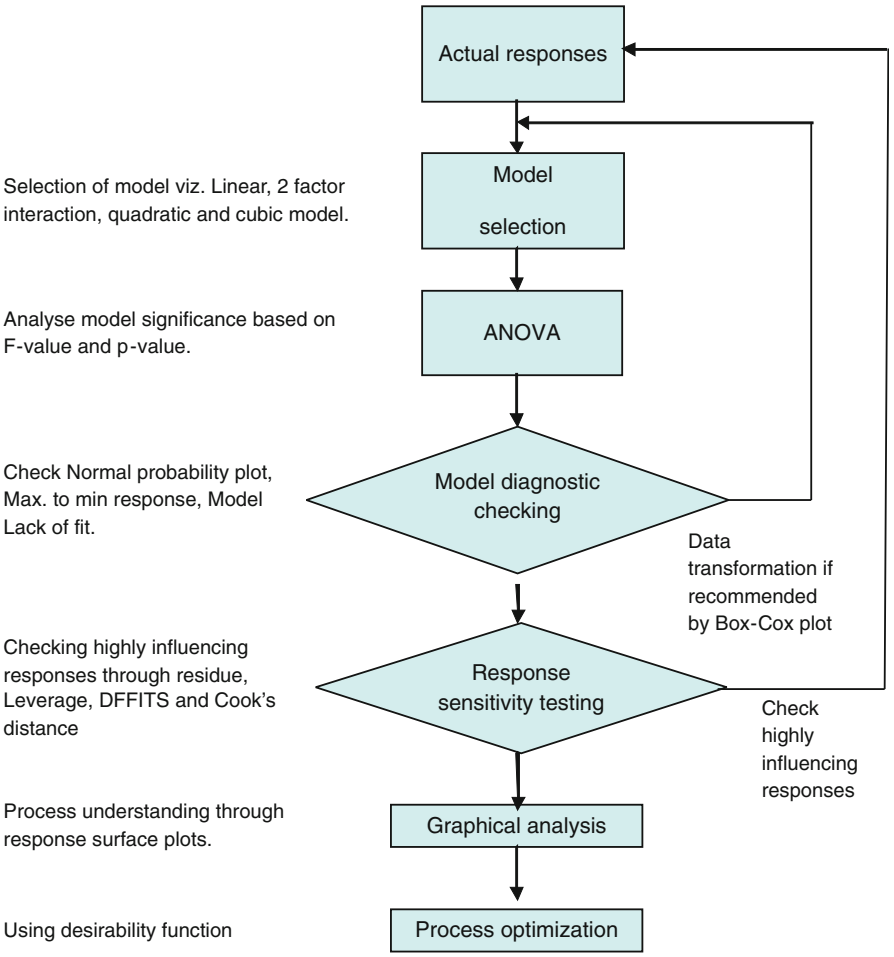

Fig. 1.2 Flow chart of model selection, model building and response optimization (Reprinted with permission from ref. Bhatti et al. (2011a). Copyright 2011 Elsevier)

minimizing energy consumption). A fully connected three-layer feed-forward network with the input, hidden and output layers was generated through optimum selection of hidden layer neurons. Each node in the input layer (five nodes) represents the value of one independent variable while the output layer (two nodes) indicates the dependent variables. ANN model (neural network toolbox v6) was trained using 'TRAINBR' function. This algorithm also computes the number of effective network parameters (weights and biases) used by the network. The convergence of effective number of network parameters was chosen as a decision tool to allocate optimum number of neurons in the hidden layer, in this case seven nodes. A number of training runs were performed to look out for the best

possible weights in error back-propagation (BP) framework and the final selected network architecture was trained.

The trained network was checked for mean square error (MSE) and correlation coefficient. GA based multi-objective optimization achieves maximizing or minimizing of an objective function. ANN model was integrated with GA (direct search toolbox v2.3) to get the non-dominated Pareto optimal front using 'gamultiobj' function. Multi-objective optimization is the simultaneous optimization of chromium removal efficiency and energy consumption. Multi-objective optimization provides a set of equally good solutions called as non-dominated or Pareto optimal solutions. Pareto front resolves the trade-offs between the competing objectives, and identifies those solutions which are non-dominated. MATLAB's 'gamultiobj' function uses a controlled elitist genetic algorithm which ranks the individuals in objective function space on the basis of degree of non-domination or dominance depth. Elitist selection mechanism selects the current best solutions in subsequent generations without applying any operators to them. Controlled elitism maintains a balance between exploration and exploitation of the objective function space. The input decision variables corresponding to each of the Pareto optimal solutions are tabulated.

2.5 Path Analysis

Path analysis reveals the structured relationships between a set of independent variables, and is studied using the decomposition and interpretation of direct, indirect and total effects of independent process variables on the response variables. Chromium removal efficiency was taken as response variable and five process variables as independent variables. In the present work an attempt is made to separate the effect of five process variables—chromium concentration, pH, current density, treatment time and effective reactor volume of 150 ml (electrode distance of 15 mm) and 250 ml (electrode distance of 25 mm) in to direct and indirect effects.

3 Results and Discussion

Four independent factors (chromium concentration, pH, current density and treatment time) at two-level factorial design were used for conducting the experiments. Responses monitored were chromium removal efficiency and energy consumption. Then, additional experiments (axial runs) were also conducted to fit second order model as per CCD. The results obtained for Fe-Fe electrode combinations is given in Table 1.1.

Table 1.1 Experimental design with observed responses for chromium removal efficiency and energy consumption for iron electrode combination

	Process variables				Response 1	Response 2
Exp. no.	Cr conc. mg/L	pH –	Current density A/m^2	Treatment time min	Cr removal efficiency (%)	Energy consumed (Wh)
1[a]	32.5	4.89	20	6.5	66.4	0.023
2	72.5	4.94	20	6.5	58.2	0.023
3	32.5	6.21	20	7.2	60.7	0.026
4	72.5	6.64	30	6.5	53.9	0.035
5	32.5	5.44	40	6.5	80.6	0.047
6	72.5	5.25	40	6.5	70.5	0.047
7	32.5	6.7	40	6.5	80.6	0.047
8	72.5	6.72	50	6.5	66.5	0.058
9	32.5	5.44	60	6.5	95.9	0.124
10	72.5	4.94	60	7.2	76.0	0.138
11	32.5	6.21	60	6.5	91.7	0.124
12	72.5	6.64	60	6.5	66.4	0.124
13	32.5	5.26	90	6.5	99.5	0.187
14	72.5	5.25	100	6.5	94.2	0.207
15	32.5	6.7	80	6.5	98.9	0.166
16	72.5	6.72	100	6.5	89.4	0.207
17	32.5	4.89	20	11.5	93.4	0.041
18	72.5	4.94	20	11.5	73.2	0.041
19	32.5	6.21	20	11.5	86.4	0.041
20	72.5	6.64	30	11.5	69.1	0.062
21	32.5	5.44	40	11.5	99.3	0.083
22	72.5	5.25	40	11.5	89.7	0.083
23	32.5	6.7	40	11.5	97.9	0.083
24	72.5	6.72	50	11.5	91.7	0.104
25	32.5	5.44	60	11.5	99.7	0.221
26	72.5	4.94	60	11.5	97.2	0.221
27	32.5	6.21	60	11.5	98.7	0.221
28	72.5	6.64	60	11.5	92.9	0.221
29	32.5	5.26	80	11.5	99.5	0.295
30	72.5	5.25	100	11.5	99.2	0.369
31	32.5	6.7	80	11.5	99.1	0.295
32	72.5	6.72	100	11.5	99.4	0.369
33	52.5	5.65	60	9.0	86.1	0.135
34	52.5	5.61	60	9.0	76.7	0.135
35	52.5	5.61	60	9.0	73.4	0.135
36	52.5	5.61	60	9.0	71.41	0.135
37	52.5	5.76	60	9.0	78.38	0.135
38	52.5	5.76	60	9.0	68.04	0.135
39	52.5	5.65	40	9.0	77.87	0.090

(continued)

Table 1.1 (continued)

Exp. no.	Process variables				Response 1	Response 2
	Cr conc.	pH	Current density	Treatment time	Cr removal efficiency	Energy consumed
	mg/L	–	A/m^2	min	(%)	(Wh)
40	52.5	5.65	40	9.0	72.90	0.090
41	52.5	2.82	50	9.0	83.75	0.113
42	52.5	7.81	60	9.0	75.80	0.135
43	52.5	5.64	60	9.0	89.72	0.135
44	52.5	5.67	10	9.0	48.66	0.008
45	52.5	5.65	100	9.0	99.87	ND
46	52.5	5.65	60	3.0	69.77	0.045
47	52.5	5.65	60	15.0	99.50	0.225

[a]Exp. no. 1–40 are used in factorial modelling and Exp. no. 1–47 are used for CCD

3.1 RSM Modelling and Optimization

Experimental data for Fe-Fe electrode combination along with actual responses is given in Table 1.1. Half probability plot predicted that current density, treatment time and chromium concentration had the highest effects on Cr(VI) removal efficiency (Fig. 1.3a). Pareto chart revealed that current density, treatment time and chromium concentration have a significant effect on chromium removal efficiency since it crossed the bonferroni limit. Similarly, 2FI between current density and treatment time had a possible significant effect as it crossed t-value limit (Fig. 1.3b). The fitted model was significant at 99.99 % level of significance (F-value = 47.29 at degree of freedom $d_f = 4$) with not-significant *lack of fit* ($p = 0.461$). Final equation in terms of unit-less regression coefficients and actual process conditions is given in Table 1.2. The regression coefficients in coded equations were used to find the relevant importance of individual terms on normalized scale. The current density had the highest positive contribution in the chromium removal efficiency followed by treatment time. The solution pH has no effect on chromium removal efficiency, and has to be maintained within the range, preferably in slightly acidic conditions. This minimises the use of acidic conditions for chromium reduction. Modelling of energy consumption has current density and treatment time along with 2FI between current density and treatment time as significant process conditions. ANOVA model was significant at 99.99 % level of significance (F-value = 287.41 at $d_f = 3$) with $R^2 = 0.965$.

3.2 Centre Composite Design

CCD is the most widely used model development strategy. Fitted ANOVA model was highly significant at 99.99 % level of significance (F-value = 36.6 at $d_f = 7$)

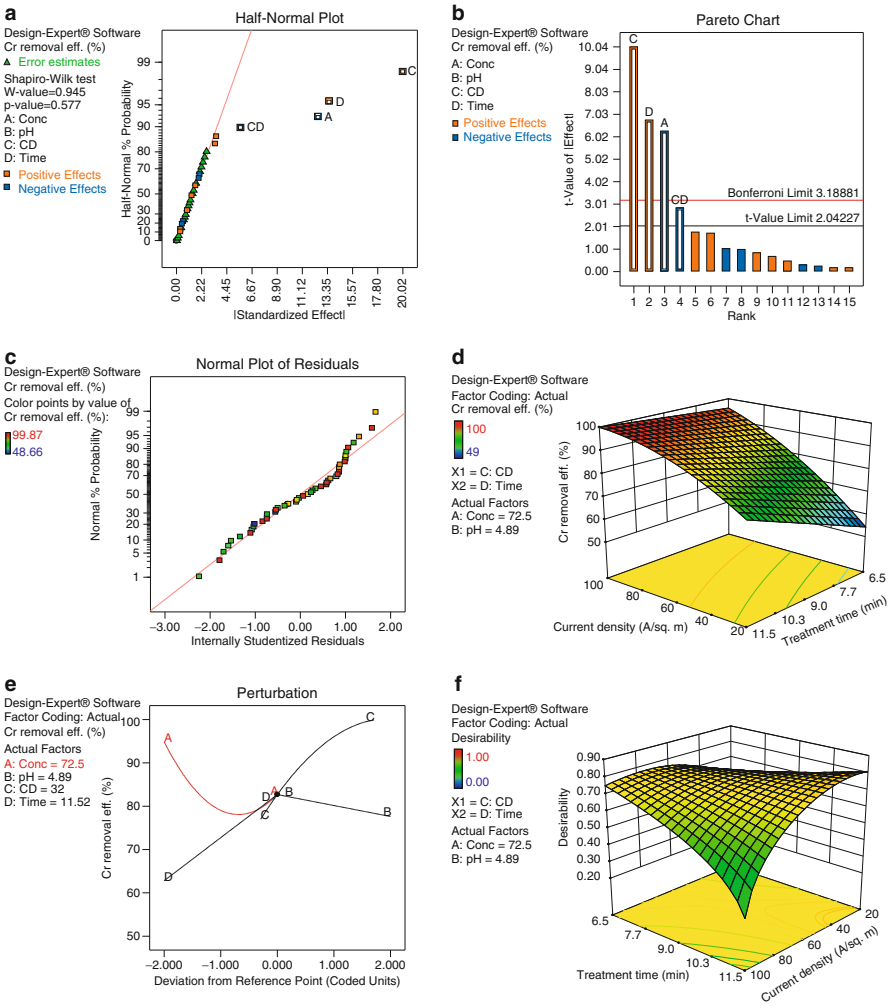

Fig. 1.3 (**a**) Half-Normal plot showing significant process variables in chromium removal efficiency. (**b**) Pareto chart showing significant levels in chromium removal efficiency. (**c**) Normal plot of residuals as per CCD. (**d**) 3D contour plot for current density and treatment time *vs.* chromium removal efficiency. (**e**) Perturbation plot showing the effect of each process variable while holding other process conditions at optimized process conditions for chromium removal efficiency. (**f**) Desirability plot showing the effect of treatment time and current density on chromium removal efficiency

with not-significant *lack of fit* ($p = 0.3319$) (Table 1.3). The proposed model has all the linear terms, one 2-factor interaction (2FI) between current density and treatment time, and squared terms for chromium concentration and current density. The model *lack of fit* was not-significant, which is indicative of a strong signal as compared to model noise. The data passed the Normal % probability test

Table 1.2 Empirical models for predicting chromium removal efficiency

Experimental design	Empirical model
	Coded equations[1]
Factorial CCD	$Y(\%) = 87.27 - 6.26A + 15.35C + 6.95D - 4.41C \times D$ $Y(\%) = 80.15 - 6.07A - 2.53B + 16.04C + 6.70D - 4.59C \times D + 9.73A^2 - 4.59C^2$
	Actual equations[2]
Factorial CCD	$Y(\%) = 32.266 - 0.313A + 0.777C + 5.383D - 0.043C \times D$ $Y(\%) = 96.502 - 2.865A - 2.764B + 1.154C + 5.389D - 0.0454 C \times D + 0.024A^2 - 2.867 \times 10^{-3}C^2$
	valid for $A = 5$–100 mg/L, $B = 2.8$–7.8, $C = 10$–100 A/m^2, $D = 3$–15 min

[1]Coded equation: Y Chromium removal efficiency, A Chromium concentration, C Current density and D Treatment time are in coded units
[2]Actual equation: Y Chromium removal efficiency, A Chromium concentration (mg/L), B pH, C Current density (A/m^2), D Treatment time (min)

Table 1.3 ANOVA statistics for chromium removal efficiency using iron electrode as per CCD

Source	Sum of squares (SS)	Degree of freedom df	Mean squares (MS)	F-value	p-value Prob. > F
Model	8244	7	1178	36.61	<0.0001*
A – Chromium conc.	1148	1	1148	35.69	<0.0001*
B – pH	219	1	219	6.82	0.0128*
C – Current density	3988	1	3988	123.96	<0.0001*
D – Treatment time	1844	1	1844	57.32	<0.0001*
$C \times D$	276	1	276	8.58	0.0056*
A^2	877	1	877	27.27	<0.0001*
C^2	166	1	166	5.16	0.0287*
Lack of Fit	1175	35	34	1.68	0.3319 (NS)
	Model statistics				
	Std. Dev.	5.7		R^2	0.868
	Mean	83.1		Adj. R^2	0.844
	C.V. %	6.8		Pred. R^2	0.819
	PRESS	1722		Adeq. Precision	23.7

* Significant at $p < 0.05$
NS = Not significant at $p < 0.05$

(Fig. 1.3c) and could be used for graphical plotting of the regression equations. The unit-less regression equation for coded factors and actual regression equation is given in Table 1.3. The unit-less regression equation indicated that current density

has the highest positive contribution in linear terms. But, 2FI showed antagonist interaction between current density and treatment time. The model revealed that beyond 100 A/m^2, there was no appreciable increase in Cr(VI) removal efficiency. But, lowering treatment time had beneficial effect on energy consumption. By keeping the treatment time around 6.5 min, the Cr(VI) removal efficiency was 96 %. Thus, there was marginal reduction in Cr(VI) removal efficiency (~3 %) if treatment time was set at lower values (Fig. 1.3d). The perturbation plot showed that three of the process variables, Cr(VI) concentration, current density and treatment time, have significant effect on Cr(VI) removal efficiency (Fig. 1.3e). Mild pH affect was observed and affected Cr(VI) removal efficiency by 5 % maximum. Current density had positive effect on chromium removal efficiency, but rate of increase decreased for current density above 40 A/m^2. Model for energy consumption comprised two linear terms (current density and treatment time) and one 2FI between current density and treatment time. The reduced 2FI model explained 95.5 % variance in the data. Multiple response optimization for maximizing chromium removal efficiency while minimizing energy consumption gave a removal efficiency of 82 % for 72.5 mg/L Cr(VI) concentration, pH of 4.9, current density of 30 A/m^2 and treatment time of 11.5 min with energy consumption of 0.065 Wh. Desirability plot revealed that lower current density favours chromium removal efficiency, whereas on the higher side (100 A/m^2), the chances of achieving desired efficiency was substantially reduced (Fig. 1.3f). It is inferred that current density should be in the range of 40 A/m^2 to 60 A/m^2 and treatment time $\leq$9 min to achieve the maximum Cr(VI) removal efficiency. The other process factors should be maintained as per influent wastewater characteristics.

3.3 ANN-GA Modelling and Optimization

Experimental data as given in Table 1.1 along with additional experimental runs obtained by varying distance between the electrodes from 15 to 25 mm was Fused for fitting ANN model. The electrode distance is confounded in current density, thus adding additional experimental runs at reduced current density to be incorporated in ANN model building. The fitted model had 77 optimum training runs and trained network along with its biases as given in Table 1.4. The trained network have mean sum of square errors (MSE) of 0.75 with correlation coefficient of 0.987. The regression plot of the trained network is depicted in Fig. 1.4a. For multi-objective optimization, ANN model was coupled with genetic algorithm. The weighted average change in the fitness function value over 50 generations was used as the criterion to stop the algorithm. The optimized Pareto front achieved after 115 iterations is depicted in Fig. 1.4b and the corresponding decision variables were taken from Table 1.5. Algorithm options were set at population size of 80, 0.75 with scattered crossover function, forward with migration fraction set to 0.2. The selection function was tournament of size two, adaptive feasible mutation function and distance measure function set as distance crowding. From the Pareto

Table 1.4 Network weights and biases for the ANN model

		Input layer to hidden layer weights (Wi)						
		W_1 *(Cr conc.)*	W_1 *(pH)*	W_1 *(Current density)*	W_1 *(Treatment time)*	W_1 *(Effective reactor volume)*	*Bias*	
	PE1[a]	−0.2163	−0.1342	−1.0506	−0.4085	−0.61409	0.4070	
	PE2	−1.6945	0.2031	0.2421	0.0710	0.1055	−0.3292	
	PE3	−0.2893	−0.3388	1.0173	0.6210	−0.4551	0.3959	
	PE4	0.0846	0.2127	−1.6124	−0.0876	0.1800	0.2392	
	PE5	0.1650	0.1067	−0.7472	0.5330	0.0934	−0.6932	
	PE6	−0.0258	0.1660	0.5996	1.1670	0.0135	0.4301	
	PE7	−0.7667	0.0679	0.86928	−1.6170	−0.0638	0.6901	
	Hidden layer to output layer weights (Wi)							
	W_2 PE_1	W_2 PE_2	W_2 PE_3	W_2 PE_4	W_2 PE_5	W_2 PE_6	W_2 PE_7	*Bias*
Output 1	−0.7891	0.9028	1.0829	0.8137	−1.0043	−0.5949	−0.91083	0.7920
Output 2	−0.3153	−0.0061	−0.1940	−0.7271	−0.9745	0.7934	−0.1841	−0.6654

[a]*PE* Processing elements, *Output* 1 Cr(VI) removal efficiency, *Output* 2 Energy consumption

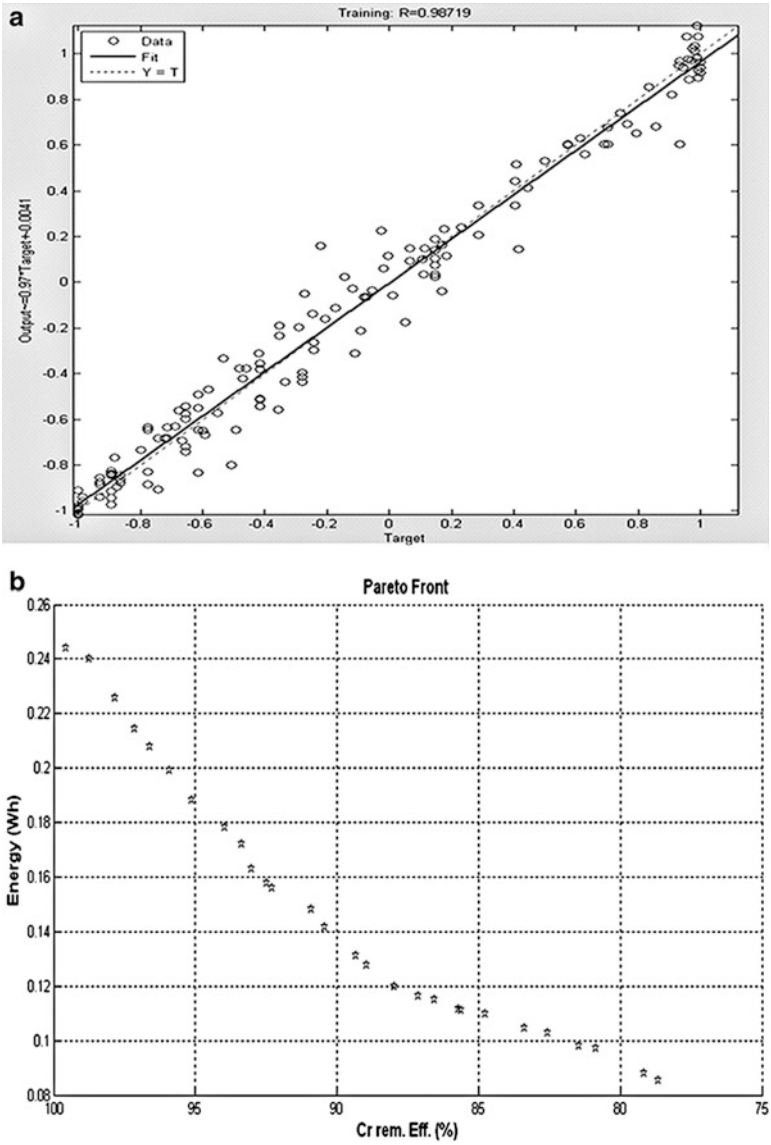

Fig. 1.4 (**a**) Regression plot (Actual *vs.* Predicted) using ANN model. (**b**) Pareto front showing multi-objective optimization of chromium removal efficiency and energy consumption

front, maximum chromium removal efficiency (99.6 %) was achieved consuming 0.244 Wh of energy, whereas minimum chromium removal efficiency (78.7 %) consumed 0.085 Wh of energy. This reduction in Cr(VI) removal efficiency from 99.6 to 78.7 % decreases energy consumption by 65 %. Minimizing energy consumption to lowest values reduces removal efficiency around 80 %. The best

Table 1.5 Process decision variables corresponding to each of the Pareto-optimal solutions depicted in Fig. 1.4b and chromium removal per unit energy consumption for iron electrode (Chromium concentration ~40 mg/L, pH between 4.5 and 5.2)

	Process variables		Response variables		Cr(VI) removal per unit energy consumption	
	Current density	Treatment time	Cr(VI) removal efficiency	Energy		
	A/m^2	min	%	Wh	Actual	Normalized
1	70	10.0	99.6	0.244	408	1.00
2	69	10.0	98.8	0.240	411	1.01
3	66	10.0	97.8	0.226	434	1.06
4	64	10.0	97.1	0.214	453	1.11
5	63	10.0	96.6	0.208	464	1.14
6	61	10.0	95.9	0.199	482	1.18
7	59	10.0	95.1	0.188	505	1.24
8	58	9.9	94.0	0.178	527	1.29
9	57	9.9	93.4	0.172	542	1.33
10	55	10.0	93.0	0.163	570	1.40
11	54	9.9	92.5	0.158	586	1.43
12	53	10.0	92.3	0.156	592	1.45
13	52	9.9	90.9	0.148	613	1.50
14	51	10.0	90.4	0.142	638	1.56
15	48	9.9	89.4	0.131	682	1.67
16	48	9.9	89.0	0.128	696	1.70
17	46	9.9	88.0	0.120	733	1.80
18	45	9.8	87.1	0.116	749	1.83
19	46	9.7	86.6	0.115	753	1.84
20	45	9.6	85.7	0.111	769	1.88
21	45	9.6	84.8	0.110	770	1.89
22	46	9.3	85.6	0.111	771	1.89
23	45	9.1	83.4	0.104	798	1.95
24	45	8.9	82.6	0.103	803	1.97
25	45	8.7	81.5	0.098	829	2.03
26	45	8.6	80.9	0.097	834	2.04
27	45	8.1	79.2	0.088	899	2.20
28	45	8.0	78.7	0.085	922	2.26

operating conditions were obtained when normalized values of chromium removal efficiency per unit energy consumption are around 1.67 (Table 1.5). This gives corresponding input variables as pH of 4.6, current density of 48 A/m^2 and 10 min of treatment time to get 89.4 % Cr(VI) removal efficiency consuming 0.131 Wh of energy (Fig. 1.4b).

Table 1.6 Path analysis for iron electrode

Independent variables	R_{yx}	Direct effect (DE)	Indirect effects (IE)					Total IE
			X_1	X_2	X_3	X_4	X_5	
X_1	−0.287	**−0.361**	0	−0.001	0.070	0.014	−0.001	0.083
X_2	0.016	−0.102	−0.003	0	0.080	−0.006	0.001	0.070
X_3	0.665	**0.708**	−0.036	−0.011	0	−0.010	0.013	−0.058
X_4	0.371	**0.402**	−0.012	0.001	−0.018	0	0.001	−0.029
X_5	−0.370	−0.029	−0.010	0.002	**−0.328**	−0.008	0	**−0.336**

X_1 Cr(VI) concentration, X_2 pH, X_3 Current density, X_4 Treatment time, X_5 Effective reactor volume

3.4 Path Analysis

Current density followed by treatment time gave maximum positive direct effect, whereas initial chromium concentration gave maximum negative direct effect on chromium removal efficiency. Effective reactor volume had negative indirect effect (–0.336) on chromium removal efficiency (Table 1.6). Negative indirect effect of effective reactor volume is mediated through current density. Therefore, increasing current density beyond optimum range had a cascading effect on chromium removal efficiency. It is therefore recommended that current density should be maintained between 20 and 40 A/m^2 for best removal efficiency.

As per Espino-Quinones et al. (2012), the optimum conditions for electrocoagulation using iron electrodes were current density of 97.7 A/m^2, pH of 6.5, reaction time of 35 min and 170 rpm as agitation velocity for 100 % chromium removal. In the similar study, Liu et al. (2014) optimized chromium removal efficiency (98.84 %) using iron electrodes at initial chromium concentration of 105 mg/L, cell voltage of 4 V, pH = 6 and 60 min treatment time. Bhatti et al. (2009, 2011a) reported electrocoagulation removal of Cr(VI) using aluminum electrodes with chromium removal efficiency of 90.4 % with energy consumption of 137.2 kWh/m^3. They further reported that energy efficient chromium removal was 50 % at 27.8 kWh/m^3. Akbal and Camci (2010, 2012) reported 99.9 % chromium removal at 100 A/m^2 in 20 min treatment time, and 100 % chromium removal in 60 min treatment time and 2 A current. Olmez (2009) proposed highly acidic pH for complete reduction of Cr(VI). The other optimized conditions were 7.4 A applied current, 33.6 mM NaCl electrolyte and 70 min treatment time. Hamdan and EI-Nass (2014) worked on chromium removal from groundwater using electrocoagulation. The optimized conditions were 79.4 A/m^2 and 5 min treatment time with 0.6 kWh/m^3 of energy consumption. In another study, researchers studied role of iron anode oxidation in two-electrode system separated by ion exchange membrane for reduction of hexavalent chromium to trivalent chromium. The process is more energy efficient under lower volumetric current density of 1.5 mA/L and follows zero order rate that is dependent on electric current density (Sarahney et al. 2012). The present study concluded maximum chromium removal

efficiency of 99.9 % and it was independent of initial chromium concentration. However, for energy efficient chromium removal, 90.3 % chromium removal efficiency was achieved at 0.063 kWh/m^3 of energy consumption. The optimum conditions were 23 A/m^2 of current density and 11.5 min of treatment time. Thus, the present study led to significant reduction in energy consumption with comparable chromium removal efficiency. For achieving discharge standards of 0.05 mg/L for Cr(VI), the wastewater would require treatments in cycles in order to be more economical and energy efficient. The present study therefore indicated that iron-iron electrode combination is a highly efficient process for chromium removal, with low energy requirements.

4 Conclusions

Electrocoagulation using iron electrodes could achieve 99.9 % chromium removal efficiency. Iron residuals (<1 mg/L) produced in the process imparts a light yellowish colour to the treated water. Current density and treatment time are important process variables for removal of hexavalent chromium from the wastewater. Models developed using response surface methodology can be used to predict chromium removal efficiency at any desired process conditions. Response surface methodology helped in empirical model building to any set of process conditions. ANN-GA helped in selecting best operating conditions for process operator with respect to the removal efficiency as well as energy consumption.

Acknowledgements The authors are thankful to University Grants Commission (UGC), New Delhi for financial support and the Head, Department of Botanical and Environmental Sciences, Guru Nanak Dev University, Amritsar for providing research facilities. The authors are thankful to the Director, Indian Institute of Technology Roorkee, India for EPMA analysis of the iron electrode.

References

Abassi, S.A., Abassi, N. and Soni, R. (1997). Heavy Metals in the Environment. Mittal Publications, New Delhi.

Aber, S., Amani-Ghadim, A.R. and Mirzajani, V. (2009). Removal of Cr(VI) from polluted solutions by electrocoagulation: Modeling of experimental results using artificial neural network. *Journal of Hazardous Materials*, **171:** 484–490.

Adhoum, N., Monser, L., Bellakhal, N. and Belgaied, J.E. (2004). Treatment of electroplating wastewater containing Cu^{+2}, Zn^{+2} and Cr(IV) by electrocoagulation. *Journal of Hazardous Materials*, **112:** 207–213.

Akbal, F. and Camci, S. (2010). Comparison of electrocoagulation and chemical coagulation for heavy metal removal. *Chemical Engineering and Technology*, **33:** 1655–1664.

Akbal, F. and Camci, S. (2011). Copper, chromium and nickel removal from metal plating wastewater by electrocoagulation. *Desalination*, **269:** 214–222.

Akbal, F. and Camci, S. (2012). Treatment of metal plating wastewater by electrocoagulation. *Environmental Progress and Sustainable Energy*, **31(3):** 340–350.

Al Anbari, R.H., Alfatlawi, S.M. and Albaidhani, J.H. (2012). Removal of some heavy metals by electrocoagulation. *Advanced Materials Research*, **468–471:** 2882–2890.

Anderson, M.J. and Whitcomb, P.J. (2004). RSM Simplified: Optimizing process using response surface methods for Design of Experiments. CRC Press, Boca Raton.

APHA, AWWA, WEF (1998). Standard Methods for the Examination of Water and Wastewater (19th ed.). American Public Health Association, Washington DC.

Arroyo, M.G., Pérez-Herranz, V., Montañés, M.T., García-Antón, J. and Guiñón, J.L. (2009). Effect of pH and chloride concentration on the removal of hexavalent chromium in a batch electrocoagulation reactor. *Journal of Hazardous Materials*, **169:** 1127–1133.

Beyazit, N. (2014). Copper(II), chromium(VI) and nickel(II) removal from metal plating effluent by electrocoagulation. *International Journal of Electrochemical Science*, **9(8):** 4315–4330.

Bhagawan, D., Poodari, S., Pothuraju, T., Srinivasulu, D., Shankaraiah, G., Yamuna Rani, M., Himabindu, V. and Vidyavathi, S. (2014). Effect of operational parameters on heavy metal removal by electrocoagulation. *Environmental Science and Pollution Research*, **21(24):** 14166–14173.

Bhatti, M.S., Reddy, A.S. and Thukral, A.K. (2009). Electrocoagulation removal of hexavalent chromium in simulated wastewater using response surface methodology. *Journal of Hazardous Materials*, **172:** 839–845.

Bhatti, M.S., Reddy, A.S., Kalia, R.K. and Thukral, A.K. (2011a). Modeling and optimization of voltage and treatment time for the electrocoagulation removal of hexavalent chromium. *Desalination*, **269:** 157–162.

Bhatti, M.S., Kapoor, D., Kalia, R.K., Reddy, A.S. and Thukral, A.K. (2011b). RSM and ANN modeling for electrocoagulation of copper from simulated wastewater: Multi objective optimization using genetic algorithm approach. *Desalination*, **274:** 74–80.

Cataldo, H.M., Barletta, L., Dogliotti, M.B., Russo, N., Fino, D. and Spinelli, P. (2012). Heavy metal removal by means of electrocoagulation using aluminum electrodes for drinking water purification. *Journal of Applied Electrochemistry*, **42:** 809–817.

CPCB (2001). Pollution Control Law Series, Pollution control Acts, Rules and Notifications issued thereunder. Central Pollution Control Board, Ministry of Environment and Forests, Govt. of India, New Delhi.

Dermentzis, K., Christoforidis, A., Valsamidou, E., Lazaridou, A. and Kokkinos, N. (2011). Removal of hexavalent chromium from electroplating wastewater by electrocoagulation with iron electrodes. *Global Nest Journal*, **13:** 412–418.

Eckenfelder, W.W. Jr. (2000). Industrial Water Pollution Control (3rd ed.). McGraw Hill, Singapore.

Espinoza-Quiñones, F.R., Módenes, A.N., Theodoro, P.S., Palácio, S.M., Trigueros, D.E.G., Borba, C.E., Abugderah, M.M. and Kroumov, A.D. (2012). Optimization of the iron electrocoagulation process of Cr, Ni, Cu, and Zn galvanization by-products by using response surface methodology. *Separation Science and Technology*, **47:** 688–699.

Hamdan, S.S. and El-Naas, M.H. (2014). Characterization of the removal of Chromium(VI) from groundwater by electrocoagulation. *Journal of Industrial and Engineering Chemistry*, **20(5):** 2775–2781.

Heidmann, I. and Calmano, W. (2008). Removal of Cr(VI) from model wastewaters by electrocoagulation with Fe electrodes. *Separation and Purification Technology*, **61:** 15–21.

Liu, Y., Lu, J., Ma, X., Li, Y. and Lin, S. (2014). Technique and mechanism of electrocoagulation process for treatment of wastewater containing chromium. *Chinese Journal of Environmental Engineering*, **8(9):** 3640–3644.

Metcalf and Eddy (2003). Wastewater Engineering Treatment and Reuse, 4th ed. Revised by Tchobanoglous G., Burton, F.L. and Stensel, H.D. Tata McGraw Hill Education Pvt. Ltd., New Delhi.

Odongo, I.E. and McFarland, M.J. (2014). Electrocoagulation treatment of metal finishing wastewater. *Water Environment Research*, **86(7):** 579–583.

Olmez, T. (2009). The optimization of Cr(VI) reduction and removal by electrocoagulation using response surface methodology. *Journal of Hazardous Materials*, **162:** 1371–1378.

Shahriari, T., Bidhendi, G.N., Mehrdadi, N. and Torabian, A. (2014). Removal of chromium(III) from wastewater by electrocoagulation method. *KSCE Journal of Civil engineering*, **18(4):** 949–955.

Sarahney, H., Mao, X. and Alshawabkeh, A.N. (2012). The role of iron anode oxidation on transformation of chromium by electrolysis. *Electrochimica Acta*, **86:** 96–101.

Vasudevan, S., Lakshmi, J. and Sozhan, G. (2012). Simultaneous removal of Co, Cu, and Cr from water by electrocoagulation. *Toxicological and Environmental Chemistry*, **94:** 1930–1940.

Verma, S.K, Khandegar, V. and Saroha, A.K. (2013). Removal of chromium from electroplating industry effluent using electrocoagulation. Journal of Hazardous, Toxic, and Radioactive Waste, 17(2): 146–152.

WHO (1996). Chromium in Drinking Water, Background Document for Development of WHO Guidelines for Drinking Water Quality. Guidelines for Drinking Water Quality, 2nd ed., vol. 2. World Health Organization, Geneva.

Xu, H.Y., Yang, Z.H., Zeng, G.M., Luo, Y.L., Huang, J., Wang, L.K., Song, P.P. and Mo, X. (2014). Investigation of pH evolution with Cr(VI) removal in electrocoagulation process: Proposing a real-time control strategy. *Chemical Engineering Journal*, **239:** 132–140.

Zaroual, Z., Chaair, H., Essadki, A.H., El Ass, K. and Azzi, M. (2009). Optimizing the removal of trivalent chromium by electrocoagulation using experimental design. *Chemical Engineering Journal*, **148:** 488–495.

Zongo, I., Leclerc, J., Maïga, H.A., Wéthé, J. and Lapicque, F. (2009). Removal of hexavalent chromium from industrial wastewater by electrocoagulation: A comprehensive comparison of aluminum and iron electrodes. *Separation and Purification Technology*, **66:** 159–166.

Chapter 2
Sunlight-Assisted Photo-Fenton Process for Removal of Insecticide from Agricultural Wastewater

Amrita Dutta, Sanjukta Datta, Mahua Ghosh, Debasish Sarkar, and Sampa Chakrabarti

1 Introduction

Pesticides and insecticides are harmful and toxic organic chemicals that are used for controlling pests and insects in agriculture, thereby considered as necessary evil. Agricultural wastewater, contaminated with such toxic pesticides, pollutes surface and groundwater. Pesticides are able to reach surface waters either directly or indirectly via the discharge of agricultural drainage water from treated land and via runoff after application on hard surfaces (Leu et al. 2004). Organophosphorus pesticides are produced in mass and are widely used in the developing country. 2,2 dichlorovinyl dimethyl phosphate, commonly referred as Dichlorvos (Fig. 2.1) is an organophosphorous insecticide, which is highly toxic, non-biodegradable and difficult to remove by conventional methods. During 2006–2010 period, consumption of Dichlorvos in India was 5833 metric tons. Due to its fairly good solubility [~10 g. L^{-1} (at 20 °C)] in water (WHO 1978, 1994) it is highly mobile in aquatic environment. Various technologies and processes have been proposed for the treatment of pesticide-contaminated waters. Some conventional techniques including flocculation, filtration and adsorption of activated carbon are only based on a phase transfer of the pollutant. These treatment procedures are either of high cost or a source of secondary pollution due to sludge formation: therefore, there is a need to seek better alternatives (Evgenidou et al. 2005). Advanced oxidation processes (AOPs) are attractive methods for the treatment of wastewaters containing

A. Dutta • D. Sarkar • S. Chakrabarti (✉)
Department of Chemical Engineering, University of Calcutta, 92, Acharya P.C. Road, Kolkata 700 009, India
e-mail: scchemengg@caluniv.ac.in

S. Datta • M. Ghosh
Department of Chemical Technology, University of Calcutta, 92, Acharya P.C. Road, Kolkata 700 009, India

F. Kurisu et al. (eds.), *Trends in Asian Water Environmental Science and Technology*, DOI 10.1007/978-3-319-39259-2_2

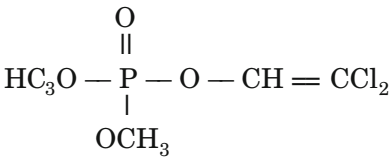

Fig. 2.1 Structure of Dichlorvos (2, 2 dichlorovinyl dimethyl phosphate)

refractory organics due to their efficiency to oxidize a great variety of organic contaminants by the generation of highly reactive hydroxyl radicals (OH•) (Espulgas et al. 2002). Many pollutants, including pesticides, pharmaceuticals and dyes can be completely mineralised by AOP as reported in the works of Chiron et al. (2000), Perez-Estrada et al. (2005) and Lucas and Peres (2006). Heterogeneous photocatalysis using titanium dioxide (TiO_2) and solar/UV radiation, combined with hydrogen peroxide (H_2O_2), and homogeneous processes such as Fenton (Fe^{2+}/H_2O_2) and photo-Fenton (Fe^{2+}/H_2O_2/UV/sunlight) reactions are proved to be useful techniques for the treatment of pesticide-contaminated wastewater. There are different ways to produce HO•, among which solar photo-Fenton process is one of the most efficient ones for the treatment of contaminated wastewater (Malato et al. 2002; Oller et al. 2006; Maldonado et al. 2007; Ortega-Liébana et al. 2012; Klamerth et al. 2013).

Degradation of triazine herbicides was reported by Burrows et al. (2002), methylparathion by Chiron et al. (2000), fenuron by Acero et al. (2002) and diuron by Burrows et al. (2002). Sakugawa et al. (2013) reported the degradation of three pesticides at pH 2.8 and 7.2 in pure and natural waters using Fe^{2+}/H_2O_2/UV-visible light and Fe^{3+}/H_2O_2 UV-visible light oxidation systems.

Dichlorvos is among the 24 insecticides registered and used in India. It has been classified in category 'C' by US-EPA as potential carcinogen. Hence the present work has been undertaken in order to explore the efficacy of sunlight-assisted photo-Fenton oxidative degradation of dichlorvos pesticide in water in a batch process. Process parameters studied were (i) dosing of H_2O_2, (ii) ferrous sulphate dosing, (iii) pH and (iv) initial concentration of the insecticide. FTIR spectroscopy was used to identify the functional groups resulting from degradation reaction. Chemical oxygen demand (COD) was monitored to examine the extent of mineralization of the insecticide. Additionally, a kinetic model, representing the initial rate of degradation as a function of initial reactant concentration, was proposed and validated by experimental results.

2 Materials and Methods

2.1 Chemicals Used

Dichlorvos (76 % purity) (molecular formula $C_4H_7Cl_2O_4P$, molecular weight 220.9 g/mol) was obtained from United Phosphorus Limited, India. Structure is

given in Fig. 2.1. Crystalline ferrous sulphate ($FeSO_4 \cdot 7H_2O$), was obtained from Sisco Research Laboratories, India. For this experiment 0.5 % of $FeSO_4$ solution has been used. Hydrogen peroxide (H_2O_2, 50 % v/v) was obtained from Merck Specialities, India. Sodium bi-sulphite ($NaHSO_3$) was obtained from Loba Chemie. 5(N) $NaHSO_3$ solutions have been used to stop the Fenton reaction at desired point. All solutions were prepared using fresh distilled water.

2.2 Experimental Procedure

Solar photo-Fenton experiments were performed in a stainless steel box-shaped batch reactor with a 3 mm thick quartz plate as its lid through which sunlight could enter. The reactor was provided with cooling water circulation to maintain the temperature at 30–32 °C. The schematic of the present experimental setup is shown in Fig. 2.2. Simulated wastewater was prepared by adding Dichlorvos insecticide into deionised water. Freshly prepared solutions of $FeSO_4 \cdot 7H_2O$ and H_2O_2 was added in the synthetic wastewater. The solutions were continuously stirred using a magnetic stirrer. Intensity of solar radiation was approximately 60–66 kLux (24.12–26.53 $mW.cm^{-2}$). Samples were withdrawn from time to time to measure the extent of degradation. The reaction was stopped by adding sodium bisulphite and analyzed for the residual pollutant with HPLC. All the experiments were carried out within the time span between 12 noon and 2 pm during May-June in eastern part of India.

2.3 Analytical Methods

Residual concentrations of the pollutant were analyzed at different time intervals using WATERS 2487 HPLC equipped with a C18 Column (ZORBAX SB-C18 5 µm, 46 × 150 mm). Mixture of acetonitrile and Milli-Q water (50/50 v/v for dichlorvos) was used as the mobile phase with a flow rate of 1 $mL.min^{-1}$ (Rice et al. 2005). Chemical oxygen demand (COD) was determined by the APHA standard total reflux method. FTIR analysis was performed in a Jasco-6300 instrument using KBr pellet.

3 Result and Discussions

Time-concentration data was collected for all the experiments varying different process parameters. Each experiment was repeated more than once and the standard deviation was less than ±5 %.

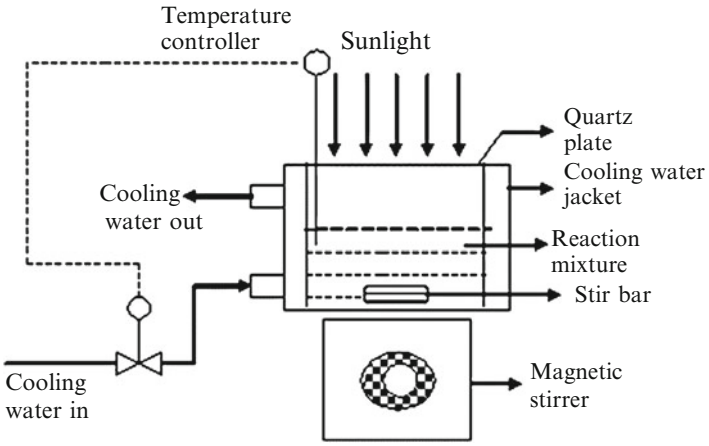

Fig. 2.2 Schematic of experimental set-up

3.1 *Effect of pH*

Photo-Fenton reactions are strongly dependent on pH (Tamimi et al., 2011). Experiments were carried out in pH range of 3–7. From Fig. 2.3a it can be seen that the photo Fenton oxidation efficiency monotonically decreases with increasing pH. This is because pH value influences both the generation of hydroxyl radicals as well as the oxidation efficiency. The degradation decreased at pH values higher than 5, because ferrous sulphate gets precipitated as hydroxide, resulting in a reduction in the penetration of solar radiation in the reaction mixture (Faust and Hoigne 1990). Moreover, Dichlorvos in acidic solution is more susceptible to hydrolysis than that in alkaline solution (Jiangtong 1981).

Figure 2.3b shows the effect of pH on the reduction of COD of wastewater containing Dichlorvos. The results show that the percent removal of COD is more at acidic pH. Raising pH from 3 to 7 decreased the removal efficiency of Dichlorvos from 83 to 57 %. Corresponding decrease in the removal of COD was from 86.6 to 61.8 % respectively. Initial rate also followed the same trend.

3.2 *Effect of Hydrogen Peroxide Concentration*

H_2O_2 itself generates active oxygen species. In this experiment, the concentration of H_2O_2 was changed from 14 to 58 mmol.L^{-1}, but the concentration of ferrous sulphate dosage was held constant (0.28 mmol.L^{-1}). Other process parameters, initial concentration of insecticide (0.133 mmol.L^{-1}), pH (3) and temperature (30 °C) were kept constant. From Fig. 2.4a it is observed that 95.33 % of 0.133 mmol.L^{-1} Dichlorvos degraded after 120 min under sunlight of 66 kLux

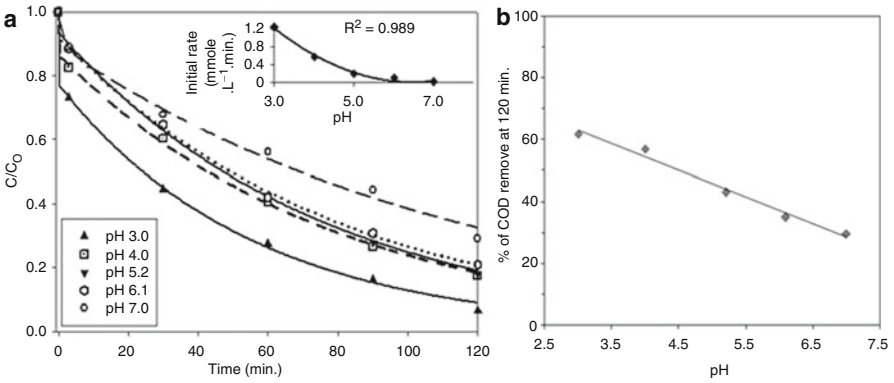

Fig. 2.3 (**a**) Effect of pH on degradation of pesticide in water. Inset shows initial reaction rate at different pH and (**b**) Effect of the pH on the COD removal

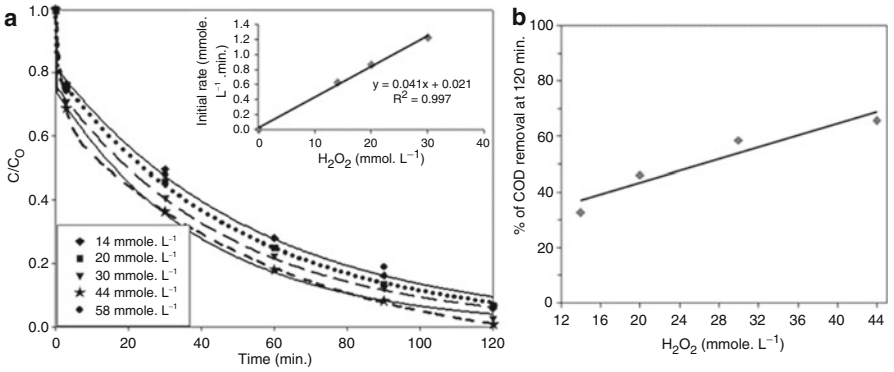

Fig. 2.4 (**a**) Effect of H_2O_2 dosage for the degradation of pesticide contaminated water. Inset shows initial reaction rate vs. H_2O_2 dosage and (**b**) Effect of dosing of H_2O_2 on the COD removal

using 30 mmol.L^{-1} of H_2O_2. Degradation of Dichlorvos was observed to increase from 93.24 to 95.33 with increasing the dosing concentration of hydrogen peroxide from 14 to 30 mmol.L^{-1}. With the increase in H_2O_2-dosing, the initial reaction rate of pesticide increased up to a particular dosing of 30 mmol.L^{-1}. After that it decreased due to the scavenging of hydroxyl radical by H_2O_2. Similar finding was reported by Ghaly et al. (2001) who found that the recombination of hydroxyl radicals and also hydroxyl radicals reaction with H_2O_2, contributes to the scavenging of OH• (Eqs. 2.1, 2.2, 2.3).

$$H_2O_2 + OH\bullet \longrightarrow H_2O + HO_2\bullet \quad (2.1)$$

$$HO_2\bullet + OH\bullet \longrightarrow H_2O + O_2 \quad (2.2)$$

$$OH\bullet + OH\bullet \longrightarrow H_2O_2 \quad (2.3)$$

It can be postulated that H_2O_2 should be added at an optimum concentration to achieve the best degradation. Hence, 30 mmol.L^{-1} of H_2O_2 was selected as the optimal dosage for the degradation of Dichlorvos in wastewater. Rongxi et al. (2009) reported that 75 mL per litre of 30 % H_2O_2 solution was the optimal dosage for the treatment of industrial triazophos pesticide wastewater. Figure 2.4b shows that percent of COD removal has increased with increasing H_2O_2 concentration from 14 to 30 mmol.L^{-1}.

3.3 *Effect of Ferrous Sulphate Dosing Concentration*

Dosing of ferrous sulphate is one of the major parameters to influence the photo-Fenton processes. Solar-assisted photo-Fenton experiments were executed with different doses of $FeSO_4{\cdot}7H_2O$ ranging from 0.072 to 0.36 mmol.L^{-1}. The results of these experiments are shown in Fig. 2.5a, b. It can be seen that 11 % of 0.133 mmol.L^{-1} insecticide degraded without ferrous sulphate solution, when H_2O_2 dosage was 30 mmol.L^{-1} and pH was 3. Moreover, the degradation and initial reaction rate decreased with decrease in the concentration of $FeSO_4{\cdot}7H_2O$ upto a critical value. Further increase in the concentration of ferrous sulphate resulted in decrease of the initial degradation rate of substrate because production of a large amount of Fe^{3+}. Fe^{3+} decomposes H_2O_2 and produces $Fe(OH)^{2+}$ in acidic condition. Tamimi et al. (2008) reported that higher the concentration of Fe^{2+}, more was the amount of Fe^{3+} generated from the process of H_2O_2 decomposition by Fe^{2+}, thus making Fe^{2+} unavailable for reaction.

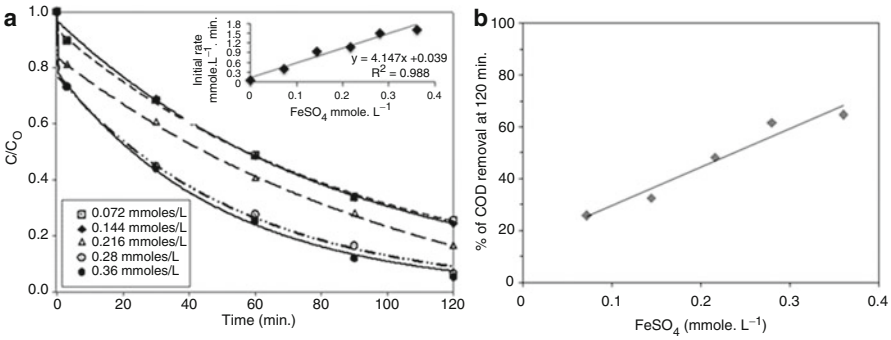

Fig. 2.5 (**a**) Effect of $FeSO_4{\cdot}7H_2O$ dosage for the degradation of pesticide contaminated water. Inset panel shows initial reaction rate vs. $FeSO_4{\cdot}7H_2O$ dosage and (**b**) Effect of dosing of $FeSO_4{\cdot}7H_2O$ on the COD removal

3.4 Effect of Initial Concentration of Insecticide

Degradation of pesticide and COD removal at various initial concentrations by photo-Fenton oxidation is shown in Fig. 2.5a, b respectively. After 120 min reaction time, degradation of pesticide were observed to be 99.42 %, 93.49 %, 95.42 %, 88.08 % and 88.22 % at initial pesticide concentration 0.069, 0.133, 0.224, 0.308 and 0.376 mmol.L^{-1} respectively when the other parameters were fixed at $FeSO_4{\cdot}7H_2O$: 0.28 mmol.L^{-1}, H_2O_2: 30 mmol.L^{-1} and pH 3. Initial rate remained almost independent of the initial concentration within the experimental range of concentration (0.068–0.224 mmol.L^{-1}). Percent degradation decreased with increasing initial concentration of substrate.

It can be seen that the removal of COD clearly increased with the decreasing amount of pesticides (Fig. 2.6).

3.5 Rate Equation and Kinetics

Degradation of the oxidation reaction is assumed to proceed via hydroxyl and peroxyhydroxyl radical attack to the pesticide molecule (represented as RH). Hence rate of degradation is the rate of free-radical attack on pesticide.

In acidic medium, the scheme of the reaction can be represented as follows:

$$H_2O_2 + h\nu \xrightarrow{k_1(I_S)} 2OH\bullet \tag{2.4}$$

$$Fe^{2+} + H_2O_2 \xrightarrow{k_2} Fe^{3+} + OH\bullet + HO^- \tag{2.5}$$

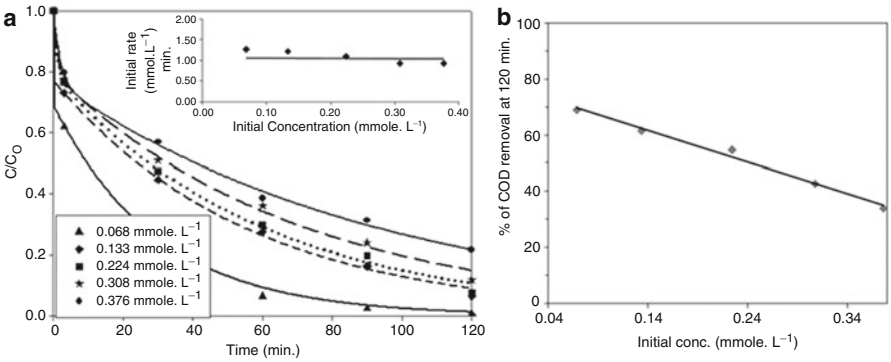

Fig. 2.6 (**a**) Effect of initial concentration for the degradation of pesticide contaminated water. The inset panel shows reaction rate vs. initial concentration. (**b**) Effect of initial pesticide concentration on the COD removal

$$Fe^{3+} + H_2O_2 \xrightarrow{k_3} Fe^{2+} + \bullet OH_2 + H^+ \tag{2.6}$$

$$Fe^{3+} + H_2O + h\nu \xrightarrow{k_4(I_S)} Fe^{2+} + \bullet OH + H^+ \tag{2.7}$$

$$RH + \bullet OH \xrightarrow{k_5} R\bullet + H_2O \rightarrow \text{Products} \tag{2.8}$$

$$RH + \bullet O_2H \xrightarrow{k_6} R\bullet + H_2O \rightarrow \text{Products} \tag{2.9}$$

Here rate constants k_1 and k_4 are considered to be dependent on the intensity of sunlight i.e., I_S. Hence $k_1 = k_1(I_S)$ and $k_4 = k_4(I_S)$.

From Eqs. (2.5) and (2.6), initial rate of degradation of pesticide, $-r_{RH}$ becomes:

$$-\frac{d}{dt}[RH] = k_5[RH][\bullet OH] + k_6[RH][\bullet O_2H] \tag{2.10}$$

Active oxidant, •OH radical is generated by the reaction steps (2.1), (2.2) and (2.4) and is consumed in the step (2.5). So the net rate of generation of •OH radical is:

$$\begin{aligned} -\frac{d}{dt}[\bullet OH] = \; & k_1(I_S)[H_2O_2] + k_2[Fe^{2+}][H_2O_2] \\ & + k_3[Fe^{3+}][H_2O_2] + k_4(I_S)[Fe^{3+}][H_2O] + k_5[RH][\bullet OH] \end{aligned} \tag{2.11}$$

Similarly the other reaction intermediates and oxidizing species, $O_2H\bullet$, Fe^{3+} and Fe^{2+} have their own pathways of generation and consumption as described in the scheme. According to well known theory of non-elementary reaction, concentration of all the intermediates are in pseudo-steady state, that is net rate of each of them is zero. Therefore, the expression for the initial rate becomes:

$$-r_{RH} = -\frac{d}{dt}[RH] = k_1(I_S)[H_2O_2] + 2k_2\left[Fe^{2+}\right][H_2O_2] \tag{2.12}$$

For constant intensity of sunlight and constant dosing of Fe^{2+} (0.28 mmol.L^{-1}),

$$-r_{RH} = m[H_2O_2] \tag{2.13}$$

where $m = \{k_1\,(I_S) + 2\,k_2\,[Fe^{2+}]\}$,

Initial rate varies with variation in dosing of H_2O_2. A plot with initial dosing of H_2O_2 and corresponding initial rates is a straight line passing through (0,0) the slope of which is m (Fig. 2.4a inset).

Similarly at constant dosing of H_2O_2 (30 mmol.L^{-1}) and constant intensity of sunlight,

$$-r_{RH} = p\left[\mathrm{Fe}^{2+}\right] + q \tag{2.14}$$

where $p = 2\,k_2\,[H_2O_2]$ and $q = k_1\,(I_S)\,[H_2O_2]$.

Here initial rate varies with variation of initial dosing of Fe^{2+}. A plot with initial dosing of Fe^{2+} and corresponding initial rates [Fig. 2.5a inset] results in a straight line with slope p and intercept q.

Solving, we get, $k_1(I_S) = 1.3 \times 10^{-3}$ min^{-1} at $I_S = 26.53$ mW.m^{-2}. Value of k_2 was determined from both the equations. The average value of k_2 is reported.

$$k_2\ (\text{average}) = 0.0705\left(\frac{mM}{L}\right)^{-1}\ \text{min}^{-1}$$

3.6 FTIR Spectra Analysis

Untreated and solar-Fenton treated pesticide aqueous solution were analyzed by FTIR spectroscopy to check for presence of organic bonds. Evgenidou et al. (2006) proposed a tentative degradation scheme of Dichlorvos during the photocatalytic oxidation of the same over TiO_2. Since this was also a case of OH• radical attack, the products and intermediates are expected to be the same in nature. In the mentioned scheme, formation of aldehydes, ketones and alcohols were proposed in addition to the ultimate oxidized products like carboxylic acid, carbon dioxide and water. Peak for $P = O$ in 1175–1300 cm^{-1} was present in the Dichlorvos solution before reaction, but not in the product; indicating breakage of the bond. After reaction, strong peaks at 2200–2300 cm^{-1} indicate CO_2 and medium peaks at 2600–3000 cm^{-1} along with strong peaks at around 1700 cm^{-1} indicate carboxylic acids (Fig. 2.7).

Strong peaks at 3200–3700 cm^{-1} and in 620–680 cm^{-1} indicate presence of alcoholic and hydrogen bonded –OH group. –OH in –COOH is indicated by peak at

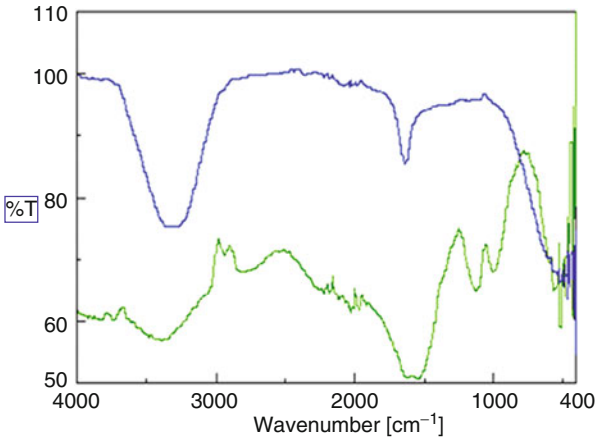

Fig. 2.7 FTIR spectra of untreated and treated insecticide aqueous solution (%T = percent of transmittance)

2400–3400 cm^{-1} and O-C = C in carboxylic acid is indicated by strong peak in 590–700 cm^{-1}. From the structure of the Dichlorvos molecule (Fig. 2.1), formation of dichloroacetic acid was envisaged. Strong peaks at 600–800 cm^{-1}, indicating Cl–C bond vibration, confirmed the proposition. Strong peaks of aldehydes and ketones were observed at 520–565 cm^{-1} and 510–560 cm^{-1} respectively. Peaks for organic ethers, indicated by medium strong peaks at 430–520 cm^{-1} and very strong peaks at 1070–1150 cm^{-1}, became more intense than that in the unreacted compound. Peaks for vinyl ethers at 1000 cm^{-1} became more intense after reaction.

All the above evidences prove well that the insecticide Dichlorvos was oxidized by sunlight-assisted photo-Fenton oxidative degradation into alcohols, aldehydes, ketones and carboxylic acid with mineralization into carbon dioxide and water. The mineralization was also evidenced by the decrease in COD as well.

4 Conclusion

Sunlight-assisted photo-Fenton oxidation reaction has been established as a very good and rapid method for the degradation of Dichlorvos insecticides. The degradation rate of insecticides and the respective COD were observed to increase with the increasing amount of ferrous sulphate and H_2O_2. The COD removal efficiencies of Dichlorvos wastewater treated by Fenton reagent are greatly influenced by the pH value, dosage of $FeSO_4 \cdot 7H_2O$ and H_2O_2. FTIR analysis of the insecticide before and after reaction indicates its degradation into lower organic fragments. In a tropical country like India with abundant solar energy, this may be considered as an economic and eco-friendly technology. The results of this work may be used to design a continuous reactor, which may be suitably scaled up to meet industrial requirement.

Acknowledgements This research was funded by the Department of Science & Technology, Government of West Bengal for their R&D grant number 749 (Sanc.)/ST/P/S&T/4G-1/2010 dated 2.2.2012. The authors are thankful to the Centre for Research in Nanoscience & Nanotechnology, CU and Prof. Arup Mukherjee, Department of Chemical Technology, CU for FTIR.

References

Acero, J., Benitez, F., Gonzalez, M. and Benitez R. (2002). Kinetics of fenuron decomposition by single-chemical oxidants and combined systems. *Ind. Eng. Chem. Res*., **41(17):** 4225–4232.

Burrows, H., Canle, M., Santaballa, J. and Steenken, S. (2002). Reaction pathways and mechanisms of photodegradation of pesticides. *J. Photochem. Photobiol. B: Biol*., **67(2):** 71–108.

Chiron, S., Fernandez-alba, A., Rodriguez, A. and Garcia-calvo, E. (2000). Pesticide chemical oxidation: State-of-the-art. *Water Res*., **34(2):** 366–377.

Espulgas, S., Giménez, J., Contreras, S., Pascual, E. and Rogríguez, M. (2002). Comparison of different advanced oxidation processes for phenol degradation. *Wat. Res*., **36(4):** 1034–1042.

Evgenidou, E., Fytianos, K. and Poulios, I. (2005). Semiconductor-sensitized photodegradation of Dichlorvos in water using TiO_2 and ZnO as catalysts. *Appl. Catal. B-Environ.*, **59(1–2):** 81–89.

Evgenidou, E., Konstantinou, I., Fytianos, K. and Albanis, T. (2006). Study of the removal of Dichlorvos and dimethoate in a titanium dioxide mediated photocatalytic process through the examination of intermediates and the reaction mechanism. *J. Hazard. Mater.*, **137(2):** 1556–1564.

Faust, B. and Hoigne, J. (1990). Photolysis of Fe(III)-hydroxyl complexes as sources of OH radicals in clouds, fog and rain. *Atmos. Environ.*, **24(1):** 79–89.

Ghaly, M., Hartel, G., Mayer, R. and Haseneder, R. (2001). Photochemical oxidation of p-chlorophenol by UV/H_2O_2 and photo-Fenton process: A comparative study. *Waste Manage.*, **21(1):** 41–47.

Jiangtong, Y. (1981). Organic Chemistry and Biochemistry of Organophosphorus Pesticides. Chemical Industry Publisher, Beijing.

Klamerth, N., Malato, S., Agüera, A. and Fernández-Alba, A. (2013). Photo-Fenton and modified photo-Fenton at neutral pH for the treatment of emerging contaminants in wastewater treatment plant effluents: A comparison. *Water Research*, **47:** 833–840.

Leu, C., Singer, H., Stamm, C., Muller, S. and Schwarzenbach, R. (2004). Simultaneous assessment of sources, processes, and factors influencing herbicide losses to surface waters in a small agricultural catchment. *Environ Sci Technol.*, **38(14):** 3827–3834.

Lucas, M. and Peres, J. (2006). Decolorization of the azo dye reactive black 5 by Fenton and photo-Fenton oxidation. *Dyes Pigm.*, **71(3):** 236–244.

Malato, S., Blanco, J., Caceres, J., Fernández-Alba, A., Aguera, A. and Rodrıguez, A. (2002). Photocatalytic treatment of water-soluble pesticides by photo-Fenton and TiO_2 using solar energy. *Catal. Today.*, **76(2–4):** 209–220.

Maldonado, M., Passarinho, P., Oller, I., Gernjak, W., Fernandez, P., Blanco, J. and Malato, S. (2007). Photocatalytic degradation of EU priority substances: A comparison between TiO_2 and Fenton plus photo-Fenton in a solar pilot plant. *J. Photochem. Photobio. A: Chem.*, **185 (2–3):** 354–363.

Oller, I., Gernjak, W., Maldonado, M., Perez-Estrada, L., Sanchez-Perez, J. and Malato, S. (2006). Solar photocatalytic degradation of some hazardous water-soluble pesticides at pilot-plant scale. *J. Hazard. Mater.*, **138(3):** 507–517.

Ortega-Liébana, M.C., Sánchez-López, E., Hidalgo-Carrillo, J., Marinas, A., Marinas, J.M. and Urbano, F.J. (2012). A comparative study of photocatalytic degradation of 3-chloropyridine under UV and solar light by homogeneous (photo-Fenton) and heterogeneous (TiO_2) photocatalysis. *Applied Catalysis B: Environmental*, **127:** 316–322.

Perez-Estrada, L., Malato, S., Gernjak, W., Aguera, A., Thurman, E., Ferrer, I. and Fernandez-Alba, A. (2005). Photo- Fenton degradation of diclofenac: Identification of main intermediates and degradation pathway. *Environ. Sci. Technol.*, **39(21):** 8300–8306.

Rice, E., Baird, R., Eaton, A. and Clesceri, L. (Eds) (2005). Standard Methods for the Examination of Water and Wastewater. American Public Health Association, AWWA (American Water Works Association). Water Environment Federation, USA, 21st ed.

Rongxi, L., Chunping, Y., Hong, C., Guangming, Z., Guanlong, Y. and Junyuan, G. (2009). Removal of triazophos pesticide from wastewater with Fenton reagent. *J. Hazard Mater.*, **167(1–3):** 1028–1032.

Sakugawa, H., Hasan, N., Olasehinde, E., Takeda, K. and Kondo, H. (2013). Applicability of solar photo-Fenton process to the remediation of water polluted with pesticides. *Nat Sci.*, **11(1):** 144–152.

Tamimi, M., Qourzal, S., Barka, N., Assabbane, A. and Ait-Ichou, Y. (2008). Methomyl degradation in aqueous solutions by Fenton's reagent and the photo-Fenton system. *Sep. Purif. Technol.*, **61(1):** 103–108.

WHO (1978). Dichlorvos. Geneva, World Health Organization (Data Sheets on Pesticides No. 2, rev. 1).

WHO/FAO (1994). Dichlorvos. *In:* Pesticide residues in food: 1993 evaluations. Part II Toxicology. Food and Agriculture Organization of the United Nations and World Health Organization, Geneva (WHO/PCS/94.4; http://www.inchem.org/documents/jmpr/jmpmono/v93pr05.htm)

Chapter 3
Catalytic Reduction of Water Contaminant '4-Nitrophenol' over Manganese Oxide Supported Ni Nanoparticles

Pangkita Deka, Debajyoti Bhattacharjee, Pingal Sarmah, Ramesh C. Deka, and Pankaj Bharali

1 Introduction

Nitroaromatic compounds (NACs) are among the largest and most important groups of industrial chemicals in use nowadays (Ju and Parales 2010; Tomei et al. 2010). The NACs, such as nitrophenol, nitrobenzene, nitrotoluene, and nitrobenzoates, are of considerable industrial importance as the main raw materials in the manufacture of various dyes, pharmaceuticals, pesticides and explosives (Tomei et al. 2010; Yi et al. 2006; Aditya et al. 2015). 4-Nitrophenol (4-NP) is one of the most common and important NACs, both in terms of quantities used and potential environmental impacts (Yi et al. 2006; Podeh et al. 1995; Aditya et al. 2015; Sarkar et al. 2011). 4-NP is mainly used for the manufacture of drugs (e.g. acetaminophen) and pesticides (e.g. methyl and ethyl parathion) and is also used in leather treatment, in dyestuff production, and for military purposes. Because of its regular and extensive use, 4-NP can be found as a pollutant in industrial wastewater streams associated with its formulation, distribution and application (Yi et al. 2006; Pozun et al. 2013). Moreover, hydrolysis of pesticides and herbicides can also release 4-NP into the subsurface and then contaminate groundwater resources (Labana et al. 2005). As the 4-NP released into the environment, its contamination can cause a significant environmental and public health risk, due to its acute toxicity and mutagenic potential (Yi et al. 2006; Podeh et al. 1995; Labana et al. 2005; Aditya et al. 2015; Pozun et al. 2013). The acute exposing of 4-NP may lead to blood disorders along with methemoglobin formation, liver and kidney damage, anemia, skin and eye irritation, and systemic poisoning. In particular, it may cause deleterious effects to ecological systems, due to the 4-NP contamination of rivers and groundwater resources [Zieris et al. (1988), Aditya et al. (2015)].

P. Deka • D. Bhattacharjee • P. Sarmah • R.C. Deka • P. Bharali (✉)
Department of Chemical Sciences, Tezpur University, Tezpur 784 028, India
e-mail: pankajb@tezu.ernet.in

F. Kurisu et al. (eds.), *Trends in Asian Water Environmental Science and Technology*, DOI 10.1007/978-3-319-39259-2_3

Therefore, 4-NP containing industrial wastewater should be uncontaminated before being discharged into the environment.

Metal nanoparticles have been extensively investigated owing to their unique physical and chemical properties compared to bulk metals and their various potential applications in the field of catalysis [Saha et al. (2010), Mori et al. (2009), Zhang et al. (2011)]. They are used as catalysts in variety of organic and inorganic transformations [Shin et al. (2009)]. Metal nanoparticles are usually dispersed on solid oxide supports to prevent agglomeration, site isolation, good accessibility of substrate molecules, mechanical robustness and so on [Jin et al. (2012)]. Moreover, supported nanoparticles exhibits high catalytic activity and selectivity compared to unsupported ones mainly through synergistic interaction with the support [Jin et al. (2012)]. In particular, supported nickel nanoparticles on various carriers have been extensively studied as heterogeneous catalysts [Wu et al. (2012b), Basagiannis and Verykios (2006)]. Nickel-based catalyst, such as Ni/Al_2O_3 [Lu et al. (1998)], Ni/TiO_2 [Wu et al. (2012b)], NiO-MgO [Choudhary et al. (1997)], Ni/m-CN [(Yang et al. 2014)] and Ni/SiO_2 (Jiang et al. 2012) shows high activity and selectivity with low cost for various catalytic reactions. In practice, Ni-based catalysts are more promising than noble metal catalysts (Wang et al. 2004). It is well known that nickel is an active and facile catalyst in hydrogenation/reduction reaction (Lu et al. 2008). 4-NP is among the most common organic pollutants in industrial and agricultural waste waters, but the 4-aminophenol (4-AP) is an important intermediate for the manufacture of analgesic and antipyretic drugs (Esumi et al. 2004; Wu et al. 2012a; Jin et al. 2012; Li et al. 2010). The nickel catalysts have been widely used in the hydrogenation of 4-NP to 4-AP (Chen et al. 2003; Du et al. 2004; Yang et al. 2014; Jiang et al. 2012). Chen et al. found that the unsupported nickel nanoparticle catalyst yields good hydrogenation activity and selectivity, but sintering of nickel nanoparticle occurs after hydrogenation.

Herein, a Ni/Mn_2O_3 catalyst, with small Ni-nanoparticles over Mn_2O_3 support, is reported for catalytic conversion of 4-NP to 4-AP efficiently at room temperature. The catalytic progress is monitored with the help of UV-visible spectrophotometric method. The UV-visible data obtained from our experiment are further supported by computational studies. In recent years, density functional theory (DFT) calculations have proved highly successful at predicting the structures and electronic properties. In addition, time-dependent DFT (TDDFT) calculations are also useful to determine the nature of the excited states of complexes and provide a better understanding of observed electronic absorption spectra.

2 Materials and Methods

2.1 Materials

Manganese chloride ($MnCl_2$ $4H_2O$) and sodium borohydrate ($NaBH_4$) were purchased from SRL chemicals. Nickel chloride hexahydrate ($NiCl_2$ $6H_2O$) and Cetyltrimethylammonium bromide (CTAB) were purchased from Rankem. 4-NP, NaOH and HPLC grade ethylene glycol were purchased from Merck, and distilled water was used throughout the whole experiment. All the reagents were used as received without further purification.

2.2 Synthesis

In the first step, 3.958 g of $MnCl_2 \times 4H_2O$ and 0.8 g of NaOH were dissolved in 40 mL of 1:1 ethylene glycol:distilled water (volume/volume) separately to form homogeneous solutions, respectively. The NaOH solution was then added dropwise to the manganese chloride solution with stirring. The mixture was then transferred to a 150 mL teflon-liner autoclave, which was sealed and heated at 120 °C for 6 h. After the autoclave was cooled to room temperature, the resulting brown precipitate was separated by centrifugation, washed three times with distilled water respectively, and dried in oven at 45 °C overnight. The dried product was then calcined at 500 °C for 3.5 h in air atmosphere. The final black powders were then obtained as manganese oxide. In the second step, to a suspension of manganese oxide particles (0.25 g) dispersed in distilled water (50 mL), a solution of $NiCl_2 \times 6H_2O$ (0.028 g, 0.118 mmol) and CTAB (0.041 g, 0.112 mmol), obtained by subsequent sonication and stirring for 30 min, was added dropwise in 1.5 mL aqueous solution of $NaBH_4$ (0.020 g, 0.526 mmol). The contents of the flask was vigorously shaken for 10 min, resulting in the generation of manganese oxide supported Ni nanocatalyst as a black suspension, which was collected by centrifugation and dried under vacuum at 45 °C for 24 h.

2.3 Characterizations

The TGA curve was obtained on a Thermal Analyzer (Model TGA-50, Shimadzu) instrument. The powder X-ray diffraction (XRD) patterns were recorded on a Rigaku Multiflex instrument using nickel-filtered CuKα (0.15418 nm) radiation source and a scintillation counter detector. Infra-red spectra were measured in a FTIR spectrophotometer, Model Nicolet Impact I-410. Measurements are performed by pelletizing the samples with KBr in the mid-infrared region. The BET surface areas were determined by N_2 adsorption using a Quantachrome

Instruments (Model: NOVA 1000e). The pore size and pore volume is determined following Barrett-Joyner-Halenda (BJH) method in the same instrument. To study the surface topography, SEM analyses were carried out with "JEOL, JSM Model 6390 LV" Scanning Electron Microscopes, operating at an accelerating voltage of 15 kV. The transmission electron microscopic investigations were carried on a JEM-2010 (JEOL) instrument equipped with a slow-scan CCD camera and at an accelerating voltage of 200 kV. In the present work, UV-visible spectra were recorded on a UV-visible spectrophotometer, Shimadzu Corporation (UV-2550).

2.4 Catalytic Reduction

To a 25 mL solution of 0.10 mmol/L 4-NP, 25 mL of freshly prepared solution of $NaBH_4$ was added which corresponds to a colour change of light yellow to yellow-green. Then to this mixture desired amount of catalyst was added, the colour of the solution faded as the reaction proceeded. Solution mixture was stirred during the reaction and the upper solution was transferred to a quartz cuvette for the measurement of UV-visible spectra. Once a spectrum was recorded, the solution was immediately transferred back to the previous reactor and stirred for another few seconds for the sequential catalytic reaction. UV-visible spectra were recorded at short intervals to monitor the progress of the reaction. This procedure was repeated during the UV-visible measurement. Blank experiments were also carried out to show that the reactions do not proceed without catalysts only in the presence of $NaBH_4$. Concentration of $NaBH_4$ and amount of catalyst were varied during the reaction.

2.5 Computational Methods

In the framework of DFT, we employed the hybrid B3LYP functional [Becke (1988), Lee et al. (1988)] to explore the stationary points on the potential energy surface. The carbon, nitrogen, hydrogen and oxygen atoms are treated with 6–311 + G(d) basis set. To study the optical properties, TDDFT approach has been used at the optimized geometries of the studied complexes both in gas phase and using water as solvent. The Polarisable Continuum Model (PCM) (Miertus et al. 1981) was applied for all gas-phase-optimized structures to study the effect of solvent (water). All the calculations are carried out using Gaussian09 program (Frisch et al. 2009).

3 Results and Discussion

Figure 3.1 represents the XRD profiles of the synthesized support and catalyst. The diffraction peaks of the support were observed at $2\theta = 23.1$, 32.9, 38.1, 43.6, 49.2, 55.1, 60.6 and 65.7° which could be assigned to (211), (222), (400), (420), (134), (440), (611) and (622) reflections, respectively (Fig. 3.1a). These reflections could be assigned to α-Mn_2O_3 having a cubic *bixbyite* structure (JCPDS card no. 89–4836), which is in good accordance with the literature values (Cao et al. 2009). Again for the catalyst the XRD pattern is shown in Fig. 3.1b. Along with cubic α-Mn_2O_3 peaks two small peaks at $2\theta = 45.0$ and 58.9° which could be indexed to (101) and (102) reflections of hexagonal primitive Ni (JCPDS card no. 89–7129). The intensity of the two peaks is very less; this may be due to presence of small amount of Ni over the α-Mn_2O_3.

The FTIR spectra for manganese oxide and Ni/α-Mn_2O_3 are depicted in Fig. 3.2a. The bands at near mid-infrared from 550 to 800 cm^{-1} in both the two spectra may be attributed to Mn-O bending vibration, asymmetric stretching bridge oxygen species (Mn-O-Mn), and symmetric stretching of Mn-O of α-Mn_2O_3 group, respectively [Cao et al. (2009)]. Elemental analysis was performed by energy dispersive X-ray spectroscopy (EDX) for the catalyst which indicates the presence of Ni with Mn and O signals devoid of any other metal and impurity (Fig. 3.2b). The EDX measurement also confirms the atomic percentage of elements present in the final product (inset of Fig. 3.2b). From the figure it is observed that Ni loading is almost 3 wt% over the α-Mn_2O_3.

Figure 3.3a shows the SEM micrographs of the α-Mn_2O_3. It is observed that the oxide particles exhibit icosahedrons-like structure with *ca.* 2–4 μm diameter in size. Further, the Ni/α-Mn_2O_3 catalyst was characterized by TEM and corresponding images are presented in Fig. 3.3b. TEM analyses demarcate that the synthesized Ni/α-Mn_2O_3 nanostructures possess sheet-like structure as presented in Fig. 3.3b. As observed from the figure the darker region correspond to α-Mn_2O_3 support, over which lighter regions correspond to Ni nanoparticles. Highly dispersed Ni nanoparticles of size 2–3 nm over the bigger α-Mn_2O_3 support are clearly visible as shown in Fig. 3.3b. The size distribution of Ni nanoparticles (inset of Fig. 3.3b) showed that most of the Ni particles fall in the size range 2–3 nm and the mean particle diameter was about 2.6 nm. N_2 adsorption–desorption (by BET method) analysis of the α-Mn_2O_3 and Ni/α-Mn_2O_3 showed type-IV isotherm with combination of H1 and H3 hysteresis loop, which is a characteristic of mesoporous material (Fig. 3.3c, d). The surface area and pore volume values are 5.62 m^2/g, 168.83 m^2/g and 0.005 cm^3/g, 0.294 cm^3/g, respectively for the α-Mn_2O_3 and Ni/α-Mn_2O_3 (An et al. 2014). The pore-size distribution curves calculated from the BJH method indicated the presence of mesoporosity in the samples, even though they support the presence of regularly ordered pores (inset in Fig. 3.3c, d). A maximum pore distribution was observed at around 30–50 Å for the α-Mn_2O_3 and 40 Å for the Ni/α-Mn_2O_3, which confirms the mesoporosity of the samples.

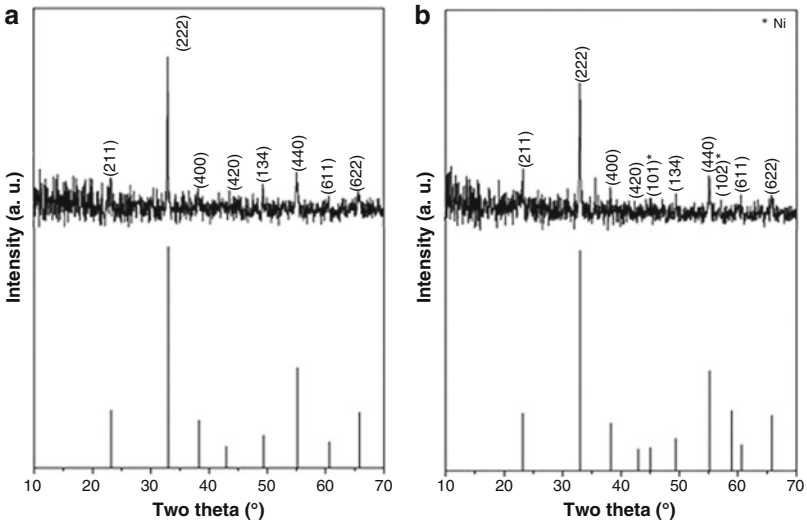

Fig. 3.1 X-ray powder diffraction patterns of α-Mn_2O_3 (**a**) and Ni/α-Mn_2O_3 (**b**)

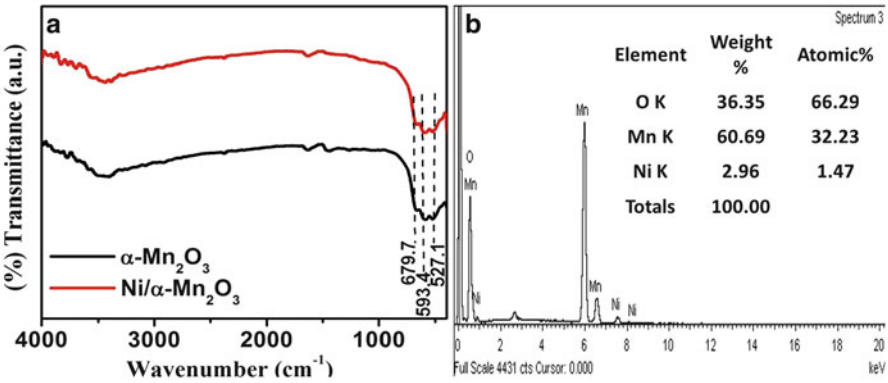

Fig. 3.2 FT-infrared spectra of α-Mn_2O_3 and Ni/α-Mn_2O_3 (**a**) and energy dispersive X-ray analysis pattern of Ni/α-Mn_2O_3 (**b**)

The catalytic activity of as-prepared α-Mn_2O_3 supported Ni nanoparticles was evaluated for the reduction of 4-NP in presence of $NaBH_4$ as mild reducing agent by the spectrophotometric studies (Fig. 3.4a, c, e). The successive decrease of the peak at 400 nm and increase of the peak at 298 nm with time indicates the catalytic reduction of 4-NP to 4-AP. The UV–vis spectra also exhibit the isosbestic points nm, which are evidently found at near 250, 270 and 325 which indicates that 4-AP is the only product of the reaction (Saha et al. 2010). Because the peak at 400 nm was much stronger than that at 298 nm, the kinetics of the reduction reaction was studied by measuring the absorbance at 400 nm as a function of time. As the concentration of $NaBH_4$ is in great excess in the reactions a pseudo-first-order

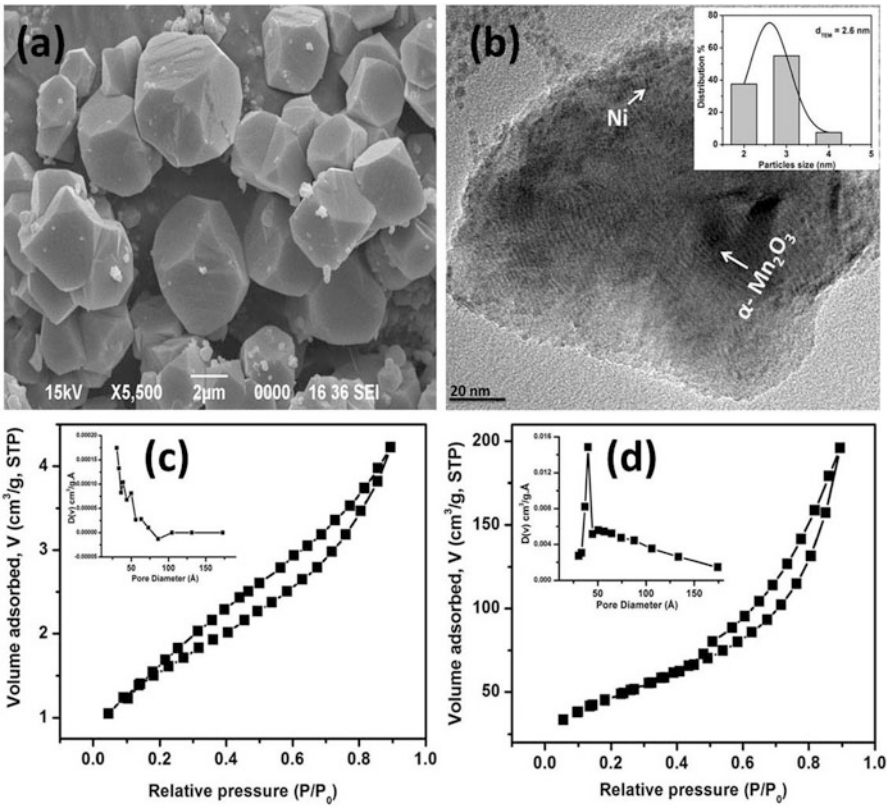

Fig. 3.3 SEM image of α-Mn_2O_3 (**a**); TEM image of Ni/α-Mn_2O_3 (inset particles size distribution of the Ni nanoparticles) (**b**); Nitrogen sorption isotherms of α-Mn_2O_3 and Ni/α-Mn_2O_3 (the insets shows pore size distribution of the respective samples) (**c**) and (**d**), respectively

kinetics can be applied with respect to concentration of 4-nitrophenolate ion. The plots of $\ln(A_t/A_0)$ against the reaction time are presented in Fig. 3.4b, d, f. The A_0 and A_t in the plot of $\ln(A_t/A_0)$ against reaction time are the absorbances of 4-nitrophenolate ion at time 0 and t, respectively. The linear fit with a coefficient of determination for the plots $\ln(A_t/A_0)$ against the reaction time very close to unity supports the assumption of pseudo-first-order kinetics.

During the course of the reaction, concentration of $NaBH_4$ has been varied to study the effect of concentration of $NaBH_4$ on the rate of the reaction (Table 3.1). From the table it is observed that the rate of the reduction reaction increases as the concentration of $NaBH_4$ increases. Also the time taken for the completion of reaction decreases as the concentration of $NaBH_4$ is increased. Besides this, according to literature (Saha et al. 2010) the concentration of $NaBH_4$ has no effect on further increasing its concentration. Therefore we took 60 mmol/L as the optimum concentration for the reduction reaction and in further studies such as recyclability test, effect of catalyst dosage are carried out by keeping the concentration of $NaBH_4$ as 60 mmol/L.

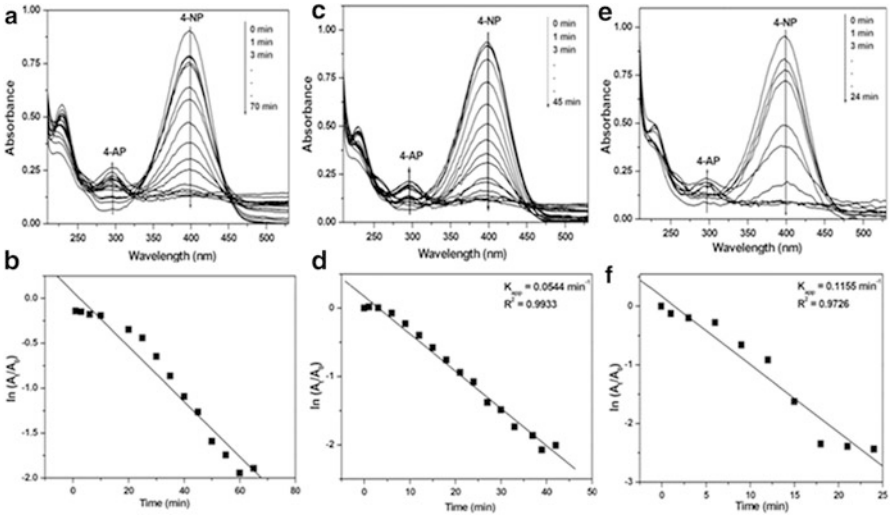

Fig. 3.4 Time-dependent UV-vis absorption spectra and plots of $\ln(A_t/A_0)$ versus time in presence of 20 mmol/L (**a**, **b**), 40 mmol/L (**c**, **d**) and 60 mmol/L (**e**, **f**) $NaBH_4$, respectively, for the reduction of 4-nitrophenol over 0.020 g Ni/α-Mn_2O_3 catalyst in aqueous media at 25 °C

Table 3.1 Reduction of 4-NP over 0.020 g Ni/α-Mn_2O_3 catalyst

Sl. No.	Conc. of $NaBH_4$ (mmol/L)	Time (min)	k_{app} (min^{-1})	R^2
1	20	70	0.0306	0.9785
2	40	45	0.0548	0.9933
3	60	24	0.1155	0.9726

The recyclability of the catalyst carried out in presence of 0.020 g of catalyst at 60 mmol/L concentration of $NaBH_4$ for four successive cycles are presented in Fig. 3.5.

In the figure it shows that for the first two cycles, reduction is completed within 40 min whereas for fourth cycle it took 80 min. The main reason for decrease in such catalytic activity may be due to the loss of catalyst during separation [Deka et al. (2014)].

The influence of catalyst dosage is studied with the 60 mmol/L concentration of $NaBH_4$. Table 3.2 presents the time of the catalytic reaction, apparent rate constant and R^2 value for different amounts of catalyst at 60 mmol/L $NaBH_4$.

It is observed from the table that the reaction proceeds faster with increasing amount of catalyst. But after reaching certain amount of the catalyst the reaction time almost does not affect the catalyst dose. It is evident from the table that ca. 0.020 g is optimum dose for complete reduction of 4-NP.

For better presentation we have compared the present work with some earlier reports and highlighted in Table 3.3. From the table it is observed that the present catalyst shows superior activity compared to the other Ni-based catalysts. The

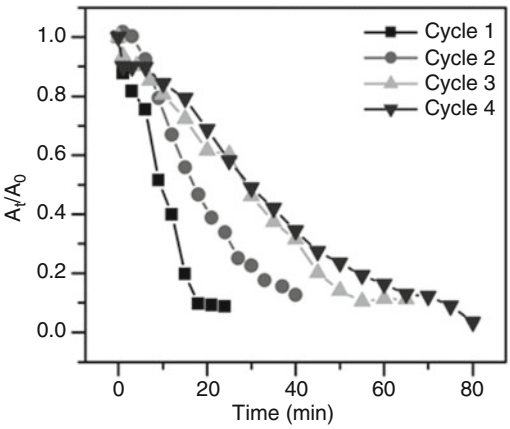

Fig. 3.5 A_t/A_0 against the reaction time over Ni/α-Mn_2O_3 for four successive cycles. Reaction condition: [$NaBH_4$] = 60 mmol/L and catalyst amount = 0.020 g

Table 3.2 Effect of catalyst dosages on the reaction time and apparent rate constants

Sl. No.	Amount of catalyst (g)	Time (min)	k_{app} (min^{-1})	R^2
1	0.010	42	0.0789	0.9776
2	0.015	39	0.0800	0.9796
3	0.020	24	0.1155	0.9726
4	0.025	25	0.1297	0.9631

Conditions: [$NaBH_4$] = 60 mmol/L and [4-NP] = 0.10 mmol/L

synergetic effect between the support and Ni may be the reason for better activity of the catalyst than the results reported earlier.

3.1 Computational Studies

The various optical properties obtained from the TDDFT level are listed in Table 3.4. From the table, it is clear that the wavelengths for the dominant peaks in both the experimental and theoretical results of our study are in close agreement with each other.

For 4-NP, we obtained two peaks in the TDDFT spectra. The dominant peak with larger oscillator strength (absorption) is observed around 317 nm in water. This is associated with the 36^{th} electronic state which is the HOMO for the molecule. Thus the peak is due to the transition from HOMO to LUMO which is a π- π* type transition with excitation energy 3.86 eV. The peak around 242 nm is found to be due to HOMO-LUMO + 1 transition. In case of 4-AP, a sharp peak is observed around 300 nm, which is also due to the transition of HOMO to LUMO and is a π- π* type transition. The other peak obtained around 242 nm is characterized by HOMO to LUMO + 3 transitions. Finally we have observed the spectra for 4-nitrophenolate ion, where a sharp peak appears around 373 nm as a result of

Table 3.3 Comparison of rate constant values for 4-NP reduction using Ni-based catalysts

Sl. No.	Catalyst	[4-NP] mmol/L	[$NaBH_4$] mmol/L	Rate constant, k_{app} (min^{-1})	Ref.
1	Ni/α-Mn_2O_3	0.1	60	0.1297	Present work
2	$NiCo_2$	0.1	60	0.0730	Wu et al. (2011)
3	Ni/SiO_2	0.1	200	0.0680	Jiang et al. (2012)
4	$FeNi_2$	0.1	60	0.0570	Wu et al. (2012a, b)

Table 3.4 Maximum absorption wavelength λ, oscillator strengths *f* and excitation energies *E* for three different complexes at TDDFT/B3LYP level

	Wavelength, λ (nm)			Oscillator strength, f		Excitation energy, E (in eV)	
Complex	Gas phase	Water	Exp.	Gas phase	Water	Gas phase	Water
4-NP	293	321	317	0.26	0.35	4.24	3.86
	228	231	225	0.05	0.06	5.41	5.36
4-AP	294	300	300	0.06	0.07	4.27	4.12
	238	242	228	0.16	0.21	5.20	5.11
4-nitrophenolate	356	373	400	0.47	0.58	3.48	3.32
	279	271	–	0.03	0.05	4.44	4.56

HOMO-LUMO transition. The ion shows a sharp peak around 271 nm in contrast to a broad peak in gas phase study at around 279 nm. The peak is a result of HOMO to LUMO + 1 transition with excitation energy 4.56 eV. Finally we plot all the UV-visible spectra in both the phases as shown in Fig. 3.6. These computational spectra provide strong evidence in support of our experimental spectral results.

4 Conclusions

In summary, a general strategy of reduction of 4-nitrophenol from industrial wastewater using as-synthesized α-Mn_2O_3 supported nickel nanoparticles catalyst is reported. The as-synthesized support and catalyst are characterized by XRD, FTIR, SEM-EDX, TEM and BET surface area analyses techniques. The Ni particles are found to be distributed over α-Mn_2O_3 surface with spherical shape in nature. The catalytic activity of the synthesized Ni/α-Mn_2O_3 were evaluated for the reduction of 4-NP in presence of $NaBH_4$. The reduction was found to be very efficient and followed pseudo first-order kinetics. The catalyst efficiency of Ni particles was determined on the basis of recyclability. The result indicates that the Ni nanoparticles catalyze the reduction very efficiently with a good recyclability upto fourth cycle at room temperature. It also indicates that these spherical Ni

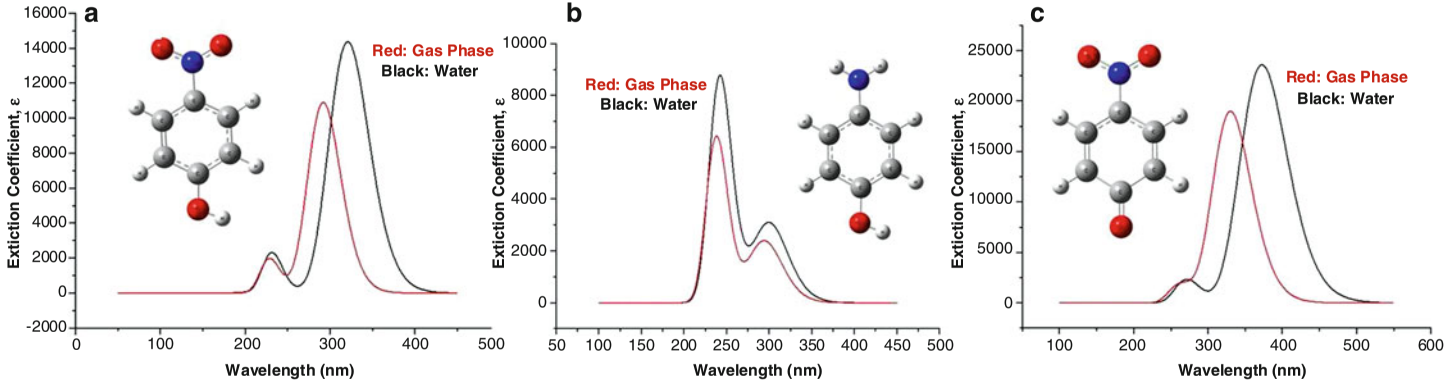

Fig. 3.6 The UV-visible spectra and optimized structures for (**a**) 4-NP, (**b**) 4-AP and (**c**) 4-nitrophenolate ion

nanoparticles can be effectively used as an attractive alternative to various noble metal catalyst for the reduction of 4-nitrophenol. Experimental results are well supported by TDDFT studies. Further works are under active process to check the selectivity of the synthesized catalyst by using real industrial wastewater and also to know the detailed mechanism of the reduction reaction. Our investigation of the synthesis of nickel nanoparticle for the catalytic reduction is highly efficient, low cost and thus has potential application for the chemical and pharmaceutical industry.

Acknowledgement This work was supported by the Tezpur University as research grant to PB. DB thanks CSIR, New Delhi for senior research fellowship. Authors also acknowledge the financial support from Department of Science and Technology, New Delhi. SAIF, North-Eastern Hill University, India and SAIC, Tezpur University, India are acknowledged for analytical supports.

References

Aditya, T., Pal, A. and Pal, T. (2015). Nitroarene reduction: A trusted model reaction to test nanoparticle catalysts. *Chem. Commun*., **51(46):** 9410–9431.

An, M., Cui, J. and Wang, L. (2014). Magnetic Recyclable Nanocomposite Catalysts with Good Dispersibility and High Catalytic Activity. *J. Phys. Chem. C*, **118(6):** 3062–3068.

Basagiannis, A.C. and Verykios, X.E. (2006). Reforming reactions of acetic acid on nickel catalysts over a wide temperature range. *Appl. Catal. A: Gen*, **308**: 182–193.

Becke, A.D. (1988). Density-functional exchange-energy approximation with correct asymptotic behaviour. *Phys. Rev. A*, **38(6):** 3098–3100.

Cao, J., Zhu, Y., Bao, K., Shi, L., Liu, S. and Qian, Y. (2009). Microscale Mn_2O_3 Hollow Structures: Sphere, Cube, Ellipsoid, Dumbbell, and Their Phenol Adsorption Properties. *J. Phys. Chem. C*, **113(41):** 17755–17760.

Chen, R.Z., Du, Y., Chen, C.L., Xing, W.H., Xu, N.P., Chen, C.X. and Zhang, Z.L. (2003). Comparative study on catalytic activity and stability of nano-sized nickel and raney nickel. *J. Chem. Ind. Eng. (China)*, **54(5):** 704–706.

Choudhary, V.R., Uphade, B.S. and Mamman, A.S. (1997). Oxidative Conversion of Methane to Syn gas over Nickel Supported on Commercial Low Surface Area Porous Catalyst Carriers Precoated with Alkaline and Rare Earth Oxides. *J. Catal*., **172(2):** 281–293.

Deka, P., Deka, R.C. and Bharali, P. (2014). In-situ generated copper nanoparticle catalyzed reduction of 4-nitrophenol. *New J. Chem*., **38:** 1789–1793.

Du, Y., Chen, H.L., Chen, R.Z. and Xu, N.P. (2004). Synthesis of *p*-aminophenol from *p*-nitrophenol over nano-sized nickel catalysts. *Appl. Catal. A: Gen*, **277(1–2):** 259–264.

Esumi, K., Isono, R. and Yoshimura, T. (2004). Preparation of PAMAM- and PPI-Metal (Silver, Platinum, and Palladium) Nanocomposites and Their Catalytic Activities for Reduction of 4-Nitrophenol. *Langmuir*, **20(1):** 237–243.

Frisch, M.J. et al. (2009). Gaussian 09: Revision B. 01. Gaussian, Pittsburgh, PA.

Jiang, Z., Xie, J., Jiang, D., Jing, J. and Qin, H. (2012). Facile Route Fabrication of Nano-Ni Core Mesoporous-Silica Shell Particles with High Catalytic Activity towards 4-Nitrophenol Reduction. *Cryst. Eng. Comm*., **14:** 4601–4611.

Jin, Z., Xiao, M., Bao, Z., Wang, P. and Wang, J. (2012). A General Approach to Mesoporous Metal Oxide Microspheres Loaded with Noble Metal Nanoparticles. *Angew. Chem. Int. Ed*., **51 (26):** 6406–6410.

Ju, K.S. and Parales, R.E. (2010). Nitroaromatic Compounds, from Synthesis to Biodegradation. *Microbiol. Mol. Biol. Rev.*, **74(2):** 250–272.

Labana, S., Pandey, G., Paul, D., Sharma, N.K., Basu, A. and Jain, R.K. (2005). Pot and Field Studies on Bioremediation of *p*-Nitrophenol Contaminated Soil Using *Arthrobacterprotophormiae* RKJ100. *Environ. Sci. Technol.*, **39(9):** 3330–3337.

Lee, C.,Yang, W. and Parr, R.G. (1988). Development of the Colle-Salvetti correlation energy formula into a functional of the electron density. *Phys. Rev. B*, **37(2):** 785–789.

Li, H., Jo, J.K., Zhang, L., Ha, C.-S., Suh, H. and Kim, I. (2010). A General and Efficient Route to Fabricate CarbonNanotube-Metal Nanoparticles and Carbon Nanotube-Inorganic Oxides Hybrids. *Adv. Funct. Mater.*, **20:** 3864–3873.

Lu, H., Yin, H., Liu, Y., Jiang, T. and Yu, L. (2008). Influence of support on catalytic activity of Ni catalysts in *p*-nitrophenol hydrogenation to *p*-aminophenol. *Catal. Commun.*, **10(3):** 313–316.

Lu, Y., Xue, J., Yu, C., Liu, Y. and Shen, S. (1998). Mechanistic investigations on the partial oxidation of methane to synthesis gas over a nickel-on-alumina catalyst. *Appl. Catal. A: Gen*, **174(1–2):** 121–128.

Miertus, S., Scrocco, E. and Tomasi, J. (1981). Electrostatic interaction of a solute with a continuum. A direct utilization of ab initio molecular potentials for the prevision of solvent effects. *Chem. Phys.*, **55(1):** 117–129.

Mori, K., Kumami, A., Tomonari, M. and Yamashita, H. (2009). A pH-Induced Size Controlled Deposition of Colloidal Ag Nanoparticles on Alumina Support for Catalytic Application. *J. Phys. Chem. C*, **113(39):** 16850–16854.

Podeh, M.R.H., Bhattacharya, S.K. and Qu, M. (1995). Effects of nitrophenols on acetate utilizing methanogenic systems. *Water Res.*, **29(2):** 391–399.

Pozun, Z.D., Rodenbusch, S.E., Keller, E., Tran, K., Tang, W., Stevenson, K.J. and Henkelman, G. (2013). A Systematic Investigation of *p*-Nitrophenol Reduction by Bimetallic Dendrimer Encapsulated Nanoparticles. *J. Phys. Chem. C*, **117:** 7598–7604.

Sarkar, S., Sinha, A.K., Pradhan, M., Basu, M., Negishi, Y. and Pal, T. (2011). Redox Transmetalation of Prickly Nickel Nanowires for Morphology Controlled Hierarchical Synthesis of Nickel/Gold Nanostructures for Enhanced Catalytic Activity and SERS Responsive Functional Material. *J. Phys. Chem. C*, **115:** 1659–1673.

Saha, S., Pal, A., Kundu, S., Basu, S. and Pal, T. (2010). Photochemical Green Synthesis of Calcium-Alginate-Stabilized Ag and Au Nanoparticles and Their Catalytic Application to 4-Nitrophenol Reduction. *Langmuir*, **26(4):** 2885–2893.

Shin, K.S., Choi, J.Y., Park, C.S., Jang, H.J. and Kim, K. (2009). Facile Synthesis and Catalytic Application of Silver-Deposited Magnetic Nanoparticles. *Catal. Lett.*, **133(1–2):** 1–7.

Tomei, M.C., Annesini, M.C., Rita, S. and Daugulis, A.J. (2010). Two-Phase Partitioning Bioreactors Operating with Polymers Applied to the Removal of Substituted Phenols. *Environ. Sci. Technol.*, **44(19):** 7254–7259.

Wang, J.G., Liu, C.J., Zhang, Y.P., Yu, K.L., Zhu, X.L. and He, F. (2004). Partial oxidation of methane to syngas over glow discharge plasma treated Ni–Fe/Al_2O_3 catalyst. *Catal. Today*, **89 (1–2):** 183–191.

Wu, K.-L., Wei, X.-W., Zhou, X.-M., Wu, D.-H., Liu, X.-W., Ye, Y. and Wang, Q. (2011). $NiCo_2$ Alloys: Controllable Synthesis, Magnetic Properties, and Catalytic Applications in Reduction of 4-Nitrophenol. *J. Phys. Chem. C*, **115:** 16268–16274.

Wu, K.-L., Yu, R. and Wei, X.-W. (2012a). Monodispersed $FeNi_2$ Alloy Nanostructures: Solvothermal Synthesis, Magnetic Properties and Size-Dependent Catalytic Activity. *Cryst. Eng. Comm.*, **14:** 7626–7632.

Wu, Z., Chen, J., Di, Q. and Zhang, M. (2012b). Size-controlled synthesis of a supported Ni nanoparticle catalyst for selective hydrogenation of *p*-nitrophenol to *p*-aminophenol. *Catal. Commun.*, **18:** 55–59.

Yang, Y., Ren, Y., Sun, C. and Hao, S. (2014). Facile Route Fabrication of Nickel based Mesoporous Carbons with High Catalytic Performance towards 4-Nitrophenol Reduction. *Green Chem.*, **16:** 2273–2280.

Yi, S., Zhuang, W.Q., Wu, B., Tay, S.T.L. and Tay, J.H. (2006). Biodegradation of *p*-Nitrophenol by Aerobic Granules in a Sequencing Batch Reactor. *Environ. Sci. Technol*., **40(7):** 2396–2401.

Zhang, Z., Shao, C., Zou, P., Zhang, P., Zhang, M., Mu, J., Guo, Z., Li, X., Wang, C. and Liu, Y. (2011). In situ assembly of well-dispersed gold nanoparticles on electrospun silica nanotubes for catalytic reduction of 4-nitrophenol. *Chem. Commun*., **47:** 3906–3908.

Zieris, F.J., Feind, D. and Huber, W. (1988). Long-term effects of 4-nitrophenol in an outdoor synthetic aquatic ecosystem. *Arch. Environ. Contam. Toxicol*., **17(2):** 165–175.

Chapter 4
Simulation of Nitrate Removal in a Batch Flow Electrocoagulation-Flotation (ECF) Process by Response Surface Method (RSM)

E. Nazlabadi and M.R. Alavi Moghaddam

1 Introduction

Electrocoagulation-flotation (ECF) is one of the newest treatment methods, which has been used successfully to remove different kinds of pollutants (Behbahani et al. 2013). ECF is a process which consists of three main parts: (1) Creating metallic hydroxide flocs within the solution by electro-dissolution of soluble anodes, (2) Formation of coagulants in aqueous phase, and (3) Adsorption of pollutants on coagulants and then removal by sedimentation/flotation (Arroyo et al. 2009; Zaroual et al. 2009).

Nitrate is a stable and highly soluble ion with low potential for co-precipitation or adsorption (El-Shazly et al. 2011). Nitrate concentration is naturally a few milligrams in litre for groundwater, but different factors like inappropriate sewage treatment/disposal, unsuitable agricultural/stockbreeding activities, and the geological structures of each region, makes this concentration to grow up. High levels of nitrate can cause severe health problems (Moghaddasi et al. 2008; Azadegan et al. 2012; Nazlabadi and Alavi Moghaddam 2014). Conventional methods of removing nitrate include biological decomposition, ion exchange, chemical treatment, reverse osmosis and membrane separation techniques (El-Shazly et al. 2011; Lakshmi et al. 2012).

In recent years, ECF as a chemical treatment method has been focused on by a large number of researchers for removal of nitrate due to its high treatment efficiency, low sludge production, easy operation and relatively low capital cost. In particular, electrocoagulation has demonstrated an attractive alternative to the other traditional methods for treating nitrate contaminated water (Li et al. 2009;

E. Nazlabadi • M.R.A. Moghaddam (✉)
Civil and Environmental Engineering Department, Amirkabir University of Technology (AUT), Hafez St., Tehran 15875-4413, Iran
e-mail: alavim@yahoo.com

F. Kurisu et al. (eds.), *Trends in Asian Water Environmental Science and Technology*, DOI 10.1007/978-3-319-39259-2_4

Emamjomeh and Sivakumar 2009; Kumar and Goel 2010; Kasiri and Khataee 2011; Lakshmi et al. 2012). However, the process is limited in practice due to formation of by-products like nitrite during treatment (Lakshmi et al. 2012; Nazlabadi and Alavi Moghaddam 2014).

The efficiency of ECF process is influenced by various factors such as initial pH, initial nitrate concentration, applied current, number of electrodes and reaction time. Simulation of these factors can be useful in order to achieve better nitrate removal efficiency. As it is well known, some limitations of classical study methods such as time consuming and high cost can be eliminated by statistical experimental design such as response surface methodology (RSM) (Zodi et al. 2010; Behbahani et al. 2013). RSM is only applicable for variables such as initial pH which is defined by a range of numbers and this technique is not useful for parameters like electrode material that are not numerical. Many research groups applied this method for removal of different pollutants by ECF (Aleboyeh et al. 2008; Krishna Prasad et al. 2008; Chavalparit and Ongwandee 2009; Sadri Moghaddam et al. 2010; Behbahani et al. 2011; Behbahani et al. 2013; Taheri et al. 2013; Radaei et al. 2014). However, to the best of our knowledge, RSM rarely has been used for nitrate removal (Koporal and Ogutveren 2002; Emamjomeh and Sivakumar 2009; Kumar and Goel 2010; Vasudevan et al. 2010; El-Shazly et al. 2011; Lacasa et al. 2011; Malakootian et al. 2011; Lakshmi et al. 2012; Sim et al. 2012).

The main objective of the present study is to simulate nitrate removal efficiency and remained nitrite as responses using an ECF unit operating in batch regime. For simulating this process, the relation between the responses and five quantitative variables (initial pH, initial nitrate concentration, reaction time, number of electrodes, applied current) is determined by a second order polynomial model.

2 Materials and Methods

2.1 ECF Reactor

A batch flow ECF reactor was made in the lab from Plexiglas with dimensions of 50 cm × 10 cm × 9 cm. Aluminum plate electrodes with the effective area of 42 cm^2 and thickness of 1 mm were used in this research. Inter-electrode distance was maintained at 10 mm and electrodes were connected to a DC power supply (Micro, PW4053R, 0–5 A, 0–40 V) in bipolar mode. Two hotplate magnetic stirrers (Labtech Hotplate Stirrer, LMS-1003, Korea) was applied for preparing complete mixed solutions in the EC reactor. The EC reactor used in this study is shown in Fig. 4.1.

Fig. 4.1 Photograph of the ECF's set-up

2.2 Experimental Procedure

Coagulation, flocculation, settling and flotation were taking place within the ECF reactor. All the experiments were carried out at room temperature. Nitrate solutions were prepared synthetically by dissolving proper amounts of $NaNO_3$ (Merck, solubility 874 g/l) in the range of 300–500 mg/lit and Na_2SO_4 (Merck, 99 %) as supporting electrolyte in 3.7 L of distilled water. The amounts of Na_2SO_4 added in each experiment are depending on the applied currents. The initial pH of the solution was adjusted before the experiment by H_2SO_4 and NaOH, and pH values were measured using pH meter (340i, WTW, Germany). All effluent samples for nitrate and some of them for nitrite were analyzed using a UV–vis spectrophotometer (DR/4000, HACH, USA) by method of 8039 (nitrate) and 8507 (nitrite). Percentage of nitrate removal was calculated by Eq. (4.1):

$$\text{Nitrate removal efficiency } (\%) = (C_r - C_t) \times 100/C_r \tag{4.1}$$

where C_r and C_t are the nitrate concentration in raw and treated solutions, respectively.

2.3 Experimental Design and Data Analysis

RSM is a well-known up-to-date approach for developing approximation models based on either physical experiments or computer experiments (simulations) with minimum number of experiments, as well as analyzing the interactions between selected parameters (Hameed et al. 2009; Raissi and Eslami Farsani 2009). The most widely used class of second-order designs called central composite design (CCD) was applied for the RSM (Nazlabadi and Alavi Moghaddam 2014). In the

present study, the CCD was selected for experimental design of the removal efficiency of nitrate and remained nitrite. Five factors, including initial pH, initial nitrate concentration, current, electrode number and reaction time with five-levels were employed for response surface modelling in the ECF process. A total of 57 experiments were carried out according to a 2^5 full factorial CCD, consisting of 32 factorial experiments, 10 axial experiments on the axis at a distance of $\pm\alpha$ from the centre, and 15 replicates at the centre of the experimental domain. The value of α for rotatability depends on the number of points in the factorial portion of the design, which is given in Eq. (4.2):

$$\alpha = (N_F)^{\frac{1}{4}} \tag{4.2}$$

where N_F is the number of points in the cube portion of the design ($N_F = 2^k$, k is the number of factors) (Behbahani et al. 2011). Therefore, α is equal to $(2^5)^{1/4} = 2.4$ according to Eq. (4.2).

The statistical software "Minitab", version 16.1.0 was also used for CCD and developing a simulation model. Several experiments were initiated as a preliminary study for determining the range of parameters prior to designing the experimental runs. Five-level factors were used to build models as shown in Table 4.1. In the case of remained nitrite, among the 57 run, the 22 critical runs were selected. The critical runs include: minimum level (five runs) and maximum level (five runs) of each factor, one factor in minimum level and other in maximum (five runs), one factor in maximum level and other in minimum (five runs), and two of replicate runs.

Nitrate removal efficiency and remained nitrite of the ECF process were taken as the responses of the experiments (Y_i) according to Eq. (4.3):

$$Y_i = b_0 + \sum_{i=1}^{n} b_i x_i + \sum_{i=1}^{n} b_{ii} x_i^2 + \sum_{i=1}^{n-1} \sum_{j=i+1}^{n} b_{ij} x_i x_j, \tag{4.3}$$

where Y_i is the response, b_0, b_i, b_{ii}, b_{ij} are the constant coefficient, the linear coefficients, the quadratic coefficients and the interaction coefficients, respectively, and x_i and x_j are the coded values of the variables.

Table 4.1 Experimental range and levels of independent variables according to RSM design

Variables	Factor	Unit	Levels				
			$-\alpha$	-1	0	$+1$	$+\alpha$
Initial pH	X_1	–	1.9	4	5.5	7	9.1
Applied current	X_2	Ampere	0.95	2	2.75	3.5	4.55
Initial concentration of nitrate	X_3	mg/L as NO_3^-	160	300	400	500	640
Electrode number	X_4	–	5	8	10	12	15
Reaction time	X_5	min	61	110	145	180	229

3 Results and Discussion

3.1 Development of Regression Model Equation

In order to study the effect of selected variables, experiments were performed for different combinations of variables using statistically designed experiments. The *P* and the *F* values for nitrate removal efficiency and remained nitrite are listed in Tables 4.2 and 4.3, respectively.

The second order polynomial equations for nitrate removal efficiency (Y_1) and remained nitrite (Y_2) in terms of coded factors are given by Eqs. (4.4) and (4.5), respectively.

Table 4.2 Analysis of variance for nitrate removal efficiency

Source	df	F value	p-value Prob > F
Model	24	49.72	<0.0001
X_1-pH	1	19.23	0.0002
X_2-Current	1	2.98	0.0974
X_3-Ini. Conc.	1	328.50	<0.0001
X_4-Elec.	1	1.67	0.2089
X_5-Time	1	160.08	<0.0001
X_1X_2	1	6.24	0.0198
X_1X_3	1	25.67	<0.0001
X_1X_4	1	2.19	0.1517
X_1X_5	1	66.98	<0.0001
X_2X_3	1	60.56	<0.0001
X_2X_4	1	6.24	0.0197
X_2X_5	1	6.85	0.0151
X_3X_4	1	1.68	0.2076
X_3X_5	1	19.40	0.0002
X_1^2	1	0.51	0.4816
X_2^2	1	25.55	<0.0001
X_3^2	1	3.02	0.0949
X_5^2	1	34.20	<0.0001
$X_1X_2X_3$	1	1.84	0.1877
$X_1X_2X_4$	1	15.44	0.0006
$X_1X_2X_5$	1	13.29	0.0013
$X_1X_3X_5$	1	36.37	<0.0001
$X_1^2X_2$	1	43.87	<0.0001
$X_1^2X_5$	1	74.27	<0.0001
Residual	24		
Lack of fit	10	0.99	0.50
Pure error	14		

Table 4.3 Analysis of variance for remained nitrite

Source	df	F value	p-value Prob > F
Model	13	40.34	0.0004
X_1-pH	1	7.54	0.0405
X_2-Current	1	58.20	0.0006
X_3-Ini. Conc.	1	260.72	<0.0001
X_4-Elec.	1	9.92	0.0254
X_5-Time	1	4.07	0.0998
X_1X_2	1	1.76	0.2416
X_1X_3	1	1.25	0.3141
X_2X_3	1	29.16	0.0029
X_1^2	1	2.93	0.1474
X_2^2	1	12.72	0.0161
X_3^2	1	39.96	0.0015
X_4^2	1	3.12	0.1377
X_5^2	1	0.06	0.8118
Residual	5		
Lack of fit	4	–	–
Pure error	1		

$$\begin{aligned} Y_1 = {} & 76.24 + 3.28\,X_1 + 1.49\,X_2 - 10.27\,X_3 + 0.68\,X_4 + 10.96\,X_5 \\ & + 1.67\,X_1X_2 + 3.81\,X_1X_3 + 0.96\,X_1X_4 + 6.15\,X_1X_5 + 5.95\,X_2X_3 \\ & + 1.60\,X_2X_4 + 2.00\,X_2X_5 - 0.87\,X_3X_4 - 3.18\,X_3X_5 - 0.40\,X_1^2 \\ & + 1.87\,X_2^2 - 0.64\,X_3^2 - 2.16\,X_5^2 + 1.06X_1X_2X_3 - 2.52\,X_1X_2X_4 \\ & - 2.84\,X_1X_2X_5 + 4.54\,X_1X_3X_5 + 7.20\,X_1^2X_2 - 9.62\,X_1^2X_5 \end{aligned} \tag{4.4}$$

$$\begin{aligned} Y_2 = {} & 12.33 + 1.99\,X_1 - 9.9\,X_2 + 11.68\,X_3 - 2.28\,X_4 - 2.61\,X_5 + 1.7\,X_1X_2 - \\ & 1.52\,X_1X_3 - 6.92\,X_2X_3 - 0.91\,X_1^2 + 2.84\,X_2^2 + 3.36\,X_3^2 + 0.94\,X_4^2 + 0.22\,X_5^2 \end{aligned} \tag{4.5}$$

Table 4.4 presents the observed nitrate removal efficiency and remained nitrite for the 57 and 22 experiments, respectively.

The most important parameters, which affect the nitrate removal efficiency are initial pH, initial nitrate concentration and time. Moreover it was found that square terms of current and time and interaction terms except X_1X_4 and X_3X_4 were significant to the response. Triple interaction terms of $X_1X_2X_4$, $X_1X_2X_5$, $X_1X_3X_5$ and $X_2X_3X_5$ were also significant to the response. In case of remained nitrite, initial nitrate concentration and current are the most effective parameters. Also interaction and square terms except of X_2X_3, X_2^2 and X_3^2, respectively, have negligible effect.

Table 4.5 shows the coefficient of determination (R^2) for nitrate removal efficiency and remained nitrite. High R^2 values of 98 % and 99 % for nitrate removal efficiency and remained nitrite, respectively, express a high correlation between the observed and predicted values. Also the "Predicted R^2" is in reasonable agreement with the "Adjusted R^2" in both response.

Table 4.4 RSM design and its observed values for nitrate removal efficiency and remained nitrite

Std	Run	Initial pH	Applied current (Ampere)	Initial concentration of nitrate (mg/L)	Electrode number	Reaction time (min)	Nitrate removal efficiency (%)	Remained nitrite (mg/L)
7	1	4.00	3.50	500	8	110.00	72.98	–
55	2	5.50	2.75	400	10	145.00	73.43	12.6
13	3	4.00	2.00	500	12	110.00	54.82	–
17	4	4.00	2.00	300	8	180.00	83.02	10.18
48	5	5.50	2.75	400	10	145.00	82.16	12.6
8	6	7.00	3.50	500	8	110.00	80.07	–
44	7	5.50	2.75	400	10	145.00	67.89	–
12	8	7.00	3.50	300	12	110.00	83.76	–
36	9	5.50	4.55	400	10	145.00	90.56	5.68
6	10	7.00	2.00	500	8	110.00	44.20	–
45	11	5.50	2.75	400	10	145.00	78.96	–
24	12	7.00	3.50	500	8	180.00	89.37	10.77
37	13	5.50	2.75	160	10	145.00	97.23	2.67
1	14	4.00	2.00	300	8	110.00	76.38	–
43	15	5.50	2.75	400	10	145.00	76.61	–
56	16	5.50	2.75	400	10	145.00	76.61	–
2	17	7.00	2.00	300	8	110.00	83.76	15.32
57	18	5.50	2.75	400	10	145.00	76.61	–
34	19	9.10	2.75	400	10	145.00	81.73	13.78
32	20	7.00	3.50	500	12	180.00	96.90	–
14	21	7.00	2.00	500	12	110.00	45.08	–
26	22	7.00	2.00	300	12	180.00	91.88	–
18	23	7.00	2.00	300	8	180.00	84.50	–
40	24	5.50	2.75	400	15	145.00	78.41	11.38

(continued)

Table 4.4 (continued)

Std	Run	Initial pH	Applied current (Ampere)	Initial concentration of nitrate (mg/L)	Electrode number	Reaction time (min)	Nitrate removal efficiency (%)	Remained nitrite (mg/L)
46	25	5.50	2.75	400	10	145.00	76.61	–
11	26	4.00	3.50	300	12	110.00	86.71	–
47	27	5.50	2.75	400	10	145.00	76.61	–
19	28	4.00	3.50	300	8	180.00	94.83	–
21	29	4.00	2.00	500	8	180.00	33.57	–
4	30	7.00	3.50	300	8	110.00	81.54	–
50	31	5.50	2.75	400	10	145.00	76.61	–
15	32	4.00	3.50	500	12	110.00	81.40	–
41	33	5.50	2.75	400	10	61.00	37.44	41.82
51	34	5.50	2.75	400	10	145.00	76.61	–
53	35	5.50	2.75	400	10	145.00	76.61	–
30	36	7.00	2.00	500	12	180.00	65.90	40.10
39	37	5.50	2.75	400	5	145.00	72.32	24.8
16	38	7.00	3.50	500	12	110.00	82.28	17.34
31	39	4.00	3.50	500	12	180.00	88.48	6.98
22	40	7.00	2.00	500	8	180.00	90.69	–
25	41	4.00	2.00	300	12	180.00	80.20	–
49	42	5.50	2.75	400	10	145.00	76.61	–
29	43	4.00	2.00	500	12	180.00	75.64	–
33	44	1.90	2.75	400	10	145.00	5.89	1.11
9	45	4.00	2.00	300	12	110.00	86.71	8.81
38	46	5.50	2.75	640	10	145.00	47.76	61.39
20	47	7.00	3.50	300	8	180.00	93.35	–
27	48	4.00	3.50	300	12	180.00	96.31	–
54	49	5.50	2.75	400	10	145.00	76.61	–

42	50	5.50	2.75	400	10	229.00	90.03	8.02
10	51	7.00	2.00	300	12	110.00	77.85	–
23	52	4.00	3.50	500	8	180.00	58.81	–
5	53	4.00	2.00	500	8	110.00	71.21	52.22
35	54	5.50	0.95	400	10	145.00	83.39	9.72
52	55	5.50	2.75	400	10	145.00	76.61	–
28	56	7.00	3.50	300	12	180.00	93.35	4.57
3	57	4.00	3.50	300	8	110.00	73.42	5.09

Table 4.5 Coefficient of determination (R^2) for nitrate removal efficiency and remained nitrite

	Value	
Parameter	Nitrate removal efficiency	Remained nitrite
R^2	0.98	0.99
Adjusted-R^2	0.96	0.96
Predicted-R^2	0.89	0.82

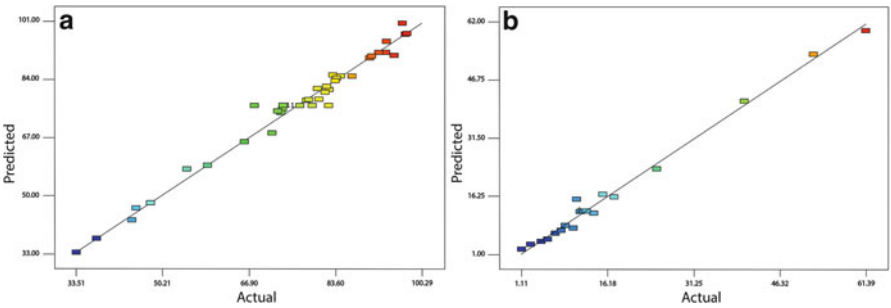

Fig. 4.2 Actual versus predicted values: (**a**) nitrate removal efficiency and (**b**) remained nitrite

Figure 4.2a, b illustrates the actual versus predicted values for nitrate removal efficiency and remained nitrite, respectively. The figure indicates a good agreement between the observed and predicted values.

4 Conclusions

In the present study, the effects of five main parameters including initial pH, initial nitrate concentration, applied current, number of electrodes and reaction time on nitrate removal efficiency by ECF, as a response, were investigated using RSM. Also, due to the formation of by-products like nitrite during treatment process, remained nitrite was also considered as a second response. According to the ANOVA results, the model indicated high *R*-squared value of 98 % and 99 % for nitrate removal efficiency and remained nitrite, respectively. The predicted *R*-squared of 89 % is in reasonable agreement with the adjusted R-squared of 96 % for removal efficiency of nitrate. Similarly, predicted *R*-squared of 96 % is in reasonable agreement with adjusted *R*-squared of 82 % for remained nitrite. Therefore the applied model showed an acceptable accuracy. In addition, it can be concluded that ECF is a very efficient technology for treatment of nitrate wastewaters and RSM is a powerful tool for simulation of nitrate removal efficiency and remained nitrite by ECF process.

Acknowledgement The authors are grateful to the Amirkabir University of Technology for the financial support. In addition, the authors wish to thank Ms. Lida Ezzedinloo for her assistance during experiments and Mr. Shahab Karimifard for English language revision of the mansucript.

References

Aleboyeh, A., Daneshvar, N. and Kasiri, M.B. (2008). Optimization of C.I. Acid red 14 azo dye removal by electrocoagulation batch process with response surface methodology. *Chem. Eng. Proc*., **47:** 827–832.

Arroyo, M.G., Perez-Herranz, V., Montanes, M.T., Garcia-Anton, J. and Guinon, J.L. (2009). Effect of pH and chloride concentration on the removal of hexavalent chromium in a batch electrocoagulation reactor. *J. Hazard. Mater*., **169:** 1127–1133.

Azadegan, M.M., Alavi Moghaddam, M.R. and Maknoon, R. (2012). Investigation of nitrate concentration in drinking water distribution network of Tehran city, Iran. 10th International Symposium on Southeast Asian Water Environment, 08–10 Nov., Vietnam.

Behbahani, M., Alavi Moghaddam, M.R. and Arami, M. (2011). Techno-economical evaluation of fluoride removal by electrocoagulation process: Optimization through response surface methodology. *Desalination*, **271:** 209–218.

Behbahani, M., Alavi Moghaddam, M.R. and Arami, M. (2013). Phosphate removal by electrocoagulation process: Optimization through response surface methodology. *Env. Eng. Mang. J. (EEMJ)*, **12:** 12.

Chavalparit, O. and Ongwandee, M. (2009). Optimizing electrocoagulation process for the treatment of biodiesel wastewater using response surface methodology. *J. Env. Sci*., **21:** 1491–1496.

El-Shazly, A.H., Al-Zahrani, A.A. and Al-Sharani, S.S. (2011). Improvement of NO_3^- removal from wastewater by using batch electrocoagulation unit with vertical monopolar aluminum electrodes. *Inter. J. Electrochem. Sci*., **6:** 4141–4149.

Emamjomeh, M.M. and Sivakumar, M. (2009). Denitrification using a monopolar electrocoagulation/flotation (ECF) process. *J. Env. Mng*., **91:** 516–522.

Hameed, B.H., Tan, I.A.W. and Ahmad, A.L. (2009). Preparation of oil palm empty fruit bunchbased activated carbon for removal of 2, 4, 6-trichlorophenol: Optimization using response surface methodology. *J. Haz. Mat*., **164:** 1316–1324.

Kasiri, M.B. and Khataee, A.R. (2011). Photooxidative decolorization of two organic dyes with different chemical structures by UV/H_2O_2 process: Experimental design. *Desalination*, **270:** 151–159.

Koporal, A.S. and Ogutveren, U.B. (2002). Removal of nitrate from water by Electroreduction and electrocoagulation. *J. Haz. Mat*., **89:** 83–94.

Krishna Prasad, R., Ram Kumar, R. and Srivastava, S.N. (2008). Design of optimum response surface experiments for electro-coagulation of distillery spent wash. *Water, Air and Soil Pol*., **191:** 5–13.

Kumar, N.S. and Goel, S. (2010). Factors influencing arsenic and nitrate removal from drinking water in a continuous flow electrocoagulation (EC) process. *J. Haz. Mat*., **173:** 528–533.

Lacasa, E., Canizares, P., Saez, C., Fernandez, J.F. and Rodrigo, M.A. (2011). Removal of nitrates from groundwater by electrocoagulation. *Chem. Eng. J*., **171:** 1012–1017.

Lakshmi, J., Sozhan, G. and Vasudevan, A. (2012). Recovery of hydrogen and removal of nitrate from water by electrocoagulation process. *Env. Sci. Pol. Res*., DOI 10.1007/s11356-012-1028-4.

Li, M., Feng, C., Zheng, Z., Shen, Z. and Sugiura, N. (2009). Electrochemical reduction of nitrate using various anodes and a Cu/Zn cathode. *Electrochem. Com*., **11:** 1853–1856.

Malakootian, M., Yousefi, N. and Fatehizadeh, A. (2011). Survey efficiency of electrocoagulation on nitrate removal from aqueous solution. *Inter. J. Env. Sci. Tech.*, **8(1):** 107–114.

Moghaddasi, M.S., Alavi Moghaddam, M.R., Maknoun, R. and Moghadasi, A.R. (2008). Investigation of nitrate concentration in tap water of Arak city, Iran. Proceedings of 6th International Symposium on Southeast Asian Water Environment, 29–31 Oct., Bandung, Indonesia.

Nazlabadi, E. and Alavi Moghaddam, M.R. (2014). Simulation of operation cost for nitrate removal using response surface method in electrocoagulation process. *Intern. J. of Env. Eng. (IJEE)*, **1(2):** 91–95.

Radaei, E., Alavi Moghaddam, M.R. and Arami, M. (2014). Removal of reactive blue 19 from aqueous solution by pomegranate residual-based activated carbon: Optimization by response surface methodology. *Iranian J. Env. Health Sci. & Eng. (IJHSE)*, **12(1):** 65. doi: 10.1186/2052-336X-12-65.

Raissi, S. and Eslami Farsani, R. (2009). Statistical process optimization through multi-response surface methodology. *World Academy of Sci., Eng. and Tec. (WASET)*, **27:** 03–25.

Sadri Moghaddam, Sh., Alavi Moghaddam, M.R. and Arami, M. (2010). Coagulation/flocculation process for dye removal using sludge from water treatment plant: Optimization through response surface methodology. *J. Haz. Mat.*, **175:** 651–657.

Sim, J., Seo, H. and Kim, J. (2012). Electrochemical denitrification of metal-finishing wastewater: Influence of operational parameters. *Korean J. Chem. Eng.*, **29:** 483–488.

Taheri, M., Alavi Moghaddam, M.R. and Arami, M. (2013). Techno-economical optimization of Reactive Blue 19 removal by combined electrocoagulation/coagulation process through MOPSO using RSM and ANFIS models. *J. Env. Mng.*, **128:** 798–806.

Vasudevan, S., Epron, F., Lakshmi, J., Ravichandran, S., Mohan, S. and Sozhan, G. (2010). Removal of NO_3^- from drinking water by electrocoagulation—An alternate approach. *Clean – Soil, Air, Water*, **38:** 225–229.

Zaroual, Z., Chaair, H., Essadki, A.H., El Ass, K. and Azzi, M. (2009). Optimizing the removal of trivalent chromium by electrocoagulation using experimental design. *Chem. Eng. J.*, **148:** 488–495.

Zodi, S., Potier, O., Lapicque, F. and Leclerc, J.P. (2010). Treatment of industrial wastewaters by electrocoagulation: Optimization of coupled electrochemical and sedimentation processes. *Desalination*, **261:** 186–190.

Part II
Wastewater Treatment and Monitoring: Biological Treatment

Chapter 5
Decolourization Studies of a Novel Textile Dye Degrading Bacterium

S. Menaka and S. Rana

1 Introduction

Textile dyes represent one of the most complicated pollutants because of their complex nature and difficulty in degradation. More than 100,000 commercially available dyes are known and the world annual production of the dyestuffs amounts to more than 7×10^5 tonnes (Robinson et al. 2001). It has been estimated that more than 10–15 % of the total dyestuff used in dye manufacturing and textile industry is released in to the environment during their synthesis and dyeing process. Almost 2,80,000 tonnes of textile dyes are discharged every year worldwide (Mass and Chaudhari 2005). In India, annual consumption of dyes by the textile industries is around 6,01,225 tonnes. The release of textile dyes into the environment is of great concern due to colourations of natural waters and also due to toxicity, mutagenicity and carcinogenicity. Various physical and chemical treatment methods are available for colour removal but use more energy and chemicals than biological processes. Moreover, they also concentrate the pollution into solid or liquid sidestreams requiring additional treatment or removal. Therefore, biological treatment is often the most economical alternatives when compared with other physical and chemical processes (Solis et al. 2012). However, it is considered that due to the recalcitrant nature of the textile dyes, the textile wastewaters impart toxicity to the microorganisms making aerobic treatment difficult. On the other hand, treatment under anaerobic conditions (by using anaerobic bacteria like *Bacteroids* sp., *Eubacterium* sp., *Clostridium* sp. etc.) produces aromatic amines which are toxic to the environment (Archna et al. 2012).

S. Menaka (✉) • S. Rana
Department of Biotechnology, Dolphin PG College of Science and Agriculture, Chunnikalan, Fatehgarh Sahib, Punjab 140406, India
e-mail: salammenaka@gmail.com

F. Kurisu et al. (eds.), *Trends in Asian Water Environmental Science and Technology*, DOI 10.1007/978-3-319-39259-2_5

Over the past decade, many organisms capable of dye decolourization at lab scale have been reported, but there are few reports available on their exploitation in treatment processes. Efforts to isolate bacterial culture capable of degrading azo dyes started in the 1970s with reports of a *Bacillus subtilis*. Bacterial isolates from soil and sludge sample belonging to *Bacillus* sp., *Alcaligenes* sp. and *Aeromonas* sp. were commonly found to have high dye decolourization ability. Other reports suggested that *Pseudomonas* sp. *Escherichia coli* and sulphate-reducing bacteria are efficient dye decolourizers. Many fungi and yeasts are also reported to be effective dye decolourizers (Banat et al. 1996). Discharge of effluents into water bodies without treatment is very common in many places. The effectiveness of these treatment systems depends upon the survival and adaptability of microorganisms during the treatment processes. Moreover, the effluents contain a diversity of dyes with different concentrations and compositions.

There is a need to discover microorganisms that are able to degrade efficiently a great number of pollutants at a very low operational cost. Therefore there is a need to find effective dye decolourizing microorganisms with ability to decolourize different types of dyes at a fast rate and under different environmental conditions. Among the synthetic dyes released by the textile industry effluents, azo dye is the most detrimental class as it is highly persistent in the aquatic environment. In the present study, therefore, decolourization of azo dyes has been studied by taking methyl orange as the supplement in the media. The main objectives undertaken for the present study were isolation and screening of dye decolorizing bacteria from textile industry effluents, morphological and biochemical characterization of the best dye decolourizing bacteria, analysis of dye decolourization under different culture conditions and evaluation of the potential to degrade a broad spectrum of reactive synthetic dyes.

2 Materials and Methods

2.1 Source of Sample

Effluent samples in liquid and solid state were collected from the vicinity of textile dying industries located in district Solan, Himachal Pradesh, India. Soil sample was also collected from the surrounding of a dyeing shop situated in Fatehgarh Sahib Road, Punjab, India. Both liquid as well as solid samples were stored under refrigerated condition at 4 °C until use.

2.2 Isolation of Dye-Decolourizing Bacteria

All samples were used for isolation of dye decolourizing bacterial cultures by enrichment culture techniques using mineral salt medium (MSM) supplemented with glucose (0.2 w/v) and yeast extract (0.2 % w/v) containing anazo dye, methyl orange, with the final dye concentration of 100 mg/L. The enrichment was carried out in three different 200 ml MSM medium in 500 ml Erlenmeyer flask by adding 10 ml industrial effluent, 10 ml of industrial soil suspension and soil suspension from dye shop (1 g soil in 10 ml water) respectively. The culture flasks were incubated in an orbital shaker with 120 rpm, at 30 °C. One ml of the enriched culture was transferred to fresh medium. Such serial transfers were performed till 7 days. At the end of incubation, 1 ml of sample was serially diluted from each flask and plated on the agar medium with same concentrations of ingredients. The pure cultures of individual bacterial strains were maintained by streaking onto nutrient agar slants and stored at 4 °C, as well as in 40 % glycerol stored at −20 °C.

2.3 Screening of Dye Decolourizing Bacteria and Decolourization Activity

MSM supplemented with dye was inoculated with 1 % of the respective inocula and incubated at 30 °C for 48 h. After 48 h, the medium was centrifuged at 8000 rpm for 15 min. Then decolourization was determined with the help of spectrophotometer at 597 nm by using methyl orange dye as standard. Uninoculated media served as blank.

The percent decolourization of dye containing medium was determined by using the formula:

$$D = [A_0 - A_1)/A_0] \times 100$$

where D is decolourization in %, A_0, initial absorbance and A_1 is final absorbance.

2.4 Optimization of Different Parameters for Maximum Decolourization

Various parameters were optimized to achieve the highest decolourization rate of the dye. They were with respect to the effect of (a) Incubation period (24–168 h), (b) pH (4–9), (c) Temperature (20–50 °C), (d) Nutrients—Carbon (sucrose, glucose and mannitol) and Nitrogen source (ammonium sulphate, beef extract, peptone), (e) inoculum percentage, and (f) dye concentration. Sucrose, mannitol and glucose were used at 10 gL^{-1} with methyl orange at 100 mgL^{-1} concentration. Ammonium

sulphate, beef extract and peptone were used at 2.5 gL^{-1} and methyl orange was added as 100 mgL^{-1}. Inoculum percentage was checked in the range 2–10 % (v/v). Effect of dye concentration on decolourization was studied by supplementing MSM with methyl orange dye at different concentrations ranging from 50 to 250 mg L^{-1}. MSM without culture was served as control. All the flasks were incubated at 30 °C under shaking conditions (150 rpm) for 6 days.

2.5 Decolourization Analysis with Optimized Condition

Experiment was set up to study the best decolourization for the methyl orange dye with all optimum parameters obtained during standardization i.e., pH, temperature, carbon and Nitrogen source, dye concentration and inoculum percentage. Decolourization activity was checked thereafter.

2.6 Decolourization of Different Dyes

To study the decolourization pattern of different dyes, Acid Red 88, Safranin, Bromophenol Blue, Mordant Red 3 and Congo red were used. Flasks were incubated at 30 °C for 3 days. Decolourization of different dyes was thereafter checked.

3 Results and Discussion

3.1 Isolation and Screening of Dye Decolourizing Bacteria

Samples were collected from the disposal site of effluent of textile dyeing industries since the chances of getting microbes having the ability to decolourize dyes are very high. There were 11 isolates which grew on the MSM with methyl orange dye as the sole carbon source. These isolates were purified by streaking on fresh nutrient agar plates and then preserved for further study on nutrient agar slants.

3.2 Dye Decolourization Activity

The decolourization activity was checked for all the 11 isolates by growing on MSM for 120 h. The percentage decolourization of one particular isolate designated as SM1 was the highest (67.8 %). Therefore, it was chosen for further study. Using Bergey's Manual of Systematic Bacteriology, the isolate was identified as

Staphylococcus sp. Previous studies have shown that strains of *Staphylococcus* sp., isolated from soil in a textile-effluent treatment plant, were able to decolourize the sulphonate azodye Congo Red (Park et al. 2005). Chen et al. (2005) isolated the gene encoding NADPH-flavinazoreductase (Azo1) from the human skin bacterium *Staphylococcus aureus* ATCC 25923, which confirmed that the enzyme responsible for dye decolourization could be an inducible flavoprotein using both NADH and NADPH as electron donors, as previously reported for other bacterial strains (Moutaouakkil et al. 2003).

3.3 Optimization for Maximum Decolourization

The operation conditions greatly influence the efficiency of decolourization. Maximum decolourization was obtained at a dye concentration of 100 mgL^{-1}. The activity decreased with increase in concentration of the dye. This might be due to the toxicity of dye to bacterial cells. Reports on similar studies show that an enzyme laccase isolated from a fungus *Tramatestrogii* had optimum dye concentration of 60 mgL^{-1} when methyl orange was used (Daassi et al. 2013). While in another report of decolourization of methyl orange, it was shown that at a dye concentration range of 50–100 mgL^{-1}, maximum decolourization was obtained by a *Pseudomonas* sp. strain (Shah et al. 2013). Among the C-sources chosen for study, glucose was found to show highest decolourization activity (upto 94 % at 120 h) for SM1. On the other hand, among the N-sources chosen for study, peptone was found to show highest decolourization activity (upto 90 % at 120 h). The type of C-source and N-source which enhances the decolourization effect depends on the microorganism under study (Ponraj et al. 2011). It was observed that by varying the pH of the medium, no significant difference in decolourization activity was observed between pH 6 and 9, but pH 9 showed slightly more favourable. The effect of temperature on decolourization activity showed that SM1 gave highest decolourization activity upto 75 % at 28 °C. It was also observed that the isolate was able to decolourize upto 48 % at 50 °C. Thus, the isolate has the potential to decolourize dyes at high pH and temperatures. While studying the effect of inoculum percentage on dye decolourization, it was seen that with 10 % bacterial inoculum, the decolourization activity was highest (upto 90 %).

The optimized conditions were pH 9, temperature 28 °C, glucose as carbon source, peptone as nitrogen source and with 10 % inoculum percentage. Under the optimized conditions, decolourization increased upto 95 % in 72 h as compared to 50.5 % in 72 h before optimization.

3.4 Decolourization Activity with Different Dyes

Among the different types of dyes based on chemical structure, azo dyes are the most commonly used dyes in the textile industries (Ayed et al. 2011). Therefore, in the present study, isolates were tested for decolourization of azo dyes mainly. But out of different dyes used, SM1 isolate was found to degrade Bromophenol blue dye with high efficiency (greater than 80 %) followed by Acid Red 88, Safranin, Mordant Red 3 and Congo red. This result shows that the isolate has the potential to decolourize varied types of dyes and can be studied for its applications in treatment of textile wastewaters.

4 Conclusions

The present study highlights the biological decolourization of azo dyes by a bacterial isolate which is identified as *Staphylococcus* sp. obtained from effluent samples of textile industries. The isolate designated as SM1 was found to be an efficient dye decolourizer. It was able to decolourize efficiently at 10 % (w/v) concentration of certain dyes which are of the sulphonated azo dye type. Optimization studies for enhancement of dye decolourization showed that upto 95 % decolourization was obtained at 72 h compared to 50.5 % before optimization. SM1 isolate was able to decolourize methyl orange even at temperature as high as 50 °C and at pH 9.

Overall, in the present study, the effluent bacterium had high potential to be used as one of a biodegrading agent because it was able to flourish even at 10 % concentration of the dyes used. Moreover, the decolourization efficiency after 24 h is more than 40 % which shows that it can decolourize at a very fast rate.

References

Archna, Lokesh, K.N. and Siva Kiran, R.R. (2012). Biological methods of dye removal from textile effluents – A review. J. Biochem. Tech., 3(5): 177–180.

Ayed, L., Mahdhi, A., Cheref, A. and Bakhrouf, A. (2011). Decolorization and degradation of azo dye Methyl red by an isolated *Sphingomonas paucimobilis*: Biotoxicity and metabolites characterization. *Desalination*, **274:** 272–277.

Banat, I.M., Nigam, P., Singh, D. and Marchant, R. (1996). Microbial decolorization of textile dye containing effluents: A review. *Bioresour. Technol.*, **58:** 217–227.

Chen, H., Hopper, H.L. and Cerniglia, C.E. (2005). Biochemical and molecular characterization of an azoreductase from *Staphylococcus aureus*, a tetrameric NADPH dependent flavoprotein. *Microbiology*, **15:** 1433**–**1441.

Daassi, D., Zouari-Mechichi, Frikha, F., Martinez, M.J., Nasri, M. and Mechichi, T. (2013). Decolorization of the azo dye acid orange 51 by laccase produced in solid culture of a newly isolated *Trametestrogii* strain 3. *Biotech*, 115–125.

Mass, R. and Chaudhari, S. (2005). Adsorption and biological decolorization of azo dye reactive red 2 in semicontinuous anaerobic reactor. *Process Biochem*, **40:** 699–705.

Moutaouakkil, A., Zeroual, Y., ZohraDzayri, F., Talbi, M., Lee, K. and Blaghen, M. (2003). Purification and partial characterization of azoreductase from Enterobacteragglomerans. *Arch Biochem Biophys*, **413(1):** 139–146.

Park, E.H., Jang, M.S., Cha, I.H., Choi, Y.L., Cho, Y.S., Kim, C.H. and Lee, Y.C. (2005). Decolorization of a sulfonated azo dye, Congo Red, by *Staphylococcus* sp. EY-3. *J. Microbiol. Biotechnol*., **15:** 221–225.

Ponraj, M., Gokila, K. and Zambare, V. (2011). Bacterial decolorization of textile dye, orange 3R. *Int. J. of Adv. Biotec. and Res*., **2(1):** 68–177.

Robinson, T., McMullan, G., Marchant, R. and Nigam, P. (2001). Remediation of dyes in textile effluent: A critical review on current treatment technologies with a proposed alternative. *Bioresour. Technol*., **77:** 247–255.

Shah, M.P., Patel, K.A., Nair, S.S. and Darji, A.M. (2013). Microbial decolorization of methyl orange dye by *Pseudomonas* spp. ETL-M. *International Journal of Environmental Bioremediation and Biodegradation*, **1(2):** 54–59.

Solis, M., Solis, A., Perez, H.I., Manjerraz, N. and Flores, M. (2012). Microbial decolorization of azo dyes: A review. *Process Biochem*., **47:** 1723–1748.

Chapter 6
Preliminary Study of Rapid Enhanced Effective Micro-organisms (REEM) in Oil and Grease Trap from Canteen Wastewater

T. Kornboonraksa

1 Introduction

Characteristics of canteen wastewater and other commercial food service facilities differ significantly from residential wastewater. Due to its high amount of organic matter, oil and grease and suspended solids, it causes higher biochemical oxygen demand (BOD). Oil and grease present in a form of low-biodegradable and frequently cause problems for both on site sewage disposal systems and public sewer systems. The water in contact with the free oil and grease (FOG) had high levels of oil approximately 800 mg/L and this may indicate the poor FOG management practices (Williams et al. 2012). Oil and grease in wastewater can exist in several forms: free, dispersed or emulsified. The differences are based primarily on size. In an oil-water mixture, free oil is characterized with droplet sizes greater than 150 μm in size while dispersed oil has a size range of 20–150 μm and emulsified oil has droplets typically less than 20 μm (Hu 2002). The majority of oil in canteen wastewater is free oil which can be removed by an overflow weir grease trap (Pollution Prevention Regional Information Center 2014). A grease trap is a chamber designed for wastewater pass through and allow any free or mechanically emulsified oil to float to the surface. Then clear wastewater can be treated in the next wastewater treatment unit. Although grease trap tanks are supposed to prevent oil and grease to enter the sanitary sewer line, high grease loads, emulsified grease, and surge wastewater loadings often cause oil and grease bypass the grease trap tanks. Some researchers found that grease trap tanks showed the removal efficiency between 43 and 80 % (Wong et al. 2007; Wongthanate et al. 2014).

From the design criteria, hydraulic retention time (HRT) of grease trap should be approximately 30 min (Karia and Christian 2006). To enhance the removal

T. Kornboonraksa (✉)
Faculty of Engineering, Burapha University, Chon Buri 20131, Thailand
e-mail: thipsuree@gmail.com

F. Kurisu et al. (eds.), *Trends in Asian Water Environmental Science and Technology*, DOI 10.1007/978-3-319-39259-2_6

efficiency of oil-water separator, effective micro-organisms could be the alternative option. Effective micro-organisms is a liquid culture of specific facultative anaerobic microbes which are capable of living in air with oxygen, as well as in low oxygen conditions. The development of effective micro-organisms mixed cultures for oil and grease removal were documented by several researchers (Wakelin and Forster 1997; Jeganathan et al. 2006; Cammarota and Freire 2006). The application of effective micro-organisms was used to hydrolyze oil and grease and could improve the biological degradation of fatty wastewaters, accelerating the process and reducing time. In this experiment, Rapid Effective Enhancements Micro-organisms (REEM) was applied to the conventional oil and grease trap. REEM contained five strains of micro-organisms (1) *Pediococcus acidilactici*, (2) *Pediococcuspentosaceus*, (3) *Baciilus amyloliquifaciens*, (4) *Pichia farinose* and (5) *Dekkera anomala*. The function of each microorganism is shown in Table 6.1. The objectives of this study were (1) to study the efficiency of REEM at different concentrations (5, 10 and 15 g), (2) to study the optimum HRT (2 and 4 h) and (3) to study the mechanism of REEM in batch experiment. Wastewater was sampled and analysed in terms of oil and grease, BOD and suspended solids.

2 Materials and Methods

2.1 Wastewater Characteristics

Wastewater in this experiment was collected from sump of canteen. On an average the wastewater samples showed following characteristics: oil and grease concentration of 1000–1300 mg/L, BOD of 1300–2700 mg/L, SS of 4600–4800 mg/L and pH 6–7.

2.2 Characteristics of Rapid Effective Enhancements Micro-organisms (REEM)

REEM contained five selected bacterial species such as *Pediococcus acidilactici*, *Pediococcus pentosaceus*, *Baciilus amyloliquifaciens*, *Pichia farinose* and *Dekkera anomala*. These bacteria were mixed with dry culture media. The dry culture media was composed of 77 % rice bran, 7 % rice flour, 10 % nutrient from soybean, 3 % whey powder, 1 % dolomite, 1 % dextrose and 1 % other nutrients. As REEM was kept as dry cells, REEM had to be inoculated in water for 12 h before use. Characteristics of REEM areas are shown in Table 6.2.

Table 6.1 Microbe functionality (Biowish Technologies Inc., 2014)

Microbe	Description	Function
Pediococcus acidilactici	Produces lactic acid and pediocins	To inhibit growth of gram negative bacteria: *Vibrio cholerae*, *Salmonella* sp. *Pseudomonas* sp., *E. coli*, Clamphylobacter, etc.
		To inhibit growth of gram positive bacteria: *Clostridium botulinum*, *Clostridium perfringens*, *Staphylococcus aureus* and *Listeria monocytogenes*
Pediococcus pentosaceus	Produces lactic acid and pediocins	To inhibit growth of gram negative bacteria: *Vibrio cholerae*, *Salmonella* sp. *Pseudomonas* sp., *E. coli*, Clamphylobacter, etc.
		To inhibit growth of gram positive bacteria: *Clostridium botulinum*, *Clostridium perfringens, Staphylococcus aureus*, *Listeria monocytogenes*
Baciilus amyloliquefaciens	Produces enzymes	To break organic matter into smaller molecules: amylase, lipase, protease, peptidase and sucrase
	Produces iturins	To inhibit growth of fungi including: Fusarium, Colletotrichum, Rhizoctonia, Aspergillus and Phytophtora
Pichia farinose	Creates toxins	To inhibit the growth of yeasts and neutralizes a wide range of toxins: Alfatoxins, Mycotoxins, Endotoxins, Exotoxins, etc.
Dekkera anomala	Produces enzymes	To break organic matter into smaller molecules: cellulase, hermicellulase, xylanase, cellobiase, amylase, pectinase, lignase, arabinase, etc.
		Ferments carbohydrate, starch and sugar into acetic acid without alcohol

Table 6.2 Characteristic of REEM

Characteristics	Value
Temperature tolerance	0–65 °C
Salinity tolerance	0–65 ppt
pH tolerance	1.5–9.6

2.3 Experimental Set-up

REEM at different concentration of 5, 10 and 15 g with HRT of 2 h and 4 h were applied to oil and grease trap (O&G trap). O&G trap was developed by using plastic container and controlling wastewater flow by static head tank. After O&G trap, wastewater was passed through filtration tank which was packed by brick, charcoal and gravel respectively. The experimental set-up is as shown in Fig. 6.1.

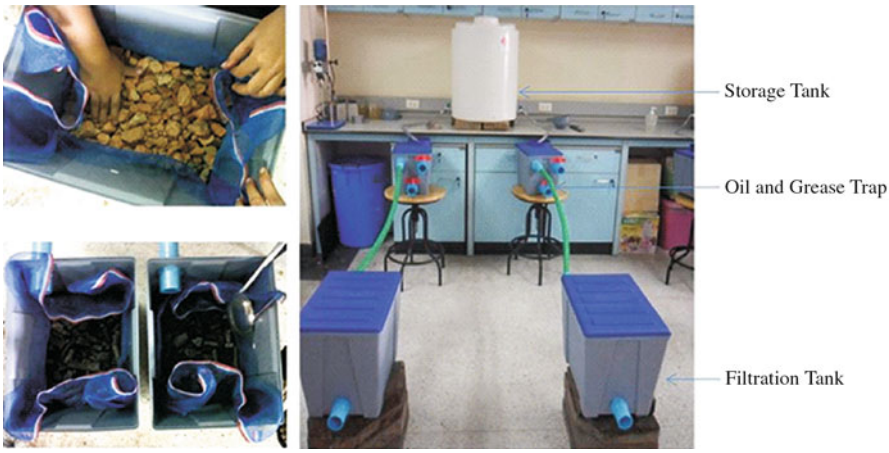

Fig. 6.1 Experimental set-up

2.4 REEM Batch Experiments

To study effects of REEM concentration, various amounts of REEM were used (5, 10 and 15 g) and these were inoculated separately each in 1000 mL of tap water to make REEM solutions of different concentrations. The solutions were kept for 12 h before mixing with canteen wastewater of 3000 mL. The wastewater then were sampled and analysed for oil and grease, BOD and SS at every 2, 4, 6 and 8 h. Figure 6.2 shows the prepared REEM solutions before mixing with wastewater.

3 Results and Discussion

3.1 Effects of REEM on Oil and Grease Removal

Figure 6.3 illustrates the canteen wastewater before and after filtration tank. The removal of oil and grease at two different hydraulic retention times (HRT) of 2 h and 4 h were as shown in Figs. 6.4 and 6.5 respectively. Wastewater without REEM was sampled and analysed at every 2, 4, 6 and 8 h. There was no significant change in removal efficiency for the conventional grease trap between HRT of 2 h and 4 h. At HRT of 2 h, the removal efficiency of conventional grease trap was only 62–64 % and after filtration tank was 68–70 %. With the increase of HRT to 4 h, oil and grease removal from trap was increased to 62–65 % and after filtration tank was 71–73 %. After REEM was applied in the grease trap, oil and grease removal efficiency was increased for REEM 5 and 10 g. At HRT of 2 h, REEM 5, 10 and 15 g, oil and grease removal from trap were 74 %–76 %, 76 %–78 % and 68 %–71 % whereas after filtration tank were 79 %–80 %, 81 %–82 % and 75 %–78 %

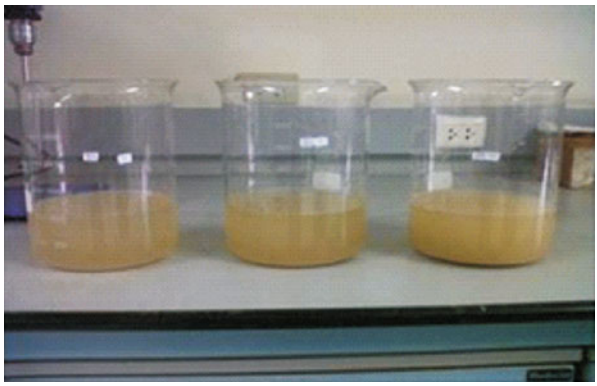

Fig. 6.2 Prepared REEM solutions

respectively. It was found that increasing HRT from 2 to 4 h caused the removal efficiency of oil and grease to increase only when REEM were 5 and 10 g. From trap, the removal efficiencies were 77 %–82 %, 80 %–87 % and then dropped to 72 %–73 % and from filtration tank were 82 %–86 %, 85 %–89 % and 78 %–80 % respectively. From these results, it could be concluded that enzymes that were produced by REEM could enhance oil and grease removal. However, the enzymes may cause a reduction in BOD removal due to the breakbond mechanisms of molecules from larger to smaller that promoted the micro-organism to degrade the substance faster compared to the treatment without REEM.

3.2 Effects of REEM on BOD Removal

The removal of BOD at different hydraulic detention times (HRT) of 2 h and 4 h were examined and are as shown in Figs. 6.6 and 6.7 respectively. Samples were collected and analysed without REEM at every 2, 4, 6 and 8 h. It was found that without REEM, there was no BOD removal efficiency after HRT of 2 h. With the increase of HRT to 4 h, the BOD removal after filtration was 19–28 %. However, with REEM the BOD removal efficiency increased. At HRT of 2 h, REEM 5, 10 and 15 g, BOD removal from trap were 3 %–10 %, 1 %–10 % and 4 %–7 % whereas after filtration tank the BOD removal were 12 %–17 %, 6 %–15 % and 5 %–9 % respectively. It was found that after increase of HRT from 2 to 4 h, the removal efficiency of BOD increased only when REEM concentrations were of 5 and 10 g. From trap, removal efficiency were 4 %–33 %, 2 %–25 % and then dropped to 2 %–8 % and from filtration tank were 21 %–40 %, 13 %–31 % and 11 %–23 % respectively. This could be because REEM worked as a facultative bacteria and they also consumed the oxygen during the 5 days of BOD incubated. Hence, there was higher oxygen demand which resulted in lower BOD removal efficiencies for all REEM concentrations.

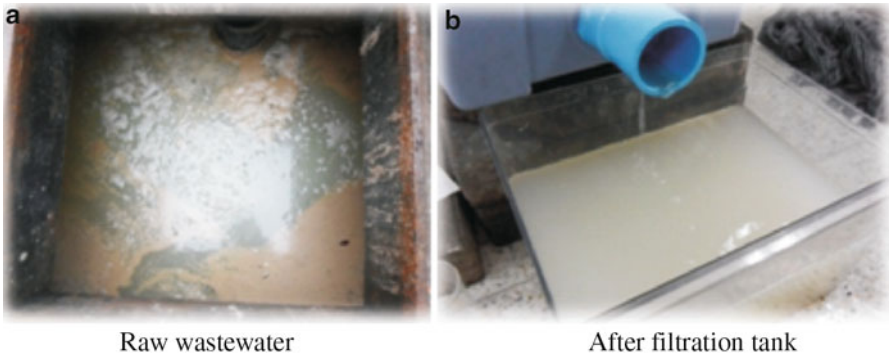

Fig. 6.3 Canteen wastewater characteristics. (**a**) Raw wastewater (**b**) After filtration tank

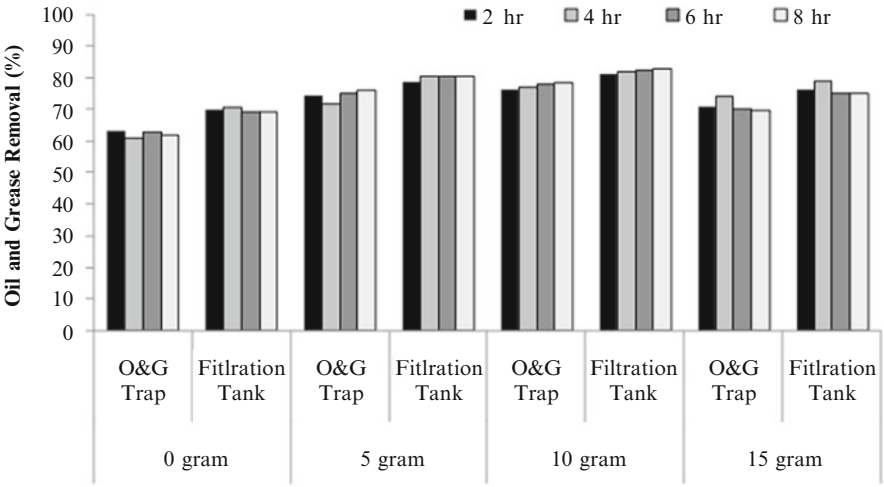

Fig. 6.4 Oil and grease removal at HRT of 2 h

3.3 Effect of REEM on SS Removal

Effects of REEM on SS removal are shown in Table 6.3. Wastewater was collected from oil and grease trap and filtration tank at every 2, 4, 6 and 8 h. It was found that with and without REEM, there were no SS removal from oil and grease trap. No SS removal was observed in oil and grease trap, may be due to the increased amount of micro-organism in the reactor. After filtration tank, SS removal at HRT of 2 h with REEM of 0, 5, 10 and 15 g were 5 %–8 %, 5 %–8 %, 1 %–7 % and 3 %–9 % respectively. When the HRT was changed to 4 h, SS removal after filtration tank were 5 %–9 %, 5 %–8 %, 2 %–8 % and 3 %–9 % respectively.

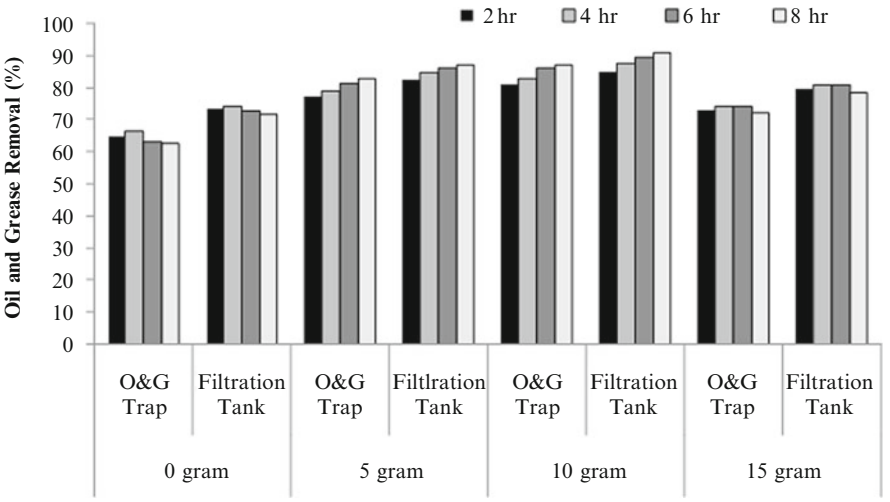

Fig. 6.5 Oil and grease removal at HRT of 4 h

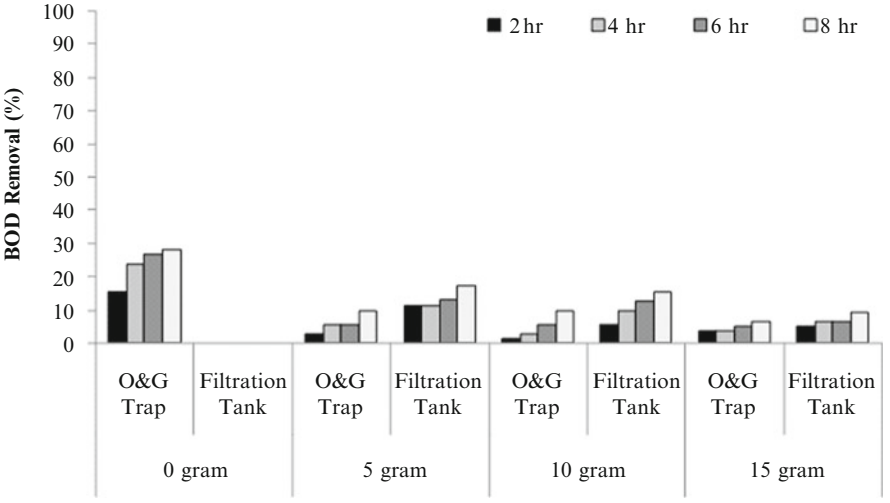

Fig. 6.6 BOD removal at HRT of 2 h

3.4 Oil and Grease Removal in Batch Experiment

The results of oil and grease removal were confirmed by batch experiments. REEM at the same concentrations were studied. The results showed that without REEM, oil and grease removal efficiency showed the lowest value. With the increase of REEM to 5, 10 and 15 g, oil and grease removal efficiency increased. The highest oil and grease removal was observed at REEM of 10 g as shown in Table 6.4.

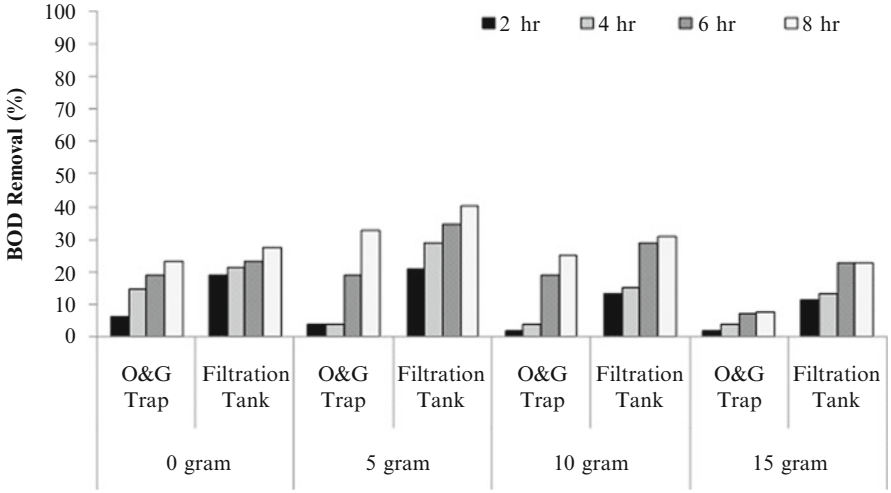

Fig. 6.7 BOD removal at HRT of 4 h

Table 6.3 Average SS removal at different REEM concentrations and HRTs

REEM (gram)	SS removal (%) HRT = 2 h		SS removal (%) HRT = 4 h	
	After O&G Traps	After filtration tank	After O&G Traps	After filtration tank
0	0	5–8	0	5–9
5	0	5–8	0	5–8
10	0	1–7	0	2–8
15	0	3–9	0	3–9

4 Conclusions

The experimental results demonstrated that the application of REEM in O&G trap could enhance O&G removal efficiency compared to w/o REEM. The range of O&G removal with REEM was in the range of 75–89 % whereas the efficiency was 68–73 % w/o REEM. The effect of HRT on O&G removal was studied at 2 h and 4 h with different REEM dosage. It was found that REEM 10 g with HRT 4 h showed the highest O&G removal efficiency (85–89 %). However, there was no significant effect on BOD and SS removals in the water treated both with REEM and w/o REEM application. The increase in REEM dosage showed the decrease in BOD and SS removal efficiency.

Table 6.4 Oil and grease removal in batch experiments

REEM (g)	Sampling time (h)	Oil and grease removal (%)
0	2	61–62
	4	63–64
	6	60–61
	8	60–61
5	2	75–76
	4	77–78
	6	78–79
	8	78–80
10	2	78–79
	4	79–80
	6	80–81
	8	80–81
15	2	62–73
	4	64–74
	6	61–73
	8	72–73

5 Recommendation

For the further research study, the kinetics of REEM on oil and grease removal should be investigated.

References

Biowish Technologies Inc. (2014). Introduction to Biowish: Aquaculture. Biowish Technologies Inc., Ohio, United States.

Cammarota, M.C. and Freire, D.M.G. (2006). A review on hydrolytic enzymes in the treatment of wastewater with high oil and grease content. *Biores. Tech*., **97(17):** 2195–2210.

Hu, X. (2002). Separation of Oil-in-Water Emulsion for Environmental Protection. Ph.D. thesis, Department of Environmental Economics, Szent István Egyetem, Élelmiszertu-dományi Doktori Iskola.

Jeganathan, J., Bassi, A. and Nakhla, G. (2006). Pre-treatment of high oil and grease pet food industrial wastewaters using immobilized lipase hydrolyzation. *J. Haz. Mat*., **137(1):** 121–128.

Karia, G.L. and Christian, R.A. (2006). Design of preliminary treatment units. *In:* Wastewater Treatment: Concepts and Design Approach. Prentice-Hall of India, New Delhi.

Pollution Prevention Regional Information Center (2014). Guidelines for Design, Installation, and Construction of North Carolina Food Establishments. Pollution Prevention Regional Information Center, Omaha, United State.

Wakelin, N.G. and Forster, C.F. (1997). An investigation into microbial removal of fats, oils and greases. *Biores. Tech*., **59(1):** 37–43.

Williams, J.B., Clarkson, C., Mant, C., Drinkwater, A. and May, E. (2012). Fat, oil and grease deposits in sewers: Characterisation of deposits and formation mechanisms. *Water Res*., **46 (19):** 6319–6328.

Wong, N.H., Law, P.L. and Lai, S.H. (2007). Field tests on a grease trap effluent filter. *Int. J. Environ. Sci. Tech.*, **4(3):** 345–350.

Wongthanate, J., Mapracha, N., Prapagdee, B. and Arunlertaree, C. (2014). Efficiency of modified grease trap for domestic wastewater treatment. *J. Indus. Tech.*, **10(2):** 10–22.

Chapter 7
Step-Feed Technology in SBR to Enhance the Treatment of Landfill Leachate

K.B.S.N. Jinadasa, T.I.P. Wimalaweera, H.M.W.A.P. Premarathne, and S.M.A.L. Senarathne

1 Introduction

Municipal solid waste leachate is the liquid leached from a landfill. The annual production of municipal solid wastes in Sri Lanka, is mostly disposed via landfilling or open dumping. The generation of leachate is caused principally by precipitation, percolating through waste deposited in a landfill. Once in contact with decomposing solid waste, the percolating water becomes contaminated and if it then flows out of the waste material, it is termed leachate. This leachate (if not collected and treated) poses dangerous environmental and health risks due to its impact on surface and ground waters. Leachate may contain large amounts of organic matter (biodegradable, but also refractory to biodegradation), where humic-type constituents consist as the important group, as well as ammonia-nitrogen, heavy metals, chlorinated organic and inorganic salts (Renou et al. 2008). It is very costly to clean up when they contaminate the groundwater. Figure 7.1 shows a typical municipal landfill.

With the age of the landfill, characteristics of the leachate vary. An immature leachate has higher C/N ratio in which biological processes can be easily adopted. But with age, the biodegradable portion decreases and with the low C/N ratio biological processes become difficult.

The sequencing batch reactor (SBR) is operated on a sequence of fill and draw cycles. The conventional SBR cycle contains four steps: Filling, Reacting, Settling and Idling. SBR treats the wastewater using microorganisms' microbial metabolism. Both natural and synthetic leachate were used in this research. In the natural

K.B.S.N. Jinadasa (✉) • S.M.A.L. Senarathne
Civil Engineering Department, University of Peradeniya, Peradeniya 20400, Sri Lanka
e-mail: shamj@pdn.ac.lk

T.I.P. Wimalaweera • H.M.W.A.P. Premarathne
SATREPS Project, Civil Engineering Department, University of Peradeniya, Peradeniya, Sri Lanka

F. Kurisu et al. (eds.), *Trends in Asian Water Environmental Science and Technology*, DOI 10.1007/978-3-319-39259-2_7

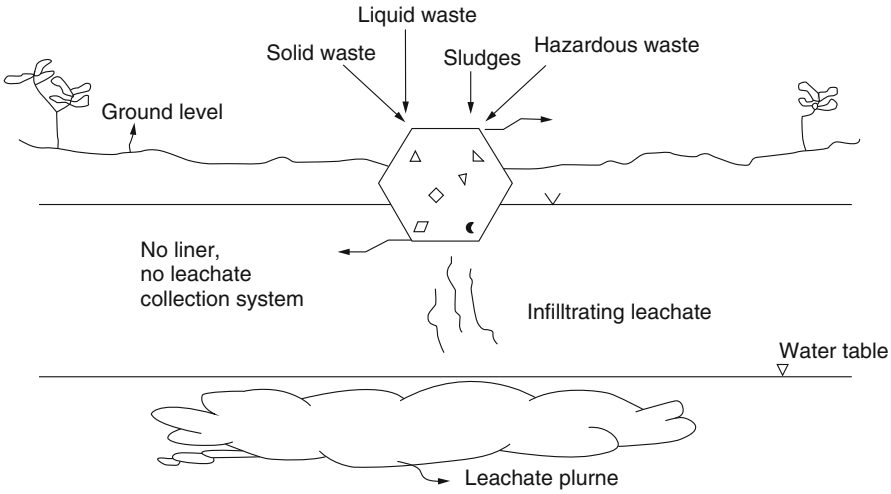

Fig. 7.1 Typical solid waste open dumping

landfill leachate, the characteristics are varied in large ranges. So at the latter part of the research, synthetic leachate was used to keep the influent quality constant. So that performances of the system can be monitored easily. Many authors have reported COD removals up to 75 %. Also, 99 % NH_4^+-N removal has been observed during the aerobic treatment of domestic leachates in a SBR with a 20–40 days residence time. Recently, nutrient reduction from pre-treated leachate was carried out using a lab-scale SBR by Uygur and Kargi. Sequential anaerobic–aerobic operations resulted in COD, NH_4^+-N and PO_4^{3-}-P removal of 62 %, 31 % and 19 %, respectively, at the end of cycle time (21 h) (Renou et al. 2008).

High concentration of organics and ammonia nitrogen is commonly feature in industrial wastewaters such as landfill leachate, textile and fertilizer wastewater.

Biological processes for nitrogen removal is very important because discharge of nitrogen into surface water results in oxygen depletion and algae bloom (Junga et al. 2004).

In order to achieve high nitrification and denitrification rate, the step-feed SBR with alternating aerobic and anoxic phases in the reaction phase can enhance the N removal (Rodríguez et al. 2010). Except for advantages of the typical SBR, the step-feed SBR can make good use of influent COD as the carbon source required in the denitrification process. This means that, by step feeding and multiple aerobic/anoxic phases, a carbon source is required to denitrify nitrite. Nitrate which is formed in each aerobic period is provided by the subsequent anoxic period influent. Moreover, step-feed strategy allows nitrification to occur under a lower organic loading in the aerobic periods, which estimates the inhibition of high organic loading on autotrophic nitrifiers and saves aeration consumption to oxidize these organic matters (Guo et al. 2007). To authors' knowledge, advanced nitrogen removal from leachate through step-feed SBR process was never reported.

Based on these concepts and analysis, the main objective of this study is not only to study the performance of SBR system for leachate treatment, but also to study the

feasibility of nitrogen removal from landfill leachate using step-feed mechanism in the SBR process and to examine the applicability of pH as a real time control strategy for the SBR process.

2 Materials and Methods

2.1 Experimental Lab-Scale Reactor

Figures 7.2 and 7.3 show the laboratory scale SBR and the cross sectional view of the reactor respectively.

A reactor of the model was made up of a cylindrical perspex tank where the bottom was modified to have a slope made up out of a 2 mm thick steel cone. This was merely to support the settling of solids during the settling phase. At the tip of the cone, a stop valve was fitted for the purpose of draining the tank and to extract samples. An influent pipe was inserted into the tank from the top opening and an effluent motor was submerged in the tank at the level of 6.7 l cm. Mechanical agitator powered by an electrical motor was fixed at the top tank and air supply was done by an aquarium air pump where the blowers are fixed at the bottom of the tank. During this research, the step-feed mechanism is introduced to the laboratory scale model and the necessary modifications are done such as connecting a mini pump to add external carbon source. The cycle operation is controlled by a programmable logic controller.

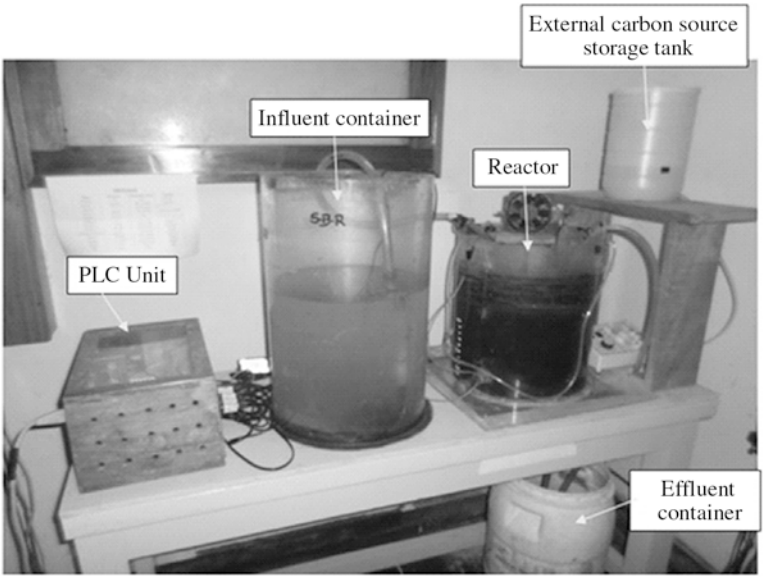

Fig. 7.2 Laboratory scale SBR model

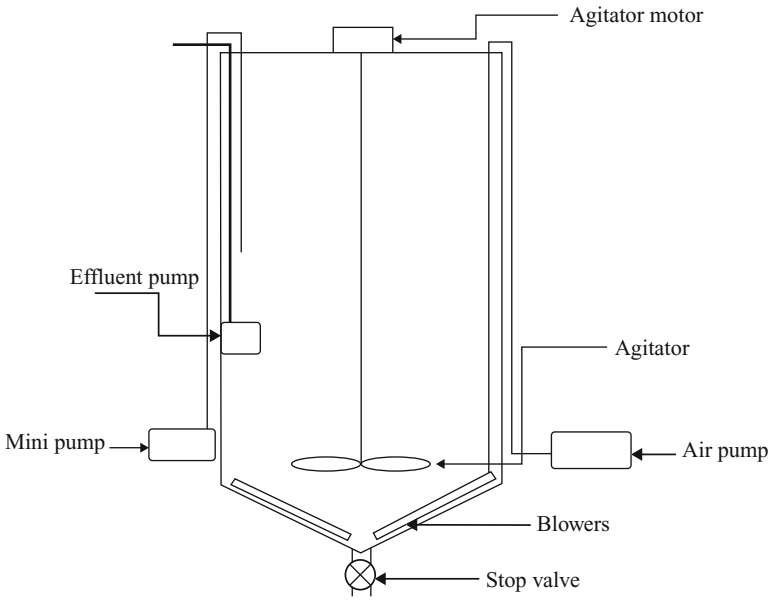

Fig. 7.3 Cross-sectional view of the reactor

2.2 Leachate Composition and Seed Sludge

The seeding sludge was obtained from Temple of Tooth Relic WWTP (Kandy, Sri Lanka). Characteristics of natural leachate which was taken from dumping yard Gohagoda, Kandy is shown in Table 7.1. Composition of synthetic leachate was K_2HPO_4, K_2CO_3, $MgCl_2.6H_2O$, $NaHCO_3$, $MgSO_4.7H_2O$, $CaCl_2$, NH_4Cl, NaCl, CH_3COONa, sugar, and trace metal solution were as 4.437 mg/l, 70.73 mg/l, 31.785 mg/l, 71.436 mg/l, 16.073 mg/l, 1400 mg/l, 19.92 mg/l, 200 mg/l, 3000 mg/l and 1 ml/l respectively.

2.3 Operating Strategy of Conventional SBR Cycle

Initially the lab scale model was operated for 2 weeks using synthetic wastewater to acclimatize the microorganisms. Then leachate was introduced to the reactor. Initially, the conventional SBR cycle was operated. Since the main objective of the conventional cycle was to treat the biodegradable waste portion, the total number of phases in a cycle was utilized as four in order to make the cycle operation simple. The fill phase was set as a static fill and react, settle and decant phases used under aerobic condition. Timing for each phase was fixed as fill, react, settle and decant as 1 min, 9 h, 2 h 54 min and 5 min respectively.

Table 7.1 Characteristics of natural leachate

Parameter	Range
BOD_5 (mg/l)	370–485
COD (mg/l)	3300–5600
NH_4^+-N (mg/l)	280–640
NO_3^--N (mg/l)	120–230
NO_2^--N (mg/l)	32–54
pH	6.7–8.0
Temp (°C)	25 ± 1

2.4 Operating Strategy of Step-Feed SBR Cycle

To enhance nitrogen removal, the step-feed mechanism was introduced. At the conventional cycle, the react phase consisted of only aeration and mixing but at the step-feed process, the react phase consisted of six phases. There were three fill phases, which are achieved in a very short time, just like pulse filling. There are three aerobic-anoxic combinations and at the last anoxic phase, an external carbon source (glucose) is added to the reactor as the electron donor for denitrification (Fig. 7.4).

Timing of these phases was determined by using pH as a real-time control parameter. Aeration and mixing took place at the aerobic phase and only mixing was done at the anoxic phase. External carbon source was added using mini pump. Aeration and mixing of the reactor ceased during the settle phase and the activated sludge was allowed to settle under quiescent conditions. During the draw phase, the clarified supernatant was withdrawn through the submersible pump fixed at the minimum liquid level. Both anoxic and aerobic durations were not fixed but distributed by real-time control.

2.5 Analytical Method

NO_3^--N, NH_4^+-N, TN, mixed liquor volatile suspended solids (MLVSS), BOD_5, COD and pH were measured in this study. The Nesslar method and cadmium reduction method were used to find NH_4^+-N and NO_3^--N respectively. Reactor Digestion method was used for the COD measurement and standard method was used for the MLVSS.

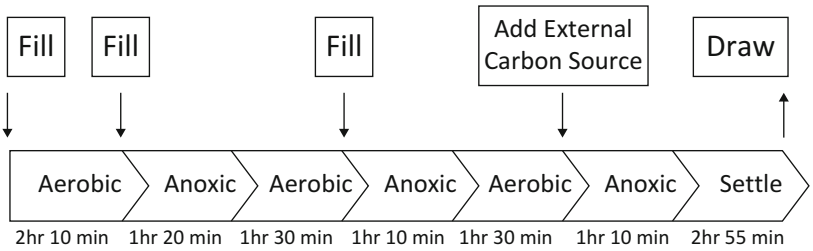

Fig. 7.4 Operational strategy in step-feed

3 Results and Discussion

3.1 Overview of System Performance

During the operation of conventional SBR cycle, accumulation of NO_3^--N was observed but organic matter removal was in a higher level. During this period, natural leachate was used. Then with the introduction of step-feed process, synthetic leachate was used to keep the influent quality constant, so that performances of the system can be monitored easily. After the introduction of step-feed process during first 3 weeks, effluent NH_3-N was higher than the influent NH_3-N. In order to rectify this issue, urea at the synthetic leachate was replaced by NH_4Cl. The colour of the activated sludge was more of a blackish nature during the first few weeks. Insufficiency of air at aerobic phase was the reason for this and it was solved by introducing a new air pump. As the study progressed NH_3-N removal and total nitrogen removal efficiency kept constant, therefore in order to increase F/M ratio BOD_5 portion of the synthetic leachate was increased. But this increase has not affected the nitrogen removal efficiency and it was kept constant further.

3.2 Performance of Conventional SBR Cycle

With the conventional cycle, BOD_5 removal was around 80 % and NH_3-N removal efficiency was around 70 %. While 80 % of COD removal was achieved. Influent and effluent BOD_5 quality is shown in Fig. 7.5.

NH_3-N also shows improvement with the conventional SBR cycle. Figure 7.6 shows the variation of NH_3-N with the time.

But there was an accumulation of NO_3^--N inside the reactor. Figure 7.7 shows the accumulation of NO_3^--N in the reactor.

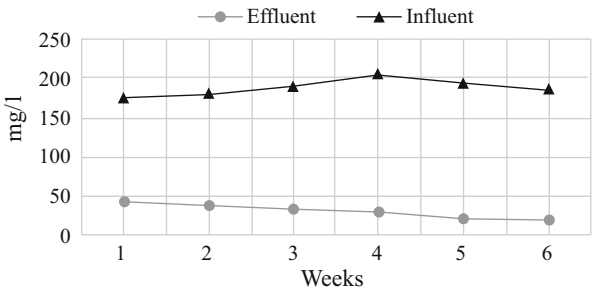

Fig. 7.5 Variation of BOD_5 at influent and effluent

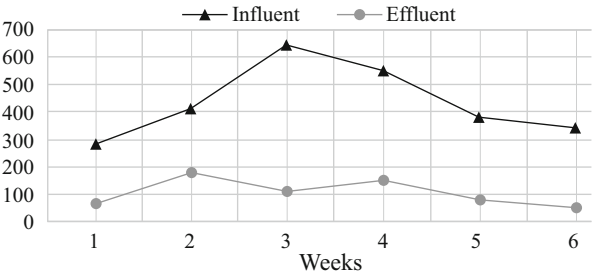

Fig. 7.6 Variation of NH_3-N in influent and effluent

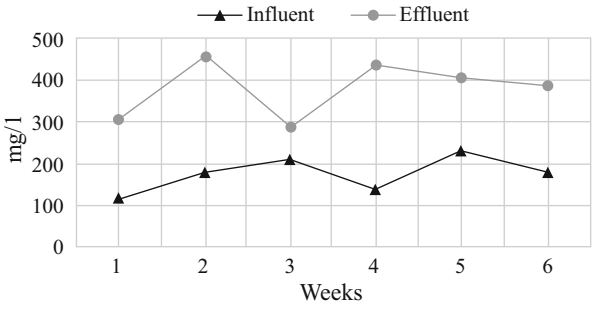

Fig. 7.7 Variation of NO_3^--N in influent and effluent

3.3 Evaluation of Conventional SBR Cycle

In this research, the SBR shows a significant role on removing BOD, COD and ammonia. However, the nitrite nitrogen (NO_2^--N) and the nitrate nitrogen (NO_3^--N) showed some accumulation process (Fig. 7.8). This may be due to lack of denitrification process. Thus the nitrate concentration was higher compared with the influent concentration.

After the nitrification, nitrate converts to nitrogen gas in the denitrification process under the anaerobic condition. The denitrification is the reduction of oxidized nitrogen compounds. The final product of complete denitrification process is nitrogen gas (N_2). Denitrification runs stepwise, from the most oxidized to the most reduced compound:

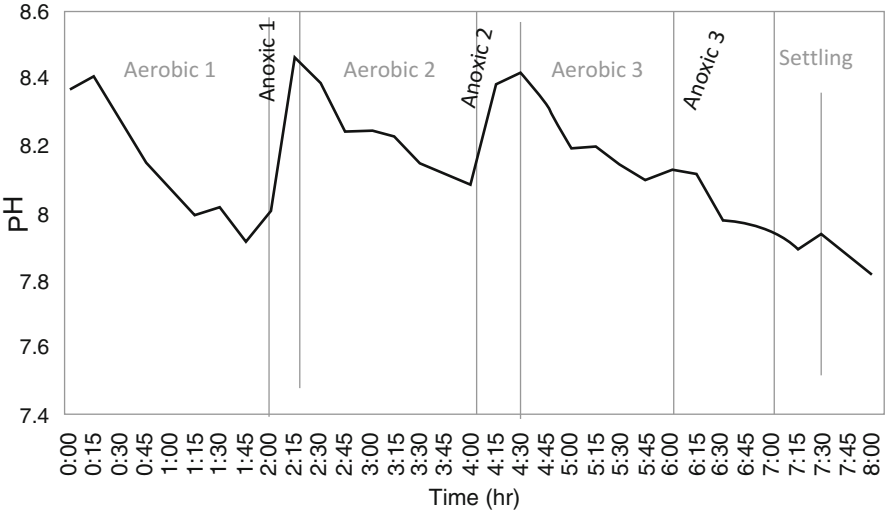

Fig. 7.8 Variation of pH value in a cycle with step-feed mechanism

$$NO_3^- \rightarrow NO_2^- \rightarrow NO \rightarrow N_2O \rightarrow N_2$$

The resulting reduction of denitrification:

$$2NO_3^- + H^+ + \text{Organic matter} \rightarrow N_2 + HCO_3^-$$

Since there is no anoxic phase in the reaction phase, the formed nitrates and nitrites remain as nitrates and nitrites in the system.

3.4 Performance of Modified SBR Cycle (Step-Feed Process)

The step-feed process was introduced to rectify this situation. The step-feed process has an anoxic phase and denitrification was achieved in that period.

pH was used to determine the durations of each phase. A decrease in pH at aerobic phase was observed and it was caused by the reduction of alkalinity and the acid production during nitrification. After completion of nitrification, the pH started to increase. The pH value continuously increased with denitrification and started to decrease after the completion of denitrification. Such variation has been observed by many authors (Changyong et al. 2007). pH variation within the cycle is shown in Fig. 7.8.

After the introduction of step-feed process, the total nitrogen amount shows a treatment, which means NO_3^--N accumulation was rectified with the step-feed process. Figure 7.9 shows the behaviour of total nitrogen within the study time.

The variation of parameters within the reaction period is also monitored. These results help to have an idea about the process taking place in each phase.

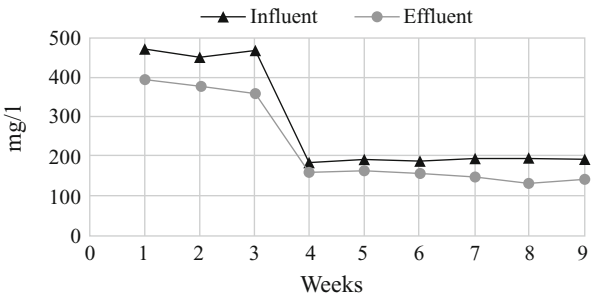

Fig. 7.9 Variation of influent and effluent TN

Due to the intermittent filling stages, BOD_5 is instantly increased before anoxic 1 and anoxic 2. The removal of BOD_5 occurs mostly at the aerobic phases. Figure 7.10 shows the BOD_5 variation within the react period.

NO_3^--N variation within the cycle is shown in Fig. 7.11. Figure 7.11 clearly shows that denitrification occurs at the anoxic phase. The lowest concentrations of NO_3^--N can be observed at the end of the anoxic phases.

3.5 Evaluation of Modified SBR Cycle

As shown in Fig. 7.11, with the step-feed process, the NO_3^--N accumulation was rectified. Average treatment efficiencies for step-feed process are shown in Table 7.2.

4 Conclusions

SBR is a promising technology all over the world to treat landfill leachate. Generally leachate has higher nitrogen concentration; therefore nitrogen removal is vital in leachate treatment. The SBR system is ideally suited to nitrification–denitrification processes since it provides an operation regime compatible with concurrent organic carbon oxidation and nitrification (Renou et al. 2008). The step-feed SBR with multiple aerobic/anoxic phases was put forward in the study. The durations of aerobic and anoxic could be distributed by real-time control using pH as nitrification and denitrification control parameters. The conventional SBR cycle has some issues with the NO_3^--N removal when treating ammonia-rich wastewater like leachate. As a solution for this issue, the step-feed process with multiple aerobic/anoxic phases was put forward.

It was observed that organic matter removal efficiency was above 80 %. Effluent BOD_5 was below 30 mg/l, which satisfy the standard to discharge into the inland surface water bodies; so it shows the validity of the modified SBR process in organic matter removal.

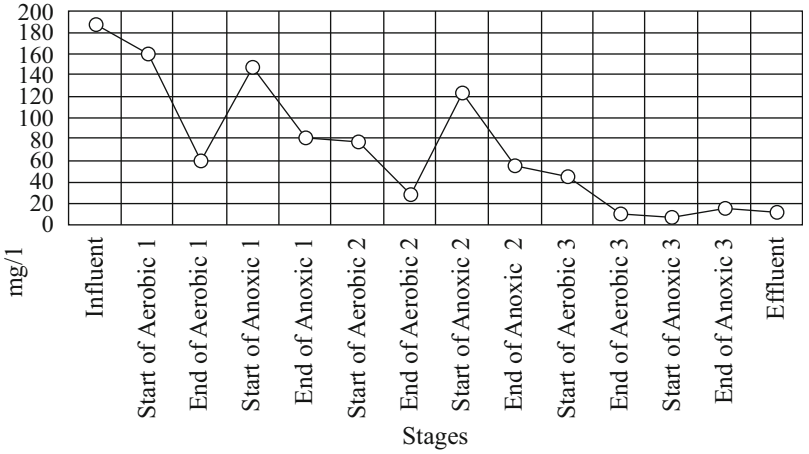

Fig. 7.10 BOD_5 variation within the react period

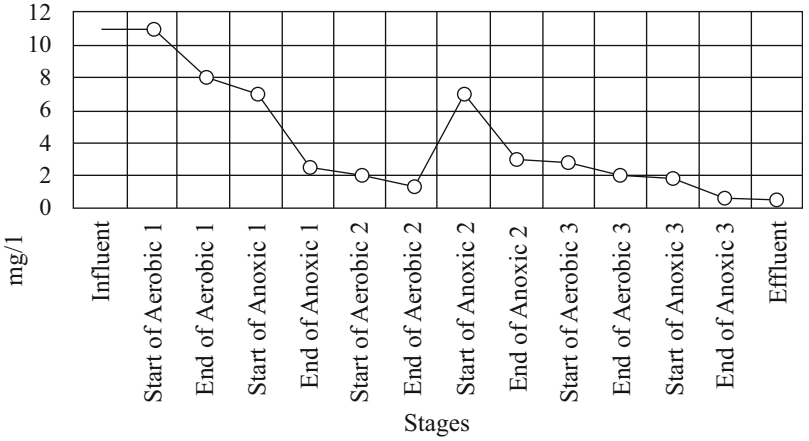

Fig. 7.11 NO_3^--N variation within the reaction period

Table 7.2 Average treatment efficiencies for the step-feed process

Parameter	Influent (mg/l)	Effluent (mg/l)	Efficiency %
BOD_5	187	15	92
COD	2560	600	75
TN	191	134	30
NH_4^+	172	127	26
NO_3^-	11	5	55

But our system has not yet provided definite evidence on the satisfactory nitrogen removal. Possible reasons for this behaviour could be under high ammonia loading conditions. Ammonia oxidizing bacteria (AOB) suffered from a shortage of O_2 because the aeration phase was not long enough. AOB were thereby gradually limited at the system. Also microorganisms would be inhibited due to the low F/M ratio of the leachate. AOB are notorious for their slow growth and low maximum growth yield, making their isolation and maintenance in pure culture difficult and time-consuming.

While maintaining the cycle time as 12 h, we were able to maintain organic, hydrological and nitrogen loading rates such as 1.2 kg COD/m^3/d, 0.3 m/d and 58.1 g/m^2/d respectively, while other usual leachate treatment options have relatively low hydraulic and pollutant loading rates.

In future, we would like to operate the system with increased hydraulic retention time. By increasing the length of aerobic phases, more time can be given to ammonification, which will convert more ammoniacal nitrogen into nitrate or nitrite.

Also rather than having all reactions in one reactor, two reactors can be maintained with one as an anaerobic reactor and the other as an aerobic reactor. Simultaneous growth of nitrifiers and heterotrophic microorganisms in a single reactor leads to low nitrification rates due to overwhelming action of heterotrophic microorganisms.

Acknowledgement This research is financially supported by the JST-JICA Science and Technology Research Partnership for Sustainable Development (SATREPS) project.

References

Changyong, Wu, Zhiqiang, Chen, Xiuhong, Liu and Yongzhen, Peng (2007). Nitrification–denitrification via nitrite in SBR using real-time control strategy when treating domestic wastewater. *Biochemical Engineering*, **36:** 87–92.

Guo, Jianhua, Yang, Qing, Peng, Yongzhen, Yang, Anming and Wang, Shuying (2007). Biological nitrogen removal with real-time control using step-feed SBR technology. *Enzyme and Microbial Technology*, **40:** 1564–1569.

Junga, Jin-Young, Chung, Yun-Chul, Shin, Hang-Sik and Son, Dae-Hee (2004). Enhanced ammonia nitrogen removal using consistent biological regeneration and ammonium exchange of zeolite in modified SBR process. *Water Research*, **38:** 347–354.

Renou, S., Givaudan, J.G., Poulain, S., Dirassouyan, F. and Moulin, P. (2008). Landfill leachate treatment: Review and opportunity. *Journal of Hazardous Materials*, **150:** 468–493.

Rodríguez, Diana Catalina, Pino, Nancy and Peñuela, Gustavo (2010). Monitoring the removal of nitrogen by applying a nitrification–denitrification process in a Sequencing Batch Reactor (SBR). *Bioresource Technology*, **102:** 2316–2321.

Chapter 8
Response Surface Optimization of Phosphate Removal from Aqueous Solution Using a Natural Adsorbent

Prangya Ranjan Rout, Puspendu Bhunia, and Rajesh Roshan Dash

1 Introduction

Phosphorous exists in the form of orthophosphate, polyphosphates, pyrophosphate, organic phosphate esters and organic phosphonates, and all these forms could be hydrolyzed to orthophosphate (Majed et al. 2012). Orthophosphate could be utilized by microorganisms, plants and animals for their growth and development. Hence, considered as a vital nutrient in most of the ecosystems and due to its low concentration occurrence in the environment, it usually serves as the limiting nutrient (Huang et al. 2013). Sustained inputs of phosphate (more than 1 mg L^{-1}) to aquatic environments lead to increased rates of eutrophication affecting the quality of domestic, industrial, agricultural and recreational water resources. Then again, phosphorous is an important element, extensively contributing towards many biological, agricultural, industrial, environmental, medical and household applications. Therefore, the excess discharge of phosphates to aquatic environments is taking place through various anthropogenic activities such as the use of fertilizers, pigments, detergents and electronic industry discharge, domestic wastewater discharge, mineral processing, rural and urban sewage disposal etc. (Wang et al. 2013). Excepting eutrophication, the increasing loads of phosphates in water bodies stimulate the activity of a damaging microbe known as *Pfisteria*, speed up the production of microsystin, a toxin that poisons aquatic animals and can cause hepatocellular carcinoma in humans, and result in depletion of desirable flora and fauna (Yuan et al. 2006; Rout et al. 2015a). In order to prevent these problems phosphorous removal from wastewater is highly desirable before discharging. The World Health Organization (WHO) recommended a maximum discharge limit of phosphorous as 0.5–1.0 mg L^{-1} (Galalgorchev 1992). Therefore, in the current

P.R. Rout • P. Bhunia • R.R. Dash (✉)
School of Infrastructure, Indian Institute of Technology, Bhubaneswar 751 013, Odisha, India
e-mail: rrdash@iitbbs.ac.in

F. Kurisu et al. (eds.), *Trends in Asian Water Environmental Science and Technology*, DOI 10.1007/978-3-319-39259-2_8

scenario, more and more stringent regulatory limits of phosphate discharge have been set by many nations and regions worldwide.

In recent past, a lot of advanced treatment methods such as physical processes, chemical precipitation, biological treatment and adsorption-based processes, etc. have been practised for phosphate abatement, since phosphate is usually difficult to remove by conventional wastewater treatment plants. Out of these various processes, adsorption with the advantage of high removal efficiency, operation simplicity, invulnerability to coexisting pollutants, economical and less sludge production has attracted immense interest (Zong et al. 2013). The efficiency of the adsorption process depends upon the adsorbent materials, which should be of low cost, easily available and exhibits high uptake capacity (Huang et al. 2013). The most useful materials are usually found among various wastes and natural substances (Mateus et al. 2012).

A number of natural materials like various soils, laterite, andesite, granite, etc. and waste materials like refuse concrete, waste paper, mussel shell, limestone waste, used bricks, dolochar, RS, Ground Burnt Patties (GBP), etc. have been reported as efficient adsorbents to reduce phosphorous concentrations in the effluents (Rout et al. 2014a, b, 2015b, c). In the present study the phosphate adsorption potential and behavior of RS, a natural substance has been examined in batch mode of experimentation. RS is the highest coverage of all soil groups of the state Odisha (India). Presence of excess amounts of oxides of iron imparts red colour to the soil. The soils are strongly to moderately acidic with low to medium organic matters and poor water retention capacity. The soils are deficient in nutrients, have low cation exchange capacity, high phosphate and sulphur adsorption property. All these characteristic features contribute to the possibility of RS to be used as a phosphate adsorbent.

With the help of conventional experimental methodologies, which are based on one-variable-at-a-time (OVAT), prediction of the effects of multiple parameters and their interaction is difficult. Moreover, by considering more experimental parameters for a particular experiment, more number of runs will have to be performed, which is cumbersome and time consuming. On the other hand, Response Surface Methodology (RSM) has been attested to be a handy tool for fulfilling the purpose of studying the effects of multiple parameters simultaneously, while performing a reduced number of experiments (Box and Draper 1987). Therefore RSM has been applied in this study to optimize experimental parameters and to develop statistical models of phosphate adsorption by RS in batch mode of operation.

2 Materials and Methods

2.1 Adsorbent

The adsorbent (RS) was collected from the Balibagada village area in Ganjam district. The adsorbent was washed several times with distilled water to remove

surface adhered particles, soluble materials and to remove the red colour of iron, and dried in hot-air oven at 100 °C for overnight. Then it was crushed, passed through 48-mesh sieve and particles less than 0.3 mm size were used in the adsorption study.

2.2 Adsorbate

Chemicals of analytical grade used in the present experimental studies, were procured from Himedia Laboratories, Mumbai, India. Phosphate stock solutions of 1000 mg L^{-1} were prepared synthetically by dissolving calculated amount of anhydrous potassium dihydrogen phosphate (KH_2PO_4) in distilled water. The stock solution was further diluted to get the desired concentrations of experimental working solution. This synthetic phosphate solution was used for optimizing different adsorption parameters in both batch and column studies. The pH of the phosphate solution was adjusted to desired value by addition of 0.1 M HCl and NaOH.

2.3 Analytical Methods

Phosphate concentration in aqueous solutions was determined by the vanado molybdo phosphoric acid method. 1 mL of vanadate-molybdate reagent, 0.5 mL of distilled water and 3.5 mL of filtered sample were mixed and the solution was analyzed after 10 min with a UV/VIS spectrophotometer (Perkin Elmer Lambd-25) at the detection wavelength of 470 nm. Elemental distribution of RS before and after adsorption was monitored using Field Emission Scanning Electron Microscope (FESEM, ZEISS SUPRA 55), equipped with EDS at an accelerating voltage of 15 kV by sprinkling adsorbents onto the carbon tape mounted on the SEM stub. To determine pHzpc, 1 g of RS was added to a series of Elnermayer flasks containing 100 mL of 0.01 M NaCl solution of variably adjusted pH (2.5–12), agitated for 48 h and then final pH was measured. The pHzpc was obtained as the point of intersection ($pH = 0$) of the resulting curve as obtained by plotting change in pH (ΔpH) against the initial pH (pH_i). The specific surface area of RS was determined by the BET nitrogen gas adsorption-desorption method using a specific surface area analyzer, QUADRASORB *SI*, USA. Design Expert version 7.0.3, Stat Ease, USA was used for the application of RSM to fit and analyze experimental data to various models. Statistical validation of the models was done by analysis of variance (ANOVA). BET analysis was done by Quadra Win software.

2.4 Adsorption Experiments

The batch study was performed for the optimization of process parameters (adsorbent dose, contact time, initial phosphate concentration and pH) involved in the adsorption process as per central composite design (CCD) using RSM. 100 mL of the phosphate solutions of varying concentrations (1.25–26.25 mg L^{-1}) and variably adjusted pH (5–12.5) were taken in 250 mL Erlenmeyer flasks, a known quantity of adsorbents (5–105 g L^{-1}) were added to each flask and agitated for a variable period of time (7.5–157.5 min) at 150 rpm in an orbital shaker at room temperature. After the completion of adsorption process a pre-determined settling period of 1 h was allowed and filtration of supernatant was done using 0.45 μm filter paper, prior to phosphate analysis. The percentage removal efficiency of phosphate was determined using Eq. (8.1):

$$\text{Removal efficiency}(\%) = \frac{(C_0 - C_e)}{C_0} \times 100 \tag{8.1}$$

where C_0 and C_e are the initial and equilibrium phosphate concentrations (mg L^{-1}),

2.5 RSM-Based Experimental Design, Modelling and Statistical Analysis

With the purpose of finding the optimum experimental conditions for the maximum phosphate adsorption in batch mode, the experiments were designed by CCD of RSM. The effects of the process parameters such as contact time (A = 7.5–157.5 min) (0.5–6.5 g L^{-1}), adsorbent dose (B = 5–105 g L^{-1}), initial phosphate concentration (C = 1.25–26.25 mg L^{-1}) and pH (D = 5–12.5) were investigated at five levels i.e. ±α (axial points), ±1 (factorial points), and 0 (centre point) and three replications of the central point is presented in Table 8.2. Quadratic model was developed based on the CCD experiments correlating all the variables as per the following equation (Rout et al. 2015b):

$$R = b + \sum_{i=1}^{n} c_i x_i + \sum_{i=1}^{n} c_{ii} x_i^2 + \sum_{i=1}^{n-1} c_{ij} x_i x_j \tag{8.2}$$

where R is the predicted response, b is the intercept coefficient, c_i is the linear coefficient, c_{ii} is the quadratic coefficient, c_{ij} is the interaction coefficient and x_i and x_j are the coded values of the variables. Statistical validation of the RSM developed models were done by ANOVA by solving the regression equation and by analyzing the individual and combined effects of the variables through contour response surface plots.

2.6 Equilibrium Kinetics and Isotherms Studies

The experimentally obtained batch adsorption data were fitted to the pseudo-first order and pseudo-second order in order to find out the best fit model. Similarly Langmuir and Freundlich isotherm models were applied to adsorption equilibrium data to figure out best fit isotherm model.

3 Results and Discussion

3.1 Characterization of Adsorbent and Adsorption Process

The chemical composition of the RS was analyzed by highly sophisticated experimental techniques such as Proton Induced X-ray Emission (PIXE) and Proton Induced γ-ray Emission (PIGE) and the major constituents are given in Table 8.1. Despite being the major component of RS, the silicon oxide has a very insignificant role in phosphate removal. Conversely, the presence of magnesium and calcium ion facilitates phosphate removal via precipitation whereas iron and aluminium oxides by ligand exchange forming inner-sphere complexes. The elemental composition of RS before and after phosphate adsorption was analyzed by EDS. EDS in fact is the easiest technique to get a direct evidence of adsorption process. Figure 8.1a displays the EDS spectra of the entire electron image of the RS sample. The presence of Fe, Al, Si, Ca, Mg, C, O, K etc. as primary elements were observed from the figure. Both elemental composition (by EDS) and chemical composition (by PIXE and PIGE) results are in accordance with each other. The presence of phosphorous peak in the EDS spectra of phosphate adsorbed RS (Fig. 8.1b) validates the successful adsorption of phosphate onto RS. Thus, the adsorption of phosphate by RS was legitimated by EDS analysis.

Table 8.1 Properties and compositions of red soil

Properties	Compositions
Particle size (mm)	<0.3
pH zpc	7.51
BET Surface area (m^2g^{-1})	25.55
SiO_2 (%)	52.45–54.3
Fe_2O_3 (%)	24.21–24.73
Al_2O_3 (%)	21.38–22.17
MgO (%)	4.85–5.01
Na_2O (%)	0.46–0.49
CaO (%)	0.31–0.34

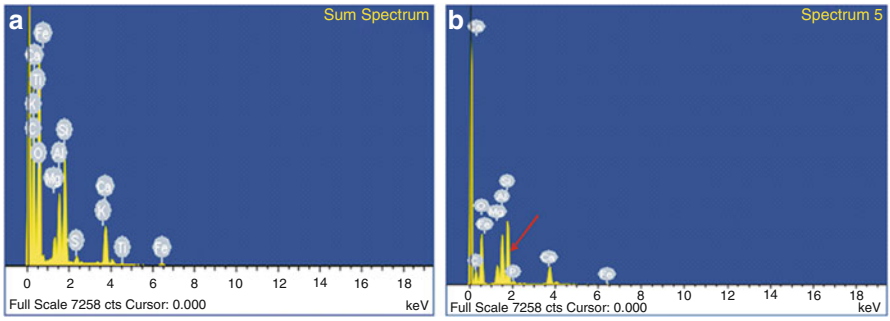

Fig. 8.1 EDS images of RS (**a**) before adsorption, (**b**) after adsorption

3.2 RSM Model Fitting and ANOVA Analysis

The individual and interactive effects of different process variables on phosphate were explored by performing CCD based experimental design. Total number of 27 five-level experiments were performed and the results are shown in Table 8.2. The results signify a wide range of percentage phosphate removal (56–99 %) for the predicted response, suggesting that the selected response is strongly related to the selected variables in this study. The CCD of RSM generated quadratic models for the response. The empirical relationships of phosphate removal with the four variables in coded values are given in Eq. (8.3).

$$\begin{aligned}\text{Percentage phosphate removal} = {} & +96 + 6.07\text{A} + 8.31\text{B} - 2.44\text{C} - 0.88\text{D} \\ & + 0.38\text{AB} + 0.51\text{AC} - 0.16\text{AD} + 1.78\text{BC} \\ & - 0.81\text{BD} - 0.068\text{CD} - 5.41\text{A}^2 - 5.74\text{B}^2 \\ & - 0.24\text{C}^2 - 2.99\text{D}^2\end{aligned} \tag{8.3}$$

where A, B, C and D are the coded terms for the independent variables of the designated response as mentioned in Sect. 2.5. The positive and negative signs indicate synergistic and antagonistic effects, respectively. The predicted values of percentage phosphate removal were calculated using Eq. (8.3) and are listed in Table 8.2. The predicted results are found to be in good agreement with experimental results as per Fig. 8.2.

The validation of the response surface quadratic model for phosphate removal was done by ANOVA and the findings are listed in Table 8.3. Generally, significance of regression models is justified by the larger F-values (Fischer's F statistics), very small *p*-values (probability), non-significant lack of fit and high values of R^2 (correlation coefficient), adjusted R^2 and predicted R^2 (Rout et al. 2015b; Box and Draper 1987). Table 8.3 illustrates that the CCD based RSM quadratic model for phosphate removal was statistically significant with high F-value 69.25, very low *p*-value <0.0001, non-significant lack of fit 48.93, R^2 0.98, adjusted R^2 0.97 and

Table 8.2 Experimental design matrix generated by CCD for phosphate removal in batch mode

		Actual variables				Removal efficiency	
Standard order	Run order	A	B	C	D	Actual	Predicted
1	19	82.5	5	13.75	7.50	56	56.42
2	24	82.5	55	13.75	12.5	81	82.29
3	15	45	80	20.00	10	82	80.12
4	8	120	80	20.00	5	96	98.76
5	16	120	80	20.00	10	93	93.72
6	13	45	30	20.00	10	61	62.31
7	2	120	30	7.50	5	81.5	82.26
8	25	82.5	55	13.75	7.5	96	96.00
9	21	82.5	55	1.25	7.5	99	99.92
10	11	45	80	7.50	10	83	83.81
11	7	45	80	20.00	5	85	84.54
12	5	45	30	20.00	5	64	63.51
13	3	45	80	7.50	5	86	85.51
14	12	120	80	7.50	10	96	95.38
15	18	157.5	55	13.75	7.5	88.75	86.51
16	22	82.5	55	26.25	7.5	91	90.17
17	26	82.5	55	13.75	7.5	96	96.75
18	14	120	30	20.00	10	75	74.38
19	17	7.5	55	13.75	7.5	59.9	62.24
20	20	82.5	105	13.75	7.5	90	89.67
21	6	120	30	20.00	5	76	76.20
22	4	120	80	7.50	5	98	97.70
23	27	82.5	55	13.75	7.5	96	95.81
24	1	45	30	7.50	5	71.3	71.59
25	23	82.5	55	13.75	2.5	87	85.81
26	10	120	30	7.50	10	81.7	83.17
27	9	45	30	7.50	10	77	73.12

predicted R^2 0.99. Moreover, Fig. 8.2 exhibits an excellent agreement between the actual and predicted values of phosphate removal. Thus, the statistical validity of the model was confirmed by the reasonable evidences.

3.3 Interaction of Variables and the Effect on Response

The interactions among the variables and their combined effects by taking two variables at a time and keeping the third one constant, on phosphate removal were evaluated with the help of contour plots as shown in Fig. 8.3a–f. All the figures clearly portray that increasing adsorbent dose and contact time increases phosphate removal efficiency whereas, decreasing initial phosphate concentration increases removal of phosphate (Rout et al. 2015c). The pH shows no significant effect on the

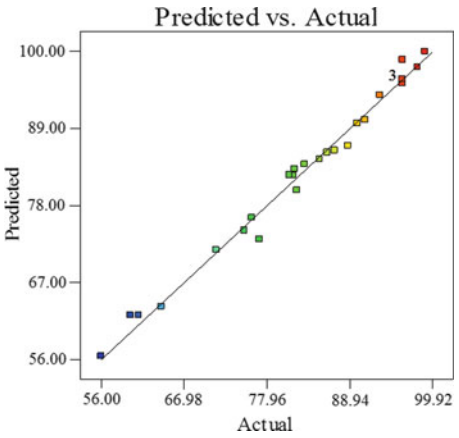

Fig. 8.2 Correlation of actual vs. predicted phosphorous removal efficiency

Table 8.3 ANOVA for response surface quadratic model of percentage phosphate removal

Source	*Sum of squares*	*df*	*Mean square*	*F value*	*p-value Prob > F*	
Model	3953.17	14	282.3	69.25	<0.0001	Significant
Residual	48.93	12	4.08			
Lack of fit	48.93	10	4.89			
Pure error	0.000	2	0.000			
Cor total Model	4002.1	26				
Model Summary Statistics						
Source	*Std. dev.*	R^2	*Adjusted* R^2	*Predicted* R^2	*PRESS*	
Linear	7.69	0.6753	0.6163	0.549	1805.05	Suggested
2FI	8.75	0.6942	0.5031	0.5047	1982.35	Aliased
Quadratic	2.02	0.9878	0.9735	0.9296	281.82	
Cubic	1.07	0.9989	0.9926	0.8364	654.57	

response. From Fig. 8.3a, it is observed that phosphate removal increases by increasing both adsorbent dose and contact time. More adsorbent dose provides more adsorption functional sites and more contact time helps in making more interaction among the adsorbate and adsorbent molecules. Therefore, their combined effect is influential in the model. The combined effect of contact time and initial phosphate concentration as shown in Fig. 8.3b, suggests neutralize effect. At higher initial phosphate concentration the adsorption saturation reached quickly resulting in lesser phosphate removal (Rout et al. 2014a), but higher contact time results in higher removal.

Figure 8.3c clearly demonstrates that the removal efficiency is solely governed by contact time. The pH value up to 7.5 results in higher removal whereas beyond 7.5 results in lower removal efficiency. The observed effect can be explained on the

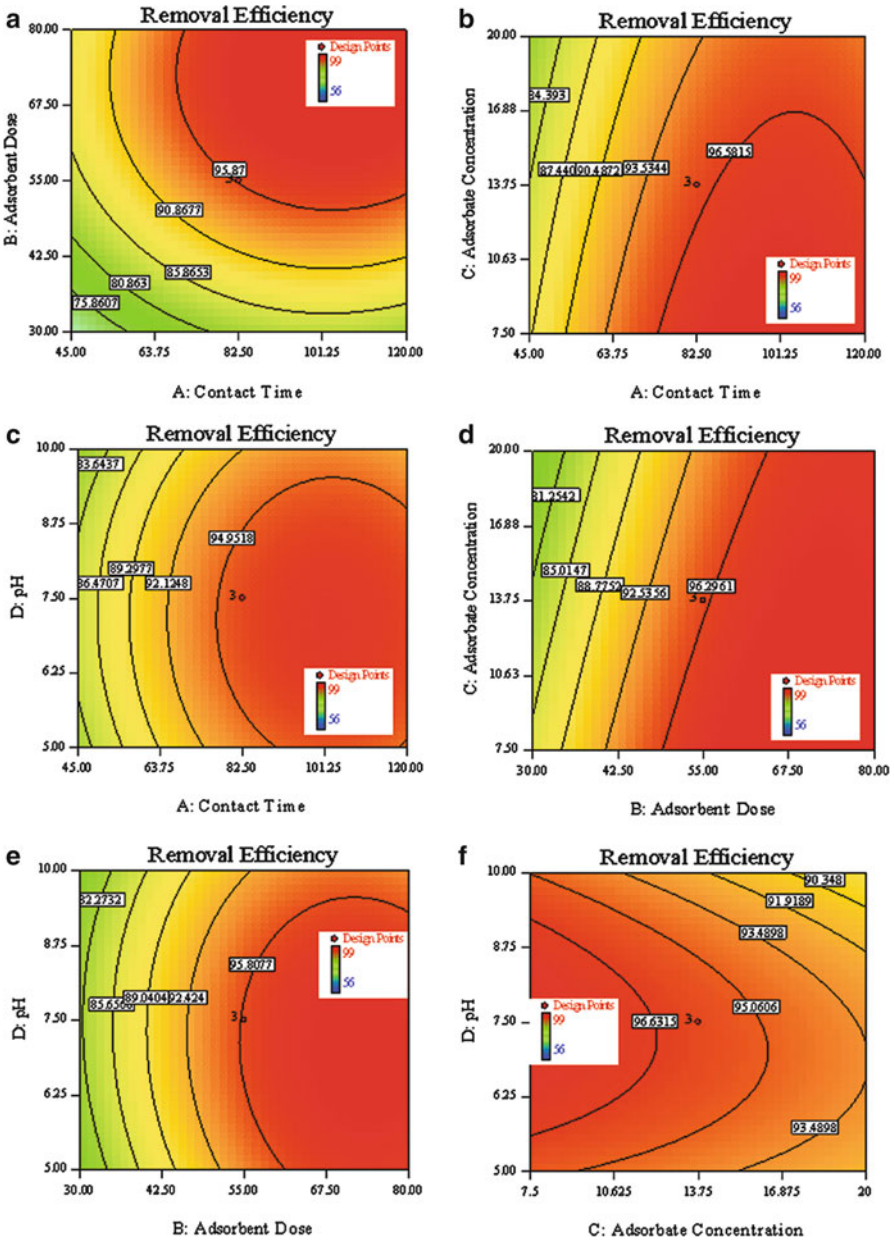

Fig. 8.3 Contour response surface plots for phosphate removal (%): (**a**) Effect of adsorbent dose and contact time. (**b**) Effect of adsorbate concentration and contact time. (**c**) Effect of pH and contact time. (**d**) Effect of adsorbate concentration and adsorbent dose. (**e**) Effect of pH and adsorbent dose. (**f**) Effect of pH and adsorbate concentration

basis that at pH less than pH_{zpc} (7.51) of the adsorbent, the surface charge of the adsorbent is positive, so Columbic attraction between the binding sites and phosphate ions leads to a higher phosphate uptake. At pH higher than $pH_{zpc,}$ the negative surface charge of the adsorbents repels the phosphate anions and resulting in lower removal efficiency (Rout et al. 2014a). In Fig. 8.3d the effect of both the parameters thwarts each other. Increasing adsorbent dose has positive effect while decreasing initial adsorbate concentration shows positive effect. So maximum removal efficiency was realized at 55 gL^{-1} of adsorbent dose and 13.75 mgL^{-1} initial phosphate concentrations. Figure 8.3e clearly demonstrates the dominance of adsorbent dose on removal efficiency while pH was showing almost no effect. In case of Fig. 8.3f, decreasing both the parameters has influential effect on removal efficiency. Maximum removal efficiency of 96.63 % was achieved at pH approximately 5.5 and initial phosphate concentration 7.5 mgL^{-1}.

3.4 Process Optimization and Experimental Validation

Optimization was done by applying a multiple response method, called desirability function (D) (Rout et al. 2015b). In point optimization of phosphate removal, maximum removal efficiency, minimum adsorbent dose, maximum initial phosphate concentration, contact time in the range (45–120 min) and pH in the range (5–10) were selected as the most desirable targeted criteria for the optimum response. Out of 18 alternative solutions, the maximum desirability was found to be a removal efficiency of 86.05 % at an adsorbent dose of 38.42 gL^{-1}, initial phosphate concentration of 20 mg L^{-1}, contact time of 104.53 min, pH 7.03 and with a desirability level of 0.835. To check the adequacy of the suggested optimum set of parameters, confirmatory experiments were carried out in replicates keeping all the optimized parameters constant. The resultant removal efficiency (85.19 %) was close to the predicted value by the model, with the percentage errors of 0.86 %. The good agreement between the predicted and experimental results validated the results of response surface optimization and its usefulness in predicting the responses at optimal operating conditions.

3.5 Equilibrium Kinetics and Isotherms Studies

The experimental data were fitted to linearized forms of Langmuir and Freundlich isotherm models and pseudo-first order and pseudo-second order kinetic models. The kinetic parameters along with R^2 values for all the models are given in Table 8.4. From the table, it is observed that the Langmuir isotherm showed good fit ($R^2 = 0.98$) to the experimental data than that of Freundlich isotherm ($R^2 = 0.96$). Thereby, confirming monolayer sorption on surfaces containing finite numbers of identical active sites (Rout et al. 2015c). Similarly good fit pseudo-second order

Table 8.4 Parameters of isotherm and kinetics models

Langmuir model	q_m (mg g^{-1})	b (L mg^{-1})	R^2
	0.56	1.67	0.98
Freundlich model	K_f (mg g^{-1})	n	R^2
	0.27	2.99	0.96
Pseudo first-order model	q_e (mg g^{-1})	k_1 (min^{-1})	R^2
	0.43	−0.078	0.54
Pseudo second-order model	q_e (mg g^{-1})	k_2 (g (mg min) $^{-1}$)	R^2
	0.35	0.26	0.99

model with R^2 value (0.99) than that of the pseudo-first order model ($R^2 = 0.54$) explains the proportionality relationship of the rate of adsorption with the square of the number of unoccupied sites on the adsorbent surface and the concentration of the adsorbate in the solution (Rout et al. 2015c).

4 Conclusions

The present study has confirmed RS as an efficient adsorbent for the phosphate removal from aqueous solution. The adsorption of phosphate was supported by the appearance of phosphorous in EDS spectrum of spent adsorbent. Statistical modelling generated quadratic model phosphate removal, with high R^2 value of 0.98. At optimized conditions of the process variables as recommended by the response surface, experimental validation resulted in 85.19 % phosphate removal. Well fitted experimental data to Langmuir isotherm model and pseudo-second order reaction kinetic models, confirms monolayer adsorption where, both adsorbent and adsorbate concentration administer the phosphate adsorption process. The statistical designing, modelling and optimization study could be able to evaluate the performance and established RS as an effective adsorbent for removal of phosphate from aqueous solutions. High efficiency and abundant availability make RS a prospective low cost adsorbent for phosphate removal from wastewater.

Acknowledgement The authors are thankful to the School of Infrastructure, Indian Institute of Technology Bhubaneswar, India, for providing facilities to carry out the research work in the concerned area.

References

Box, G.E.P. and Draper, N.R. (1987). Empirical Model-Building and Response Surfaces. Wiley, New York.

Galalgorchev, H. (1992). WHO guidelines for drinking water quality. *Iwsa Specialized Conference on Quality Aspects of Water Supply*, **11:** 1–16.

Huang, W.Y., Zhu, R.H., He, F., Li, D., Zhu, Y. and Zhang, Y.M. (2013). Enhanced phosphate removal from aqueous solution by ferric-modified laterites: Equilibrium, kinetics and thermodynamic studies. *Chem. Eng. J*., **228:** 679–687.

Majed, N., Li, Y. and Gu, A.Z. (2012). Advances in techniques for phosphorous analysis in biological sources. *Curr. Opin. Biotech*., **23:** 852**–**859.

Mateus, D.M.R., Vaz, M.M.N. and Pinho, H.J.O. (2012). Fragmented limestone wastes as a constructed wetland substrate for phosphorous removal. *Ecol. Eng*., **41:** 65–69.

Rout, P.R., Dash, R.R. and Bhunia, P. (2015a). Nutrient removal from domestic wastewater: An Environmental Biotechnology approach. *In:* Advances in Environmental Sciences and Engineering, A.K. Dash and M. Das (eds), vol. 1. Astral International Pvt. Ltd., New Delhi.

Rout, P.R., Bhunia, P. and Dash R.R. (2015b). Effective utilization of a sponge iron industry by-product for phosphate removal from aqueous solution: A statistical and kinetic modeling approach. *J. Taiwan Inst. Chem. Eng*., **46:** 98–108.

Rout, P.R., Bhunia, P. and Dash, R.R. (2015c). A mechanistic approach to evaluate the effectiveness of red soil as a natural adsorbent for phosphate removal from wastewater. *Desalin. Water. Treat*., **54:** 358–373.

Rout, P.R., Bhunia, P. and Dash R.R. (2014a). Modelling isotherms, kinetics and understanding the mechanism of phosphate adsorption onto a solid waste: Ground Burnt Pattie. *J. Environ. Chem. Eng*., **2:** 1331**–**1342.

Rout, P.R., Dash, R.R. and Bhunia, P. (2014b). Modeling and packed bed column studies on adsorptive removal of phosphate from aqueous solutions by a mixture of ground burnt patties and red soil. *Adv. Environ. Res*., **3:** 231–251.

Wang, X.H., Liu, F.F., Lu, L., Yang, S., Zhao, Y., Sun, L.B. and Wang, S.G. (2013). Individual and competitive adsorption of Cr (VI) and phosphate onto synthetic Fe-Al hydroxides. *Colloid Surface A*., **423:** 42–49.

Yuan, M., Carmichael, W.W. and Hilborn, E.D. (2006). Microcystin analysis in human sera and 469 liver from human fatalities in Caruaru, Brazil 1996. *Toxicon*, **48:** 627–640.

Zong, E., Wei, D., Wan, H., Zheng, S., Xu, Z. and Zhu, D. (2013). Adsorptive removal of phosphate ions from aqueous solution using zirconia-functionalized graphite oxide. *Chem. Eng. J*., **221:** 193–203.

Chapter 9
Removal of Pharmaceuticals from Water Using Adsorption

V. Arya and Ligy Philip

1 Background

Drinking water should be free from any kind of contamination. The source of water can be surface water or groundwater. The conventional water treatment plant takes care of most of the organic contaminants and pathogens. However, analysis of water samples by various researchers showed that the water bodies are contaminated with more complex compounds which are toxic at very low concentrations. Extensive research on these compounds started in mid 1990s with the use of more sophisticated instruments (Santos et al. 2010). These compounds are known as emerging contaminants (ECs) which are widely being studied because of their potential to cause long-term effects to living organisms. Even at very low concentration (μg/L to ng/L), these compounds have very high hazard quotient. Many studies have reported the presence of ECs in surface water and ground water. There is lack of knowledge of their impact in long-term effect on human health, environment and aquatic environments (Deblonde et al. 2011).

Emerging contaminants include endocrine disrupting compounds (EDCs), pharmaceutically active compounds (PhACs) and personal care products (PCPs). ECs can cause serious health effects to the ecosystem (Daughton and Ternes 1999). The removal of these compounds become difficult as these are present at very low concentrations. There is no regulation in the water quality standards for these contaminants. Hence, there is no measure to monitor these compounds in the effluents of wastewater treatment plants (WWTPs). Besides, complete information about the toxicity of these compounds is also not available. These compounds are getting into the water through municipal sewage. Major part of the ingested

V. Arya • L. Philip (✉)
Environmental and Water Resources Engineering Division, Department of Civil Engineering, IIT Madras, Chennai 600 036, India
e-mail: ligy@iitm.ac.in

F. Kurisu et al. (eds.), *Trends in Asian Water Environmental Science and Technology*, DOI 10.1007/978-3-319-39259-2_9

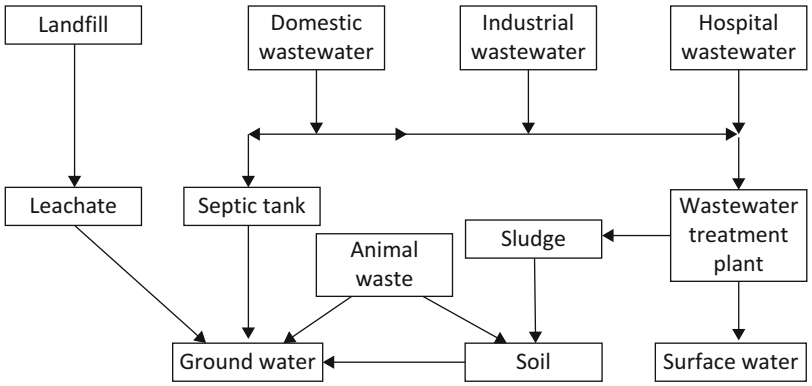

Fig. 9.1 Major sources and pathways of ECs in the environment

pharmaceuticals is excreted from the body, and subsequently gets discharged into the wastewater. Most of the conventional WWTPs are incapable of removing these contaminants (Petrovic 2003). As a result, these compounds will be present in WWTP effluent discharged into the water bodies. Many a time, this water will be used as the source for water supply in the cities located downstream. As a result, human beings are getting exposed to these compounds very regularly. Many studies have identified the presence of these compounds in WWTP effluent (Kumar et al. 2008; Mutiyar and Mittal 2014), surface water (Selvaraj et al. 2014; Shanmugam et al. 2014), groundwater (Sacher et al. 2001), and even in drinking water (Benotti et al. 2009). Figure 9.1 shows various sources and pathways of ECs in the environment.

The ECs were first identified in surface water three decades ago in USA. After that, numerous studies were carried out in USA, Europe and some parts of Asia which reported the presence of various ECs in surface water posing threat to human and aquatic life. There are only a few studies reporting the concentration of emerging contaminants in surface water in India. The most significant study was the analysis of pharmaceuticals from the effluents of pharmaceutical industries in Patancheru (Larsson et al. 2007), which is one of the leading production sites in world market. Studies reported the presence of antibiotics and EDCs in WWTP effluents and in hospital wastewater (Diwan et al. 2010; Kumar et al. 2008; Mutiyar and Mittal 2014). Ramaswamy et al. (2011) analyzed antiepileptic, antimicrobial and preservative compounds in surface water and sediment from the Kaveri, Vellar and Tamiraparani rivers, and in the Pichavaram mangrove in Tamil Nadu, India. Recent studies reported the presence of bisphenol A, alkylphenol ethoxylates and non-steroidal anti-inflammatory drugs, namely, diclofenac, ketoprofen, naproxen, ibuprofen, and acetylsalicylic acid in ng/L in the above locations (Selvaraj et al. 2014; Shanmugam et al. 2014).

2 Adverse Effects of ECs

Pharmaceuticals are extremely important as emerging contaminants because continuous consumption through drinking water even at very low concentrations can cause irreversible effect on human health. Studies have been conducted on aquatic organisms to measure toxicity in terms of growth rate, bioaccumulation, reproduction, geno-toxicity and morphological and physiological abnormalities (Santos et al. 2010). There have been evidences on feminization of fish and significant changes in physiological functions due to the presence of EDCs in surface water and wastewater effluent (Beijer et al. 2013; Larsson et al. 1999). Antibiotics are widely studied because of their utmost importance. Continuous exposure to antibiotics may lead the microbes to become resistant against these medicines. There have been evidences on the presence of antibiotic resistant bacteria in wastewater effluents (Diwan et al. 2010; Kümmerer 2004). Studies have reported the undesired effects of ECs, in particular EDCs, in higher organisms such as rats and alligators (Guillette Jr. et al. 1994; Kumar et al. 2008). All these data show that even in trace amounts, ECs can cause significant effects to the environment. There is not much data available on the toxicity to humans due to consumption of water containing ECs (Daughton and Ternes 1999; Stackelberg et al. 2004). However, possibility of future generations getting affected irreversibly cannot be ignored.

The fate of the compound during treatment depends on the nature of compound and treatment schemes adopted. Even though the compound is not identified in effluent, it may be present in some other form as a metabolite (Daughton and Ternes 1999). Hence, it is important to understand the fate of these compounds in generally adopted treatment schemes. The increased toxicity at very low concentrations, bioaccumulation, antibacterial resistance and the persistence of ECs after conventional WWTP necessitates the use of advanced treatment technologies or modifying the existing treatment schemes for water treatment. Various treatment technologies are available for the removal of emerging contaminants from water. Depending on the technology adopted, the compounds get completely mineralized, converted to intermediate forms, adsorbed to material used for removal or become more hydrophilic and more persistent. Hence, suitable technology should be selected considering the objective.

3 Treatment Technologies

Even though the treatment plants are efficient in removing the pollutant load and nutrients from wastewater, the removal of ECs is not promising. The removal of ECs in conventional treatment is complex because of their diverse physicochemical properties. Removal efficiencies in WWTPs range from 20 to 90 % depending on the technology adopted and the compound to be removed. A lot of studies have been conducted to assess the ability of the conventional treatment methods to

Table 9.1 Removal of ECs by various conventional treatment technologies

Treatment	Advantages	Disadvantages	References
Adsorption using activated carbon	Efficient in removing non-polar compounds (log Kow > 2). It can be coupled with ozonation and coagulation to improve the efficiency.	Polar compounds are not removed. Presence of DOM, solubility of compounds and contact time affect the efficiency.	Kim et al. (2007), Snyder et al. (2007), and Westerhoff et al. (2005)
Activated sludge process	Commonly used in WWTPs and cheapest treatment option. Only less number of ECs are removed efficiently.	Most of the compounds present as ions at neutral pH bypass the treatment. Increase in SRT enhances the removal.	Bolong et al. (2009) and Clara et al. (2005)
MBR	Flexibility to operate at high MLSS concentration and increased SRT. MBR coupled with RO shows higher removal efficiency. More diversity of microbes, over effluent quality is improved.	Removal due to biosorption requires further sludge treatment, high capital and operating costs.	Clara et al. (2005), Dolar et al. (2012)
Advanced oxidation processes	Use of reactive oxygen species with high oxidation potential. Can be used as tertiary treatment for the compounds escaping the pretreatment processes.	Needs UV for most of the treatments which makes the system expensive. High doses are required for efficient removal of ECs.	Adams et al. (2002), Andreozzi et al. (2004), and Pereira et al. (2007)

remove ECs. Comparison of different treatment technologies is presented in Table 9.1. Previous studies reported that coagulation and flocculation are not effective in removing ECs from water (Adams et al. 2002; Westerhoff et al. 2005). However, Snyder et al. (2007) reported that compounds with log Kow value greater than 5 can be removed by coagulation if they are present in anionic form. Adsorption, membrane processes and advanced oxidation are reported to remove ECs from water to some extent.

4 Clay as Adsorbent

There are many studies on the removal of pharmaceuticals using activated carbon (Westerhoff et al. 2005; Snyder et al. 2007). However, the fate of pharmaceuticals during adsorption depends on their partition coefficient, pH of solution and sorption coefficient. Clay is a natural adsorbent for most of the pollutants. Use of clay as an alternative to conventional adsorbents can reduce the cost of the treatment. Clay minerals are hydrous aluminum or magnesium phyllosilicates containing iron, magnesium, alkali and alkaline earth metals and other cations present either in

the interlayer space or in the clay lattice (Zhou and Keeling 2013). The layered structure of clay minerals makes them good adsorbent by adsorbing guest species to the interlayer space. The ions present in the interlayer spaces are Ca^{2+}, Mg^{2+}, Na^{+}, K^{+} etc. These ions have high hydration energies thereby making clay minerals hydrophilic in nature.

Clay minerals obtained considerable attention in adsorption due to their large surface area, swelling properties, strong electrostatic interactions and micro to nano sized particles (Zhou and Keeling 2013). There are a number of methods to change the adsorption properties and surface characteristics of clay particles. Commonly used method is modifying clay minerals by cationic or anionic surfactants and the clay synthesized using organic molecules is termed as organo clay. Organo clay is synthesized by intercalation of organic molecule to the interlayer space of clay. This happens mainly through cation exchange mechanism. During the preparation of organoclays, organic cations replace the inorganic cations in the interlayer spaces and on the external surfaces of clay particles (Wu et al. 2014). This leads to an increase in interlayer spacing, thereby accommodating large organic molecules from water. Changes in the interlayer structure of clay are shown in Fig. 9.2. While modifying clay using surfactant, surfactant retention occurs within the interlayer space of clay and other layers of silicates present. These modified clay exhibits hydrophobicity and can adsorb organic contaminants. Adsorption of non-polar organics will be followed by the uptake of counter ions and these counter ions further enhance the adsorption of anionic pollutants from water (Xu and Boyd 1995). A number of studies using organo clay for the removal of contaminants from water have been conducted in the past. However, studies aiming at the removal of pharmaceuticals from water are less. Table 9.2 lists studies conducted using different types of clays in removing pharmaceuticals from water.

Proper selection of treatment is important in the removal of ECs from the environment. Low cost adsorbents can be an alternative to conventional adsorbents. Clay adsorbents are proven to be efficient in batch studies and as adsorption column. Modified adsorbents can be applied in field as permeable barrier which can improve the natural treatment processes. Research in this area requires more attention. The main problem faced in adsorption is the regeneration of adsorbent. Thermal regeneration is not feasible in most of the cases as it can affect the stability of the adsorbent. Other methods such as biodegradation, photo-oxidation and

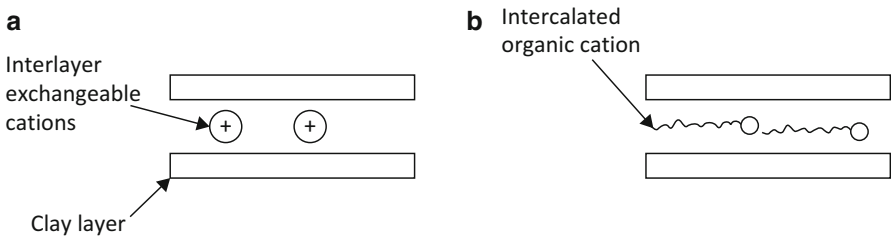

Fig. 9.2 Layered structure of clay before (**a**) and after (**b**) modifying using organic cations

Table 9.2 Selected studies on removal of pharmaceuticals using different clay adsorbents

Material used	Target pollutants	Observations	References
BDMHDA modified montmorillonite	Tetracycline and sulfonamide antibiotics	Micelle-clay adsorption column was efficient compared to activated carbon column.	Polubesova et al. (2006)
Organo clay modified using tetrabutyl ammonium	Flurbiprofen	High adsorption capacity, mainly chemisorption and was found to be exothermic.	Akçay et al. (2009)
Montmorillonite and rectorite	Tetracycline	Clays can remove hydrophilic compounds by intercalation, adsorption is highly dependent on the pH.	Chang et al. (2009)
Aluminum pillared K10 and KSF (Al-K10 and Al-KSF)	Trimethoprim	Removal was dependent on pH of the solution, electrostatic interactions dominated adsorption process.	Molu and Yurdakoç (2010)
Montmorillonite, illite and rectorite	Ciprofloxacin	Adsorption was due to the electrostatic attraction of functional groups and hydrogen bonding.	Wang et al. (2011)
Zeolites and pure and modified clays using organic cations and transition metals	Salicylic acid, acetylsalicylic acid and atenolol	Adsorption capacities are dependent on the characteristics of the pharmaceuticals such as hydrophobicity and functional groups present.	Rakić et al. (2013)

chemical extraction of pollutants for regeneration of organo clay are reported (Zhu et al. 2009).

5 Experimental Studies on Organo Clay in Adsorbing Ciprofloxacin from Water

Previous studies have reported considerable adsorption of ciprofloxacin on montmorillonite minerals (Wang et al. 2011). Ciprofloxacin is a commonly used antibiotic. More than 70 % of the concentration consumed is excreted (Mompelat et al. 2009). Studies were done to compare the adsorption capacities of Na-Bentonite and organically modified bentonite. Surfactant CTAB (Cetyltrimethyl ammonium bromide) [$C_{16}H_{33}(CH_3)_3NBr$] was used to modify bentonite which had a CEC of 70 meq/100 g. Intercalation of the surfactant into the clay layer was verified by FTIR spectroscopy. Figure 9.3 shows the FTIR spectra of Na-Bentonite before and after modifying with CTAB. The common bands present in both the samples include -OH stretching of Al-OH and Si-OH at

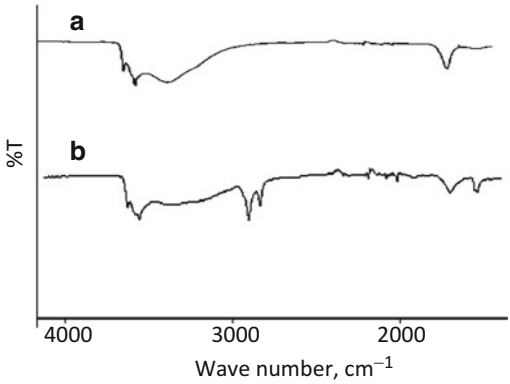

Fig. 9.3 FTIR spectra of bentonite (**a**) and modified bentonite (**b**)

3622 cm^{-1} and 3695 cm^{-1}, respectively (Suchithra et al. 2012). The bands near 2927 cm^{-1} and 2850 cm^{-1} represents the symmetric stretching vibrations of $–CH_2$ bonds and asymmetric stretching vibration of C-H bonds (Praus et al. 2006). This clearly indicates the intercalation of modifier in the interlayer space of clay. CTA ions get adsorbed on the clay due to electrostatic forces causing ion exchange (Praus et al. 2006). Further, it was reported that longer the surfactant chain length and higher the charge density of the clay, interlayer spacing of the clay will be increased (Rakic et al. 2013). Moreover, charge density of the layer would determine the orientation of organic cations in the clay lattice. Orientation of exchanged cations in organo clay could be identified by XRD analyses by observing the basal spacing.

In the present case, the surfactant loading was not exceeded above the cation exchange capacity (CEC) of the clay. It is evident that the properties of the clay will change with respect to the surfactant loading, chain length of the surfactant and clay mineral used. He et al. (2010) reported that the basal spacing of the clay minerals increased with increase in surfactant loading. However, for the experimental study, surfactant loading was not exceeded above CEC of the clay as it would increase the hydrophobicity. Depending on the requirement, optimized loading of the surfactant could be found out experimentally.

During kinetic adsorption studies, 1 g/L of adsorbent was used in solution containing 1 mg/L of ciprofloxacin. Adsorption equilibrium was reached within 6 h. Adsorption of ciprofloxacin was higher in modified bentonite. Nearly, 50 % of the compound was adsorbed to pure bentonite whereas 67 % of ciprofloxacin was adsorbed to organo clay as given in Fig. 9.4. Ciprofloxacin is polar in nature with low Kow values. In case of organically modified clay, hydrophilic head and hydrophobic tail of the surfactant in the interlamellar space of the clay will attract the polar and non-polar part of the molecules in the solution (Rakic et al. 2013). Ciprofloxacin would be present in zwitterionic form at neutral pH. Even then the main mechanism of adsorption to clay is assumed to be cation exchange, there could be limited amount of adsorption owing to the interaction of COO- group in ciprofloxacin with the cations in the interlayer space of clay (Wang et al. 2011).

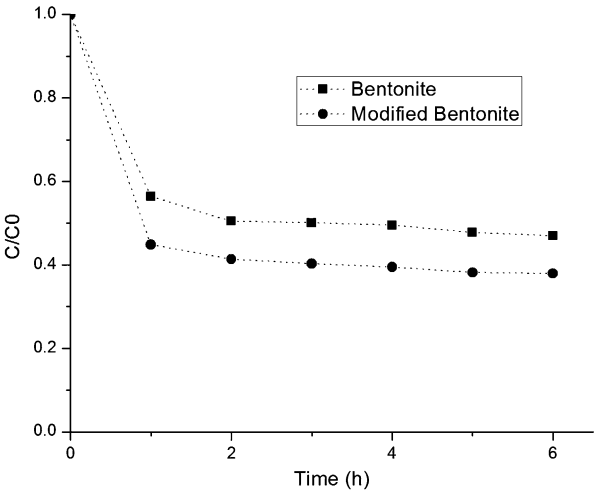

Fig. 9.4 Adsorption of ciprofloxacin on bentonite and modified bentonite

6 Conclusions

Removal of ECs from water and wastewater is not completely achieved in conventional treatment methods due to the complex nature of these compounds and their diverse chemical properties. Adsorption is found to be efficient in removing ECs from water and is used as a tertiary treatment. Modified clay adsorbents can be used to remove the pharmaceuticals from water if these materials possess the desired surface characteristics. Clay is mainly hydrophilic in nature which limits its applications in water treatment. Hydrophilic nature of the clay can be altered by incorporating surfactants into the interlayer space of the clay. Presence of surfactants significantly alters the hydrophilic-hydrophobic nature of the organoclay. Pharmaceuticals present in the water can get adsorbed onto the organo clay due to hydrophobic interactions or the bonding between the functional groups in the compounds to the clay surface. Surface characteristics of the organo clay can be controlled by the surfactant loading. However, extent of removal of the compound depends on the ionic form in which it is present at the desired pH. Column studies need to be done and a suitable method should be adopted for regeneration of adsorbents. The effect of DOM and presence of other ions in water should be considered before developing treatment scheme.

References

Adams, C., Wang, Y., Loftin, K. and Meyer, M. (2002). Removal of antibiotics from surface and distilled water in conventional water treatment process. *J. Env. Eng.*, **128:** 253–260.

Akçay, G., Kilinç, E. and Akçay, M. (2009). The equilibrium and kinetics studies of flurbiprofen adsorption onto tetrabutylammonium montmorillonite (TBAM). *Colloids Surfaces A Physicochem. Eng. Asp.*, **335(1–3):** 189–193.

Andreozzi, R., Campanella, L., Fraysse, B., Garric, J., Gonnella, A., Lo Giudice, R., Marotta, R., Pinto, G. and Pollio, A. (2004). Effects of advanced oxidation processes (AOPs) on the toxicity of a mixture of pharmaceuticals. *Water Sci. and Tech.*, **50(5):** 23–28.

Benotti, M.J., Trenholm, R.A., Vanderford, B.J., Holady, J.C., Stanford, B.D. and Snyder, S.A. (2009). Pharmaceuticals and endocrine disrupting compounds in U.S. drinking water. *Environ Sci Technol*, **43:** 597–603.

Beijer, K., Gao, K., Jönsson, M.E., Larsson, D.G.J., Brunström, B. and Brandt, I. (2013). Effluent from drug manufacturing affects cytochrome P450 1 regulation and function in fish. *Chemosphere*, **90(3):** 1149–1157.

Bolong N., Ismail F., Salim M. R., and Matsuura T. (2009). A review of the effects of emerging contaminants in wastewater and options for their removal. *Desalination*, **239(1–3):** 229–246.

Chang, P.-H., Li, Z., Jiang, W.-T. and Jean, J.-S. (2009). Adsorption and intercalation of tetracycline by swelling clay minerals. *Appl. Clay Sci.*, **46(1):** 27–36.

Clara M., Kreuzinger N., Strenn B., Gans O., and Kroiss H. (2005). The solids retention time-a suitable design parameter to evaluate the capacity of wastewater treatment plants to remove micropollutants. *Water Res.*, **39(1):** 97–106.

Daughton, C.G. and Ternes, T.A. (1999). Pharmaceuticals and personal care products in the environment: Agents of subtle change? *Environ. Health Perspect.*, **107(Suppl 6):** 907–938.

Deblonde, T., Cossu-Leguille, C. and Hartemann, P. (2011). Emerging pollutants in wastewater: A review of the literature. *Int. J. Hyg. Environ. Health*, **214(6):** 442–448.

Diwan, V., Tamhankar, A.J., Khandal, R.K., Sen, S., Aggarwal, M., Marothi, Y., Iyer, R.V., Sundblad-Tonderski, K., Stålsby-Lundborg, C. (2010). Antibiotics and antibiotic-resistant bacteria in waters associated with a hospital in Ujjain, India. *BMC Public Health*, **10:** 414.

Dolar, D., Gros, M., Rodriguez-Mozaz, S., Moreno, J., Comas, J., Rodriguez-Roda, I. and Barceló, D. (2012). Removal of emerging contaminants from municipal wastewater with an integrated membrane system, MBR-RO. *J. Hazard. Mater.*, **239–240:** 64–69.

Guillette Jr., L. J., T. S. Gross, G. R. Masson, N. M. Matter, H. F. Percival, and A. R. Woodward. (1994). Developmental abnormalities of the gonad and sex hormone concentrations in juvenile alligators from contaminated and control lakes in Florida. *Environmental Health Perspectives*, **104:** 680–688.

He, H., Ma, Y., Zhu, J., Yuan, P. and Qing, Y. (2010). Organoclays prepared from montmorillonites with different cation exchange capacity and surfactant configuration. *Appl. Clay Sci.*, **48 (1–2):** 67–72.

Kim, S.D., Cho, J., Kim, I.S., Vanderford, B.J. and Snyder, S.A.(2007). Occurrence and removal of pharmaceuticals and endocrine disruptors in South Korean surface, drinking, and waste waters. *Water Research*, **41:** 1013–1021.

Kumar, V., Chakraborty, A., Viswanath, G. and Roy, P. (2008). Androgenic endocrine disruptors in wastewater treatment plant effluents in India: Their influence on reproductive processes and systemic toxicity in male rats. *Toxicol. Appl. Pharmacol.*, **226(1):** 60–73.

Kümmerer, K. (2004). Resistance in the environment. *J. Antimicrob. Chemother.*, **54(2):** 311–320.

Larsson, D.G.J., Adolfsson-erici, M., Parkkonen, J., Pettersson, M. and Berg, A.H. (1999). Ethinyloestradiol—An undesired fish contraceptive ? *Aquat. Toxicol.*, **45:** 91–97.

Larsson, D.G.J., de Pedro, C. and Paxeus, N. (2007). Effluent from drug manufactures contains extremely high levels of pharmaceuticals. *J. Hazard. Mater.*, **148(3):** 751–755.

Molu, Z.B. and Yurdakoç, K. (2010). Preparation and characterization of aluminum pillared K10 and KSF for adsorption of trimethoprim. *Microporous Mesoporous Mater.*, **127(1–2):** 50–60.

Mompelat, S., LeBot, B. and Thomas, O. (2009). Occurrence and fate of pharmaceutical products and by-products, from resource to drinking water. *Environ Int*, **35:** 803–814.

Mutiyar, P.K. and Mittal A.K. (2014). Occurrences and fate of selected human antibiotics in influents and effluents of sewage treatment plant and effluent-receiving river Yamuna in Delhi (India). *Environ. Monit. Assess*., **186(1):** 541–557.

Petrovic, M. (2003). Analysis and removal of emerging contaminants in wastewater and drinking water. *TrAC Trends Anal. Chem*., **22(10):** 685–696.

Pereira, V. J.,Linden, K. G., and Weinberg, H. S.(2007) Evaluation of UV irradiation for photolytic andoxidative degradation of pharmaceutical compounds inwater. *Water Res* **41:**4413–23.

Polubesova, T., Zadaka, D., Groisman, L. and Nir, S.(2006).Water remediation by micelle–clay system: case study for tetracycline and sulfonamide antibiotics. *Water Res*., **40:** 2369–2374.

Praus P., Turicová M., Studentová S., and Ritz M. (2006). Study of cetyltrimethylammonium and cetylpyridinium adsorption on montmorillonite. *J. Colloid Interface Sci*., **304(1):** 29–36.

Rakić V., Rajić N., Daković A., and Auroux A. (2013). The adsorption of salicylic acid, acetylsalicylic acid and atenolol from aqueous solutions onto natural zeolites and clays: Clinoptilolite, bentonite and kaolin. *Microporous Mesoporous Mater*., **166:** 185–194.

Ramaswamy, B.R., Shanmugam, G., Velu, G., Rengarajan, B. and Larsson, D.G.J. (2011). GC-MS analysis and ecotoxicological risk assessment of triclosan, carbamazepine and parabens in Indian rivers. *J. Hazard. Mater*., **186(2–3):** 1586–1593.

Santos, L.H.M.L.M., Araújo, A.N., Fachini, A., Pena, A., Delerue-Matos, C. and Montenegro, M. C.B.S.M. (2010). Ecotoxicological aspects related to the presence of pharmaceuticals in the aquatic environment. *J. Hazard. Mater*., **175(1–3):** 45–95.

Selvaraj, K.K., Shanmugam, G., Sampath, S., Larsson, D.G.J. and Ramaswamy, B.R. (2014). GC-MS determination of bisphenol A and alkylphenol ethoxylates in river water from India and their ecotoxicological risk assessment. *Ecotoxicol. Environ. Saf*., **99:** 13–20.

Shanmugam, G., Sampath, S., Selvaraj, K.K., Larsson, D.G.J. and Ramaswamy, B.R. (2014). Non-steroidal anti-inflammatory drugs in Indian rivers. *Environ. Sci. Pollut. Res. Int*., **21(2):** 921–931.

Snyder S., Wert E., and Lei H. (2007). Removal of EDCs and pharmaceuticals in drinking and reuse treatment processes. AWWA Research Foundation, IWA Publishing.

Stackelberg, P.E., Furlong, E.T., Meyer, M.T., Zaugg, S.D., Henderson, A.K., and Reissman, D.B. (2004) Persistence of pharmaceutical compounds and other organic wastewater contaminants in a conventional drinking-water-treatment plant. *Sci. Total Environ*., **329 (1–3):** 99–113.

Wang, C.-J., Li, Z. and Jiang, W.-T. (2011). Adsorption of ciprofloxacin on 2:1 dioctahedral clay minerals. *Appl. Clay Sci*., **53(4):** 723–728.

Westerhoff P., Yoon Y., Snyder S., and Wert E. (2005). Fate of endocrine-disruptor, pharmaceutical, and personal care product chemicals during simulated drinking water treatment processes. *Environ. Sci. Technol*., **39(17):** 6649–6663.

Wu, L., Liao, L., Lv, G., Qin, F. and Li, Z. (2014). Microstructure and process of intercalation of imidazolium ionic liquids into montmorillonite. *Chem. Eng. J*., **236:** 306–313.

Xu, S., and Boyd, S. A.(1995). Cationic surfactant sorption to a vermiculitic subsoil via hydrophobic bonding. *Environ. Sci. Technol*., **29:** 312–320.

Zhou, C.H. and Keeling, J. (2013). Fundamental and applied research on clay minerals: From climate and environment to nanotechnology. *Appl. Clay Sci*., **74:** 3–9.

Zhu R., Zhu J., Ge F., and Yuan P. (2009). Regeneration of spent organoclays after the sorption of organic pollutants: A review. *J. Environ. Manage*., **90(11):** 3212–6.

Part III
Hydrological and Quality Issues: Surface Water

Chapter 10
Hydrological Regimes and Zooplankton Ecology at Tempe Floodplains, Indonesia: Preliminary Study Before the Operation of the Downstream Barrage

Reliana Lumban Toruan and Fajar Setiawan

1 Introduction

Floodplain is one of a very productive ecosystems (Ning et al. 2013) and harbours high biodiversity of micro-invertebrate (Shiel et al. 1998). Flood and drought cycles induce high biodiversity, and thus productivity, in the floodplain systems where connectivity between terrestrial and aquatic component plays an important role (Schöll et al. 2012; Armitage et al. 2003). Floodplain ecosystem features a network of riverine, and ditches habitats (Armitage et al. 2003), where flood events form a large inundated area by which the terrestrial and aquatic ecosystems are connected. During drought phase, habitats in riverine-floodplain systems are fragmented and isolated from the main river channel forming distinct habitats with distinctive abiotic and biotic characteristics (Thomaz et al. 2007). As opposed to dry condition, floods will reconnect the fragmented habitats, allowing the connectivity between riverine and floodplain systems; and reduce spatial variability within patchy habitats which are formed during low water period. A number of studies suggest that increasing water level during floods event results in increasing similarity between habitats as the connectivity established (Thomaz et al. 2007; Tockner et al. 2000). It is clear that hydrological regime is the key driving force of ecological function and biodiversity in floodplain systems. There have been little study conducted about zooplankton from the floodplain of tropical regions, especially, Indonesia, one of the world's biodiversity "hotspots". This preliminary study has, therefore, summarised the diverse assemblages of zooplankton of Lake Tempe as a response to changing water level during dry and flood seasons. Planktonic organisms, including zooplankton, are the key elements in the aquatic environment (Palmer

R.L. Toruan (✉) • F. Setiawan
Research Centre for Limnology, Indonesian Institute of Sciences, Cibinong Science Centre and Botanical Garden, Jl. Raya Bogor Km 46 Cibinong, 16911 West Java, Indonesia
e-mail: reliana@limnologi.lipi.go.id

F. Kurisu et al. (eds.), *Trends in Asian Water Environmental Science and Technology*, DOI 10.1007/978-3-319-39259-2_10

and Yan 2013). The responses of zooplankton to changing environment due to fluctuated water level are fundamental to our understanding of the dynamic of planktonic organisms in floodplain habitats, mainly where they are moderately or heavily regulated.

Lake Tempe is a riverine floodplain lake undergoing significant changes on water level that affected the adjacent water course. Hydrological regimes of Lake Tempe floodplain provide a chance to study the zooplankton dynamic in the lake. The area of wetland was highly influenced by fluctuating water level resulting in periodical inundation and drying cycles. Tempe system surface area ranges from 280 to 430 km^2 with a maximum depth of 9 m during extreme high water level where only about 10 km^2 remain inundated during low water period with a maximum depth of 1.5 m. In 2012, barrage at the downstream point was constructed in order to regulate water level of the lakes and was planned to operate in late 2013. The barrage will be closed during dry period to maintain water level at 5 m above sea level (asl) or 3 m water depth. Floodplain ecosystem is the most productive ecosystem where drying and flooding cycles play an important factor in ecosystem richness. Zooplankton responds differently to hydrological variable depending on the environmental factors and the biology of zooplankton (Crome and Carpenter 1988). Our study aims to look at the hydrological characteristic of Tempe floodplain and its association with zooplankton community. The study was conducted during low water (LW) period in 2012 and high water (HW) period in 2013 to look at the characteristics of hydrological parameters and its association with zooplankton community specifically before the operation of the downstream barrage.

2 Materials and Methods

As part of multidisciplinary study on limnological and hydrological characteristics of floodplain lakes in Indonesia, field surveys were conducted in October 2012 (LW) and June 2013 (HW) in Tempe Floodplain to measure hydrological parameter including water discharge, water level and sedimentation rate, in situ water quality measurement and qualitative sampling of zooplankton. Sampling for all water quality parameters and zooplankton was done in seven stations; TMP1, 2, 3, 4, 5, 6 and 7, where TMP refers to Lake Tempe. Sedimentation rates were measured by placing sedimentation trap at fixed point for a minimum of 24 h; sedimentation rate was then calculated as settling velocity of suspended solid per day ($mg/cm^2/day$). In situ water quality data were recorded by use of HORIBA water quality checker while other chemical parameters were analysed in laboratory according to standard method for water and waste analysis (APHA 2013). Samples for qualitative analyses of zooplankton were taken from the pelagial and littoral zone with a vertical tow of plankton net. Thirty litres water integrating the water column from bottom to surface was collected and filtered through a 40-μm mesh sieve plankton net and preserved with 4 % formalin. The period of sampling coincided with extreme drought in 2012 and large flood event in 2013. Figure 10.1 shows landsat imagery

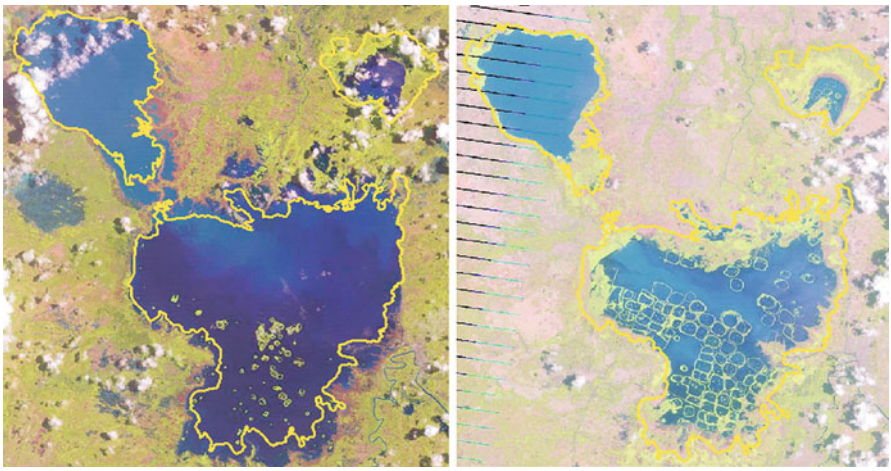

Fig. 10.1 Landsat images showing high water level (*left*) observed in April 1989 and low water level (*right*) observed in October 2012 (Landsat images were processed by F. Setiawan in 2013)

of the recorded large flood event back in 1989 and drought condition recorded during sampling period. We were not able to produce image of flood event in 2013 due to time and data limitation. The figures show habitat disconnectivity between the main floodplain (Lake Tempe) and the adjacent water courses during dry condition.

3 Results and Discussion

3.1 Environmental Variables

Lake Tempe experienced hydrological changes associated with variation in discharge from three river systems feeding the lake and with the rainfall events. During our study period, significant increase of water level in Lake Tempe was observed from May to July where the maximum area of inundation reached in July; then water slowly decreased and reached the lowest water level in November. Maximum and minimum water levels during LW and HW were 1.5 m and 0.4 m; and 1.7 m and 5 m respectively. Sedimentation rate was 49.9 mg/cm^2/day (the highest rate) at TMP1 and 13.1 mg/cm^2/day (the lowest) at TMP7 (Table 10.1).

Annual precipitation rate in Lake Tempe is highly variable with the highest rate being recorded was 5300 mm which usually occurs in April to June, while the lowest rainfall data has been observed at only 980 mm which occurs during October to November. Highly variable precipitation rate at the catchment reflected in water level fluctuation as shown in Fig. 10.2.

Table 10.1 Summary of average in-situ water quality parameters and zooplankton species composition

Env. parameter	LW	HW
Max depth (cm)	95	350
Min depth (cm)	25	300
Sechi depth (cm)	5–15	54–70
Average temperature (°C)	30.5	29
Dissolved oxygen (mg/L)	5.6–9.03	2.4–8.02
pH	7.1	7.5
Conductivity (μS/cm)	265	191.5
Total nitrogen (TN) (mg/L)	0.506	1.398
Total phosphate (TP) (mg/L)	0.161	0.129
Total suspended solid (TSS) (mg/L)	171.14	95
Zoop. composition		
Copepods	10	22
Cladocers	11	11
Rotifers	47	15
Total abundancy (ind/L)	2680	844

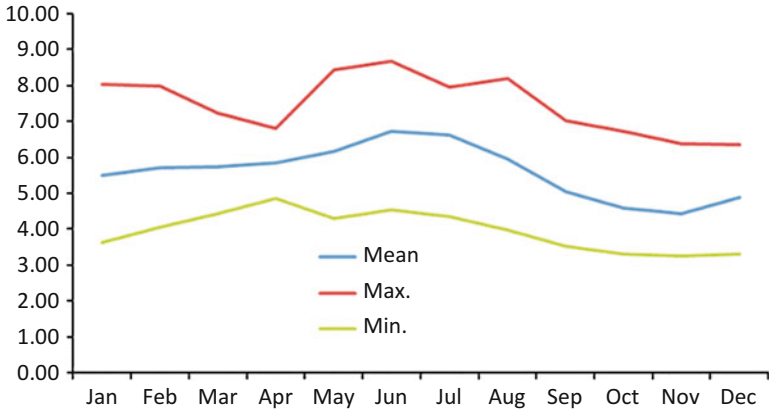

Fig. 10.2 Monthly water level fluctuation at Lake Tempe (graph was generated according to data from 1978 to 2001)

3.2 Zooplankton

Sixty-eight zooplankton species were identified during LW including ten copepods, 11 cladocerans, and 47 rotifers, whereas 48 species were identified during HW consisting of 22 copepods, 11 cladocerans and 15 rotifers. Rotifer was dominant during LW period which then were shifted by micro crustacean population during HW, showing a clear species succession between the two hydrological periods. Rotifers, which were well adapted to low water habitat, were the most abundant species, with species from genus Brahchionus dominant in LW. Copepods of the family Diapthomidae (naupli, copepodit and adults) were the most abundant group

in HW followed by cyclopoid and cladocerans. Figure 10.3a, b shows the separation of the main zooplankton group, shifting the community structure from LW species to HW species. The list of species and code used for ordination purposes is presented in Table 10.2.

Species numbers as well as the abundance were higher in LW than in HW period suggesting that low water period is the period where zooplankton recruitment is high especially for benthic and littoral species (e.g. Rotifers). Rotifers are food resources for micro crustacean that will start to colonise as flood occurs, and further support fish productivity. Thus, low water period is also critical as it provides suitable environment for food recruitment to support the foodweb.

During large flood events, habitat connectivity between river and the lakes is high and there are larger freshly inundated areas allowing plankton groups to dominate the habitat before the higher trophic organisms taking over. At this stage it is suggested that the bottom up pressure (e.g. water quality, hydrological regimes and other abiotic factors) regulate the zooplankton assemblage (Shiel et al. 2006; Pinel-Alloul and Mimouni 2013) before top-down forces influence the habitat when all biotic groups are established. Our study indicates that beta diversity is also decreasing in flood season, and thus spatial variability within study site is also lessened. Similar finding was observed by Deksne and Škute (2011) who studied the relationship between ecohydrological factors and the zooplankton assemblages in the Daugava River. They suggested that during dry period the abundance of rotifers is also correlated with the low concentration of dissolved oxygen. Rotifers are more tolerant to low oxygen compared to cladocerans and copepods as they respire through their body surface and, thus, utilise the available oxygen effectively. Furthermore, high turbidity and suspended solid during dry period are negatively correlated with the abundance and biomass of micro crustaceans (Škute et al. 2008). In this condition, rotifers fared better as they indirectly benefited from the alleviated impact of competition and predation with other zooplankton groups in high turbidity and suspended solid during low water period (Thorp and Mantovani 2005). This result is also in agreement with other findings from various studies of different floodplain systems (Shiel 1985; Beaver et al. 2013; Shiel et al. 2006).

Overall, our result revealed low species richness in Lake Tempe floodplain compared to other related studies that relate hydrological regimes with zooplankton assemblages. For example, Shiel et al. (1998) identified more than a 100 species of rotifers from arid floodplain of Australia; similarly 164 rotifers species have been recorded from Brahmaputra basin (Sharma 2005). A recent study shows that floodplain ecosystem is a home for high value of biodiversity (Shiel et al. 2006). Therefore, we suggest that tropical floodplain ecosystems potentially harbour higher biodiversity and species richness than our current records. In addition, the abiotic and biotic condition in lotic systems of the riverine sections of the floodplain are varied and changeable. Consequently data can differ time to time and, hence long-term study is needed to fully understand the effect of hydrological regimes on floodplain planktonic organism, importantly in tropical regions.

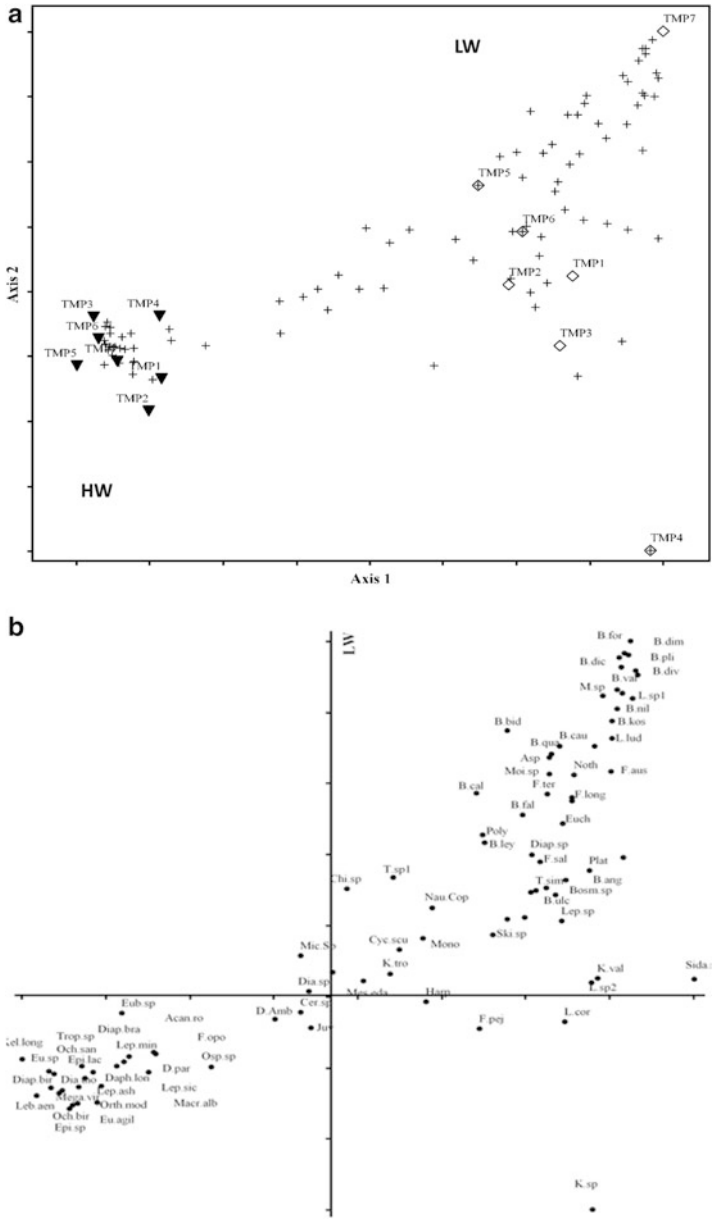

Fig. 10.3 (**a**) Ordination of Nonmetric Multi-Dimensional Scale (NMDS) graph showing the separation of zooplankton assemblages between the two hydrological phases (High and Low water periods). (**b**) NMDS ordination showing the separation of zooplankton species between the two hydrological phases (High and Low water periods)

Table 10.2 Zooplankton species list identified from Lake Tempe

Species code	Species list	Species code	Species list
Dia.sp	*Diaptomus* sp.	B.ley	*B.leydigi*
Ski.sp	*Skistodiaptomus* sp.	B.cau	*B.caudatus*
Lep.sp	*Leptodiaptomus* sp.	B.fal	*B.falcatus*
Och.san	*Ochyodiaptomuss sanguenensis*	B.for	*B.forficula*
Och.bir	*Ochyodiaptomuss birgei*	B.bid	*B.bidentatus*
Lep.min	*Leptodiaptomus minutus*	B.qua	*B.quadridentatus*
Lep.sic	*Leptodiaptomus sicilis*	B.var	*B.variabilis*
Lep.ash	*Leptodiaptomus ashlandi*	B.kos	*B.kostei*
Epi.lac	*Epischura lacustris*	B.ses	*B.sesilis*
Epi.sp	*Epischura* sp.	B.pli	*B.plicatilis*
Osp.sp	*Ospranticum* sp.	B.dim	*B.dimidiatus*
Nau.Cop	Nauplius copepod	B.nil	*B.nilsoni*
Mic.Sp	*Microcyclops* sp.	B.ser	*B.sericus*
Dia.sp	*Diacyclops* sp.	B.ang	*B.angularis*
Dia.tho	*Diacyclops thomasi*	B.ulc	*B.ulceolaris*
Acan.ro	*Acanthocyclops robustus*	B.dic	*B.dichotomus*
Cyc.scu	*Cyclops scutiffer*	B.div	*B. diversicornis*
Mes.eda	*Mesocyclops edax*	B.sp	*B.sp1*
Trop.sp	*Tropocyclops* sp.	K.tro	*Keratella tropica*
Orth.mod	*Orthocyclops modestus*	K.val	*K.valga*
Macr.alb	*Macrocyclops albidus*	K.sp	*Keratella* sp.
Eu.agil	*Eucyclops agilis*	Kel.long	*Keliotica longispina*
Eu.sp	*Eucyclops* sp.	Noth	*Notholca* sp.
Mega.vir	*Megacyclops viridis*	Plat	*Plationus platulus*
Harp	*Harpaticoidea* sp.	Anur	*Anuraeopsis*
D.mag	*Daphnia magna*	F.long	*Filinia longiseta*
D.Amb	*Daphnia ambigua*	F.sal	*F.saltator*
D.Pul	*Daphnia pulex*	F.fas	*F.fassa*
D.men	*Daphnia mendotae*	F.pej	*F.pejleri*
D.par	*Daphnia parvula*	F.opo	*F.opoliensis*
Cer.sp	*Ceriodaphnia* sp.	F.ter	*F.terminalis*
Simo.sp	*Simocephalus* sp.	F.aus	*F.australensis*
Juv	*Juvenile cladoceran*	L.cor	*Lecane cornuta*
Diap.bra	*Diaphanosoma brachyurum*	L.sp2	*Lecane* sp1
Diap.bir	*Diaphanosoma birgei*	L.sp2	*Lecane* sp2
Daph.lon	*Daphnia longiremis*	L.lud	*Lecane ludwigi*
Bosm.sp	*Bosmina* sp.	M.cop	*Monostyla copies*
Eub.sp	*Eubosmina* sp.	M.sp	*Monostyla* sp.
Moi.sp	*Moina*	T.sim	*Trichocerca similis*
Sida.sp	*Sida* sp.	T.rou	*Trichocerca rouselleti*
Chi.sp	*Chidorus* sp.	T.sp1	*Trichocerca* sp1
Leb.aeb	*Leberis aenigmatosa*	Euch	*Euclanis* sp.
B.cal	*Brachionus calyciflorus*	Asp	*Asplanchna* sp.
Dicra	*Dicranophoroides* sp.	Poly	*Polyarthra remata*
		Mono	*Monoarthra* sp.

4 Conclusions

Based on our survey for each hydrological phase, we can say that Lake Tempe harbours a rich zooplankton community characterised by dense population of rotifers during low water period followed by a succession to crustacean community. Our results reveal that the connectivity between lakes and riverine ecosystems strongly influence zooplankton composition and succession from high water period to low water period. It is suggested that water level fluctuations benefit adaptation strategies of dominant species while species that are poorly adaptable to drought will undergo scarcity (Chaparro et al. 2011). The heterogeneity in zooplankton between the two hydrological phases reflects the heterogeneity of habitats in floodplain systems (Shiel et al. 1998). The importance of floodplain habitats in terms of biodiversity and the ecosystem services they provide remain largely uninvestigated and lagged behind other issues (e.g. fisheries and aquatic macrophyte) in Indonesia while the subsequent hydrological regimes modification continues to happen. It is no doubt that flow modification will have deleterious effect on floodplains biodiversity which has hardly been addressed in this region. Further study to investigate the potential loss of biodiversity, and thus lake productivity, of Lake Tempe, and probably elsewhere in Indonesia, in relation to environmental changes, particularly due to human intervention, is essential. Importantly, the concept of designing network of reserve in a floodplain habitats, comparing the increase of water retention time due to flow regulation to the overall lake's productivity and biodiversity is worthy of further study.

Acknowledgement This study was fully supported by the Research Centre for Limnology, Indonesian Institute of Sciences under the annual research grant financial years 2012 and 2013. We would like to gratefully acknowledge the staff of South Sulawesi Province Marine and Fisheries Agency and our colleagues and technicians of the laboratory in the Research Centre for Limnology, Indonesian Institute of Sciences for water chemicals analysis and landsat image processing.

References

APHA (2013). Standard Methods for the Examination of Water and Wastewater. General Books LLC.

Armitage, P.D., Szoszkiewicz, K., Blackburn, J.H. and Nesbitt, I. (2003), Ditch communities: A major contributor to floodplain biodiversity. *Aquatic Conservation: Marine and Freshwater Ecosystems*, **13:** 165–185.

Beaver, J., Jensen, D., Casamatta, D., Tausz, C., Scotese, K., Buccier, K., Teacher, C., Rosati, T., Minerovic, A. and Renicker, T. (2013). Response of phytoplankton and zooplankton communities in six reservoirs of the middle Missouri River (USA) to drought conditions and a major flood event. *Hydrobiologia*, **705:** 173–189.

Chaparro, G., Marinone, M.C., Lombardo, R.J., Schiaffino, M.R., De Souza Guimarães, A. and O'farrell, I. (2011). Zooplankton succession during extraordinary drought–flood cycles: A case

study in a South American floodplain lake. *Limnologica – Ecology and Management of Inland Waters*, **41:** 371–381.

Crome, F.H.J. and Carpenter, S.M. (1988). Plankton community cycling and recovery after drought – Dynamics in a basin on a flood plain. *Hydrobiologia*, **164:** 193–211.

Deksne, R. and Škute, A. (2011). The influence of ecohydrological factors on the cenosis of the Daugava River Zooplankton. *Acta Zoologica Lituanica*, **21:** 133–144.

Ning, N.P., Gawne, B., Cook, R. and Nielsen, D. (2013). Zooplankton dynamics in response to the transition from drought to flooding in four Murray–Darling Basin rivers affected by differing levels of flow regulation. *Hydrobiologia*, **702:** 45–62.

Palmer, M.E. and Yan, N.D. (2013). Decadal-scale regional changes in Canadian freshwater zooplankton: The likely consequence of complex interactions among multiple anthropogenic stressors. *Freshwater Biology*, **58:** 1366–1378.

Pinel-Alloul, B. and Mimouni, E.-A. (2013). Are cladoceran diversity and community structure linked to spatial heterogeneity in urban landscapes and pond environments? *Hydrobiologia*, **715:** 195–212.

Schöll, K., Kiss, A., Dinka, M. and Berczik, Á. (2012). Flood-Pulse Effects on Zooplankton Assemblages in a River-Floodplain System (Gemenc Floodplain of the Danube, Hungary). *International Review of Hydrobiology*, **97:** 41–54.

Sharma, B.K. (2005). Rotifer communities of floodplain lakes of the Brahmaputra basin of lower Assam (N.E. India): Biodiversity, distribution and ecology. *Hydrobiologia*, **533:** 209–221.

Shiel, R., Green, J. and Nielsen, D. (1998). Floodplain biodiversity: Why are there so many species? *Hydrobiologia*, **387–388:** 39–46.

Shiel, R.J. (1985). Zooplankton of the Darling River System, Australia. Verhandlungen Internationale Vereinigung. *Limnologie*, **22:** 2136–2140.

Shiel, R.J., Costelloe, J.F., Reid, J.R.W., Hudson, P. and Powling, J. (2006). Zooplankton diversity and assemblages in arid zone rivers of the Lake Eyre Basin, Australia. *Marine and Freshwater Research*, **57:** 49–60.

Škute, A., Gruberts, D., Soms, J. and Paidere, J. (2008). Ecological and hydrological functions of the biggest natural floodplain in Latvia. *Ecohydrology and Hydrobiology*, **8:** 291–306.

Thomaz, S., Bini, L. and Bozelli, R. (2007). Floods increase similarity among aquatic habitats in river-floodplain systems. *In:* Hydrobiologia, pp. 1–13.

Thorp, J.H. and Mantovani, S. (2005). Zooplankton of turbid and hydrologically dynamic prairie rivers. *Freshwater Biology*, **50:** 1474–1491.

Tockner, K., Malard, F. and Ward, J.V. (2000). An extension of the flood pulse concept. *Hydrological Processes*, **14:** 2861–2883.

Chapter 11
Organics and Heavy Metals Content in River Receiving the Effluent of Municipal Landfill Leachate Treatment

Indah R.S. Salami and Dimas K. Rizaldi

1 Introduction

Municipal solid waste in Indonesia is commonly disposed in a landfill with leachate treatment facility before the effluent is discharged to river. Sarimukti landfill is located 5 km to the southeast of Cirata Reservoir, covers around 21.2 ha area and accepts municipal solid wastes from cities of Bandung, Cimahi and West Bandung. Cirata Reservoir is one of the cascade reservoirs along Citarum River and the sustainability of Citarum River is important since it is utilised for electricity, water supply, irrigation and also fishery activity for many cities along its catchment area.

Leachate of solid waste disposal contains potentially significant concentration of dissolved organic matter, xenobiotic organic compounds, inorganic macro components as anions and cations and heavy metals (Christensen et al. 2001; Kjeldsen et al. 2002). Their existence may contaminate the river water and potentially pose adverse effect on aquatic environments. Study of contaminants in Cirata Reservoir suggested that heavy metals content in the reservoir were originated from the upper stream sources (Salami and Octaviana 2008; Salami et al. 2008). On the other hand, Sarimukti leachate effluent is discharged to Cipanawuan River, one of the tributary rivers of Citarum leading to Cirata Reservoir.

Therefore, this study was aimed to identify the concentration of certain pollutants in river water due to Sarimukti landfill leachate effluent discharge to downstream flow rivers leading to Cirata Reservoir.

I.R.S. Salami (✉) • D.K. Rizaldi
Department of Environmental Engineering, Faculty of Civil and Environmental Engineering, Institut Teknologi Bandung (ITB), Jl. Ganesha 10, Bandung, 40132, Indonesia
e-mail: indahrss@tl.itb.ac.id

F. Kurisu et al. (eds.), *Trends in Asian Water Environmental Science and Technology*, DOI 10.1007/978-3-319-39259-2_11

2 Materials and Methods

Water samples were collected from 12 sampling locations starting from the landfill outlet, Cipanawuan River, in the upper stream of Cipanawuan, to downstream rivers of Cipicung River, Cimeta River, Citarum River and ended in Cirata Reservoir. Some locations in the upper stream of the river flow also measured to evaluate the water quality before it was mixed with landfill leachate effluent. The water sampling collection was conducted two times which were on July 2011 (SP I, dry season) and December 2011 (SP II, rainy season). The sampling locations were noted by GPS and the total length of the stream sampled was approximately 12.56 km (Table 11.1). Locations of sampling is illustrated in Fig. 11.1. The sizes

Table 11.1 The altitude of sampling locations

Sampling locations	Positions		Distance from the landfill outlet (km)
1	6°48′21.07″ S	107°20′55.90″ E	0
2	6°48′20.94″ S	107°20′56.24″ E	–
3	6°48′21.29″ S	107°20′55.43″ E	–
4	6°48′35.48″ S	107°20′51.30″ E	0.6
5	6°48′35.75″ S	107°20′51.65″ E	–
6	6°48′37.47″ S	107°20′51.39″ E	0.66
7	6°49′7.66″ S	107°19′56.34″ E	–
8	6°49′6.85″ S	107°19′55.24″ E	3.36
9	6°49′2.84″ S	107°19′24.52″ E	4.46
10	6°48′57.06″ S	107°19′8.90″ E	–
11	6°47′44.20″ S	107°18′16.99″ E	8.06
12	6°46′11.74″ S	107°17′5.93″ E	12.56

Fig. 11.1 Sampling locations (Google Earth, 2011)

of the rivers varied, started from 30 cm depth to 40 m in Cirata Reservoir. Sampling locations deeper than 2 m were sampled with three depths (0.2, 0.5 and 0.8 of total depth). These three depth samples were collected from sampling locations 10, 11 and 12. During the first sampling period it was not possible to collect water samples from locations 9 and 10 because all the surface of the river was covered by dense water hyacinth and the small boat could not pass through the area.

Parameters measured and analyzed in this study consisted of physical, chemical and microbiological characteristics. Physical parameters analyzed included temperature and microbiological parameters measured total coliform using MPN methods. Chemical parameters assessed comprised pH, conductivity, solids (Total Dissolved Solids/TDS and Total Suspended Solids/TSS), dissolved oxygen/DO, organics content, BOD, COD, total phosphate, ammonium, nitrite, nitrate, sulphate, and metals (iron, copper, lead, zinc, nickel, cadmium, chromium and mercury). The methods of analyses were based on Standard Methods procedures. Samples were collected in different bottles for chemical parameters, for metals, BOD and microbial samples analyzed.

The water quality results were compared to governmental regulations for effluent standard for landfill effluent and stream standard for water quality in the rivers. Governmental effluent standards used were based on the Decree of West Java Governor No. 6 year 1999 about Industrial Wastewater Effluent Standards, specifically waste Class II. Stream standard used was the Indonesian Government Decree No. 82 year 2001 about Water Quality Management and Water Pollution Control, specifically water Class III for freshwater fishery, animal husbandry and agriculture.

3 Results and Discussion

The results of effluent samples measurement are described in Table 11.2. Wastewater quality of effluent from Sarimukti landfill contained high TDS, BOD and COD. TDS concentrations from effluent was 4235.41 ± 247.54 mg/L and the allowable standard was 4000 mg/L. BOD was 477.22 ± 63.12 mg/L at average (standard of maximum effluent BOD = 150 mg/L) and COD was 2000 ± 188.56 mg/L (maximum COD effluent = 300 mg/L). The effluent was also shown high in pH (average pH = 8.26 ± 0.09) and very low DO of 1.25 ± 0.07 mg/L. The treatment facility had to be improved to comply with the regulation. The effluent analyses showed that the time of samplings did not significantly measure different values. Dry season in July and rainy season in December did not change the effluent quality significantly. Limited water sampling number and period were the reasons of having different results with other studies. Dan'azumi and Bichi (2010) measurement of water pollution at Challawa River in Kano, Nigeria demonstrated rainy season pollution lower than those in dry season. Hydrological observations demonstrated that the driest period was at the

Table 11.2 Results of landfill effluent quality analysis

No.	Parameters	Units	Concentrations
1	pH		8.26 ± 0.09
2	TDS	mg/L	4235.41 ± 247.54
3	TSS	mg/L	225.7 ± 7.89
4	Conductivity	mS/cm	19.08 ± 1.87
5	DO	mg/L	1.25 ± 0.07
6	Organics	mg/L	2361.15 ± 361.09
7	BOD	mg/L	477.22 ± 63.12
8	COD	mg/L	2000 ± 188.56
9	Total phosphate	mg/L	9.26 ± 0.47
10	Ammonium	mg/L	2511.76 ± 281.41
11	Nitrite	mg/L	1.82 ± 0.30
12	Nitrate	mg/L	12.99 ± 1.69
13	Sulphate	mg/L	343.10 ± 68.81
14	Iron	mg/L	9.54 ± 0.75
15	Copper	mg/L	0.10 ± 0.07
16	Lead	mg/L	0.025 ± 0.01
17	Zinc	mg/L	0.221 ± 0.02
18	Nickel	mg/L	0.16
19	Cadmium	mg/L	0.001
20	Chromium	mg/L	0.1835
21	Mercury	ppb	0.45
22	Total coliform	MPN/100 mL	315

end of dry season, and also the wettest condition was detected at the end of rainy season.

The average temperature of water was 28.73 ± 1.24 °C whereas average air temperature was 30.98 ± 2.56 °C. During the rainy season the air and water temperatures were not statistically different (at $\alpha = 5\,\%$). However, in dry season the air temperature (33.45 ± 0.69 °C) was higher than those in water (28.67 ± 1.47 °C). The water temperatures in both seasons were not statistically different but air temperature differed between dry and rainy seasons (Fig. 11.2a). Water temperature from the outlet of landfill leachate treatment to the water in Cirata Reservoir decreased. Some slight increase of temperature inputs however were found around Sampling Locations 7 and 8 which were occupied by agriculture and human inhabitants.

Conductivity in the effluent (19.08 ± 1.87 mS/cm) was high but lower in the downstream flow due to dilution. Landfill leachate was characterized by high conductivity especially in the first year operation (Purwanta 2007). The dilution was occurred soon as around 0.66 km downstream the conductivity was detected less than 1 mS/cm. TDS of the effluent (4235.41 ± 247.54 mg/L) was higher than the government's effluent standard (4000 mg/L) and similar to conductivity the TDS also diluted and complied with the standard at 0.6 km downstream of the

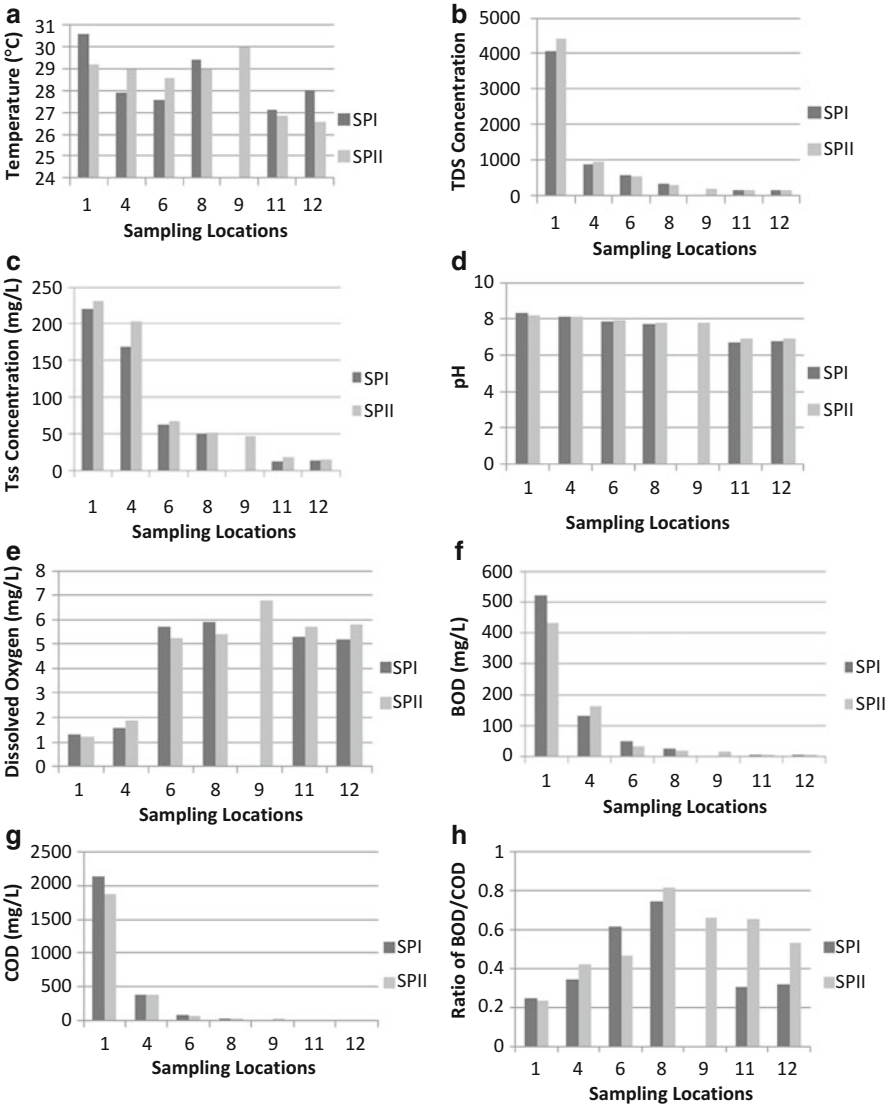

Fig. 11.2 Water quality condition in each sampling location: (**a**) Temperature, (**b**) TDS, (**c**) TSS, (**d**) pH, (**e**) DO, (**f**) BOD, (**g**) COD and (**h**) ratio of BOD/COD

outlet. There was no seasonal interference in terms of conductivity and TDS values (Fig. 11.2b). TSS at the outlet of landfill facility (225.7 ± 7.89 mg/L) was high but not exceeding the standard (maximum of 400 mg/L). However it was noted that other input (Sampling Location 3) in the upper stream river contained quite high TSS concentrations. TSS content was statistically shown to be affected by season (Fig. 11.2c). The TSS during rainy season was significantly higher than those in dry

season. TSS concentration considerably reduced in the downstream flow of the river.

The pH of the effluent was alkaline with the pH higher than 8. The farther from the landfill outlet the pH was becoming more neutral (Fig. 11.2d). There was no significantly different pH between rainy and dry seasons. The pH of leachate represented the stability of the process in the landfill. At the early stage of landfill decomposition the pH of leachate was close to neutral under aerobic condition. Later when anaerobic condition developed the acidogenic/acetogenic phase produced strong acidic pH. After months or years the process of degradation then stabilized under methanogenic condition that created leachate with neutral or slightly alkaline pH. Aerobic condition might return later and indicated hazardous material ceased (Environment Agency 2003). Sarimukti landfill has been operated more than 5 years, so this suggested that the process of waste degradation has been stabilized under methanogenic condition.

The oxygen content in the river dropped as the effluent entered the river flow. Before receiving the effluent, the Dissolved Oxygen (DO) in the river was higher than 5.3 mg/L (Sampling Locations 2, 3 and 5), but it dropped to average DO of 1.7 mg/L after landfill effluent input (Sampling Location 4). At around 0.6 km downstream (Sampling Location 6), the DO recovered to 5 mg/L again. The DO in Sampling Locations 11 and 12 slightly reduced that has been influenced by the activity in Cirata Reservoir. The fishery adds high amount of organics as the feed for fish.

The effluent of landfill contained high organic content that utilized the oxygen content in the river. The organic content of the effluent was very high (average of 2361.15 ± 361.09 mg/L) and as BOD was measured at average 477.22 ± 63.12 mg/L and COD was equal to 2000 ± 188.56 mg/L. Both BOD and COD of effluent were higher than the standard for wastewater effluent (BOD max. 150 mg/L and COD 300 mg/L). However, the organics, BOD and COD contents decreased farther away from the outlet. Similarly to the DO situation, before the effluent input the BOD of the upper stream river was lower than 26 mg/L and lower than 35 mg/L for COD (Sampling Locations 2, 3 and 5). These conditions of BOD and COD were recovered after 3.36 km downstream of the input. This suggested that the self purification of the river occurred in field and stated that the river was able to recover within the distance of 3.36 km. The reason of longer distance recovery perhaps was related to type of organics in the effluent. Calculating the BOD/COD ratio, it was shown that the effluent contained lower biodegradable organics than chemically degraded organics. This was in agreement with Christensen et al. (2001) that stated ratio BOD/COD was lower under methanogenic condition. The ratio BOD/COD in the upper stream of the outlet was higher than 0.5. After effluent input, the ratio of BOD/COD in adjacent areas was lower than 0.5 and then increased again in the Sampling Location 8 which was estimated around 3.36 km downstream. It was also noted that during rainy season the BOD/COD ratio was slightly higher explaining more biodegradable component existing in the river flow. However, some other possible sources of more chemically degraded materials discharges entered the flow

around Sampling Locations 11 and 12. This possibly originated from pollution of industrial areas before Cirata Reservoir mouth.

With regard to inorganic components, the study indicated that landfill treatment effluent generated high ammonium of average 2511.76 ± 281.41 mg/L. This concentration of effluent was considered very high compared to treated ammonium effluents studied by Ozturk et al. (2003) that obtained ammonium of 250 mg/L in the effluent. The Sarimukti landfill treatment facility had not successfully removed the ammonium content. River water without effluent input showed low ammonium of less than 10 mg/L except at Sampling Location 3 that was detected at average of 28 mg/L. It was also noted, that deeper the water the ammonium increased. Higher nitrite and nitrate were also found in the effluent but the concentrations did not exceed the standard. However, nitrate concentration was found to be higher than nitrite. This showed that aerobic degradation of ammonium occurred in the river. Total phosphate in the outlet (Location 1) and surrounding (Locations 2, 3 and 4) was considered high as detected above 2 mg/L. Other locations contained total phosphate of the highest as 0.94 mg/L. Total phosphate originated not only from landfill effluent but also agriculture activity in the area. In the dry season, Sampling Locations 9 and 10 were covered by water hyacinth and the calculation of data showed that average total phosphate during dry season was higher than those in the rainy season. Sulphate concentration from the effluent was the highest measured (at average 343.10 ± 68.81 mg/L) compared to the water in the upper stream river which only contained less than 10 mg/L sulphate. The concentration of sulphate however decreased and in the reservoir it was detected at 21.3 ± 2.6 mg/L.

Heavy metals measurement analyzed eight metals namely Fe, Cu, Pb, Zn, Ni, Cd, Cr and Hg. Among these metals, only Cu in the water of Sampling Locations 3, 11 and 12 showed concentration slightly above stream standard. Heavy metals concentrations in the effluent were higher than those in the river water, but all still were lower than the effluent standard. Fe concentration decreased along the river flow (Fig. 11.3a). Ni, Cd and Hg concentrations could be measured in the effluent but still complied with the standard. In some sampling locations these heavy metals concentrations were under the range of detection limit of the equipment/analyzer. Some sampling locations in the downstream river exhibited an increase of heavy metals concentration. This suggested that heavy metals in the river came from other sources such as agriculture and industrial activities. Other sources of Cu concentration inputs were predicted and found in Sampling Locations 3, 11 and 12. Figure 11.3b showed that Pb received other inputs beside landfill effluent. At Sampling Location 12, Pb was considerably increased. Zn also increased in Sampling Locations 10, 11 and 12 (Fig. 11.3c) whereas Cr had other inputs from Sampling Locations 7 and 9. Heavy metals inputs were possibly originated from agriculture origin because the land use in these areas are dominated by agriculture. Some human inhabitant was also found around Sampling Location 7.

This study found that the heavy metals concentrations were considered in low concentration. Christensen et al. (2001) stated that heavy metals were not significant pollutants from landfill because of strong attenuation of heavy metals by sorption and precipitation. However, complexation of heavy metals with dissolved

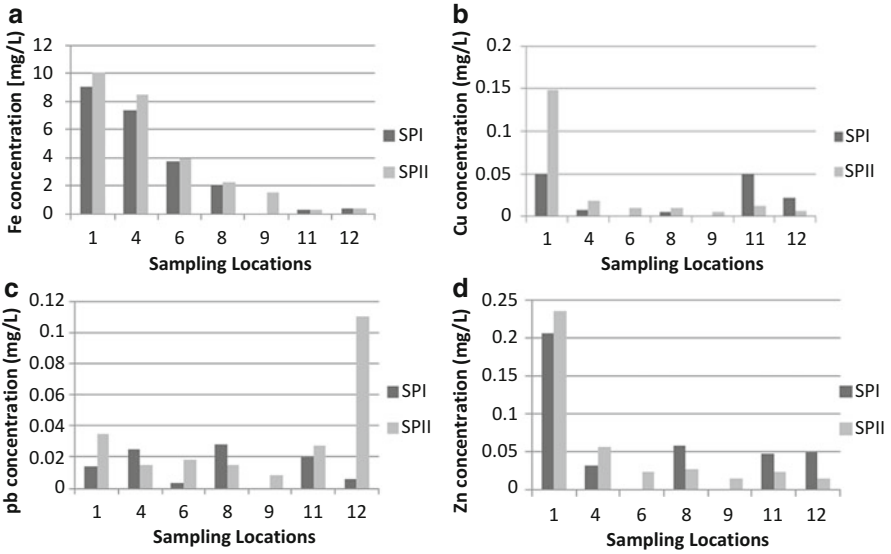

Fig. 11.3 Heavy metals content in each location: (**a**) Fe, (**b**) Cu, (**c**) Pb and (**d**) Zn

organic matter could be performed. Colloids also posed high affinity for heavy metals. Furthermore, it was observed that attenuation of heavy metals to groundwater would not exceed 1000 m from the landfill site. This study noted that at Sampling Location 4 with a distance of 600 m, all heavy metals concentrations were lower than stream standard. This study also found that the highest concentration of heavy metals detected in the leachate was in the order of Zn > Cr > Ni > Cu > Pb > Cd > Hg. Talalaj and Dzienis (2007) reported the heavy metals contents could be ordered as follows: Zn > Ni > Cu > Cd. This was shown that similar orders were detected in both landfill leachates. High Zn concentration in the leachate was also found by Adewuyi and Opasina (2010) at dumpsite in Abadan Nigeria (Zn > Pb > Cu > Ni > Cd), and also Nubi and Ajuonu (2011) in groundwater closed to dumpsite area in Oyo State, Nigeria (Zn > Ni > Pb > Cu > Cr > Cd). In all studies it was noted that Zn was detected as the highest concentration, followed by metals group of Cu, Pb and Ni. Cd was always found to be in the lowest concentration. Only Cr was considered in different concentration order. Pollutant concentration and mixtures in leachate very much depended on waste types dumped in the landfills.

Total coliform analyses showed that the effluent of landfill treatment did not contribute to the total coliform in the river water. The landfill effluent only contained at average total coliform of 315 MPN. The highest total coliform was measured at Sampling Locations 3 and 5 that indicated of human activities origin. The total coliform measurement during dry season demonstrated a slightly higher number than those estimated in rainy season (Fig. 11.4).

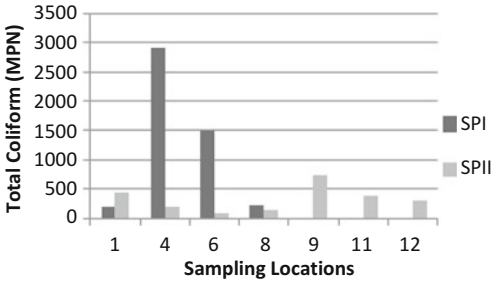

Fig. 11.4 Total coliform number in each location

The impact of landfill leachate has been considered as a hazard leading to increase risk on water and ecosystem. Experiment of local fish cultivation using the river water receiving landfill leachate in the area of study between Sampling Locations 6 and 8 showed that the fish were not capable to grow and the fish mortality was found after 2 days' exposure (Tobing 2012). The experiment was an evidence for that leachate contamination to surface water created toxicity to ecosystem. Therefore method to predict the impact of leachate to water and ecosystem has been developed by other researchers. One among them was method to quantify the hazard of leachate pollution reviewed by Kumar and Alappat (2003) using Leachate Pollution Index (LPI) that by measuring leachate characteristics the composite influence of it can be quantified at any site, any stage of landfill processes. Leachate composition is always unique and site specific. Factors affecting the composition of leachate include type of wastes, composition of wastes, the particle sizes, compaction degree, the hydrology of the site, climate, age of fill, and other site specific conditions (Kumar and Alappat 2003).

4 Conclusions

This study showed that Sarimukti landfill produced leachate effluent that had to be further treated because some parameters namely TDS, BOD and COD were still higher than effluent standard. The river water downstream also was affected by leachate effluent up to some distance of the inputs. However it was concluded that the effect of landfill effluent did not reach the Cirata Reservoir. Organic pollutants represented by BOD and COD decreased along the river flow and recovered at 3.36 km after outlet discharge. Some other pollutants input beside landfill effluent were also noted in the study. In the upper stream area (Location 3) some parameters namely TSS, conductivity, total phosphate (including Location 2), ammonium and Cu were contributed by agriculture and domestic activities. Total coliform origin was definitely generated from human inhabitants in Locations 3 and 5. Other pollutant sources predominated by heavy metals inputs were found in the downstream flow especially around Sampling Locations 11 and 12. Because the landfill leachate contained potential hazardous pollutants it was recommended that the

efficacy of landfill leachate treatment should be maintained. Surface water receiving landfill leachate effluent should also be monitored periodically to reduce any adverse risk to ecosystem and human health.

Acknowledgement Appreciation is conveyed to Mr. Yaya Hudaya from Cirata Reservoir Management Agency (Badan Pengelola Waduk Cirata – BPWC) for valuable information of the landfill activity.

References

Adewuyi, G.O. and Opasina, M.A. (2010). Physicochemical and Heavy Metals Assessment of Leachate from Aperin Abandoned Dumpsite in Ibadan City, Nigeria. *E-Journal of Chemistry*, **7 (4):** 1278–1283.

Christensen, T.H., Kjeldsen, P., Bjerg, P.L., Jensen, D.L., Christensen, J.B., Baun, A., Albrechtsen, H.J. and Heron, G. (2001). Biogeochemistry of Landfill Leachate Plumes. *Applied Geochemistry*, **16:** 659–718.

Dan'azumi, S. and Bichi, M.H. (2010). Industrial Pollution and Heavy Metals Profile of Challawa River in Kano Nigeria. *Journal of Applied Science in Environmental Sanitation*, **5(1):** 23–29.

Environment Agency, UK (2003). Guidance on Monitoring of Landfill Leachate, Groundwater and Surface Water (www.environment-agency.gov.uk/static/documents/Business/report_1_533191.pdf).

Kjeldsen, P., Barlaz, M.A., Rooker, A.P., Baun, A., Ledin, A. and Christensen, T.H. (2002). *Critical Reviews in Environmental Science and Technology*, **32(4):** 297–336.

Kumar, D. and Alappat, B.J. (2003). Analysis of Leachate Contamination Potential of Municipal Landfill using Leachate Pollution Index. Workshop on Sustainable Landfill Management, 3–5 December 2003, Chennai, India,

Nubi, O.A. and Ajuonu, N. (2011). Impacts of Industrial Effluent and Dumpsite Leachate Discharges on the Quality of Groundwater in Oyo State, Nigeria. *Journal of Biodiversity and Environmental Sciences (JBES)*, **1(3):** 13–18.

Ozturk, I., Altinbas, M., Koyuncu, I., Arikan, O. and Gomec-Yangin, C. (2003). Advanced physico-chemical treatment experiences on young municipal landfill leachates. *Waste Management,* **23:** 441–446.

Purwanta, W. (2007). Study of Leachate Treatment Technology in Municipal Solid Waste Final Disposal, BPPT. *JAI*, **3(1):** 57–63.

Salami, I.R.S., Rahmawati, S., Sutarto, R.I.H. and Jaya, P.M. (2008). Accumulation of Heavy Metals in Freshwater Fish in Cage Aquaculture at Cirata Reservoir, West Java, Indonesia. *Ann. N.Y. Acad. Sci*., **1140:** 290–296.

Salami, I.R.S. and Octaviana, I.S. (2008). Floating Cage Fish Aquaculture and Its Effects on Water Quality of Cirata Reservoir, West Java, Indonesia. Proceeding of International Seminar on South East Asia Technology University Consortium (SEATUC), ITB, Bandung, January 2008.

Talalaj, I.A. and Dzienis, L. (2007). Influence of Leachate on Quality of Underground Waters. *Polish J. of Environ. Stud*., **16(1):** 139–144.

Tobing, D.I. (2012). Accumulation of Cu and Pb on Fish (*Pangasius*) Cultured in Water from Cipicung River. Final Project, Undergraduate Program, Department of Environmental Engineering, Faculty of Civil and Environmental Engineering, ITB.

Part IV
Hydrological and Quality Issues: Groundwater Contamination

Chapter 12
Tracing the Significance of River for Arsenic Enrichment and Mobilization

Manish Kumar, Nilotpal Das, and Kali Prasad Sarma

1 Introduction

Arsenic contamination of groundwater has been found to be prominent in many of the flood plain regions of the world where recent Holocene sediments are predominant (Berg et al. 2008; Kumar et al. 2010; Shah 2010). Reductive hydrolysis of metal (hydr)oxides, particularly those of Fe has been found to be the dominant mode of As mobilization in groundwater of such regions (McArthur et al. 2001; Smedley and Kinniburgh 2002; Berg et al. 2008; Kumar et al. 2010). Some of the most well known regions with high groundwater As, where the aforementioned conditions have been detected are Bangladesh, India, Vietnam and Cambodia (Bhattacharya et al. 1997; Acharyya et al. 1999; Smedley and Kinniburgh 2002; Ahmed et al. 2004; Berg et al. 2007, 2008).

Most studies on As contamination have concentrated on the hydrogeochemical aspects, however closer observation of previous studies show that the rivers play a very important role in the occurrence and distribution of As. High groundwater As levels were found at close proximity to the river in the Red River Delta region of Vietnam, indicating that proximity to the river played an important role in As distribution and occurrence (Berg et al. 2008). A similar observation could be made from the study of Shah (2010) wherein it was reported that very high groundwater As levels were detected at close proximity to the river Ganga in the Middle Gangetic plains (MGP).

A probable reason behind the observation of high As levels at close proximity to the river could be the pre-dominance of newer sediments near the river. Arsenic bearing minerals have been detected in both the Himalayan as well the older

M. Kumar (✉) • N. Das • K.P. Sarma
Department of Environmental Science, Tezpur University, Napaam, Tezpur, Assam 784028, India
e-mail: manish.env@gmail.com

F. Kurisu et al. (eds.), *Trends in Asian Water Environmental Science and Technology*, DOI 10.1007/978-3-319-39259-2_12

mountain ranges from peninsular India (Shah 2010). It has been proposed by Shah (2010), that the weathering of As bearing rocks from these mountain ranges and their deposition in the flood plains ultimately lead to high As in the groundwater of these regions. Taking the above factor into consideration it can be said that there is a greater chance of occurrence of elevated As at close proximity to the river. As already mentioned earlier, redox conditions play a very important role in mobilization of As. Freshly deposited sediments close to the river are expected to be relatively un-oxidized, which could be another reason for occurrence of high As close to the river.

Apart from proximity, the course and stage of the river has also been found to play important roles in the occurrence and distribution of As. Deposition of higher loads of sediments along concave parts of river meanders has been linked to higher As levels in those regions. This can be observed in the studies of Berg et al. (2008) in Red river delta of Vietnam, and Shah (2010) in the MGP. Previous works on As contamination of groundwater also report much higher As in the plain and the deltaic regions of rivers. Arsenic has been reported more from middle and late stages of rivers like the MGP (Kumar et al. 2010; Shah 2010) and the Ganga Meghna Brahmaputra Delta (Bangladesh) (Halim et al. 2008; Reza et al. 2010) respectively. This indicates the role played by river stage in controlling the occurrence and distribution of As. Enhanced rate of sedimentation in the aforementioned regions could be the cause behind higher As levels in such areas.

The Brahmaputra flood plains (BFP) is a system of extensive alluvial deposition where high groundwater As levels have been detected (Singh 2004). The process of As mobilization has not been studied extensively in this region; therefore the mechanism and controls on As mobilization and distribution is not properly understood. This study was conducted in order to shed some light on the impact of the river on distribution and occurrence of As in fluvial regions.

2 Materials and Methods

2.1 Study Area

The BFP has been reported to be of tectonic origin (Evans 1964; Mahanta 1995), the valley portion was formed due to compaction between the European and the Indian plates; the same process was also responsible for giving rise to the Himalayan mountain (Evans 1964; Mahanta 1995). Subsequent sedimentation by river Brahmaputra and its tributaries laid the foundation for the extensive plains that are now known as the BFP. The major types of sediments in the BFP have been reported to be undifferentiated alluvium (Jain et al. 2007) (Fig. 12.1). Based on the mode of formation, the soil types have been classified into: (i) residual and (ii) transported (Mahanta 1995). Younger alluvium has been found mainly in the river banks, while the age of the sediments has been found to increase with distance

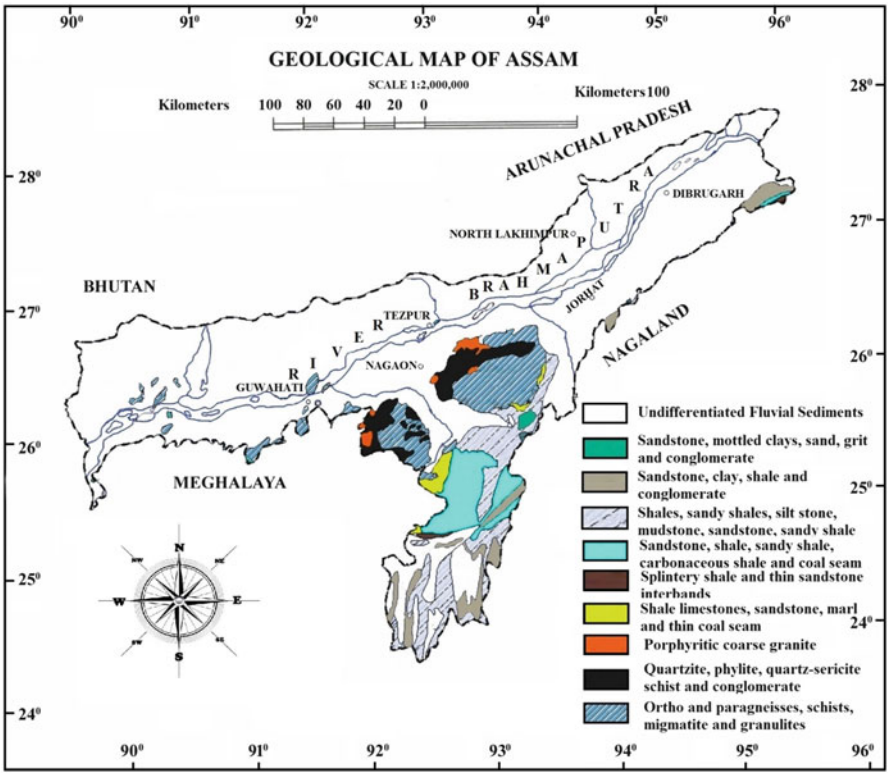

Fig. 12.1 Geological base map of Assam modified from Geological Survey of India showing the different geological formations

from the rivers. The climate of this region has been classified as "Tropical Monsoon Climate", characterized by warm and humid summers and mild winters. Brahmaputra River and its tributaries flow through and weather a number of different types of rocks (Huizing 1971; Heroy et al. 2003). The deposition of these weathered sediments determines the mineralogy of the region. The BFP has been divided into two major hydrogeological units: (i) the dissected alluvial plains and (ii) the inselberg zone (Jain et al. 2007). The Barpeta town lies in the BFP at close proximity of two small tributaries of the river Brahmaputra, which are: Nakhanda and Chawlkhowa (Fig. 12.5).

2.2 Groundwater Sampling

Groundwater sampling was conducted in the BFP from 2011 to 2012. A total of 129 groundwater samples were collected for major cations and anions analyses using standard methods prescribed by APHA (2005). Arsenic and Fe were analyzed

by atomic absorption spectroscopy (AAS, Thermoscientific ICE 3000) and inductively coupled plasma optical emission spectroscopy (ICP-OES, Perkin Elmer Optima 2100 DV) respectively. A second set of groundwater sampling ($n = 7$) was conducted in the Barpeta town area in 2014 (Fig. 12.5) for more detailed observation of the influence of river proximity and course in the distribution and occurrence of As. The As levels for the second set of groundwater samples were also determined using AAS. Mineralogy was determined using X-ray powder diffraction (Rigaku miniflex) and scanning electron microscope-energy dispersive X-ray spectroscopy (SEM-EDX, JEOL, JSM-6390LV). Contour maps were prepared for seasonal variation from the data on As levels generated from pre and post-monsoon seasons of 2011 using the software ARC GIS 9.1. Total organic carbon (TOC) was analysed using a total organic carbon analyzer [Multi C/N 2100 Analyzer (Analytik Jena AG, Germany)].

3 Results and Discussion

The general hydrochemistry of the BFP can be observed from the result of the descriptive statistics (Table 12.1).

The unit for TDS, DO, Na^+, K^+, Ca^{2+}, Mg^{2+}, HCO_3^-, Cl^-, SO_4^{2-}, PO_4^{3-} and Fe is mgL^{-1}, while the units for EC, ORP and As are μScm^{-1}, mV and μgL^{-1} respectively.

Table 12.1 Summary of descriptive statistics for different variables

Parameters	Range	Average ± SD	Co-efficient of variance
pH	10.12–5.04	6.99 ± 0.81	0.12
EC	1789–43.4	258.49 ± 197.7	0.76
TDS	851–21.5	160.10 ± 111.71	0.70
ORP	185–(−135.7)	−4.90 ± 51.24	−10.45
Na^+	49.6–0.96	15.78 ± 9.88	0.63
K^+	14–0.1	3.34 ± 2.78	0.83
Ca^{2+}	118.5–3.12	23.71 ± 16.18	0.68
Mg^{2+}	35.5–2.38	9.18 ± 6.37	0.69
HCO_3^-	400–50	177.66 ± 83.68	0.47
Cl^-	332.28–5.68	28.53 ± 29.8	1.04
SO_4^{2-}	142.36–.03	12.18 ± 16.14	1.33
PO_4^{3-}	2.56–0.16	0.45 ± 0.38	0.84
NO_3^-	2.10–0 (ND)	0.45 ± 0.53	1.18
F^-	1.31–0 (ND)	0.23 ± 0.29	3.70
Fe	5.70–0.01	1.24 ± 1.37	1.10
As	22.1.10–0.80	3.49 ± 3.91	1.12

The groundwater type in the BFP appears to be mainly of HCO_3^- type with mixed contribution from the cations (Fig. 12.2) (Piper 1953). Elevated levels of As (>10 μgL^{-1}) appear to be influenced by alkaline water type (Fig. 12.2).

The highest level of As detected in the BFP was 22.1 μgL^{-1}, most of the groundwater had As levels within the permissible limit for As in drinking water (WHO 1993). Arsenic was found to exhibit a positive relation with proximity to the river (Fig. 12.3a), while at the same time negative relation was observed with redox potential (ORP) (Fig. 12.3b), indicating towards the presence of reductive hydrolytic processes. This is proved to be true by the high regression observed between As and Fe in both the north and the south banks (Fig. 12.3d). Depth did not have a significant influence on As distribution, but it appears that As decreased with an increase in depth (Fig. 12.3c). Greater depths have been linked with sulphide formation leading to reduction in the As levels again by co-precipitation (Kim et al. 2012).

Contour maps based on As levels were prepared for pre and post-monsoon seasons. Close observation shows that As level in groundwater decreased with increase in the distance from the river (Fig. 12.4). Arsenic bearing minerals like arsenopyrite (FeAsS) and walpurgite [$(BiO)_4(UO_2)(AsO_4)_2.3H_2O$] have been detected in the sediments of the BFP (Unpublished data). Sediments which occur close to the river are newer and are relatively less oxidized; therefore such sediments may contain more of such As bearing minerals compared to older sediments away from the river. Another possibility is that, the river could be directly involved in recharging and mobilization of As in the groundwater resulting in higher As levels close to the river and lower levels away from it.

The groundwater flow pattern depends on the surface topography to a large extent; it is a very important factor considering the fact that groundwater flow is

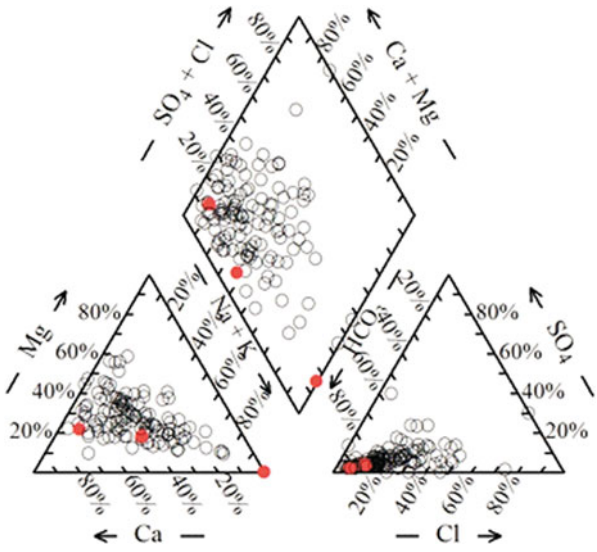

Fig. 12.2 Groundwater types in the BFP, the *red dots* represent samples with As level >10 μgL^{-1}

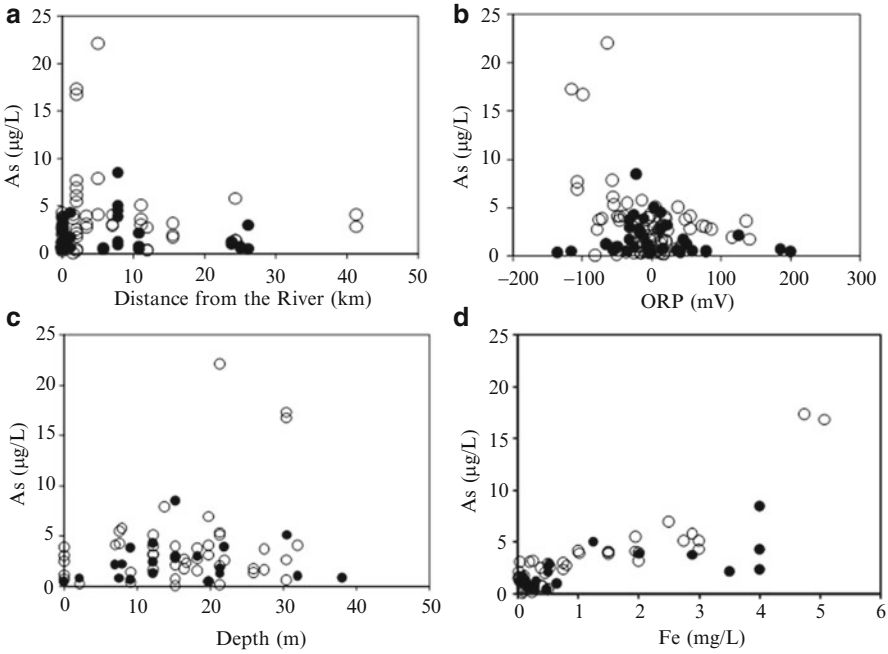

Fig. 12.3 Distribution and occurrence of As versus (**a**) proximity, (**b**) ORP, (**c**) Depth and (**d**) Fe. *Black dots* represent north bank

also responsible for the transportation and circulation of different chemical and mineral species including pollutants. When it comes to pollutants, the groundwater flow path can be used to predict zones of recharge and discharge in larger areas with inter-connected aquifers. Contour mapping in both the pre and the post-monsoon seasons (Fig. 12.4) show the presence of isolated hotspots of high As groundwater in the BFP. It is observed that there are at least two major recharge points for groundwater As in both the pre as well as the post-monsoon seasons. One is located close to the Kaliabor region in the Nagaon district in the south bank of river Brahmaputra (Fig. 12.4). The other recharge point is close to the Majuli river island in the north of Jorhat district. In the rest of the BFP there appears to be mainly isolated recharge points or hotspots rather than major recharge units.

Also contour maps suggest that the overall As level may be higher in the pre-monsoon than in the post-monsoon season. Groundwater recharge due to precipitation in the post-monsoon season could lead to dilution of As level throughout the BFP, although on an average, the recorded groundwater As values were found to be higher in the post-monsoon season in our study. The sudden increase in groundwater As levels in the Jorhat district in the post-monsoon could be due to mobilization of the highly mobile fractions of the As in the sediments which are easily replaceable by other anions like SO_4^{3-} and PO_4^{3-} (Wenzel et al. 2001). It is also evident from the pre-monsoon contour map that the level of groundwater As

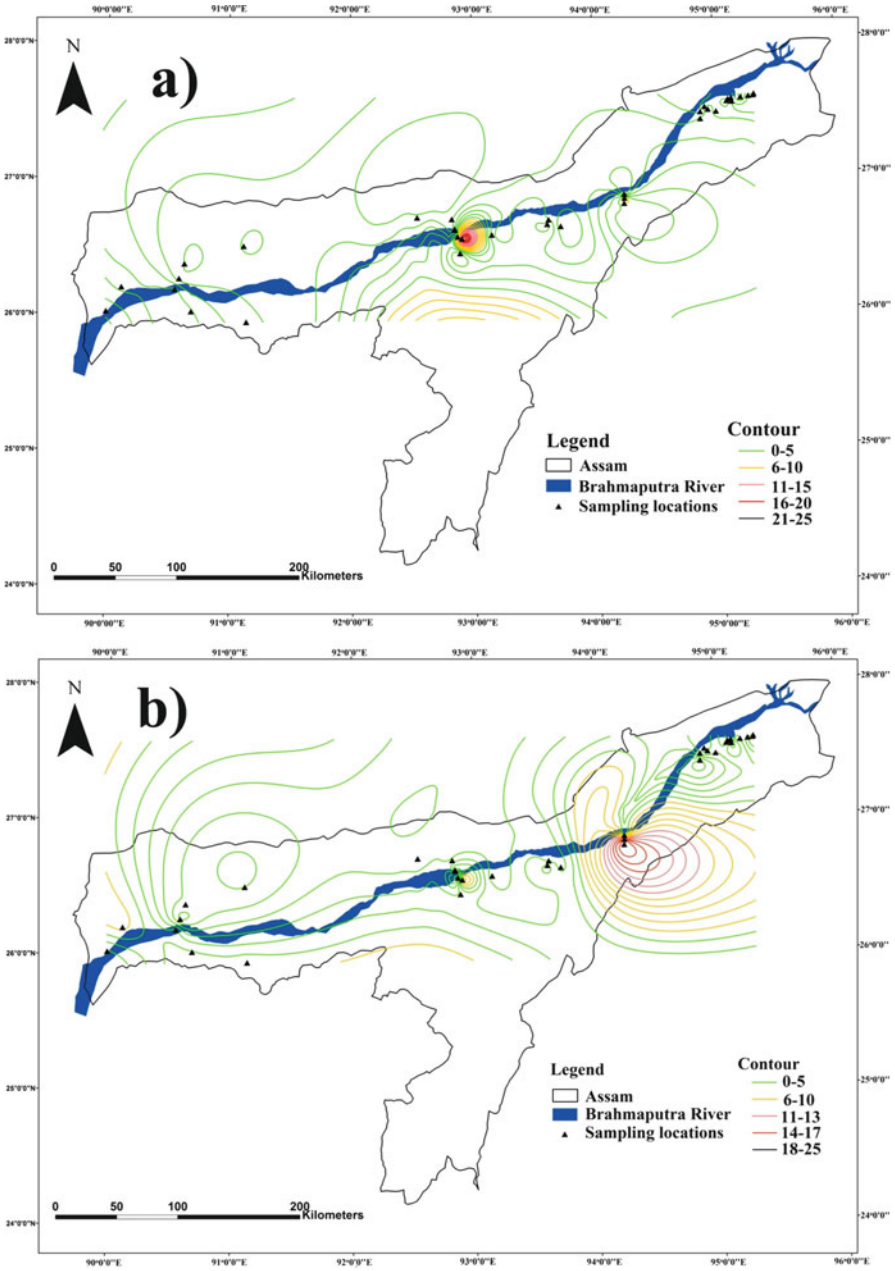

Fig. 12.4 (**a**, **b**) Contour map of As distribution in the pre and post-monsoon season respectively in the BFP

increases towards the west or downstream of the river Brahmaputra. This could be due to an increase in the rate of sedimentation caused by the decrease in the velocity of the river downstream. As the source of the groundwater As is most likely to be the sediment brought down by the river, so higher rate of sedimentation would also mean higher As in the sediments.

The town of Barpeta which lies in the BFP has a very unique hydrology; it lies close to the river Brahmaputra, which is about 7 km away, while at the same it is flanked by two minor tributaries of river Brahmaputra which are: Nakhanda and Chawlkhowa. Very high levels of groundwater As were recorded in Barpeta town, the highest recorded level of As was 131.5 μgL^{-1} (Fig. 12.5). The distribution of As however showed a great peculiarity, it was observed that high groundwater As levels were recorded only in the southern part of Barpeta, which borders the river Nakhanda (Fig. 12.5). Field inspection and interaction with the local inhabitants revealed that the aforementioned part of the town actually lied in a dead or a paleo channel of the Nakhanda river (Fig. 12.5). Arsenic levels were found to change with very little spatial variation (Fig. 12.5). The highest level of As was found to lie closest to the river, and a quick drop in As levels were observed with increase in distance from the river. The grab soil sample from this part showed a very high TOC level (15.2 mgL^{-1}), and SEM-EDX showed the presence of As along with high amounts of Fe and Mn (Fig. 12.6).

Barpeta is a small town with a population of 48,826 as per the 2011 census, the highly localized behaviour of As in such a small region is very interesting and

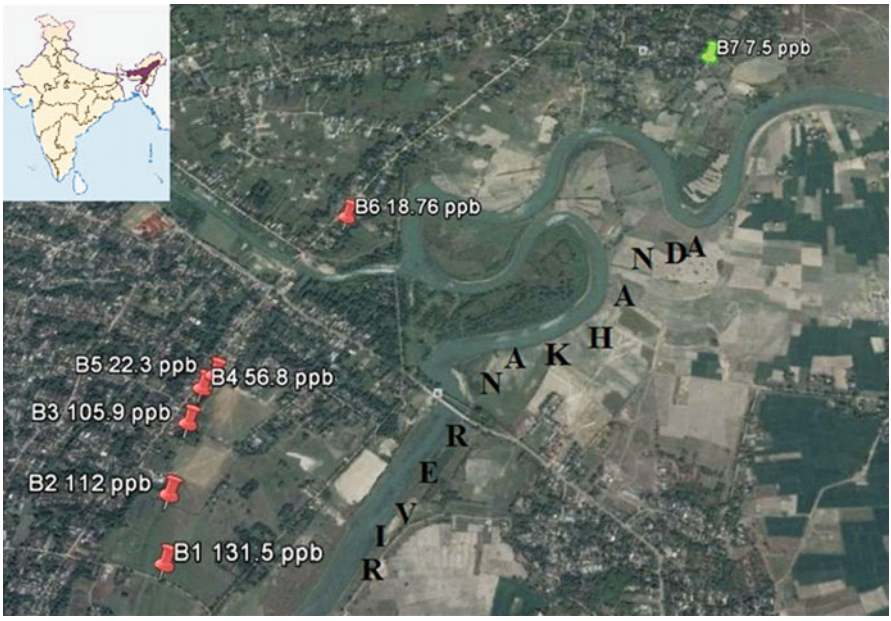

Fig. 12.5 Groundwater samples in Barpeta town with the As values

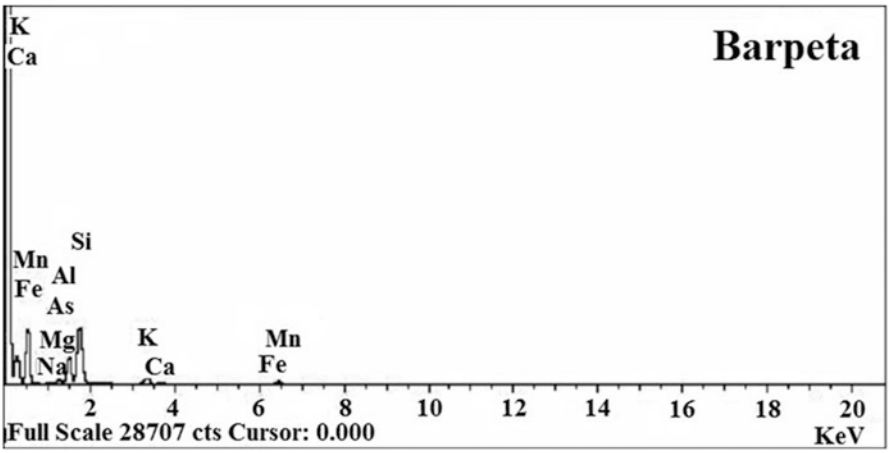

Fig. 12.6 EDX of grab soil sample from Barpeta town

highlights the influence of river course and proximity in As occurrence and distribution. Deposition of recent sediments which are high in organic matter and enriched in As bearing minerals along the Nakhanda river appears to be the reason behind the unique pattern of As occurrence in the Barpeta town.

4 Conclusions

The process of As mobilization in the BFP appears to be reductive hydrolysis of Fe (hydr)oxides, and proximity to the river appears to be a major influence on the distribution and occurrence of the contaminant. This could be due to deposition of recent sediments close to the river which are rich in As bearing minerals like arsenopyrite. The newer sediments are also likely to be deposited more along inner sides of river meanders, which explains the abundance of groundwater As in such regions as seen from the micro case study of groundwater in Barpeta town, Assam, India. Organic matter was found to be high in such sediments indicating their relatively un-oxidized condition indicating the high potential of such sediments for As mobilization. We could not observe a clear relation between As occurrence and river stage in this study. But it is likely that higher rate of sedimentation in mid stages of rivers e.g. the BFP and late stages like the GMB deltaic regions could be a reason for the elevated levels of groundwater As in such regions. Thus it can be concluded that hydrogeochemical factors which are responsible for mobilization of groundwater As in alluvial plains are regulated or influenced by the river.

Acknowledgement We thank the Department of Science and Technology (DST), under Govt. of India for funding the research project.

References

Acharyya, S.K., Chakraborty, P., Lahiri, S., Raymahasay, B.C., Guha, S. and Bhowmik, A. (1999). Arsenic Poisoning in Ganges Delta. *Nature*, 401: 545.

Ahmed, K.M., Bhattacharya, P., Hasan, M.A., Akhter, S.H., Alam, S.M.M., Bhuyan, M.A.H., Imam, M.B., Khan, A.A. and Sracek, O. (2004). Arsenic enrichment in groundwater of the alluvial aquifers in Bangladesh: An overview. *Appl. Geochem.*, 19(2): 181–200.

APHA. Standard methods for the examination of water and wastewater, (19th Ed.). American Public Health Association, Washington, D.C, 2005.

Berg, M., Trang, P.T.K., Stengel, C., Buschmann, J., Viet, P.H., Dan, N.V., Giger. W. and Stüben, D. (2008). Hydrological and Sedimentary Controls Leading to Arsenic Contamination of Groundwater in the Hanoi Area, Vietnam: The Impact of Iron-Arsenic Ratios, Peat, River Bank Deposits, and Excessive Groundwater Abstraction. *Chemical Geology*, 249(1–2): 91–112.

Berg, M., Stengel, C., Trang, P.T.K., Viet, P.H., Sampson, M.L., Leng, M., Samreth, S., Fredericks, D. Magnitude of Arsenic Pollution in the Mekong and Red River Deltas-Cambodia and Vietnam, The Science of the total environment, 372 (2–3), 413–425, 2007.

Bhattacharya, P., Chatterjee, D. and Jacks, G. (1997). Occurrence of arsenic contamination of groundwater in alluvial aquifers from Delta Plain, Eastern India: Option for safe drinking supply. *Int J Water Resour D.*, 13(1): 79–92.

Evans, P. (1964). The tectonic framework of Assam. *Jour. Geol. Soc. India*, 5: 80–96.

Guidelines for Drinking-Water Quality, 2nd edition. WHO, Geneva, 1993.

Halim, M.A., Majumder, R.K., Nessa, S.A., Hiroshiro, Y., Uddin, M.J., Shimadab, J. and Jinnoa, K. (2008). Hydrogeochemistry and Arsenic Contamination of Groundwater in the Ganges Delta Plain, Bangladesh. *Journal of Hazardous Materials*, 164(2–3): 1335–1345.

Heroy, D.C., Kuehl, S.A. and Goodbred Jr. S.L. (2003). Mineralogy of the Ganges and Brahmaputra Rivers: Implications for river switching and Late Quaternary climate change. *Sedimentary Geology*, 155(3–4): 343–359.

Huizing, H.G.J. (1971). A reconnaissance study of the mineralogy of sand fractions from East Pakistan sediments and soils. *Geoderma.*, 6(2): 109–133.

Jain, K.S., Agarwal, P.K. and Singh, V.P. (2007). Hydrology and Water Resources of India, Water Sci and Technology Library. Springer, 57: 419–472.

Kim, S.H., Kim, K., Ko, K.S., Kim, Y. and Lee, K.S. (2012). Co-Contamination of Arsenic and Fluoride in the Groundwater of Unconsolidated Aquifers under Reducing Environments. *Chemosphere*, 87(8): 851–856.

Kumar, Manish, Kumar, Pankaj, Ramanathan, A.L., Bhattacharya, Prosun, Thunvik, Roger, Singh, Umesh K., Tsujimura, M. and Sracek, O. (2010). Arsenic enrichment in groundwater in the middle Gangetic Plain of Ghazipur District in Uttar Pradesh, India. *J. Geochem. Explor.,* 105 (3): 83–94.

Mahanta, C. (1995). Distribution of nutrients and toxic metals in the Brahmaputra River Basin. Ph. D thesis, Jawaharlal Nehru University, India.

McArthur, J.M., Ravenscroft, P., Safiullah, S. and Thirlwall, M.F. (2001). Arsenic in groundwater: Testing pollution mechanisms for sedimentary aquifers in Bangladesh. *Water Resources Research*, 37(1): 109–117.

Piper, A.M. (1953). A graphic procedure in the chemical interpretation of water analysis. US Geol Surv Groundwater Note 12.

Reza, A.H.M., Selim, Jean, J.S., Yang, H.J., Lee, M.K., Woodall, Brian, Liu, C.C., Lee, J.F. and Luo, S.D. (2010). Occurrence of Arsenic in Core Sediments and Groundwater in the Chapai-Nawabganj District, Northwestern Bangladesh. *Water Research*, 44(6): 2021–2037.

Shah, B.A. (2010). Arsenic contaminated groundwater in Holocene sediments from parts of Middle Ganga Plain, Uttar Pradesh. *Curr Sci.*, 98(10): 1359–1365.

Singh, A.K. (2004). Arsenic Contamination in Groundwater of North Eastern India. Proceedings of National Seminar on Hydrology with Focal Theme on Water Quality. National Institute of Hydrology, Roorkee.

Smedley, P.L. and Kinniburgh, D.G. (2002). A review of the source, behavior and distribution of arsenic in natural waters. *Appl Geochem*, 17(5): 517–568.

Wenzel, W.W., Kirchbaumer, N., Prohaska, T., Stingeder, G., Lombic, Enzo and Adriano, D.C. (2001). Arsenic fractionation in soils using an improved sequential extraction procedure. *Analytica Chimica Acta*., 436(2): 309–323.

Chapter 13
Evaluation of Groundwater Quality in 14 Districts in Sri Lanka: A Collaboration Research Between Sri Lanka and Japan

S.K. Weragoda and Tomonori Kawakami

1 Introduction

Groundwater is an indispensable source of drinking water in many rural communities in the dry zone of Sri Lanka. However in most of the areas in dry zone, many residents suffer from health problems associated with high fluoride concentration in drinking water (Tennakoon 2004). In addition, current medical data of these regions have shown a significant increase of number of patients of Chronic Kidney Disease of Unknown Etiology (CKDu) during the recent past. It is evident with several studies done in recent past that there is an increasing trend on the reporting of patients admitted with CKDu (Bandara 2008; Chandrajith 2010).

It is found that at least 87 % of the population in the Anuradhapura administrative district in the north central region, where most areas are affected by CKDu, use either dug well or tube well water (Perera et al. 2008 cited in Chandrajith 2010). Over one thousand people have been reported as dead due to CKDu and more than 35,000 patients have registered at renal clinics of several government hospitals in the dry zone of the island (Weragoda et al. 2013). From many studies, it has been clearly shown that the etiology behind the increased number of CKD patients in NCP is neither diabetes nor hypertension (Bandara 2008). Etiology for this mysterious disease is suggested to be a combination of several environmental factors. Chandrajith (2010) suggests that even though no single geochemical parameter could be clearly and directly related to the CKD etiology, it is very likely that the unique hydrogeochemistry of the drinking water is closely associated with the incidence of the disease. Also many studies stresses the specialty of the spatial

S.K. Weragoda (✉)
National Water Supply and Drainage Board, Ratmalana, Sri Lanka
e-mail: skwera7@gmail.com

T. Kawakami
Toyama Prefectural University, Imizu, Japan

F. Kurisu et al. (eds.), *Trends in Asian Water Environmental Science and Technology*, DOI 10.1007/978-3-319-39259-2_13

distribution of this disease, which is highly associated to the north central dry zone of the country.

As the areas that have well water with high fluoride, overlapped with CKDu prevalent regions, it is suspected that fluoride may be responsible for the disease. Recently, a hypothesis has arisen saying that arsenic or cadmium is the etiology of CKDu. Regrettably, long term data on water quality of these areas in Sri Lanka is not available due to the civil war that lasted more than 30 years and also due to lack of facilities available in the country. Therefore, investigation of groundwater with special emphasis on contamination of fluoride and heavy metals was carried out using groundwater samples obtained from 14 districts of Sri Lanka to explore the possibilities for existing a relationship between the prevalence of health problems and the contaminants in drinking water.

2 Materials and Methods

Water samples ($n = 491$) were collected from wells in 14 districts in Sri Lanka from 2010 to 2012. Samples were filtrated on site to remove particulate matters and microorganisms by a membrane filter with a pore size of 0.45 μm before the samples were brought to Toyama Prefectural University, Japan for appropriate analyses. Major ion concentrations were determined by an ion chromatograph. Heavy metals including arsenic and cadmium were measured by an ICP-MS.

3 Results and Discussion

The average concentration of fluoride from Anuradhapura, Trincomalee, Hambantota, Kurunegala, Polonnaruwa and Vavuniya districts exceeded the Sri Lankan standard of 0.6 mg/L (Table 13.1). The highest concentration of 7.0 mg/L was observed in Anuradhapura District. The GIS mapping on density of CKDu patients and F concentration has shown a clear correlation. In addition, $CaCO_3$ (mg/L) was also measured to understand the hardness of water. Only Nuwara Eliya District has water termed as soft based on average value of $CaCO_3$ present. All other waters were found as "hard" water (>250 as $CaCO_3$ mg/L). Though there is not any direct health impact reported from high hardness on CKDu, temporary hardness which makes white colour deposits in water boiling pans causes reluctance among villagers to consume groundwater.

Excessive fluoride amounts cause critical health issues such as dental caries, bone fluorosis, and lesions of the thyroid, endocrine glands, and brain. This problem is widespread in many parts of the world, and still many millions of people consume groundwater with high amounts of fluoride which exceeds the recommended guideline value by World Health Organization (WHO). As a country in the tropical region, Sri Lanka has the upper limit value of F concentration as 0.6 mg/l. In Sri

Table 13.1 Maximum and average F concentration (mg/L) in groundwater of dry zone, Sri Lanka

District	Max.	Average	SD[a]
Anuradhapura	7.0	1.1	0.8
NuwaraEliya	0.1	0.0	0.0
Puttalam	2.2	0.3	0.4
Mannar	1.2	0.4	0.4
Jaffna	1.3	0.2	0.2
Trincomalee	2.4	0.8	0.7
Batticaloa	0.7	0.2	0.2
Hambantota	1.5	0.6	0.4
Matale	0.8	0.3	0.4
Kurunegala	5.0	0.7	1.2
Polonnaruwa	1.8	0.8	0.6
Vavuniya	3.1	0.8	0.6
Killinochchi	1.3	0.2	0.3
Mullattivu	1.1	0.1	0.2

[a]*SD* Standard deviation

Lanka, dental and skeletal fluorosis is a widespread health issue in majority of the residents in dry zone.

From the groundwater quality survey conducted including both CKDu endemic and non- endemic regions it is reported that high fluoride amounts is a widespread problem in dry zone Sri Lanka, highly relating with the regions associated with CKDu prevalence. Anuradhapura, which is one of the most affected regions, has reported the highest fluoride content of 7.03 mg/l with a mean value of 1.13 mg/l. Polonnaruwa has reported a mean value of 0.84 mg/l with a maximum fluoride content of 3 mg/l, while Badulla which is another endemic region resulting with a mean fluoride content of 0.56 mg/l and a maximum value of 2 mg/l, which clearly illustrate the excessive fluoride amounts in the CKDu endemic regions. In comparison to these results, Batticaloa reports a mean fluoride level of 0.21 mg/l and a maximum fluoride level of 0.7 mg/l. However according to Jayatilake et al. (2014), Hambantota is a non-endemic area, with no reported CKDu cases. But the present study reports 0.59 mg/l mean fluoride content along with a maximum fluoride level of 2.0 mg/l.

Arsenic concentration of few well water from coastal belt exceeded the Sri Lankan standard of 10 μg/L. Comparing the other heavy metal concentrations in each district, none of heavy metal other than Fe in the well waters exceeded the Sri Lankan standards. Although, As and Cd were reported recently to be the etiology of CKDu, the well water analyses clearly indicated that As and Cd in well water was not the etiology of CKDu, since no wells with their high concentration in groundwater was found.

Arsenic has long been known as a poison and is best known for its harmful acute effects. Long-term exposure to this poison through drinking water and/or food can result in adverse health effects including dermal diseases such as melanosis (dark and light spots on the skin) and keratosis (hardening of skin on hands and feet);

Table 13.2 Maximum and average as concentration (μg/L) in groundwater of dry zone, Sri Lanka

District	Max.	Average	SD[a]
Anuradhapura	1	0	0.2
NuwaraEliya	0	0	0.0
Puttalam	15	4	4.1
Mannar	66	7	11.7
Jaffna	6	2	1.7
Trincomalee	9	1	1.7
Batticaloa	14	3	3.1
Hambantota	3	1	0.9
Matale	0	0	0.1
Kurunegala	1	0	0.1
Polonnaruwa	1	0	0.2
Vavuniya	2	1	0.6
Killinochchi	2	1	0.6
Mullattivu	13	3	3.6

[a]*SD* Standard deviation

vascular diseases; birth defects; low IQ; cancer of lung, kidney, skin and others (Ngai et al. 2005). WHO recommended guideline value is 10 μg/l (WHO 2011). According to this groundwater survey results, none of considered districts' mean arsenic concentrations exceeds this guideline value. Only in one location the arsenic concentrations has exceeded this guideline value, and that is from Uppodai Lake Road in Batticaloa out of all 504 well points water samples. All other reported values are almost below 3.25 μg/l. According to the results in Table 13.2, high arsenic values are reported only in four districts; they are 15 μg/l, 66 μg/l, 13 μg/l and 14 μg/l in Puttalam, Mannar, Mullattivu and Baticcaloa respectively. But the mean value in any district has not exceeded the WHO recommended value. According to the data of Weragoda et al. (2012), it could be noticed when one closely studies the well point locations of higher concentrations of arsenic levels, that they are located nearby sea or bay. Hence, there can be a direct relation with environmental factors associated with coastal area, to result with high arsenic levels in four different well points in coastal regions in Sri Lanka. But according to overall results a common relation with CKDu and the arsenic concentrations, could not be recognized.

4 Conclusions

Investigation of well water in 14 districts in Sri Lanka was carried out to determine the concentrations of fluoride, hardness and heavy metals. High concentration of fluoride was detected in the north central region of Sri Lanka where CKDu are prevailing, while high concentration of arsenic was detected only in the coastal area and the concentration of cadmium was as low as 0 μg/L. This indicated that arsenic

and cadmium in the well water could not be an etiology of CKDu. Hence, researches on identification of causes for CKDu have to be diverted towards other means of uptake.

Acknowledgements This work was in part supported by Grant-in-Aid for Scientific Research from the Ministry of Education, Culture, Sports, Science and Technology, Sri Lanka (No. 23404003). Authors would like to be grateful to Dr Chaminda Thushara, Senior Lecturer, Ruhuna University and Mr Gayan Amarasuriya, Researcher, Post Graduate Institute of Science for their contribution in data collection.

References

Bandara, J. (2008). Chronic renal failure among farm families in cascade irrigation systems in Sri Lanka associated with elevated dietary cadmium levels in rice and freshwater fish (Tilapia). Springer.

Chandrajith, R. (2010). Chronic Kidney Disease of Uncertain Etiology (CKDu) in Sri Lanka: Geographic Distribution and Environmental Implications. Springer.

Jayatilake, N., Mendis, S., Maheepala, P. and Mehta, F.R. (2014). Chronic Kidney Disease of uncertain etiology: Prevalence and causative factors in a developing country. *BMC Nephrology*, 14(180): 1–13. doi: 10.1186/1471-2369-14-180.

Ngai, T., Dangol, B., Murcott, S. and Shrestha, R. (2005). Kanchan Arsenic Filter, Kathmandu, Nepal. Massachusetts Institute of Technology (MIT) and Environment and Public Health Organization (ENPHO).

Perera, A.P.G.R.L., Gonawala, J.M.L. and Wijekoon, D. (2008). Groundwater quality in Anuradhapura District with special reference to fluoride, Groundwater in Sri Lanka, National Academy of Science, pp.48–64.

Tennakoon, T.M.M.H (2004). Dental fluorosis in Anuradhapura District, Sri Lanka. In Proceedings of the 4th international workshop on fluorosis prevention and defluoridation of water, Colombo, Sri Lanka. pp 19 – 22.

Weragoda, S., Kodithuwakku, S. and Kawakami, T. (2012). Geological Distribution of Pollutants in Groundwater: Case Study in Eight Districts. Sri Lanka, Int. Symposium on Water Quality and Human Health: Challenges Ahead.

Weragoda, S., Kawakami, T., Motoyama, A. and Kodithukakku, S. (2013). Is groundwater in Dry Zone, Sri Lanka Safe to Drink? Sri Lanka, Collaborative Research.

WHO (2011). Guidelines for drinking-water quality, 4th ed. World Health Organization, Switzerland.

Chapter 14
Arsenic Contamination in Groundwater Affecting Holocene Aquifers of India: A Review

Babar A. Shah

1 Introduction

Groundwater arsenic (As) contamination have been reported in many parts of the world such as Bangladesh, India, Pakistan, Nepal, China, Hungary, Vietnam, Thailand, Cambodia, Taiwan, Inner Mongolia, Ghana, Egypt, Japan, Argentina, Mexico, USA and Chile (Mandal and Suzuki 2002; Ravenscroft et al. 2009). The mode of occurrence, origin and mobility of As in sedimentary aquifers are influenced by local geology, geomorphology, hydrogeology and geochemistry of sediments (Acharyya et al. 2000; Kinniburgh and Smedley 2001). The upper permissible limit of As in drinking water is 10 µg/l, as per the World Health Organization (WHO 1993), which has been endorsed by Bureau of Indian Standards (BIS 2003).

Groundwater As contamination in Quaternary aquifers are reported in India (Fig. 14.1) viz., Bengal Delta (West Bengal), Middle Ganga Plain (Uttar Pradesh-Bihar), Ghaghara Valley (Uttar Pradesh), Brahmaputra Valley (Assam), Barak Valley (Assam) and Imphal Valley (Manipur). Groundwater As concentrations in tubewell waters were tested within the Holocene Newer Alluvium aquifers, as well as the Pleistocene Older Alluvium aquifers. The main objective of study is to investigate the distribution of groundwater As in entrenched channels and floodplains in Quaternary domains under fluvial geomorphologic setting.

B.A. Shah (✉)
Department of Geological Sciences, Jadavpur University, Kolkata 700032, India
e-mail: bashahju@yahoo.com

F. Kurisu et al. (eds.), *Trends in Asian Water Environmental Science and Technology*, DOI 10.1007/978-3-319-39259-2_14

2 Materials and Methods

The tubewell samples were collected from Bengal Delta, Middle Ganga Plain, Ghaghara Valley, Imphal Valley and Barak Valley. The geographic locations of all samples were recorded by a handheld Global Positioning System (GPS). The information of tubewell depth was acquired from owner of the tubewell. GPS location of all samples were recorded.

Iron (Fe) in tubewell water samples was analysed by 1,10 phenanthroline method by the use of UV spectro-photometer. Arsenic in tubewell water and sediments was analysed through flow injection hydride generation atomic absorption spectrometry (FI-HG-AAS) system. Details of the reagents and glassware are given elsewhere (Samanta et al. 1999). Groundwater As-contaminations affecting different geological domains in India are presented in Fig. 14.1.

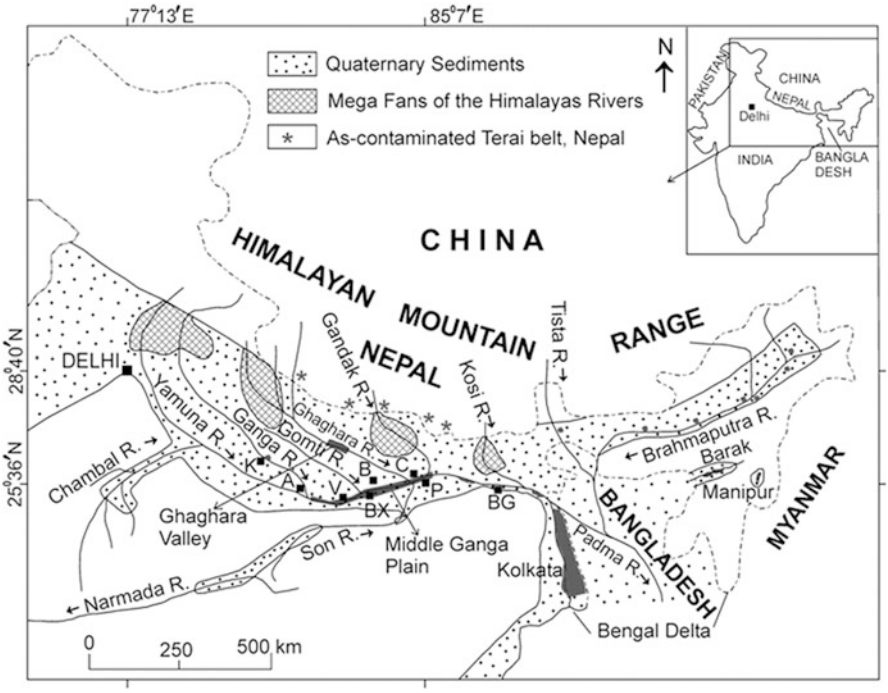

Fig. 14.1 Quaternary sediments in the Indo-Ganga foredeep and Bengal Basin. Arsenic affected areas of six geological domains in India are shown in the map. Abbreviations: K – Kanpur, A – Allahabad, V – Varanasi, BX – Buxar, B – Ballia, C – Chhapra, P – Patna, BG – Bhagalpur

3 Results and Discussion

3.1 Bengal Delta (West Bengal)

Four geomorphic and morphostratigraphic units have been identified in West Bengal and bordering Bihar and Jharkhand States in India. The western uplands of undulating hills of older rocks framing the delta are divisible into three stepped alluvial plains, e.g., western belt of undulating hills of older rocks, the Laterite Plain, Older Alluvial Plain (OAP) and the Younger Delta Plain (YDP) of the Bhagirathi-Ganga river system, which gradually come down in elevation in the east and southeast. The presence of characteristic soil profiles e.g., laterite/ferrisol and calcrete are recognized at subsurface (Mallick and Niyogi 1972; Acharyya and Shah 2007a).

Garai et al. (1984) first reported groundwater As-contamination in the Bengal Delta (West Bengal). Currently, nine districts in West Bengal (Fig. 14.1) have As-contamination in groundwater as reported by various workers (Mandal et al. 1996; Bhattacharya et al. 1997; Acharyya et al. 2000; Mandal and Suzuki 2002; Acharyya and Shah 2007a, 2010; McArthur et al. 2008; Ravenscroft et al. 2009; Bhattacharyya and Mukherjee 2009). Arsenic contaminated aquifers are mainly confined in the Holocene entrenched channels and floodplains of the Bhagirathi River. The Quaternary sequence along the western flank of the Bengal basin usually has a wedge-like shape and thickens eastward. Areas covering ODP and older surfaces are free of As contamination, which affects parts of YDP mainly to the east of the Bhagirathi River.

Arsenic affected areas confined to the western part of the Bhagirathi River are mainly discussed here. About 355 tubewell water samples were analysed from Howrah and Hooghly districts in the western part of the Bhagirathi River. About 51 % of tubewells have As >10 μg/l and 30 % of tubewells have As >50 μg/l. Maximum As and Fe concentrations in tubewell waters are 500 μg/l and 13 mg/l in Ulubaria and Balagarh blocks, respectively. Arsenic contaminated aquifers are mainly confined in the Holocene entrenched channels and floodplains of the Bhagirathi River. Many affected areas in the Balagarh Block of Hooghly district are located over the Damodar fan-delta, where maximum As concentrations of 85–90 μg/l have been recorded. The As-affected areas in Amta and Bagnan blocks of Howrah district are located on either side of the present Damodar channel but south of the Damodar fan-delta. Amta and Bagnan areas recorded maximum As concentrations of 50 and 90 μg/l, respectively (Acharyya and Shah 2007a).

3.2 Middle Ganga Plain

Groundwater As-contamination has been reported from different parts of the Middle Gangetic Basin (Fig. 14.1) in the states of Uttar Pradesh, Bihar and

Jharkhand (Chakraborti et al. 2003; Shah 2008, 2014; Kumar et al. 2010; Raju 2012; Bhattachaerjee et al. 2005). The As-affected districts in Bihar are Buxar, Bhojpur, Patna, Saran, Vaishali, Begusarai, Samastipur, Lakhisarai, Purnea, Katihar, Khagaria, Darbhanga, Bhagalpur, Kishanganj and Munger. Most of the As-contaminated tubewells are located within the depth of 15–40 m in the Holocene Newer Alluvium sediments (Chakraborti et al. 2003; Nickson et al. 2007; Shah 2008, 2010; Kumar et al. 2010; Saha et al. 2010; CGWB 2010). The low-lying entrenched channel and floodplain of the Ganga River that flank the northern tip of the Rajmahal Hills and parts of the Sahibganj district in Jharkhand are As-contaminated (Bhattacharjee et al. 2005).

Groundwater As-contamination has been reported in Ballia, Ghazipur and Bahraich districts of Uttar Pradesh in the Middle Gangetic Basin, where most of the contaminated (>10 µg/l) tubewells are located within the depth of 30 m. However, the temporal variation of As concentrations in Ghazipur district are greater in the pre-monsoon than that of the post-monsoon season (Ahmed et al. 2006; Shah 2008; Kumar et al. 2010). Lakhimpur Kheri district of Uttar Pradesh lies in Terai region along the Himalayan foothills. About 41 % (42 out of 102) of handpumps of these blocks have As above 10 µg/l (Pathak et al. 2013). Arsenic contamination in groundwater above 50 µg/L is reported in Allahabad and Kanpur districts of Uttar Pradesh. Most of the tubewells are shallow with depth ranging from 15 to 35 m (Chakraborti et al. 2009).

From Middle Ganga Plain, 224 tubewell water samples were analysed. About 73 % of tubewells have As concentrations above 10 µg/l and 41 % of tubewells have As above 50 µg/l. About 77 % of As-contaminated tubewells are from shallower depth (21 to 40 m) in the Holocene aquifers. Maximum concentrations of As and Fe in tubewell waters are 1300 µg/l and 12.93 mg/l at Semariya Ojjha Patti and Pandey Tolla villages, respectively. Most of the As contaminated tubewells are located within the depth of 20–50 m in the Newer Alluvium aquifers. The Fe content in tubewell waters varies from 0.1 to as much as 12.9 mg/l. About 85 % of tubewells have Fe beyond its permissible limit of 1 mg/l (Shah 2014).

Arsenic contaminated tubewells in Vaishali, Patna, Ballia, Bhojpur, Buxar, Mirzapur and Ghazipur districts are mostly located in entrenched channels and floodplains of the Ganga River in the Holocene Newer Alluvium surfaces. Tubewells located in Ballia, Ara, Chhapra, Patna, Hazipur, Buxar, Muhammadabad, Ghazipur, Saidpur, Varanasi, Chunar and Mirzapur towns are As-safe in groundwater because of their positions on the Older Alluvium upland surfaces (Shah 2008, 2014).

3.3 Ghaghara Valley

In the Ghaghara Valley, 231 tubewell water samples were analysed from Faizabad, Gonda and Basti districts (Fig. 14.1). About 38 %, 61 % and 42 % of tubewells in Faizabad, Gonda and Basti districts, respectively have As >10 µg/l. Moreover,

15 %, 45 % and 26 % of tubewells in Faizabad, Gonda and Basti districts, respectively have As above 50 μg/l. Mean As concentrations in tubewells from Faizabad, Gonda and Basti districts are 28.97 μg/l, 101.72 μg/l and 26.40 μg/l, respectively. Maximum concentrations of As in tubewells from Faizabad, Gonda and Basti districts are 350 μg/l, 510 μg/l and 150 μg/l, respectively (Shah 2013). Faizabad, Ayodhya and Nawabganj towns in the Ghaghara Valley are located on the yellow-brown coloured oxidized Pleistocene Older Alluvium upland surfaces and tubewells are As-safe (<10 μg/l) in groundwater. About 47 % As-contaminated (As >10 μg/l) tubewells in these three districts are located within the depth of 10–35 m (Shah 2013).

3.4 Terai Plain of Nepal and West Bengal

Arsenic contamination of groundwater also affects Terai belt of Nepal (Shrestha et al. 2003; Gurung et al. 2005). Major rivers in Terai belt (Fig. 14.1) originate from the Higher Himalaya and minor rivers emanate from the nearby Siwalik hills and deposit sediments in the form of fans along the flank of the Terai belt (Fig. 14.1). Fine sediments and organic material are deposited in inter-fan lowlands in wetlands and swamps. It was observed that sediments carried from the Siwalik hills by the minor rivers release more As than those carried by major rivers from the Higher Himalaya (Shrestha et al. 2003; Gurung et al. 2005). Terai belt of West Bengal has similar sediments characters with Terai belt of Nepal and is As-contaminated in groundwater (Bhattacharyya and Mukherjee 2009). The geology of the Terai Basin of Nepal and West Bengal is similar, based on geochemistry, stratigraphy and carbon-14 age. Average As content (9 mg/kg) of the Terai sediments is within the range of normal sediments (Gurung et al. 2005).

3.5 Brahmaputra Valley

The Brahmaputra is one of the most sediment charged large river of the world. The Brahmaputra Plain in Assam is located between the eastern Himalayas on the north and east, the Patkai and Naga Hills on the northeast and Mikir Hills and Shillong Plateau on the south. The Recent sediments in the Brahmaputra valley are deposited as alluvial fan and braid-cum-flood plain sediments of the Brahmaputra and its several tributaries.

The problem of As contamination in groundwater of Assam has been investigated by various researchers (Singh 2004; Borah et al. 2009; Chetia et al. 2011; Goswami et al. 2013). Arsenic has been detected in 21 of the total 27 districts of Assam. Maximum As content was observed in Jorhat, Dhemaji, Golaghat, Lakhimpur and Majuli Island in the state of Assam. Most of the arsenic contaminated tubewells are located in the entrenched channels and floodplains of

Brahmaputra valley (Fig. 14.1). The concentration of As was relatively high in shallow tubewell (15–40 m deep) as compared to deep tubewell. Available literature shows that groundwater of Assam valleys is highly ferruginous (Borah et al. 2009; Chetia et al. 2011; Goswami et al. 2013).

3.6 Barak Valley

The major parts of the Barak Valley consist of Tertiary upland surfaces with the presence of shale, sandstone, ferruginous sandstone, mottle clay, pebble bed and boulder beds or lowland valley areas with thin cover of Holocene Newer Alluvium sediments on top. The sediments deposited in this valley areas are characterized by organic-rich grey to black coloured, fine grained, argillaceous sediments and are poorly flushed by groundwater. Arsenic-contaminated tubewells are confined in Holocene Newer Alluvium aquifers (Fig. 14.1). Groundwater survey (sample 86) in Cachar and Karimganj districts shows that 66 % of tubewells have As concentrations above 10 µg/l and 26 % of tubewells have As above 50 µg/l (Shah 2012). Maximum As reported from these districts is 350 µg/l. About 90 % of installed tubewells in these two districts are from shallower depth (14 to 40 m). Arsenic-contaminated tubewells are confined in the Holocene Newer Alluvium aquifers (Shah 2012).

3.7 Manipur Valley

The Manipur Valley has been infilled by thick alluvium which is subdivided into the Older (Pleistocene) and Newer Alluvium. The Older Alluvium is made up of clay, silt, coarse sand, gravel, pebble and boulders, deposited adjacent to the foothills and forming older river terraces in the lower part of Manipur Valley. The Newer Alluvium is composed of clay, sand, silt and dark clay with carbonaceous matter, deposited mainly in the central and upper part of the Manipur Valley. About 628 tubewell water samples were analysed from Imphal East, Imphal West, Thoubal and Bishnupur districts of Manipur Valley (Fig. 14.1). About 63 % of tubewells have As >10 µg/l and 40 % of tubewells have As >50 µg/l (Chakraborti et al. 2008). Arsenic-contaminated aquifers in the Manipur Valley are mainly located within the Holocene Newer Alluvium, where the depth of tubewells varies from 5 to 120 m (Singh 2004; Chakraborti et al. 2008; Devi Oinam et al. 2011).

4 Source and Release of Arsenic to Groundwater

Arsenic-bearing minerals deposits in the Himalayan hill range include hydrothermal pyrite-chalcopyrite-arsenopyrite-galena mineralization associated with quartz veins in Buniyal, Doda, Almora and J&K Hills (Tewari and Gaur 1977). The Indus-Tsangpo suture in north India is marked by ophiolitic rocks, including olivine serpentinites. These ophiolites are composed of serpentinized peridotite, layered mafic to ultramafic rock, volcanic and oceanic sediments that contain high As (Guillot and Charlet 2007).

Many coal seams from the Raniganj and Jharia coalfields of the Damodar Valley, which flank the Bengal Basin, have As concentrations from 65 to 360 mg/kg. Biogenic As bearing pyrite often grow as cement-like overgrowth on iron-rich heavy mineral like titaniferous magnetite (Acharyya and Shah 2007a).

The Peninsular India is also accounted for source of As where pyrite–bearing shale in Amjhore mine has As 2.6 g/kg (Das 1977). In the gold mineralization belt of Son Valley, As concentrations in bedrock locally range 1–28 g/kg (Mishra et al. 1996).

Mineralogical studies on sediment cores and tubewell sludges from the Bhagirathi-Ganga delta, Middle Ganga Plain and Bengal Delta in Bangladesh corroborate that As-rich pyrite or any other As minerals are rare or absent in the aquifers from affected areas. However, rare presence of biogenic pyrite is recorded in reducing environment often in association of degraded plant remains. Biogenic As-bearing pyrite often grow as cement-like overgrowth on iron-rich heavy mineral like titaniferous magnetite (Acharyya and Shah 2007b). Studies on cores of aquifer sediments from As-contaminated and adjacent safe zones from Chakda and Baruipur areas, West Bengal, reveal following aquifer sediment fractions to be As bearing: iron-oxide-coated quartz and clay (illite) grains, iron-manganese-siderite, magnetite and biotite/chlorite. The XRD studies on iron-coated blackened mineral grains and other grains have revealed the presence of chlorite and amphibole. Arsenic is associated with some of these fractions (Acharyya and Shah 2007b).

Arsenic sorbed in discrete phases of hydrated Fe-Mn oxide was preferentially entrapped in argillaceous and organic-rich Holocene floodplain and deltaic sediments (Bhattacharya et al. 1997; Kinniburgh and Smedley 2001). The anaerobic heterotrophic Fe^{3+} reducing bacteria (IRB) preferentially reduce and dissolve least crystalline discrete phases of hydrate iron oxide (HFO), with consequent release of its sorbed As and other trace elements to groundwater (Islam et al. 2004; Saunders et al. 2005).

5 Conclusions

Groundwater As contamination is reported from Ganga-Meghna-Brahmaputra (GMB) plains under fluvial geomorphology and Quaternary morphostratigraphic setting. The river channels with the Newer Alluvium deposits are incised as narrow entrenched river valley terraces, which normally occur above the active flood plain. Tubewells in the Holocene Newer Alluvial aquifers are mostly As-contaminated in groundwater.

The Pleistocene Older Alluvium upland surfaces are As-safe in groundwater. Most of the towns on the GMB plains are As-safe in groundwater because of their locations on the Pleistocene Older Alluvium upland surfaces. Most of the As-affected villages are preferentially located close to abandoned or present meander channels.

The Pleistocene oxidizing yellow-brown coloured sediments are well flushed by groundwater flow due to high–hydraulic head and are low in As and devoid of organic matter. The environment of the Pleistocene aquifers is not favourable to release sorbed As to groundwater and aquifers are generally As-safe in groundwater.

Acknowledgement The author thanks School of Environmental Studies, Jadavpur University for the As and Fe analyses. The financial support of this study came from DST Young Scientist Scheme, and CSIR Scientists' Pool Scheme, which is gratefully acknowledged.

References

Acharyya, S.K., Lahiri, S., Raymahashay, B.C. and Bhowmik, A. (2000). Arsenic toxicity of groundwater of the Bengal Basin in India and Bangladesh: The role of Quaternary stratigraphy and Holocene sea level fluctuation. *Environ. Geol.*, **39:** 1127–1137.

Acharyya, S.K. and Shah, B.A. (2007a). Arsenic contaminated groundwater from parts of Damodar fan-delta and west of Bhagirathi River, West Bengal, India: influence of fluvial geomorphology and Quaternary morphostratigraphy. *Environ. Geol.*, **52:** 489–501.

Acharyya, S.K. and Shah, B.A. (2007b). Groundwater arsenic contamination affecting different geologic domains in India-a review: Influence of geological setting, fluvial geomorphology and Quaternary stratigraphy. *Environ. Sci. Health. Part A*, **42:** 1795–1805.

Acharyya, S.K. and Shah, B.A. (2010). Groundwater arsenic pollution affecting deltaic West Bengal, India. *Curr. Sci.*, **99:** 1787–1794.

Ahamed, S., Sengupta, M.K., Mukherjee, A., Hossain, A., Das, B., Nayak, B., Pal, A., Mukherjee, S.C., Pati, S., Dutta, R.N., Chatterjee, G., Mukherjee, A., Srivastava, R. and Chakraborti, D. (2006). Arsenic groundwater contamination and its health effects in the state of Uttar Pradesh (UP) in upper and middle Ganga plain, India: A severe danger. *Sci. Total. Environ.*, **370:** 310–322.

Bhattacharyya, D. and Mukherjee, P.K. (2009). Contamination of shallow aquifers by arsenic in upper reaches of Tista river at Siliguri–Jalpaiguri area of West Bengal, India. *Environ. Earth. Sci.*, **57:** 1687–1692.

Bhattacharya, P., Chatterjee, D. and Jacks, G. (1997). Occurrence of arsenic-contaminated groundwater in alluvium aquifers from delta plains, Eastern India: Options for safe water supply. *Water Resour. Devel.*, **3:** 79–92.

Bhattacharjee, S., Chakravarty, S., Maity, S., Dureja, V. and Gupta, K.K. (2005). Metal contents in the groundwater of Sahebganj district, Jharkhand, India, with special reference to As. *Chemosphere*, **58:** 1203–1217.

Borah, K., Bhuyan, B. and Sarma, H.P. (2009). Lead, arsenic, fluoride and iron contamination of drinking water in the tea garden belt of Darrang district, Assam, India. *Environ. Monit. Assess.*, **169:** 347–352.

Bureau of Indian Standards (2003). Indian standard: Drinking water Specification (first revision), Amendment No. 2, New Delhi.

Central Ground Water Board (2010). Ground water quality in shallow aquifers of India. Faridabad.

Chakraborti, D., Mukherjee, S.C., Pati, S., Sengupta, M.K., Rahman, M.M., Chowdhury, U.K., Lodh, D., Chanda, C.R. and Chakraborty, A.K. (2003). Arsenic groundwater contamination in Middle Ganga Plain, Bihar, India: A future Danger? *Environ. Health Perspect.*, **111:** 1194–1200.

Chakraborti, D., Ghorai, S., Das, B., Pal, A., Nayak, B. and Shah, B.A. (2009). Arsenic exposure through groundwater to the rural and urban population in the Allahabad-Kanpur track in the Upper Ganga Plain. *J. Environ. Monit.*, **11:** 1455–1459.

Chakraborti, D., Singh, E.J., Das, B., Shah, B.A., Hossain, M.A., Nayak, B., Ahamed, S. and Singh, N.R. (2008). Groundwater arsenic contamination in Manipur, one of the seven North-Eastern Hill states of India: A future danger. *Environ. Geol.*, **56:**, 381–390.

Chetia, M., Chatterjee, S., Banerjee, S., Nath, M.J., Singh, L., Srivastava, R.B. and Sarma, H.P. (2011). Groundwater arsenic contamination in Brahmaputra river basin: A water quality assessment in Golaghat (Assam), India. *Environ. Monit. Assess.*, **173:** 371–385.

Das, S. (1977). A note on prospecting of Amjhore pyrite, Rohtas district, Bihar with discussion on the origin of the deposits. *Ind. Min.*, **31:** 8–22.

Devi Oinam, J., Ramanathan, AL., Linda, A. and Singh, G. (2011). A study of arsenic, iron and other dissolved ion variations in the groundwater of Bishnupur District, Manipur, India. *Environ. Earth Sci.*, **62:** 1183–1195.

Garai, R., Chakraborty, S., Dey, B. and Saha, K.C. (1984). Chronic arsenic poisoning from tubewell water. *Ind. Med. Assoc.*, **82:** 34–35.

Goswami, R., Rahman, M.M., Murril, M., Sarma, K.P., Thakur, R. and Chakraborti, D. (2013). Arsenic in the groundwater of Majuli, the largest river island of the Brahmaputra: Magnitude of occurance and human exposure. *Journal of Hydrology*, doi: http://dx.doi.org/10.1016/j.jhydrol.2013.09.022.

Guillot, S. and Charlet, L. (2007). Bengal arsenic, an archive of paleohydrology and Himalayan erosion. *Environ. Sci. Health Part A*, **42:** 1785–1794.

Gurung, J.K., Ishiga, H. and Khadka, M.S. (2005). Geological and geochemical examination of arsenic contamination in groundwater in the Holocene Terai Basin, Nepal. *Environ. Geol.*, **49:** 98**–**113.

Islam, F.S., Gault, A.G., Boothman, C., Polya, D.A., Charnock, J.M., Chatterjee, D. and Lloyd, J.R. (2004). Role of metal-reducing bacteria in arsenic release from Bengal delta sediments. *Nature*, **430:** 68–71.

Kinniburgh, D.G. and Smedley, P.L. (2001). Arsenic contamination of groundwater in Bangladesh. *British Geological Survey Report, WC/00/19*, Dhaka.

Kumar, M., Kumar, P., Ramanathan, AL., Bhattacharya, P., Thunvik, R., Singh, U.K., Tsujimura, M. and Sracek, O. (2010). Arsenic enrichment in groundwater in the middle Gangetic plain of Ghazipur district in Uttar Pradesh, India. *J. Geochem. Explor.*, **105:** 83–94.

Mallick, S. and Niyogi, D. (1972). Application of geomorphology in groundwater prospecting in the alluvial plains around Burdwan, West Bengal. *Ind. Geohydrology*, **8:** 86–98.

Mandal, B.K., Roy Choudhury, T., Samanta, G., Basu, G.K., Chowdhury, P.P., Chandra, C.R., Lodh, D., Karan, N.K., Dhar, R.K., Tamili, D.K., Das, D., Saha, K.C. and Chakroborti, D. (1996). Arsenic in groundwater in Seven districts of West Bengal, India – The biggest arsenic calamity in the world. *Curr. Sci*., **70:** 976–986.

Mandal, B.K. and Suzuki, K.T. (2002). Arsenic round the world: A review. *Talanta*, **58:** 201–235.

McArthur, J.M., Ravenscroft, P., Banerjee, D.M., Milsom, J., Hudson-Edwards, K.A., Sengupta, S., Bristow, C., Sarkar, A., Tonkin, S. and Purohit, R. (2008). How paleosols influence groundwater flow and arsenic pollution: A model from the Bengal Basin and its worldwide implication. *Water Resour. Res*., **44:** 1–30.

Mishra, S.P., Sinha, V.P., Tripathi, A.K., Sharma, D.P., Dwivedi, G.N., Khan, M.A., Yadav, M.L. and Melhrotra, R.D. (1996). Arsenic incidence in Son valley gold belt. *In:* Shanker, R., Dayal, H.M., Shome, S.K., Jangi, B.L. (eds). Symp. Earth Sciences in Environmental Assessment and Management, invited papers and abstracts. Lucknow. *Geol. Surv. Ind.*

Nickson, R., Sengupta, C., Mitra1, P., Dave, S.N., Banerjee, A.K., Bhattacharya, A., Basu, S., Kakoti, N., Moorthy, N.S., Wasuja, M., Kumar, M., Mishra, D.S., Ghosh, A., Vaish, D.P., Srivastava, A.K., Tripathi, R.M., Singh, S.N., Prasad, R., Bhattacharya, S. and Deverill, P. (2007). Current knowledge on the distribution of arsenic in groundwater in five states of India. *Environ. Sci. Health Part A*, **42:** 1707–1718.

Pathak, V.K., Agnihotri, N., Khatoon, N., Khan, A.H. and Rahman, M. (2013). Hydrochemistry of groundwater with special reference to arsenic in Lakhimpur Kheri district, Uttar Pradesh, India. *IOSR Jour. Appl. Chem*., **6:** 61–68.

Raju, N.J. (2012). Arsenic Exposure through Groundwater in the Middle Ganga Plain in the Varanasi Environs, India: A Future Threat. *J. Geol. Soc. India*, **79:** 302–314.

Ravenscroft, P., Brammer, H. and Richards, K. (2009). As pollution: A global synthesis. Wiley-Blackwell, Chichester.

Saha, D., Sreehari, S.S., Shailendra, N.D. and Kuldeep, G.B. (2010). Evaluation of hydrogeochemical processes in arsenic contaminated alluvial aquifers in parts of mid-Ganga basin, Bihar, eastern India. *Environ. Earth Sci*., **61:** 799–811.

Samanta, G., Roy Chowdhury, T., Mandal, B., Biswas, B., Chowdhury, U., Basu, G., Chanda, C., Lodh, D. and Chakraborti, D. (1999). Flow Injection Hydride Generation Atomic Absorption Spectrometry for determination of arsenic in water and biological samples from arsenic-affected districts of West Bengal, India, and Bangladesh. *Microchem. J*., **62:** 174–191.

Saunders, J.A., Lee, M.K., Uddin, A., Mohammad, S., Wilkin, R.T., Fayek, M. and Korte, N.E. (2005). Natural arsenic contamination of Holocene alluvial aquifers by linked tectonic, weathering, and microbial processes. *Geochem. Geophy. Geosys*., **6:** doi:10.1029/2004GC000803.

Shah, B.A. (2008). Role of Quaternary stratigraphy on arsenic-contaminated groundwater from parts of Middle Ganga Plain, UP-Bihar, India. *Environ. Geol*., **53:** 1553–1561.

Shah, B.A. (2010). Arsenic-contaminated groundwater in Holocene sediments from parts of Middle Ganga Plain, Uttar Pradesh, India. *Curr. Sci*., **98:** 1359–1365.

Shah, B.A. (2012). Role of Quaternary stratigraphy on arsenic-contaminated groundwater from parts of Barak Valley, Assam, North–East India. *Environ. Earth Sci*., **66:** 2491–2501.

Shah, B.A. (2013). Status of groundwater arsenic pollution in Holocene aquifers from parts of the Ghaghara Basin, India: Its relation to geomorphology and hydrogeological setting. *Phy. Chem. Earth*, **58–60:** 68–76.

Shah, B.A. (2014). Arsenic in groundwater, Quaternary sediments, and suspended river sediments from the Middle Gangetic Plain, India: Distribution, field relations, and geomorphological setting. *Arab. J. Geosci*., **7:** 3525–3536.

Singh, A.K. (2004). Arsenic Contamination in Groundwater of North Eastern India. Proceedings of national seminar on 'Hydrology with focal theme on Water Quality' held at National Institute of Hydrology, Roorkee during Nov. 22–23.

Shrestha, R.R., Shrestha, M.P., Upadhyay, N.P., Pradhan, R., Khadka, R., Maskey, A., Maharjan, M., Tuladhar, S., Dahal, B.M. and Shrestha, K. (2003). Groundwater arsenic contamination, its health impact and mitigation program in Nepal. *J. Environ. Sci. Health A*, **38:** 185–200.

Tewari, A.P. and Gaur, R.K. (1977). Geological conditions of formation of Pyrite-Polymetallic deposits of the Himalaya and the Great Caucasus – A comparison. *Him. Geol*., **7:** 235–245.
World Health Organisation (1993). Guideline for drinking water quality. *Recommendations* 2nd edn., 1993, **1**, Geneva.

Chapter 15
Water Quality Evaluation in a Rural Stretch of Tezpur, Assam (India) Using Water Quality Index and Correlation Matrix

K.U. Ahamad, N. Medhi, V. Kumar, and N. Nikhil

1 Introduction

Groundwater resources have a major role in ensuring livelihood security across the world, especially in economies that depends on agriculture. In India it is the major source of drinking water in both urban and rural and its importance cannot be over emphasized. It accounts for more than 85 % of the rural domestic water needs, and 50 % of the urban water needs (Ganeshkumar and Jaideep 2011). With an estimated use of 230 km^3 of groundwater every year, i.e. more than a quarter of the global level, India is the largest user of groundwater in the world. At present apart from depletion of groundwater level, India is also facing problems regarding the increments of pollutant concentration present in it. In the North Eastern region of India, natural springs and dug wells are the only cost effective viable means of fulfilling the domestic needs for present population. Information on groundwater quality of northeast India is scanty (Suryawanshi et al. 2004). It has been reported that the concentration of fluoride (F^-), and iron [Fe(II)] in the groundwater is much higher than the permissible limits of drinking water at different areas of Assam (Sushella 2001). Fluoride in the groundwater of Assam has been reported in the range of 5–23 mg/L (Meenakshi and Maheshwari 2006) and iron in the range of 1–25 mg/L (Das et al. 2003; Mahanta et al. 2004). The permissible limit in drinking water is 1–1.5 mg/L for fluoride and 0.3 mg/L for iron (IS 10500 1991; WHO 1993). The iron present in the groundwater causes visible colouration to the water, but fluoride doesn't impart any colour to the water. Therefore the quality of drinking water is of vital importance for human being, though most consumers are unaware of the various pollutants present in the groundwater.

K.U. Ahamad (✉) • N. Medhi • V. Kumar • N. Nikhil
Department of Civil Engineering, Tezpur University, Napaam, 784028 Tezpur, Assam, India
e-mail: kahamad@tezu.ernet.in

F. Kurisu et al. (eds.), *Trends in Asian Water Environmental Science and Technology*, DOI 10.1007/978-3-319-39259-2_15

Whether water is safe for drinking or not cannot be judged simply by vision, taste and smell. The levels of pollutants present in it are actually the deciding factor. Extensive research and analysis are needed over a longer specified time to evaluate the levels of pollutants and to study the seasonal variations and the causes of such variation during the period. Attention on groundwater pollutants and its management has become a need of the hour because of its far reaching impact on human health. Therefore an attempt has been made in the present study to achieve the same by evaluating the quality of groundwater and comparing the same with the standard desirable limits as prescribed by World Health Organization (WHO) in a rural stretch of Tezpur, Assam – a northeastern hilly province of India. People living in rural and semi urban Tezpur are unaware of the various other pollutants present in the groundwater except for iron, as it gives visible colouration to water. The use of WQI could be of particular interest for developing countries, because they provide cost-effective water quality assessment as well as the possibility of evaluating trends. Water quality indices are intended to provide a simple and understandable tool for managers and decision makers on the quality and possible uses of a given water body (Horton 1965; Handa 1981; Suki et al. 1988; Sahu et al. 1991; Palupi et al. 1995). Correlation, basically, is a statistical measurement of the relationship between two variables. It is a useful statistical tool to determine the extent to which changes in the value of an attribute are associated with the changes in another attribute. The present study has been made to evaluate the current status of pollutant and an effort has been made to study the inter-relationship between different components of groundwater using Pearson correlation matrix.

2 Material and Methods

2.1 Sampling Area

Figure 15.1 shows the map of study area covering all the sampling locations. These points were chosen for study after careful consideration. The sampling locations selected are Panchmile, Dolabari, Neriwalm, Aambagan, Tribeni, Mission Chariali, Parowa Chariali, Parowa Gaon, Near Kabristan and TU Main gate. Each location is at a distance of 3 km from the previous covering an area of 30 km periphery.

2.2 Sampling and Analysis

The sampling strategy was designed to cover a range of determinants at sampling sites that accurately represent the groundwater quality of Tezpur region. Sampling was carried out at an interval of 10 days for 5 months (Aug–Dec 2013) to monitor changes caused by the seasonal hydrological cycle. Sampling, preservation and

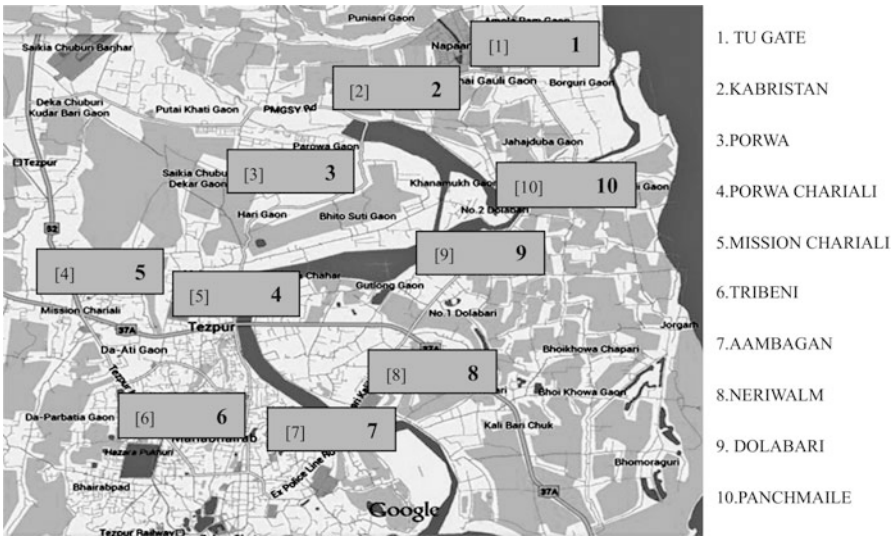

Fig. 15.1 Location of the study area (*Source:* Google map, 2014)

analytical protocols were conducted by standard methods for surface waters (APHA 1998). All samples were collected in 1 L plastic bottles. Each was rinsed three times before collecting, ensuring no adulteration and samples were collected from hand pumps. Although as per WHO recommendations, the time between sample collection and analysis should, in general, not exceed 6 h and 24 h is considered the absolute maximum. However for the present study samples were analyzed within 2–3 h of the collection. The physical characteristics were measured at the location of sampling itself using calibrated digital equipment. The various water quality parameters namely pH, electrical conductivity (EC), turbidity, total dissolved solids (TDS), hardness, alkalinity, dissolved oxygen (DO), iron and fluoride were analysed in laboratory using standard methods determined by American Public Health Association (APHA 1998) and Bureau of Indian Standards (IS 1991).

2.3 Ground Water Quality Index

The Ground Water Quality Index (*GWQI*) is calculated using Weighted Arithmetic Index method as suggested by Brown et al. (1970). The quality rating/sub index (Q_i) corresponding to the *ith* parameter is calculated using following expression.

$$Q_i = \sum_{i=1}^{n} \left[\frac{|M_i - I_i|}{|S_i - I_i|} \right] \times 100 \tag{15.1}$$

where M_i is estimated values of the ith parameter in the laboratory; I_i is ideal values of the ith parameter and S_i is standard values of the ith parameter. All the ideal values (I_i) are taken as zero except for pH for which ideal value is taken as 7. The unit weight (W_i) was calculated by a value inversely proportional to the recommended standard (S_i) of the corresponding parameter.

$$W_i = \frac{I}{S_i} \tag{15.2}$$

The overall ground water quality index (GWQI) is calculated by aggregating the quality rating (Q_i) with unit weight (W_i) linearly. Status of water quality based on WQI is as follows: From 0 to 25 = Excellent, 26–50 = Good, 51–75 = Poor, 76–-100 = Very poor, 100 and above = Unsuitable for drinking.

$$\text{WQI} = \frac{\sum_{i=1}^{n} Q_i W_i}{\sum_{i=1}^{n} W_i} \tag{15.3}$$

2.4 Statistical Analysis

Correlation provides a "unitless" measure of association between two variables, ranging from −1 (indicating perfect negative association) to 0 (no association) to 1 (perfect positive association). Both variables are treated equally in that neither is considered to be a predictor or an outcome. The most commonly used version is the Pearson product moment coefficient of correlation, r_{xy}. The Pearson correlation coefficient (r_{xy}) is computed by using the formula:

$$r_{xy} = \frac{n\Sigma(x_i y_i) - \Sigma(x_i)\Sigma(y_i)}{\sqrt{\left[n\left[\Sigma x_i^2 - (\Sigma x_i)^2\right]\right]\left[n\Sigma y_i^2 - (\Sigma y_i)^2\right]}} \tag{15.4}$$

where the variables x and y represent two different water quality parameters; and n is the number of data points/number of groundwater samples. The inter dependency of each water quality parameter over another was evaluated on the basis of r_{xy} from Eq. (15.4). Interpretation of the Pearson correlation coefficients, adopted in the present study are: $r = -1$ to -0.7 (strong negative association); $r = +0.7$ to $+1.0$ (strong positive association); $r = -0.7$ to -0.3 (weak negative association); $r =$ +0.3 to +0.7 (weak positive association); $r = -0.3$ to +0.3 (negligible or no association). For the nine water quality parameters, the possible correlations between every pair were computed and arranged into a correlation matrix. Precisely, a correlation matrix is a table of all possible correlation coefficients between a set of variables.

3 Results and Discussions

3.1 Water Quality Parameters

The water quality parameters were analyzed for ten batches of samples collected from the sampling sites and presented in Table 15.1, which summarizes the results and basic statistics of the dataset. The various water quality parameters tested are pH, electrical conductivity (EC), total dissolved solids (TDS), alkalinity, iron, total hardness, turbidity, fluoride and dissolved oxygen (DO). Although not definitive, pH of the system is an important indicator of water quality and extent of pollution. WHO sets a desirable range of 6.5–8.0 of pH for drinking water. It has been observed from the analysis of the data of the studied area that pH is almost within the permissible limit (6.5–8.5).

Natural water possesses low conductivity but contamination increases the level of conduction. For the studied area the values of conductivity varies in the range of 73–775 μS/cm, with a mean value of 351.46 μS/cm, which is within the permissible limit of 400 μS/cm as recommended by WHO. The higher value of conductivity beyond permissible limit of 400 μS/cm was found in the groundwater of Aambagan, Neriwalm, Dolabari and Tribeni. The high value of conductivity represents the presence of high concentration of dissolved salts. No health-based guideline is proposed by WHO for TDS. TDS higher than 500 mg/L imparts taste to the water, therefore, a desirable value of 500 mg/L is proposed by WHO. It is observed in the present study that TDS values are well below the upper desirable value of 500 mg/L for all the locations. The maximum TDS of 367 mg/L was found in Kabristan area, which is within the permissible limit (500 mg/L). A variation in alkalinity has been observed: maximum and average alkalinity is 524 mg/L and 133.67 mg/L, but are below the permissible limit (600 mg/L), but substantially higher than WHO desirable level of 200 mg/L. The data indicates high concentration of alkaline salts in the drinking water of these areas.

The variation of hardness in the study area has been observed to be varied within the range of 16–280 mg/L which lies well within the permissible limit of 600 mg/L as prescribed by WHO. It is evident from the analysis of the collected water samples that at all the sampling stations, except Panchmile, Parowa Charali and Parowa, the turbidity in water is less than the desirable limit of 0.5 NTU. On the other hand a value upto 5 NTU is considered acceptable to the consumers (WHO 1993). It is evident that values of turbidity at all the sampling locations except Panchmile is well below 5 NTU. For Panchmile mean value of turbidity for sampling period is 20.25 NTU which is very high above permissible limit and is a matter of concern.

Among the studied parameters iron and fluoride play the most important role in the intend use of water in terms of aesthetic as well as health. Iron gives visible colouration to water which is aesthetically unpleasant. The concentration of iron lies well within the regulatory limits as prescribed by WHO and BIS for all the sampling locations except in Panchmile—exceeding the regulatory limits and

Table 15.1 Summary of water sample analyses and basic statistics

Stations		pH	TDS	EC	Turbidity	Iron	Fluoride	Hardness	Alkalinity	DO
Panchmile	Range	6.53–5.79	90–65	183–165	47.80–9.40	2.84–0.31	0.63–0.00	88–48	126–60	4.39–2.72
	Ave ± SD	6.17 ± 0.28	80 ± 9	175 ± 7	20.25 ± 12.1	1.66 ± 0.94	0.26 ± 0.22	61 ± 15	101 ± 19	3.45 ± 0.63
Dolabari	Range	6.59–5.82	360–201	721–484	3.00–0.50	0.31–0.06	0.66–0.00	136–80	180–118	5.24–2.68
	Ave ± SD	6.24 ± 0.29	295 ± 50	643 ± 68	1.54 ± 0.79	0.15 ± 0.08	0.31 ± 0.23	103 ± 21	150 ± 17	3.56 ± 0.90
Neriwalm	Range	6.83–6.28	324–175	679–430	5.10–0.40	0.20–0.08	0.76–0.00	176–128	312–158	4.27–2.88
	Ave ± SD	6.58 ± 0.20	281 ± 52	571 ± 86	1.32 ± 1.38	0.12 ± 0.04	0.31 ± 0.25	146 ± 14	196 ± 53	3.55 ± 0.55
Aambagan	Range	6.90–6.14	318–191	772–382	1.80–0.40	0.22–0.05	0.62–0.00	280–64	524–82	4.22–2.30
	Ave ± SD	6.45 ± 0.29	267 ± 45	576 ± 167	1.01 ± 0.50	0.10 ± 0.05	0.26 ± 0.26	224 ± 60	270 ± 139	3.41 ± 0.75
Tribeni	Range	6.93–5.84	310–76	775–151	3.50–1.00	0.17–0.07	0.40–0.00	176–120	282–70	4.76–2.85
	Ave ± SD	6.24 ± 0.38	255 ± 68	580 ± 196	2.39 ± 0.78	0.12 ± 0.04	0.13 ± 0.15	164 ± 17	145 ± 70	3.47 ± 0.67
Mission Chariali	Range	6.87–5.80	53–46	149–93	1.60–0.60	0.24–0.08	0.88–0.00	48–16	116–58	4.36–2.81
	Ave ± SD	6.29 ± 0.39	49 ± 2	113 ± 17	0.84 ± 0.29	0.15 ± 0.06	0.31 ± 0.35	30 ± 11	84 ± 19	3.51 ± 0.59
Parowa Chariali	Range	6.48–5.27	61–35	151–73	21.50–3.80	0.87–0.08	0.33–0.00	48–16	98–32	5.04–2.84
	Ave ± SD	5.97 ± 0.40	40 ± 8	97 ± 28	12.98 ± 6.44	0.22 ± 0.24	0.07 ± 0.13	32 ± 11	56 ± 20	3.80 ± 0.85
Parowa Gaon	Range	6.65–5.89	76–66	168–140	9.70–5.70	0.24–0.07	0.89–0.02	64–48	162–90	4.40–2.87
	Ave ± SD	6.27 ± 0.29	70 ± 3	158 ± 9	6.92 ± 1.19	0.14 ± 0.05	0.41 ± 0.33	55 ± 7	117 ± 30	3.55 ± 0.65
Near Kabristhan	Range	6.78–5.81	367–81	734–163	1.60–0.80	0.34–0.08	0.66–0.02	152–56	198–52	4.57–2.88
	Ave ± SD	6.32 ± 0.34	168 ± 82	387 ± 214	1.27 ± 0.22	0.17 ± 0.10	0.37 ± 0.25	94 ± 31	111 ± 42	3.54 ± 0.70
TU Main Gate	Range	6.68–5.84	131–66	263–167	1.30–0.20	0.16–0.07	0.49–0.00	88–40	154–68	4.87–2.82
	Ave ± SD	6.29 ± 0.32	98 ± 24	216 ± 35	0.52 ± 0.40	0.11 ± 0.03	0.14 ± 0.18	64 ± 16	107 ± 32	3.59 ± 0.73

Units: Concentration in mgL^{-1}; conductivity in μScm^{-1}, turbidity in NTU

therefore this water has to be treated for iron before it can be used for drinking. Variation in iron concentration at Panchmile area is quite abrupt throughout the sampling period. However the variation in the concentration of fluoride in the studied area has been found as quite low and it is within the limit as prescribed by WHO and BIS. The presence of dissolved oxygen in groundwater is not desirable. The maximum amount of dissolved oxygen is obtained in samples collected just after rainfall.

3.2 Ground Water Quality Index

Ground Water Quality Index (GWQI) is calculated as per the procedure explained in Sect. 2.3 for different stations using mean values of selected parameters during the study period. The GWQI calculations are shown in Table 15.2, whereas the status of groundwater based on GWQI calculations are presented in Table 15.3 for each of the location. It has been observed from Table 15.3 that groundwater in the Panchmile area is not suitable for drinking which is due to high iron concentration along with turbidity. Same holds true for Parowa Chariali where high turbidity has rendered water poor for drinking purpose. For remaining stations groundwater quality is good.

3.3 Statistical Analysis

3.3.1 Basic Statistics

The maximum and minimum values of the water quality parameters namely pH, electrical conductivity (EC), turbidity, total dissolved solids (TDS), hardness, alkalinity, dissolved oxygen (DO), iron, and fluoride are tabulated in Table 15.4 along with the mean, standard deviation and variance for the entire study period. The variation in the mean value from the standard value (as prescribed by WHO) of various estimated parameters are presented in Fig. 15.2. It can be observed from Table 15.4 that TDS, alkalinity, EC, fluoride, hardness, iron and pH lies within the acceptable limit as prescribed by WHO. However at some places maximum value for electrical conductivity exceeds the acceptable limit. Groundwater in Panchmile area has a severe problem of iron as the concentration of iron is beyond the permissible standard and hence requires treatment before used for drinking water.

The mean value of turbidity is just within the range specified by WHO while the maximum value is quite high. Iron and fluoride are two parameters among the studied nine parameters, significant from both potability and palatability point of view.

Table 15.2 Ground water quality index calculations

				Panchmile			Dolabari			Neriwalm			Aaambagan			Tribeni		
Parameters	S_i	I_i	W_i	Mean	Q_i	$Q_i \times W_i$	Mean	Q_i	$Q_i \times W_i$	Mean	Q_i	$Q_i \times W_i$	Mean	Q_i	$Q_i \times W_i$	Mean	Q_i	$Q_i \times W_i$
Alkalinity	600	0	0.00	101.20	16.87	0.03	149.6	24.93	0.04	196.4	32.73	0.05	270.4	45.07	0.08	145.2	24.20	0.04
Conductivity	500	0	0.00	174.80	34.96	0.07	643	128.60	0.26	570.9	114.18	0.23	575.6	115.12	0.23	580	116.00	0.23
Fluoride	1.5	0	0.67	0.26	17.51	11.67	0.31	20.81	13.87	0.31	20.66	13.77	0.26	17.59	11.73	0.13	8.33	5.56
Hardness	600	0	0.00	61.20	10.20	0.02	103	17.10	0.03	146	24.38	0.04	224	37.40	0.06	164	27.32	0.05
Iron	0.3	0	3.33	1.66	552.96	1843.19	0.15	49.91	166.38	0.12	39.75	132.51	0.10	34.21	114.03	0.12	39.66	132.19
pH	8.5	7	0.12	6.17	55.20	6.49	6.243	50.47	5.94	6.58	28.00	3.29	6.45	36.67	4.31	6.24	50.67	5.96
TDS	500	0	0.00	80.00	16.00	0.03	295	58.94	0.12	281	56.12	0.11	267	53.46	0.11	255	50.92	0.10
Turbidity	10	0	0.10	20.25	202.50	20.25	1.54	15.40	1.54	1.32	13.20	1.32	1.01	10.10	1.01	2.39	23.90	2.39
Σ			4.22		1861.50			186.63			150.01			130.54			144.13	

				Mission Chariali			Parowa Chariali			Parowa Gaon			Near Kabristhan			TU Main Gate		
Parameters	S_i	I_i	W_i	Mean	Q_i	$Q_i \times W_i$	Mean	Q_i	$Q_i \times W_i$	Mean	Q_i	$Q_i \times W_i$	Mean	Q_i	$Q_i \times W_i$	Mean	Q_i	$Q_i \times W_i$
Alkalinity	600	0	0.00	84.4	14.07	0.02	56	9.33	0.02	116.5	19.42	0.03	110.5	18.42	0.03	106.5	17.75	0.03
Conductivity	500	0	0.00	113	22.60	0.05	96.7	19.34	0.04	157.6	31.52	0.06	386.6	77.32	0.15	216.4	43.28	0.09
Fluoride	1.5	0	0.67	0.31	20.71	13.81	0.07	4.68	3.12	0.41	27.58	18.39	0.37	24.99	16.66	0.14	9.64	6.43
Hardness	600	0	0.00	30	5.05	0.01	32	5.25	0.01	55	9.20	0.02	94	15.72	0.03	64	10.60	0.02
Iron	0.3	0	3.33	0.15	49.32	164.39	0.22	71.78	239.28	0.14	45.55	151.82	0.17	56.21	187.37	0.11	36.77	122.58
pH	8.5	7	0.12	6.288	47.47	5.58	5.97	68.67	8.08	6.265	49.00	5.76	6.324	45.07	5.30	6.288	47.47	5.58
TDS	500	0	0.00	49	9.76	0.02	40	8.02	0.02	70	14.00	0.03	168	33.54	0.07	98	19.62	0.04
Turbidity	10	0	0.10	0.84	8.40	0.84	12.98	129.80	12.98	6.92	69.20	6.92	1.27	12.70	1.27	0.52	5.20	0.52
Σ			4.22		183.88			250.55			176.11			209.61			134.76	

Table 15.3 Status of groundwater for each location

Stations	GWQI	Status
Panchmile	445	*Unsuitable for drinking*
Dolabari	45	Good
Neriwalm	36	Good
Aaambagan	31	Good
Tribeni	35	Good
Mission Chariali	44	Good
Parowa Chariali	62	*Poor*
Parowa	43	Good
Kabristan	50	Good
TU Gate	32	Good

Table 15.4 Basic statistics of groundwater for the study period

Parameters	Standards	Mean	Min	Max	Std Dev	Variance
TDS	500	160.19	35.00	367.00	108.02	11668.54
Alkalinity	600	133.67	32.00	524.00	79.83	6372.81
EC	500	351.46	73.00	775.00	237.73	56516.37
DO	–	3.54	2.30	5.24	0.68	0.47
Fluoride	1.5	0.26	0.00	0.89	0.26	0.07
Hardness	300	97.33	16.00	280.00	64.87	4208.49
Iron	0.3	0.29	0.05	2.84	0.55	0.30
Turbidity	5	4.90	0.20	47.80	7.61	57.88
pH	6.5–8.5	6.28	5.27	6.93	0.34	0.12

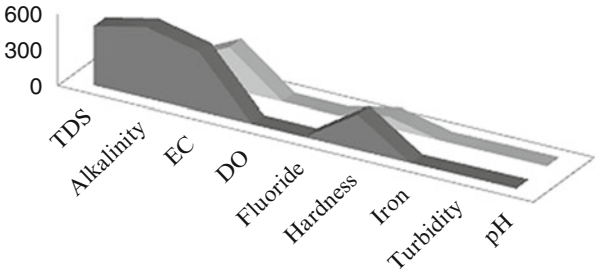

	TDS	Alkalinity	EC	DO	Fluoride	Hardness	Iron	Turbidity	pH
Standards	500	600	500	4	1.5	300	0.3	5	7
Mean	160.19	133.67	351.46	3.54	0.26	97.33	0.29	4.9	6.28

Fig. 15.2 Variation of mean value from the standard value prescribed by WHO

3.3.2 Correlation Coefficient

Correlation coefficient (r) provides a measure of degree of association between two variables. It can be used to assess the interdependence of one variable upon other. Table 15.5 provides the correlation matrix for the nine parameters which has been

Table 15.5 Correlation matrix (Tezpur)

	TDS	Alkalinity	EC	DO	Fluoride	hardness	Iron	Turbidity	pH
TDS	1.00								
Alkalinity	0.62	1.00							
EC	0.96	0.66	1.00						
DO	−0.12	0.17	0.01	1.00					
Fluoride	0.04	0.09	−0.02	−0.45	1.00				
Hardness	0.78	0.72	0.75	−0.11	0.07	1.00			
Iron	−0.21	−0.16	−0.23	−0.17	0.00	−0.18	1.00		
Turbidity	−0.41	−0.26	−0.40	0.02	−0.02	−0.35	0.47	1.00	
pH	0.25	0.10	0.16	−0.54	0.28	0.25	−0.03	−0.21	1.00

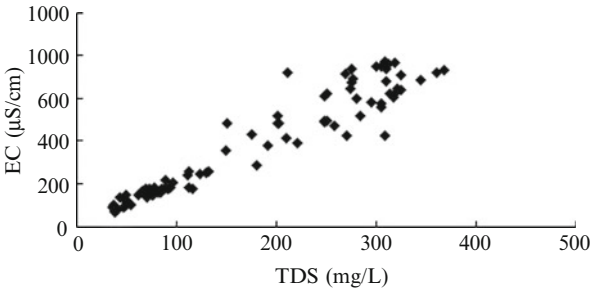

Fig. 15.3 Scatter plot between TDS and EC

analyzed during the study period. From the matrix it can be observed that there is a very Strong Positive Association ($r = 0.7$–1) between TDS – EC. This is on the basis of the fact that ionized substances which leads to conductivity of water also contribute to total dissolved solids. However this association is not on one to one basis as organic molecules and compounds dissolved in water without ionizing are not measured. It can also be seen that there exists strong positive association between TDS – Hardness, Alkalinity – Hardness and EC – Hardness. There exists weak Positive Association ($r = 0.3$–0.7) between Alkalinity – TDS and Alkalinity – EC, which may be accounted on the basis of the fact that alkalinity is a measure of bicarbonates, carbonates and hydroxides present in water which contribute somewhat to conductivity and total dissolved solids. Similarly there exists weak positive association between Turbidity – Iron concentration. It can also be seen that there exists Weak Negative Association ($r = -0.3$–0.7) between TDS – Turbidity, Turbidity – EC, DO – Fluoride, DO – pH and Turbidity – Hardness. The remaining parameters have no association with each other. Figure 15.3 shows a scatter plot between total dissolved solids and electrical conductivity. It can be seen from the plot that for low values, these two parameters are related on nearly one to one basis. However for the higher values their interdependence is not so pronounced.

4 Conclusions

Following conclusions are drawn from the present study:

- The groundwater quality of the studied area is good, except for the Panchmile area where the groundwater has iron beyond permissible limit as prescribed by WHO.
- Groundwater quality index indicates that groundwater of Panchmile is unsuitable for drinking whereas it indicated the quality of groundwater of Parowa Chariali as Poor.
- Statistical analysis suggests that the mean value of turbidity is just within the range specified by WHO while the maximum value is quite high. The concentration of fluoride is well within the permissible limits as specified by WHO. However the concentration of iron in the groundwater at one of the stations (Panchmile) is very high.

- Correlation matrix suggests a very Strong Positive Association between TDS – EC, TDS – Hardness, Alkalinity – Hardness and EC – Hardness. A weak Positive Association between Alkalinity – TDS, Alkalinity – EC and Turbidity – Iron concentration, whereas weak Negative Association between TDS – Turbidity, Turbidity – EC, DO – Fluoride, DO – pH and Turbidity –Hardness.
- Modelling techniques like linear regression, artificial neural network, fuzzy logic etc. can be applied to predict the level of significance.

References

APHA (1998). Standard methods for the examination of water and wastewater. 19th edition, American Public Health Association, American Water Works Association, Water Environment Federation, Washington DC.

Brown, R.M., McClelland, N.I., Deininger, R.A. and Tozer, R.G. (1970). A water quality index: Do we dare? *Water and Sewage Works*, **117:** 339–343.

Das, B., Talukdar, J., Sarma, S., Gohain, B., Dutta, R.K., Das, H.B. and Das, A.C. (2003). Fluoride and other inorganic constituents in groundwater of Guwahati, Assam, India. *Curr. Sci.*, **85:** 657–661.

Ganeshkumar, B. and Jaideep, C. (2011). Groundwater quality assessment using Water Quality Index (WQI) approach – Case study in a coastal region of Tamil Nadu, India. *Int. J. Env. Sci. & Res.*, **1(2):** 50–55.

Handa, B.K. (1981). An integrated water-quality index for irrigation use. *J. Agr. Sci.*, **51:** 422–426.

Horton, R.K. (1965). An index number system for rating water quality. *J. Water Pollut. Control Fed.*, **37:** 300–305.

IS 10500 (1991). Specification for Drinking Water. Bureau of Indian Standards, New Delhi.

Mahanta, D.B., Das, N.N. and Dutta, R.K. (2004). A chemical and bacteriological study of drinking water in tea gardens of central Assam. *Indian J. Environ. Prot.*, **24:** 654–660.

Meenakshi and Maheshwari, R.C. (2006). Fluoride in drinking water and its removal. *J. Hazard. Mater.*, **137(1):** 456–463.

Palupi, K., Sumengen, S., Inswiasri, S., Agustina, L., Nunik, S.A., Sunarya, W. and Quraisyn, A. (1995). River water quality study in the vicinity of Jakarta. *Water Sci. Technol.*, **31(9):** 17–25.

Sahu, B.K., Panda, R.B., Sinha, B.K. and Nayak, A. (1991). Water quality index of the river Brahmani at Rourkela industrial complex of Orissa. *J. Ecotoxicol. Environ. Monit.*, **1(3):** 169–175.

Suki, A., Kamil, M.Y. and Mok, T.P. (1988). Water quality profile of Sg. Langat. *Pertanika*, **11(2):** 273–281.

Suryawanshi, B.M., Kalyankar, K.B. and Pande, B.N. (2004). Ground water analysis in industrial zone chikalthanna (Aurangabad). *Pollut. Res.*, **23(4):** 649–653.

Sushella, A.K. (2001). Treatise on Fluorosis. *Fluoride*, **34(3):** 181–183.

WHO (1993). Guidelines for Drinking Water Quality (2nd Edition, Vol. I): Health Criteria and Supporting Information. Recommendations. World Health Organization, Geneva, Switzerland.

Part V
Hydrological and Quality Issues: Water Resource in Changing Paradigm

Chapter 16
Meltwater Quality and Quantity Assessment in the Himalayan Glaciers

Virendra Bahadur Singh and AL. Ramanathan

1 Introduction

Glaciers are the largest reservoir of fresh water on the earth. They play a vital role in the hydrological cycle (Sangewar 2012). Snow field areas of the Himalayan glaciers store about 12,000 km^3 of fresh water and are the main source of water for great Asian rivers: Ganga, Brahmaputra and Indus (Cruz et al. 2007). There are approximately 9600 glaciers found in the Indian Himalayan region, covering an area of about 40,000 km^2 (Raina and Srivastava 2008). Himalayan glaciers control the global climate change and are considered as a sensitive indicator for climate change (Sharma et al. 2013a). Since last century, majority of the Himalayan glaciers have been retreating significantly due to climate change (Kulkarni and Bahuguna 2002; Kulkarni and Alex 2003; Kulkarni et al. 2005) and effecting the meltwater runoff from the glaciers of Himalaya (Kulkarni et al. 2002). Discharge from the Himalayan glaciers is important for the generation of hydroelectric power, irrigation and drinking water supply (Singh et al. 2006).

Studies on hydrology and suspended sediment transport from the Himalayan glaciers play a vital role for the management of water resource in the downstream region (Singh et al. 2015a). These glaciers have large lateral and terminal moraines and are responsible for generation of large quantity of rock debris (Hasnain and Thayyen 1999a). Suspended sediment transport from the Himalayan glaciers was carried out at very fast rate during the summer season (Kumar et al. 2014). Himalayan glaciers contribute extensively to the continental solute budget; hence these are recognised as the most important glaciers in the world (Kumar et al. 2009). Solute chemistry of glacier meltwater has been used to understand the solute acquisition processes in the subglacial environment (Raiswell 1984; Souchez and

V.B. Singh • AL. Ramanathan (✉)
School of Environmental Sciences, Jawaharlal Nehru University, New Delhi 110067, India
e-mail: alrjnu@gmail.com

F. Kurisu et al. (eds.), *Trends in Asian Water Environmental Science and Technology*, DOI 10.1007/978-3-319-39259-2_16

Lemmens 1987; Tranter et al. 1993; Brown et al. 1994). Weathering of rock forming mineral along with minor input from atmosphere is the main sources of dissolved ions in the melt water of glacier (Berner and Berner 1987). Various studies are available on the assessment of meltwater quality (i.e. hydrogeochemistry) and quantity (i.e. hydrology) of the Central Himalayan glaciers (Hasnain and Thayyen 1999a; Kumar et al. 2002, 2009; Singh et al. 1995, 2004, 2005a, 2006, 2011; Kumar et al. 2014; Srivastava et al. 2014; Singh et al. 2012, 2014, 2015a; Pottakkal et al. 2014) and Western Himalayan glaciers (Singh 2011; Sharma et al. 2013b; Singh et al. 2013, 2015b, c, d, e; Singh and Ramanathan 2015).

2 Assessment of Meltwater Quality

In this review paper we have mainly focused on meltwater quality assessment of the Central and Western Himalayan glaciers of India.

2.1 Chemical Weathering and Hydrogeochemical Processes

The dominancy of major ions in the water can be understood by weathering of various rock minerals in the drainage basin (Das and Kaur 2001). Table 16.1 summarizes chemical compositions of the meltwater draining from some selected Central and Western Himalayan glaciers. Sulphate is the major anion in the meltwater of Gangotri, Bagni, Dudu and Chaturangi glaciers, whereas bicarbonate is the dominant anion in the meltwater of Dokriani, Kafni, Patsio, Chhota Shigri and Bara Shigri glaciers. Calcium is the dominant cation in the meltwater of Himalayan glaciers. The scatter plot between (Ca + Mg) vs TZ^+ (Fig. 16.1a–e) shows strong correlation among the plotted sampling points with high average ratio 0.71, 0.82, 0.94, 0.72 and 0.85 for Gangotri, Chaturangi, Patsio, Chhota Shigri and Bara Shigri glaciers, respectively. The average (Na + K) vs TZ^+ ratio in these glacier meltwaters was found to be 0.29, 0.18, 0.06, 0.29 and 0.15, respectively. These high inputs of (Ca + Mg) to the TZ^+ (total cations) and low (Na + K) vs TZ^+ ratios indicate that hydrogeochemical characteristics of the meltwater of Central and Western Himalayan glaciers are predominantly regulated by carbonate type weathering followed by silicate type weathering (Singh et al. 2012, 2015a, b, c, d). For weathering of carbonate rocks, hydrogen ions (proton) sources are required (Khadka and Ramanathan 2013). The C-ratio ($HCO_3/HCO_3 + SO_4$) is used for assessment of two main proton delivery mechanisms i.e. sulphide oxidation and carbonation (Brown et al. 1996). The average C-ratio for the meltwater of Gangotri and Chaturangi glaciers were calculated to be 0.43 and 0.26, respectively. These ratios show that sulphide oxidation is the dominant proton producing mechanism in these glaciers meltwaters (Singh et al. 2012, 2015a). The average C-ratio for the meltwater of the Patsio and Chhota Shigri glaciers were computed to be 0.58 and 0.67,

Table 16.1 Chemical compositions of meltwater of some selected Central and Western Himalayan glaciers

Glaciers	EC	pH	H_4SiO_4	HCO_3^-	SO_4^{2-}	Cl^-	NO_3^-	Ca^{2+}	Mg^{2+}	K^+	Na^+	References
Gangotri	81.0	7.2	64.0	266	401	11.2	1.9	206	197	83	75	Singh et al. (2012)
Dokriani	48.2	7.0	–	625	406	16.0	–	271	100	116	64	Ahmad and Hasnain (2000)
Bagni	122	7.6	–	1557	1710	13.4	–	680	269	457	21.0	Ahmad and Hasnain (2000)
Kafni	89.2	7.2	28.0	623	76.0	35.0	–	587	165	31.0	65.0	Singh et al. (1998)
Dudu	31.9	6.3	36.0	52.3	85.4	5.0	14.9	91.1	6.5	24.6	42.7	Ahmad and Hasnain (2001)
Chaturangi	124	5.8	62.9	288	837	12.8	2.86	490	405	85.8	105	Singh et al. (2015a)
Patsio (2010/ 2011/2012)	155/ 143/ 156	7.0/ 6.8/ 7.1	15.5/ 20.2/ 21.1	671/ 707/ 800	586/ 483/ 541	11.2/ 13.9/ 12.5	9.39/ 4.55/ 5.04	890/ 982/ 1035	275/ 320/ 305	38.1/ 52.6/ 46.4	34.8/ 42.2/ 42.5	Singh et al. (2015b)
Chhota Shigri (2008/2009)	56.2/ 42.5	6.7/ 6.5	71.8/ 33.4	261/ 219	160/ 104	10.6/3.3	1.31/ 1.50	128/104	118/ 98.8	51.7/ 28.9	58.3/ 38.8	Singh et al. (2015c)
Bara Shigri	40.6	6.6	17.9	232	192	15.4	3.28	274	60.2	28.4	28.8	Singh et al. (2015d)

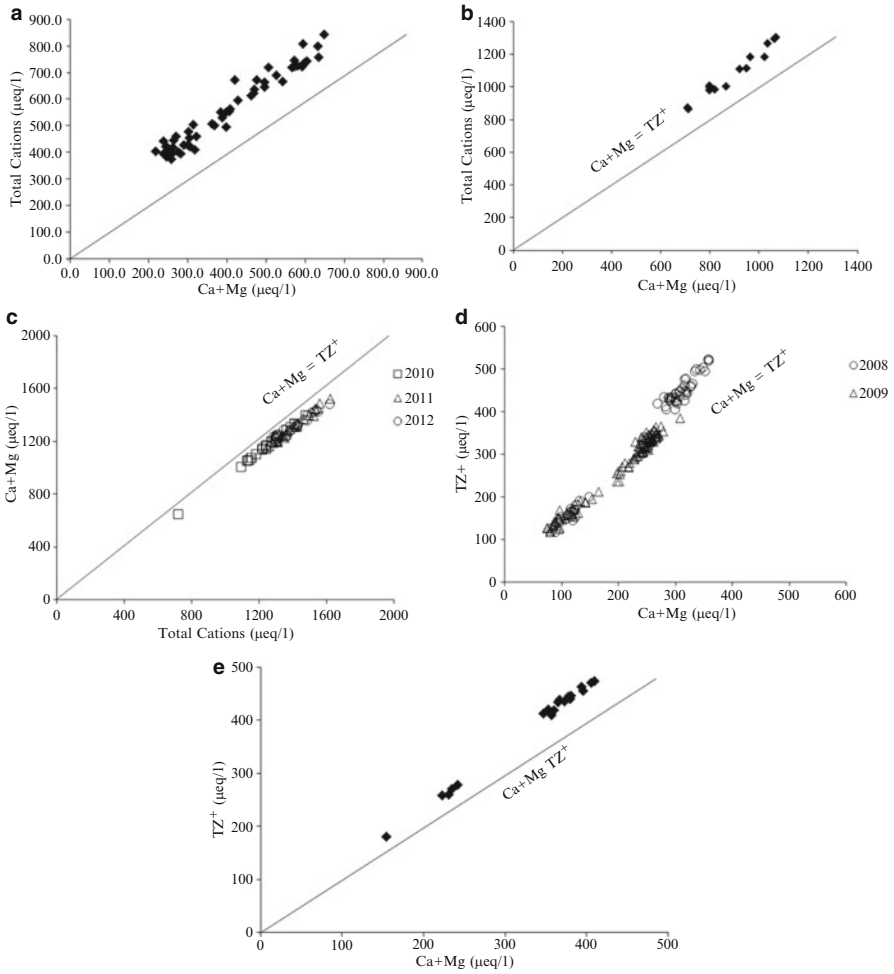

Fig. 16.1 Scatter plots between (Ca + Mg) vs TZ^+ (total cations) for (**a**) Gangotri glacier, (**b**) Chaturangi glacier, (**c**) Patsio glacier, (**d**) Chhota Shigri glacier and (**e**) Bara Shigri glacier

respectively, which indicate dominance of carbonate dissolution and dissociation of atmospheric carbon dioxide is the dominant protons producing mechanism in these glaciers meltwaters (Brown et al. 1996; Hasnain and Thayyen 1999b; Singh and Hasnain 2002; Khadka and Ramanathan 2013; Singh et al. 2015b, c).

Mild acidity generated by dissolution of carbon dioxide plays an important role for weathering capability of the natural water (Panigrahy and Raymahashay 2005). The average Pco_2 (carbon dioxide partial pressure) value for the meltwater of Central and Western Himalayan glaciers was higher than the atmospheric Pco_2 value, showing disequilibrium with respect to atmosphere and open system weathering (Sharma et al. 2013b; Singh et al. 2012, 2015b, c). The Piper plot is a

trilinear representation of the dominant ions present in the water and is applied for classification of water type or hydrogeochemical facies (Anshumali et al. 2014). $CaSO_4$ is the dominant hydrogeochemical facies in the meltwater of Gangotri and Chaturangi glaciers (Singh et al. 2012, 2015a), whereas for Patsio, Chhota Shigri and Bara Shigri glaciers, $CaHCO_3$ is the dominant hydrogeochemical facies (Singh et al. 2015b, c, d).

2.2 Input from Atmospheric Precipitation and Anthropogenic Activities

Although weathering of rocks is the dominant sources of various ions in the glacierized area, atmospheric precipitation may also have some contribution to the hydrogeochemistry of the glaciers meltwaters. Generally, sodium and chloride are the dominant ions in the rainfall dominated water (Meybeck 2003). Chloride is not much reactive within the ecosystem and not usually generated by rock weathering; therefore it is utilized as a reference ion for the determination of atmospheric precipitation to the solute budget of the river water (Meybeck 1983). The significance of atmospheric input to the hydrochemistry of river water can be understood by element to chloride ratio or by comparing the hydrochemistry of river water with the local rain water (Sarin et al. 1989; Pandey et al. 1994, 1999; Singh et al. 2005b). The average ratio of Na/Cl and K/Cl in the meltwater of Gangotri, Chaturangi, Patsio, Chhota Shiri and Bara Shigri glaciers is significantly higher than the sea aerosols, indicating relatively small input of these ions from atmospheric fallout to the hydrogeochemistry of these glaciers meltwaters (Kumar et al. 2009; Sharma et al. 2013b; Singh et al. 2012, 2014, 2015a, b, c, d). Trace quantity of nitrate and phosphate was reported from the Central and Western Himalayan glaciers, indicating palatability of these glaciers meltwaters. Many pilgrims and tourists visit the Gangotri and Chaturangi glaciers; therefore anthropogenic activities may be the possible source of these ions in these study areas (Singh et al. 2012, 2014, 2015a). In the Chhota Shigri and Bara Shigri glaciers, many shepherds arrive with lot of sheep and goats. Hence this could be one of the possible sources of nitrate and phosphate in these glaciers meltwaters (Singh et al. 2014; 2015c).

3 Assessment of Meltwater Quantity

3.1 Meltwater Runoff

Huge areas in the Himalayas are covered by snow and glaciers, which are the main source of water (Singh et al. 2011). Hydrological investigation of mountainous

areas' mainly snow and glacier hydrology is lagging behind in proportion due to lots of difficulties in data collection from mountainous areas (Singh et al. 2006). Hydrological investigations for the Chhota Shigri glaciers in Himachal Pradesh were carried out during the multi-disciplinary expeditions (1986–1989) sponsored by the Department of Sciences and Technology, Government of India. Velocity-area method was used for discharge measurements in Chhota Shigri meltwater stream. Researchers from the School of Environmental Sciences, Jawaharlal Nehru University, New Delhi also conducted the hydrological measurement on this glacier meltwater stream since 2003 onward.

The average daily meltwater runoff from the Chhota Shigri glacier has ranged from 7 to 12 cumecs between July and August 1987. Maximum runoff was observed between 3.30 pm and 7.00 pm, while minimum runoff was observed between 3.00 am and 7.00 am. The time lag between ice melting at the surface of glacier and meltwater runoff at the discharge site was 2–3 h (NIH 1988). Central Water Commission had observed Chhota Shigri glacier from 1986 to 1989. Average discharge during the study period August and September was measured to be 9.30 cumecs and 5.38 cumeces, respectively. Meltwater runoff varies directly with temperature and it alone can explain about 60 % of discharge (Vohra 1991a). Study carried out by Singh et al. (2015g) on the Chhota Shigri glacier indicates that meltwater runoff is showing increasing trend from May onward and attains its maximum value in August and then starts decreasing.

Total discharge volume of meltwater draining from the Gangotri glacier was estimated to be 581.87 and 547.47×10^6 m^3 in May-October 1999 and 2000, respectively (Kumar et al. 2002). The daily discharge for June, July, August, September and October in 1999 was observed to be 53.87 ± 34.04, 66.96 ± 11.83, 57.22 ± 12.85, 30.75 ± 6.90 and 7.97 ± 5.89 m^3/s while in 2000 it was observed to be 35.56 ± 9.16, 65.94 ± 23.67, 48.13 ± 13.61, 26.76 ± 8.88 and 15.20 ± 1.77 m^3/s, respectively (Kumar et al. 2002). The study carried out by Singh et al. (2006) on the Gangotri glacier showed that mean monthly discharge for May, June, July, August, September and October (2000 to 2003) was measured to be 27, 74, 122, 106, 61 and 22 m^3/s, respectively.

3.2 Suspended Sediment Transport

Transportation of suspended sediment from meltwater of the Himalayan glaciers is highly variable due to variability in types of weathering, rock, tectonic setting, sources of sediment, climatic conditions and debris entrainment processes (Kumar et al. 2002). Huge amount of sediment materials such as moraines, boulders and debris are found on the surface of Himalayan glaciers. They play an important role for the production of sediment from the glaciers. Ablation zone of the Himalayan glaciers have large amount of sediment materials, hence this zone of glaciers supplies a huge amount of sediment to the meltwater streams of the Himalayan glaciers. Suspended sediment concentrations of the Central and Western Himalayan

Table 16.2 Suspended sediment concentration of Central and Western Himalayan glaciers meltwater

Glaciers	Regions	Suspended sediment concentration (mgl^{-1})	References
Dokriani	Uttarakhand, India	2196	Kumar et al. (2014)
Patsio (2011/2012)	Himachal Pradesh, India	28.1/48.8	Singh et al. (2015e)
Dunagiri	Uttarakhand, India	229	Srivastava et al. (2014)
Gangotri	Uttarakhand, India	1815	Singh et al. (2014)
Chhota Shigri (2008/2009)	Himachal Pradesh, India	143/137	Singh et al. (2015c)

glaciers are given in Table 16.2. Suspended sediment concentrations of the Gangotri and Dokriani glaciers are higher than the Patsio, Dunagiri and Chhota Shigri glaciers, may be due to high discharge and geology of the study areas. Daily mean suspended sediment load of the meltwater of selected Himalayan glaciers are shown in Table 16.3. Meltwaters of the Gangotri glacier have very high suspended sediment load as compared to other selected Himalayan glaciers. Such type of result may be due to high meltwater runoff, geology and high availability of rock debris in the Gangotri glacier (Singh et al. 2014).

4 Conclusions

This review paper is focussed on assessment of meltwater quality and quantity of the Himalayan glaciers. Table 16.1 shows that pH of the meltwater is acidic to alkaline in nature. Among all anions, sulphate is the dominant anion in the meltwater of majority of Central Himalayan glaciers (except Kafni and Dokriani glaciers), whereas bicarbonate is the major anion in the meltwater of Western Himalayan glaciers. Calcium is the dominant cation in the meltwater of Himalayan glaciers. Carbonate weathering is a predominant mechanism regulating hydrochemistry of the Himalayan glaciers. In the Gangotri and Chaturangi glaciers meltwaters, Ca-SO_4 is the major hydrogeochemical facies (Singh et al. 2012, 2015a), whereas $CaHCO_3$ is the dominant hydrogeochemical facies in the meltwater of Patsio, Chhota Shigri and Bara Shigri glaciers (Singh et al. 2015b, c, d). The reported low levels of NO_3^- and PO_4^{3-} reflect good quality of meltwater of the Himalayan glaciers.

Discharge from the Chhota Shigri glacier (Western Himalaya) shows increasing tendency from May onward and attains its maximum value in August and then starts declining (Singh et al. 2015g). Mean monthly meltwater runoff from the Gangotri glacier (Central Himalaya) for May-October (2000–2003) was observed

Table 16.3 Suspended sediment load of the selected Himalayan glaciers

Glacier	Region	Basin area (km^2)	Suspended sediment load (ton day^{-1})	References
Chhota Shigri	Himachal Pradesh, India	45	135	Vohra (1991b)
Dokriani	Uttarakhand, India	16.1	447	Singh and Ramasastri (1999)
Patsio	Himachal Pradesh, India	7.82	2.83	Singh et al. (2015e)
Dunagiri	Uttarakhand, India	17.9	47	Srivastava et al. (1999)
Changme Khangpu	Sikkim, India	4.5	18	Puri (1999)
Gangotri	Uttarakhand, India	556[a]	11,673	Singh et al. (2014)

[a]Data taken from Singh et al. (2006)

to be 27, 74, 122, 106, 61 and 22 m^3/s, respectively (Singh et al. 2006). Meltwaters draining from Gangotri and Dokriani glaciers have high suspended sediment concentrations as compared to the Patsio, Dunagiri and Chhota Shigri glaciers. This may be due to geology and high meltwater runoff from the study areas.

Acknowledgements The authors are thankful to the Department of Science and Technology (DST), Government of India for funding the research project on the Chhota Shigri glacier. First author (Virendra Bahadur Singh) is also grateful to the Commonwealth Scholarship Commission, UK for providing him Commonwealth Split-site Scholarship tenable at University of Bristol, UK.

References

Ahmad, S. and Hasnain, S.I. (2000). Meltwater characteristics of Garhwal Himalayan glaciers. *J Geol Soc India*, **56:** 431–439.

Ahmad, S. and Hasnain, S.I. (2001). Chemical characteristics of stream draining from Dudu glacier: An Alpine meltwater stream in Ganga Headwater, Garhwal Himalaya. *J China Univ Geosci*, **12:** 75–83.

Anshumali, Rani M., Yadav, S.K. and Kumar, A. (2014). Geochemical alterations in surface waters of Govind Ballabh Pant Sagar, Northern Coalfield, India. *Environ Earth Sci*, **71:** 3181–3193.

Berner, E.K. and Berner, R.A. (1987). The global water cycle: Geochemistry and environment. Prentice Hall, Englewood Cliffs.

Brown, G.H., Sharp, M.J., Tranter, M., Gurnell, A.M. and Nienow, P.W. (1994). The impact of post–mixing chemical reactions on the major ion chemistry of bulk meltwaters draining the Haut Glacier d'Arolla, Valais, Switzerland. *Hydrol Proc*, **8:** 465–480.

Brown, G.H., Tranter, M. and Sharp, M. (1996). Subglacial chemical erosion: Seasonal variations in solute provenance, Haut Glacier d'Arolla, Switzerland. *Ann Glaciol*, **22:** 25–31.

Cruz, R.V., Harasawa, H., Lal, M., Wu, S., Anokhin, Y., Punsalmaa, B. et al. (2007). Asia Climate Change 2007: Impacts, Adaptation and Vulnerability. *In:* Parry, M.L., Canziani, O.F., Palutikof, J.P., Linden, P.J., van der and Hanson, C.E. (eds). Contribution of Working Group

II to the Fourth Assessment Report of the Intergovernmental Panel on Climate Change. Cambridge University Press, Cambridge, UK.

Das, B.K. and Kaur, P. (2001). Major ion chemistry of Renuka Lake and weathering processes, Simaur District, Himachal Pradesh, India. *Environ Geol*, **40:** 908–917.

Hasnain, S.I. and Thayyen, R.J. (1999a). Discharge and suspended sediment concentration of meltwaters, draining from the Dokriani glacier, Garhwal Himalaya, India. *J Hydrol*, **218:** 191–198.

Hasnain, S.I. and Thayyen, R.J. (1999b). Controls of major-ion chemistry of the Dokriani glacier meltwaters, Ganga basin, Garhwal Himalaya. *J Glaciol*, **45(149):** 87–92.

Khadka, U.R. and Ramanathan, AL. (2013). Major ion composition and seasonal variation in the Lesser Himalayan lake: Case of Begnas Lake of Pokhara Valley, Nepal. *Arab J Geosci*, **6:** 4191–4206.

Kulkarni, A.V. and Alex, S. (2003). Estimation of recent glacial variations in Baspa Basin using remote sensing techniques. *J Indian Soc Remote Sens*, **31:** 81–90.

Kulkarni, A.V. and Bahuguna, I.M. (2002). Glacial retreat in the Baspa Basin, Himalayas, monitored with satellite stereo data. *J Glaciol*, **48:** 171–172.

Kulkarni, A.V., Mathur, P., Rathore, B.P., Alex, S., Thakur, N. and Kumar, M. (2002). Effect of global warming on snow ablation pattern in the Himalaya. *Curr Sci*, **83(2):** 120–123.

Kulkarni, A.V., Rathore, B.P., Mahajan, S. and Mathur, P. (2005). Alarming retreat of Parbati Glacier, Beas basin, Himachal Pradesh. *Curr Sci*, **88(11):** 1844–1850.

Kumar, A., Verma, A., Dobhal, D.P., Mehta, M. and Kesarwani, K. (2014). Climatic control on extreme sediment transfer from Dokriani glacier during monsoon, Garhwal Himalaya (India). *J Earth Syst Sci*, **123(1):** 109–120.

Kumar, K., Miral, M.S., Joshi, S., Pant, N., Joshi, V. and Joshi, L.M. (2009). Solute dynamics of meltwater of Gangotri glacier, Garhwal Himalaya, India. *Enviro Geol*, **58:** 1151–1159.

Kumar, K., Miral, M.S., Joshi, V. and Panda, Y.S. (2002). Discharge and suspended sediment in the meltwater of Gangotri Glacier, Garhwal Himalaya, India. *Hydro Sci J*, **47(4):** 611–619.

Meybeck, M. (1983). Atmospheric inputs and river transport of dissolved substances. *In:* Webb, B.W. (ed.). Dissolved loads of rivers and surface water quality/quantity relationships. IAHS Publication Number 141.

Meybeck, M. (2003). Global occurrence of major elements in rivers. *In:* Drever, J.I. (ed.). Treatise on Geochemistry, Surface and Ground Water, Weathering, and Soils. Elsevier.

NIH (1988). Hydrological investigations in Chhota Shigri Glacier, Himachal Pradesh, Multi-disciplinary expedition to Chhota Shigri Glacier. Department of Science and Technology, Government of India, New Delhi. Technical Report Number 2.

Pandey, K., Sarin, M.M., Trivedi, J.R., Krishnaswami, S. and Sharma, K.K. (1994). The Indus River system (India–Pakistan): Major ion chemistry, uranium and strontium isotopes. *Chem Geol*, **116:** 245–259.

Pandey, S.K., Singh, A.K. and Hasnain, S.I. (1999). Weathering and geochemical processes controlling solute acquisition in Ganga Headwater-Bhagirathi River, Garhwal Himalaya, India. *Aquat Geochem*, **5(4):** 357–379.

Panigrahy, B.K. and Raymahashay, B.C. (2005). River water quality in weathered limestone: A case study in upper Mahanadi basin, India. *J Earth Syst Sci*, **114:** 533–543.

Pottakkal, J.G., Ramanathan, AL., Singh, V.B., Sharma, P., Azam, M.F. and Linda, A. (2014). Characterization of subglacial pathways draining two tributary meltwater streams through the lower ablation zone of Gangotri glacier system, Garhwal Himalaya, India. *Cur Sci*, **107(4):** 613–621.

Puri, V.M.K. (1999). Glaciohydrological and suspended sediment load studies in the melt water channel of Changme Khangpu Glacier, Mangam district, Sikkim. Symposium on Snow, Ice and Glaciers—Himalayan Prospective. Lucknow.

Raina, V.K. and Srivastava, D. (2008). Glacier Atlas of India. Geological Society of India Bangalore.

Raiswell, R. (1984). Chemical models of solute acquisition in glacial meltwaters. *J Glaciol*, **30 (104):** 49–57.

Sangewar, C.V. (2012). Remote sensing applications to study Indian glaciers. *Geocarto International*, **27(3):** 197–206.

Sarin, M.M., Krishnaswami, S., Dilli, K., Somayajulu, B.L.K. and Moore, W.S. (1989). Major ion chemistry of Ganga-Brahmaputra river system: Weathering processes and fluxes of the Bay of Bengal. *Geochim Cosmochim Acta*, **53:** 997–1009.

Sharma, A.K., Singh, S.K., Kulkarni, A.V. and Ajai (2013a). Glacier Inventory in Indus, Ganga and Brahmaputra Basins of the Himalaya. *Nat Acad Sci Lett*, **36(5):** 497–505.

Sharma, P., Ramanathan, AL. and Pottakkal, J.G. (2013b). Study of solute sources and evolution of hydrogeochemical processes of the Chhota Shigri Glacier meltwaters, Himachal Pradesh, India. *Hydro Sci J*, **58(5):** 1128–1143.

Singh, A.K. and Hasnain, S.I. (2002). Aspects of weathering and solute acquisition processes controlling chemistry of sub-Alpine proglacial streams of Garhwal Himalaya, India. *Hydrol Proc*, **16:** 835–849.

Singh, A.K., Mondal, G.C., Singh, P.K., Singh, S., Singh, T.B. and Tewary, B.K. (2005b). Hydrochemistry of reservoirs of Damodar River basin, India: Weathering processes and water quality assessment. *Enviro Geol*, **8:** 1014–1028.

Singh, A.K., Pandey, S.K. and Panda, S. (1998). Dissolved and sediment load characteristics of Kafni glacier meltwater, Pindar valley, Kumaon Himalaya. *J Geol Soc India*, **52:** 305–312.

Singh, P., Haritashya, U.K. and Kumar, N. (2004). Seasonal change in meltwater storage and drainage characteristics of the Dokriani Glacier, Garhwal Himalayas (India). *Nord Hydrol*, **34:** 15–29.

Singh, P., Haritashya, U.K., Kumar, N. and Singh, Y. (2006). Hydrological characteristics of the Gangotri Glacier, central Himalayas, India. *J Hydrol*, **327:** 55–67.

Singh, P., Haritashya, U.K., Ramasastri, K.S. and Kumar, N. (2005a). Diurnal variations in discharge and suspended sediment concentration, including runoff-delaying characteristics of the Gangotri Glacier in the Garhwal Himalayas. *Hydrol Proc*, **19:** 1445–1457.

Singh, P., Kumar, A. and Kishore, N. (2011). Meltwater storage and delaying characteristics of Gangotri Glacier (Indian Himalayas) during ablation season. *Hydrol Proc*, **25:** 159–166.

Singh, P. and Ramasastri, K.S. (1999). Project report on Dokriani glacier. National Institute of Hydrology, Roorkee, India.

Singh, V.B. and Ramanathan, AL. (2015). Assessment of solute and suspended sediment acquisition processes in the Bara Shigri glacier meltwater (Western Himalaya, India). *Environ Earth Sci*, doi: 10.1007/s12665-015-4584-3.

Singh, P., Ramasastri, K.S., Singh, U.K., Gergan, J.T. and Dobhal, D.P. (1995). Hydrological characteristic of Dokriani Glacier, Garhwal Himalaya. *Hydrol Sci J*, **40(2):** 243–257.

Singh, V.B. (2011). Hydro-meteorological and hydro-geochemical characteristics of Chhota Shigri glacier, Lahaul-Spiti Valley, Himachal Pradesh, India. M.Phil Dissertation, Jawaharlal Nehru University, New Delhi.

Singh, V.B., Ramanathan, AL. and Kuriakose, T. (2015d). Hydrogeochemical assessment of meltwater quality using major ion chemistry: A case study of Bara Shigri Glacier, Western Himalaya, India. *Natl Acad Sci Lett*, **38(2):** 147–151.

Singh, V.B., Ramanathan, AL., Mandal, A. and Angchuk, T. (2015e). Transportation of Suspended Sediment from Meltwater of the Patsio Glacier, Western Himalaya, India. *Proc Natl Acad Sci India, Sect A Phys Sci*, **85(1):** 169–175.

Singh, V.B., Ramanathan, AL. and Pottakkal, J.G. (2015g). Glacial runoff, transport of suspended sediment transport from Chhota Shigri, Western Himalaya, India. *Environ Earth Sci* (under review).

Singh, V.B., Ramanathan, AL., Pottakkal, J.G. and Kumar, M. (2014). Seasonal variation of the solute and suspended sediment load in Gangotri glacier meltwater, central Himalaya, India. *J Asian Earth Sci*, **79:** 224–234.

Singh, V.B., Ramanathan, AL., Pottakkal, J.G. and Kumar, M. (2015a). Hydrogeochemistry of meltwater of the Chaturangi Glacier, Garhwal Himalaya, India. *Proc Natl Acad Sci India, Sect A Phys Sci*, **85(1):** 187–195.

Singh, V.B., Ramanathan, AL., Pottakkal, J.G., Linda, A. and Sharma, P. (2013). Temporal variation in the major ion chemistry of Chhota Shigri glacier meltwater, Lahaul-Spiti Valley, Himachal Pradesh, India. *Natl Acad Sci Lett*, **36(3):** 335–342.

Singh, V.B., Ramanathan, AL., Pottakkal, J.G., Sharma, P., Linda, A., Azam, M.F. and Chatterjee, C. (2012). Chemical characterisation of meltwater draining from Gangotri Glacier, Garhwal Himalaya, India. *J Earth Syst Sci*, **121(3):** 625–636.

Singh, V.B., Ramanathan, AL. and Sharma, P. (2015b). Major ion chemistry and assessment of weathering processes of the Patsio glacier meltwater, Western Himalaya, India. *Environ Earth Sci*, **73:** 387–397.

Singh, V.B., Ramanathan, AL., Sharma, P. and Pottakkal, J.G. (2015c). Dissolved ion chemistry and suspended sediment characteristics of meltwater draining from Chhota Shigri Glacier, western Himalaya, India. *Arab J Geosci*, **8:** 281–293.

Souchez, R.A. and Lemmens, M.M. (1987). Solutes. *In:* Gurnell, A.M. and Clark, M.J. (eds). Glacio-fluvial Sediment Transfer, Wiley, Chichester.

Srivastava, D., Kumar, A., Verma, A. and Swaroop, S. (2014). Characterization of suspended sediment in Meltwater from Glaciers of Garhwal Himalaya. *Hydrol Proc*, **28:** 969–979.

Srivastava, D., Swaroop, S., Mukerji, S., Gautam, C.K. and Roy, D. (1999). Suspended sediment yield and its variation in Dunagiri glacier melt stream, Garhwal Himalaya. Symposium on Snow, Ice and Glaciers—A Himalayan Perspective, Lucknow.

Tranter, M., Brown, G.H., Raiswell, R., Sharp, M.J. and Gurnell, A.M. (1993). A conceptual model of solute acquisition by Alpine glacier meltwaters. *J Glaciol*, **39(133):** 573–581.

Vohra, K. (1991a). Chhota Shigri glacier run-off characteristics. Technical Report on Multi Disciplinary Glacier Expedition to Chhota Shigri, Vol. 4. Department of Science and Technology.

Vohra, K. (1991b). Sediment Load of Chhota Shigri Glacier. Technical Report on Multi Disciplinary Glacier Expedition to Chhota Shigri, Vol. 4. Department of Science and Technology.

Chapter 17
Delineation of Point Sources of Recharge in Karst Settings

Gh. Jeelani and Rouf A. Shah

1 Introduction

Karst, a geomorphic landscape that arises from the combination of high rock solubility and well developed subsurface drainage networks on rock types that are easily dissolved by water notably carbonate rocks such as limestone, dolomite or marble (Bretz 1942; Sweeting 1981; Jennings 1985; Palmer 1991, 2007; Bloom 1998; Klimchouk et al. 2000; Gunn 2004; Culver and White 2005; Ford and Williams 2007) and to a lesser extent evaporites such as gypsum, anhydrite and halite (Kozary et al. 1968; Klimchouk 2002; Johnson and Neal 2003; Ford and Williams 2007), constitutes 20–25 % of the earth's land surface (Ford and William 2007; Bakalowicz 2005). These areas are regraded to represent the earth's most diverse, scenic and resource-rich terrains with much of their wealth hidden underground including minerals, oil and natural gas, limestone quarries, apart from beautiful housing sites for urban development (Lamoreaux et al. 1993; Schmitz and Schroeder 2006). It is worldwide observed that nearly 40–50 % of the human population utilizes drinking water derived from karst aquifer systems, either directly or indirectly (Cost 1995; Ford and Williams 2007; Cooper et al. 2011; Brinkmann and Parise 2012). However, the unique hydrologic, geomorphologic and hydrogeologic features of karst (White 1988; Ford and Williams 2007; Palmer 2007; Parise and Gunn 2007) make these aquifers more vulnerable to pollution and contaminants (Drew and Hötzl 1999; Böhlke 2002; Parise and Pascali 2003; Bonacci 2004; Kovačič and Ravbar 2005; Ford and Williams 2007; Parise 2010).

Pollutants move rapidly from the land surface through large conduits in the limestone down to the water table. Sinking streams, solution hollows, or dolines provide direct entry points to groundwater, with little or no filtration or attenuation

G. Jeelani (✉) • R.A. Shah
Department of Earth Sciences, University of Kashmir, Hazratbal, Srinagar 190006, India
e-mail: geojeelani@kashmiruniversity.ac.in

F. Kurisu et al. (eds.), *Trends in Asian Water Environmental Science and Technology*, DOI 10.1007/978-3-319-39259-2_17

of contaminants (Williams 1993; Vesper et al. 2001; Parise and Pascali 2003; Sauro 2006; Ford and Williams 2007; Lerch 2011), which potentially have a serious impact on sensitive karst environments and can degrade the quality of water resource (Giné 1999; Vesper et al. 2001; Mijatović 1987; DelleRose et al. 2007; Parise and Gunn 2007; Gunn 2007; North et al. 2009). The delicate equilibrium of karst ecosystems, therefore, changes very easily, sometimes dramatically and irreversibly, up to its destruction. This may occur as a consequence of both natural and anthropogenic controls (Nicod 1972; Gunn 1993a, b; 2004; Urich 2002; Spizzico et al. 2005; Brinkmann et al. 2007; Parise 2012). Consequently, karst groundwater requires specific and appropriate protection against contaminants and pollutants. The dumping and/or throwing of solid/municipal wastes at recharge sites is one of the most important confronting environmental issue (Sauro 1993; Frumkin 1999; Giné 1999; Kacaroglu 1999; De Waele and Follesa 2004; Spizzico et al. 2005; Delle Rose et al. 2007; Gunn 2007). Attention on such contamination and its management has become a need of the hour because of its far reaching impact on human health, as the value of groundwater lies not only in its wide spread occurrence and availability but also in its consistent good quality (Rajmohan et al. 2000; UNESCO 2000). This lies in delineating the catchment and actual source areas that feed the aquifer to prevent the important resource from contamination. The number of approaches are used to identify the capture zone or the recharge areas of groundwater/springs, which include geological, geomorphological, hydrogeochemistry, tracer tests and stable isotopes.

Kashmir Valley, a region that underwent an intricate and highly complex geological and geomorphological evolution (Middlemiss 1910, 1911; Wadia 1975), provides a good general view of the most significant karst geomorphic features and peculiar characteristics of karst landforms. Carbonate lithology in the form of triassic limestone constitutes significant karst geomorphologic imprints including solution features, swallow holes, conduits, shafts, caves and large springs, which makes it as potential groundwater reservoir (Jeelani 2008). Kashmir karst has a substantial socio-economical importance as it provides pristine water supply for drinking and irrigation purposes in the form of karst springs. Keeping in view the multi-faceted importance of karst landscapes in the region, very little information is available on the karst geomorphology, hydrology, karst functioning, potential recharge areas and geometry of karst network (e.g., Coward et al. 1972; Jeelani 2005). The present study is first of its kind towards this effort, which aims to identify and to delineate recharge area of the Achabalnag karst spring located in Bringi watershed of western Himalaya (Fig. 17.1), using multiple approaches so that recharge areas can be protected, restricted and conserved from human activities. The watershed lies between latitudes 33°20′–33°45′ N and longitudes 75°10′–75°30′ E and covers an area of 595 km^2. The elevation of this mountainous catchment ranges from 1650 m above mean sea level (amsl) at Achabal town to more than 4000 m amsl near Sinthan top. The Bringi watershed is drained out by Bringi stream which is fed by a number of tributaries of which the most important are east Bringi and west Bringi.

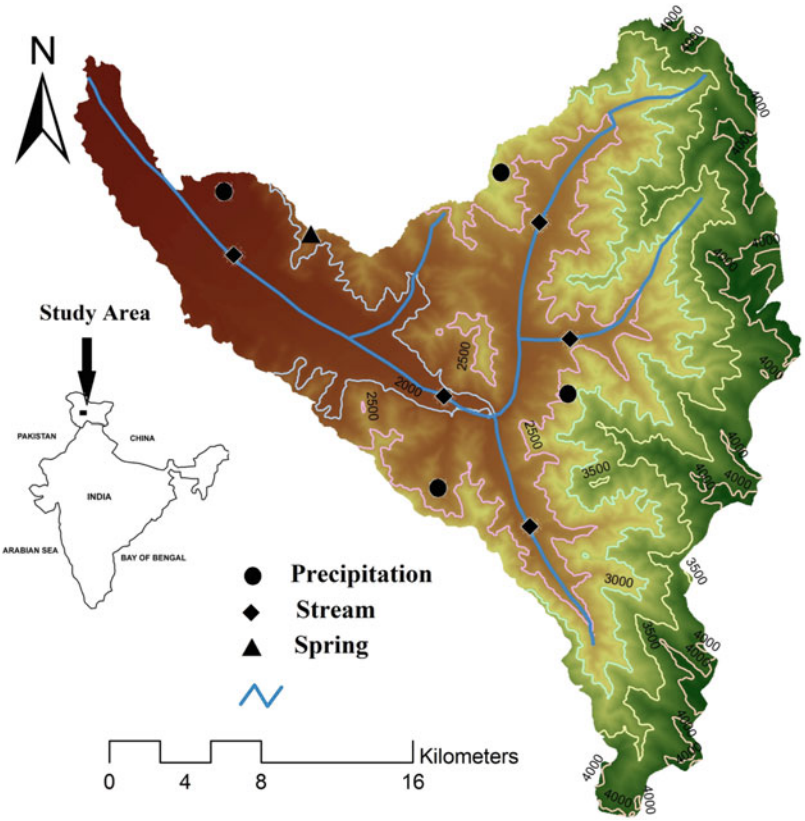

Fig. 17.1 Location map showing the sampling sites

The area receives an average annual precipitation of ~1200 mm amsl. During the past two decades the mean monthly maximum and minimum temperatures ranged from 4 to 27 °C and −4.6 to 15 °C, respectively (Fig. 17.2). March received the maximum rainfall of the year (161 mm) and October the least (34 mm). However, during the observation period (2013) the average temperature varied between 21 °C and −1 °C which is higher than that observed in last decade. The precipitation was recorded higher in March (173 mm) and lower in November (34 mm). It can be clearly seen from the data that March received above normal precipitation in 2013. The lower precipitation recorded in November showed a shift of 1 month compared to last two decades precipitation data (Fig. 17.2).

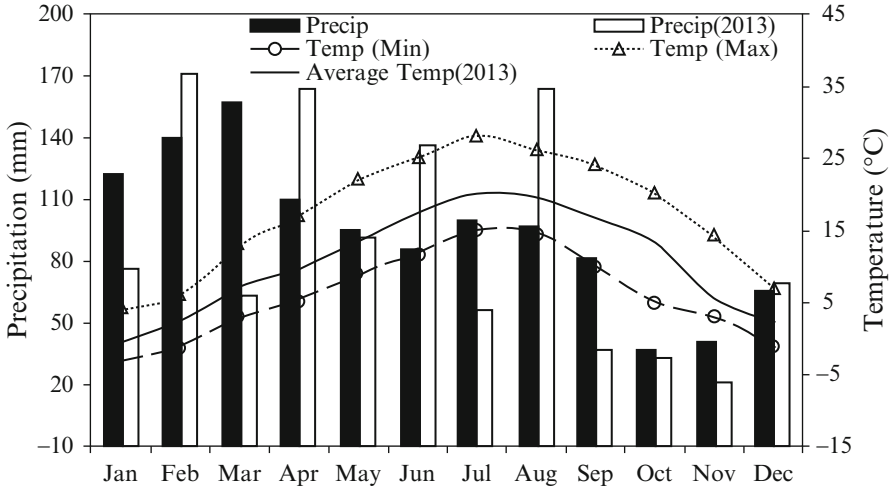

Fig. 17.2 Average monthly variation of temperature and precipitation (average for last two decades, from 1990–2009) and its relation with average temperature and precipitation during 2013

2 Materials and Methods

Precipitation, stream water and groundwater samples were collected across the mountainous watershed of Western Himalaya, for chemical and ($\delta^{18}O$ and δD) isotopic analysis (Fig. 17.1). The samples were collected during 2013 on monthly basis. The precipitation samples were generally collected as rain, except in winter when the samples were collected as snow at lower altitudes (accessible areas). Rainwater samples were collected using a standard rain gauge with a long narrow tube attached to the plastic container, fitted with a funnel, to minimize the evaporative loss of stored rainwater. Groundwater samples were collected from springs. The chemical analysis were carried out at the Department of Earth Science, University of Kashmir. For chemical analysis the water samples were filtered through 0.45 μm nucleopore membrane and collected in 500 ml HDPE bottles. The parameters including temperature, pH, electrical conductivity (EC) and alkalinity were measured in situ. Alkalinity was measured by HCl titration; Ca^{2+}, Mg^{2+}, Na^{+} and K^{+} by AAS; Cl^{-} by $AgNO_3$ titration; and $SO_4{}^{-}$ and $NO_3{}^{-}$ by spectrophotometer. During the analytical procedures, blanks and standards were run to check the reliability of the methods adopted. In most of the water samples, the total cation charge ($TZ^{+} = Ca^{2+} + Mg^{2+} + Na^{+} + K^{+}$ in meq/l) balances that of the total anions ($TZ^{-} = HCO_3{}^{-} + Cl^{-} + SO_4{}^{-} + NO_3{}^{-} + F^{-}$ in meq/l) within analytical uncertainties and the normalized inorganic charge balance is $\left[\text{NCB} = \frac{TZ^{+} - TZ^{-}}{TZ^{+}} \times 100\%\right]$ found to be within ±8 %. The isotopic analysis ($\delta^{18}O$ and δD) were carried out at the Isotope Application Division, Bhabha Atomic Research Centre (BARC) Mumbai and Physical Research Laboratory (PRL) using an isotope ratio mass spectrometer (Europa Geo 20–20) equipped with an equilibration unit (Europa WES) and

following the gas equilibration method (Epstein and Mayda 1953). Secondary standards used in the batch were pre-calibrated using the primary standards and pre-analysed samples procured from the International Atomic Energy Agency, Vienna (IAEA/WMO 1999). The $\delta^{18}O$ and δD values, in per mil (‰) are reported relative to Vienna Standard Mean Ocean Water (V-SMOW). In order to check the consistency in measurements, few samples were analysed in duplicate in each cycle of measurements. The precision of the measurements was within ± 0.1‰ for $\delta^{18}O$ and ± 1.0‰ for δD. Tracer test was performed during August 2013. Rhodamine WT was injected at the identified sink at Adigam/Dewalgam along the course of Bringi stream. Background Rhodamine WT concentrations were set using stream water measurements prior to the start of an injection. Portable Fluorometer GGUN-FL30 (Albilla University of Neuchatel, Switzerland) (Schnegg 2002, 2003; Schnegg and Flynn 2002) was used for the detection of Rhodamine WT dye.

3 Results and Discussion

3.1 Spring Hydrology

Hydrogeologists perceive a spring as an opening that allows to have a look into the underground system of water circulation and its functioning. Hydrographs are regarded as the valuable tools, which provide information about the internal structural of the aquifer. The spring hydrograph of Achabalnag spring showed that the spring discharge is highly fluctuating (Fig. 17.3) ranging 0.30–2.7 m^3/s. The higher discharge was observed in July/August whereas lower discharge in January.

It is clear from the spring hydrograph (Fig. 17.3) that the temporal trend of the spring discharge is similar to that of the ambient temperature trend. With increase in ambient temperature the spring discharge showed an increase while as the decrease in temperature decreased the spring flow. However, the higher temperature in July with lesser spring flow is due to the fact that the seasonal snow pack completely melted before July during the monitoring year. The peak discharge in August is attributed to higher rainfall. The higher precipitation from December to February with lowest spring flow reflects negligible melting and precipitation in the form of snow. The high spring flow in August indicates the maximum potential of the karst aquifer to store groundwater or the maximum recharge through point and nonpoint sources. These observations suggest that the snow melt in the mountainous catchment is the dominant contributor to spring flow. The stream hydrograph was similar to that of spring hydrograph (Fig. 17.4) suggesting a strong link between the two.

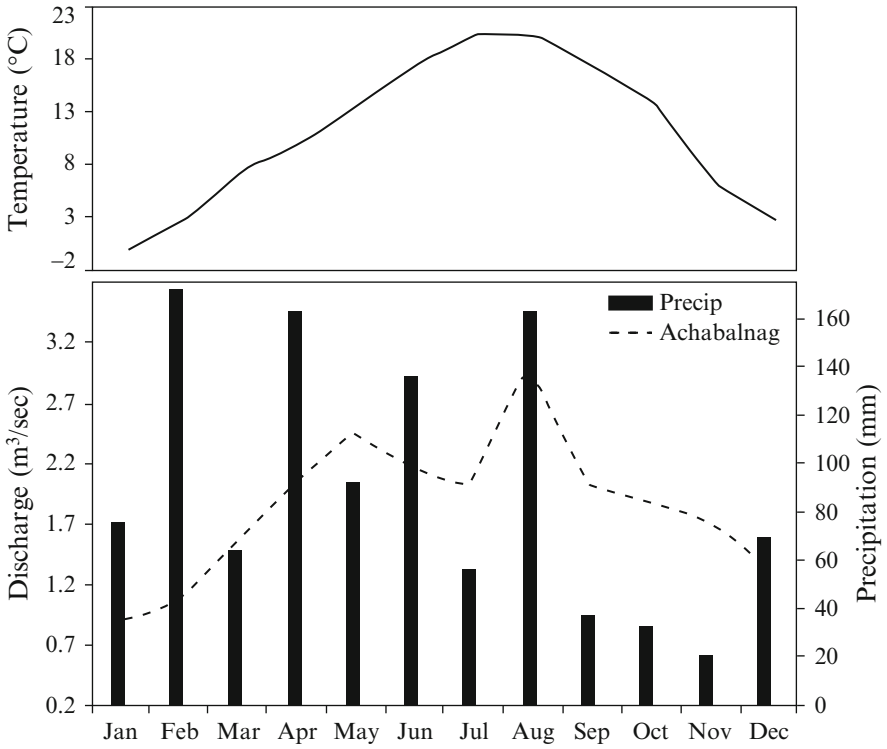

Fig. 17.3 Monthly variation of discharge of Achabalnag karst spring and its relation with ambient temperature and precipitation

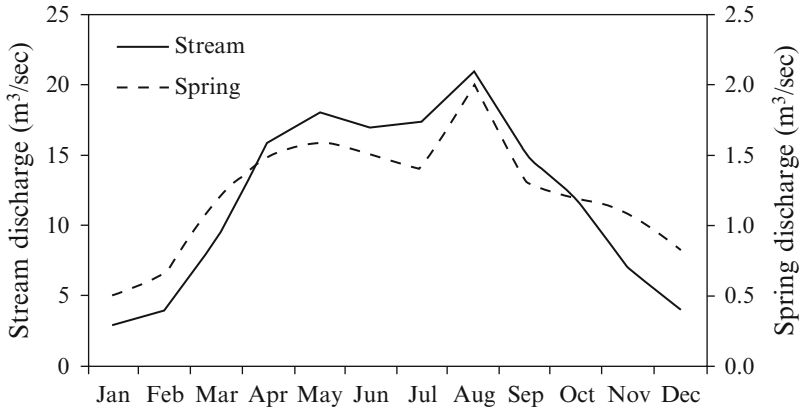

Fig. 17.4 Monthly variation of spring and stream discharges

3.2 Hydrogeochemistry

The hydrochemical data of both the stream and spring was plotted in Piper trilinear and Ludwig-Langliar diagrams (Fig. 17.5), which showed that both the surface water and karst groundwater were of Ca-Mg-HCO_3 water type. Ca^{2+} and Mg^{2+} dominate the cation budget whereas HCO_3^- dominate the anion budget and the order of major ions was $Ca > Mg > Na > K > Fe$ in cations and $HCO_3 > SO_4 > Cl > NO_3 > F$ in anions. However, the concentration of the solutes in surface water is less than that in the spring water reflecting more water-rock interaction of groundwater primarily due to the dissolution of carbonate minerals, limestone and dolomite. The solutes exhibited high concentrations at low discharge during winter and low concentrations at high discharge during summer. The decrease in the concentration of chemical constituents in the spring water with increase of discharge reflects the simultaneous response of the spring to arrival of new water. The decrease of water temperature in the stream and the spring with the increase of discharge also indicate the onset of the melting season. The stream and spring hydrogeochemistry suggest that the streams and springs have hydrological connectivity.

3.3 Water Isotopes in Catchment Waters

Due to the peculiar distribution of precipitation throughout the year, the isotopic signature of precipitation shows a significant spatio-temporal variation across the globe. These isotopic signatures are modified by a multitude of processes, like temperature and continual loss of moisture during the travel of airmass, i.e., Rayleigh distillation (Dansgaard 1964; Rozanski et al. 1993; Kendall and McDonnell 1998), mixing of air masses from local vapour sources and storm

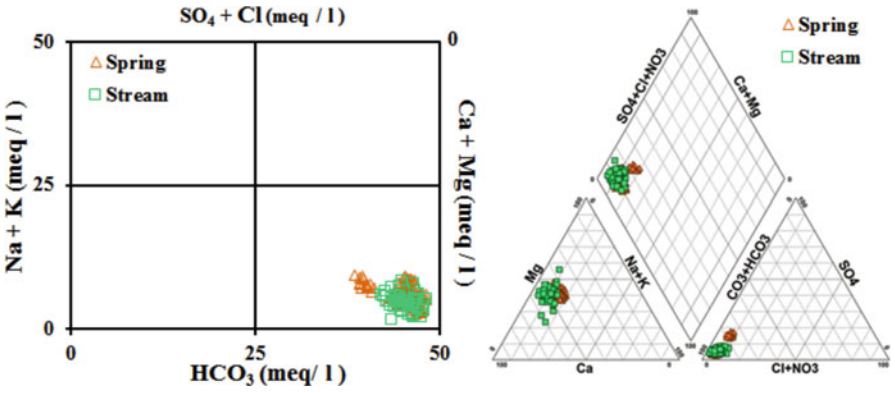

Fig. 17.5 Piper trilinear and Ludwig-Langliar plots (Piper 1994 and Ludwig 1942)

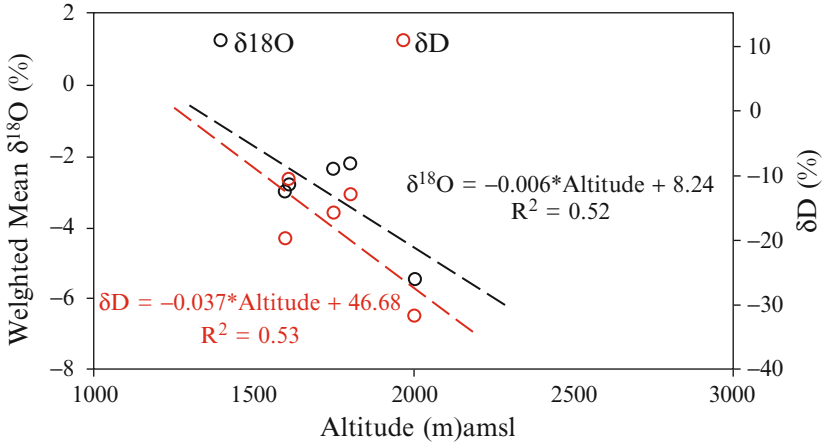

Fig. 17.6 Relationship of stable isotopes with altitude

trajectory (Friedman et al. 1992; Clark and Fritz 1997), altitude, amount and continental effect (Dansgaard 1964; IAEA 1967; Rozanski et al. 1993; Clark and Fritz 1997; Kendall and McDonnell 1998; Araguas-Araguas et al. 2000; Fleitmann et al. 2004; Mook 2000; Lachniet 2009; Gat 2010). In the Bringi mountainous catchment, the water isotopes of the catchment (precipitation, stream and spring) were used to identify the recharge areas of the karst spring. The results showed that $\delta^{18}O$ and δD isotopic values in precipitation samples varied from −1% to −9.8% and 10% to −54%, respectively. The lighter isotopic values (depleted in heavier isotopes) in precipitation were found in the samples collected from higher elevations while as the heavier isotopic values (enriched in heavier isotopes) were found in precipitation samples collected at lower altitude (Fig. 17.6). The altitude gradient of −0.64‰ and −2.9‰ per 100 m changes in elevation amsl was observed for $\delta^{18}O$ and δD, respectively. The estimated gradient was used to infer the recharge altitude of the Achabalnag karst spring.

The variation in temperature at a particular location generated the strong temporal variation in isotopic composition of precipitation with more depleted values in colder months and enriched values during warm period. January recorded the most depleted value and July recorded the enriched isotopic value during the monitoring period (Fig. 17.7).

In mountainous catchments $\delta^{18}O$ and δD of the runoff water is considered to be equal to that of the local or regional precipitation. However, the temporal variation of $\delta^{18}O$ and δD will be larger in streams/rivers where recent precipitation is the main source of flow, and smaller in those streams/rivers where baseflow is the dominant contributor. In Bringi watershed, the similar pattern was observed in stream and spring water with depleted values during the melting season of winter precipitation and enriched values in July. The stream water was observed more depleted in mountainous areas towards the source and enriched values at lower

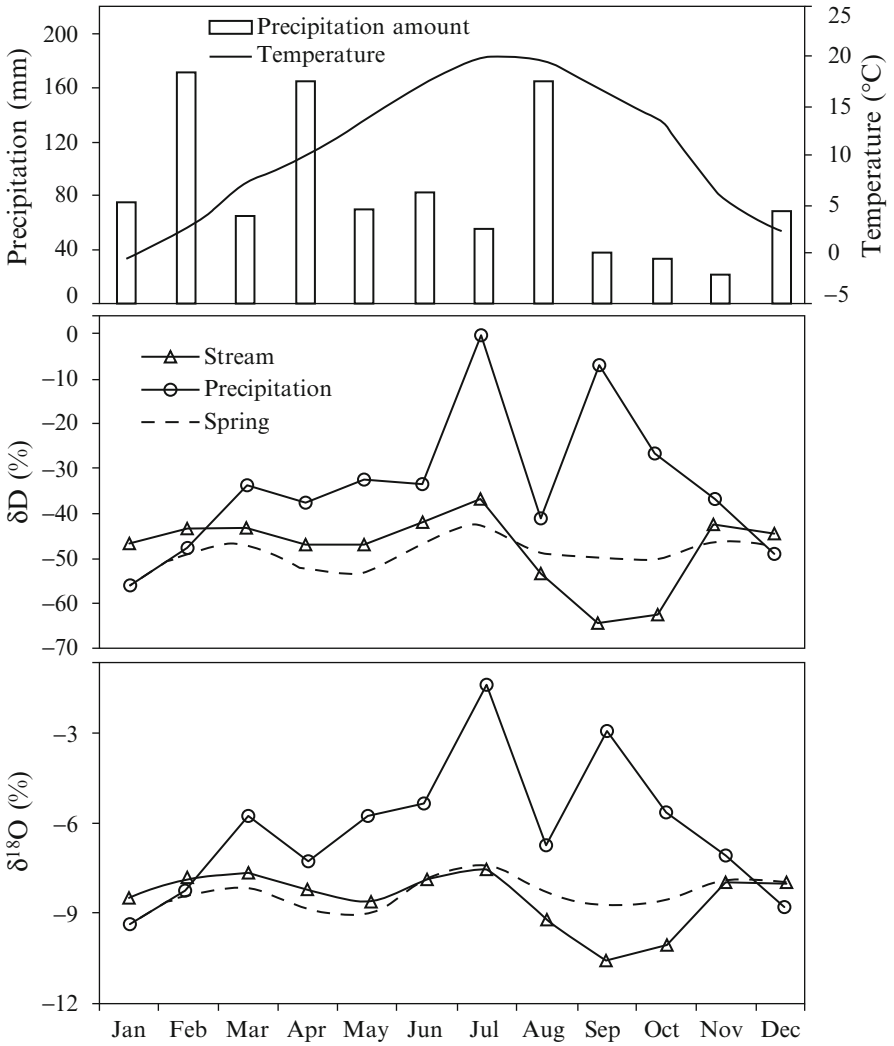

Fig. 17.7 Monthly variation of stable isotopes in precipitation, stream water and spring water and their relationship with ambient temperature and precipitation

parts towards the Valley floor. The enriched values during the February, March, June and July reflect the response of rainfall event (Fig. 17.7). The negligible snow melting/glacial melting due to sub-zero temperature and low discharge during winter represents exchange of baseflow to stream. The similarity of isotopic behaviour of stream and spring reflect recharge is dominantly contributed from the melting of snow. The temporal variation in the $\delta^{18}O$ and δD of Achabalnag karst spring showed best correlation ($r^2 = <0.96$) with the Bringi stream which indicate potential recharge stream. With the help of the local vertical isotopic gradient of

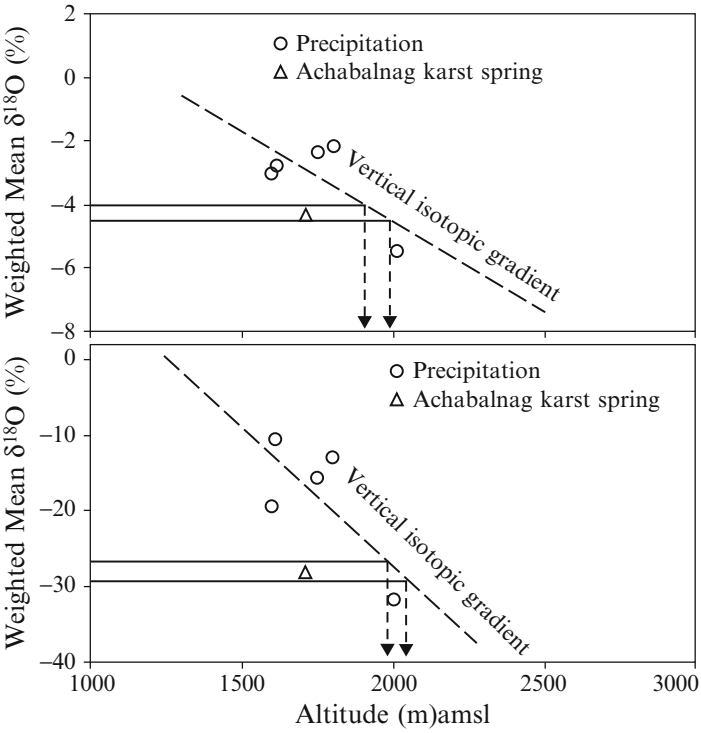

Fig. 17.8 Weighted mean $\delta^{18}O$ (*lower* panel) and δD (*upper* panel) vs. altitude of the samples

precipitation which has turned out to be the most powerful tool for tracing groundwater as it distinguishes groundwaters recharged at high altitude from those at low altitude (Clark and Fritz 1997), obtained from the weighted mean isotopic data and elevation data of precipitation, the mean elevation of precipitation where the recharge occurs was estimated as of −0.64‰ and −2.9‰ per 100 m increase in elevation, for $\delta^{18}O$ and δD, respectively. Since most of the groundwater samples show mean oxygen and hydrogen isotope ratios ranging from −3.8‰ and −31‰, respectively, the altitude of the recharge areas ranging from 1900 to 2000 m amsl (based on $\delta^{18}O$) and 1900 to 2100 m amsl (based on δD) as calculated by equation 2 (Fig. 17.8). The average estimated recharge elevation of an individual karst spring may be estimated by the following regression equations:

1. Using $\delta^{18}O$ tracer: $\delta^{18}O = -0.006\ (\pm 0.00027) \times \text{altitude} + 8.24\ (\pm 0.48)$
2. Using δD tracer: $\delta D = -0.0037\ (\pm 0.0018) \times \text{altitude} + 46.6\ (\pm 4.0)$

The inferred recharge altitude estimated by these tracers could also be overestimated or underestimated in areas where the depleted seasonal snowmelt at higher altitudes is brought down by the stream flow to lower altitudes (recharge sites) without much fractionation and in areas where effect of evaporation is prevalent on groundwater.

3.4 Field Investigations

The hydrogeological field examination was carried out, at an altitude of 1800–2500 m amsl across the Bringi catchments. The dominant surficial karren fields and various conduits were identified across the catchment. A reduction in discharge was noticed along the course of the Bringi stream at Dewalgam and Adigam (Fig. 17.9). During dry period number of karst conduits were also identified along the stream bank at these places. During high flow periods these conduits along the stream banks remain under water. These conduits are the feeding channels of karst groundwater.

3.5 Tracer Test

Tracer testing is an invaluable, commonly used, well-established technique in carbonate aquifers for determining flow direction and transport parameters (Smart and Laidlaw 1977; Käss 1998; Ford and Williams 2007). Given the hydrology of karst terraines, dye tracing is generally the most applied and acceptable method to delineate point-to-point connections between discrete recharge areas and discharge points. Although injection of dye was performed at number of conduits, only two sites (Dewalgam and Adigam) showed hydrological connectivity with the karst spring. The tracer breakthrough curve obtained (Fig. 17.10) suggests less travel time of less than 48 h. Because the flow is rapid and direct, dispersion, dilution and retardation of contaminants is likely to be minimal and the spring is vulnerable to contamination. Therefore, the recharge area of the spring must be protected, restricted and conserved from human activities.

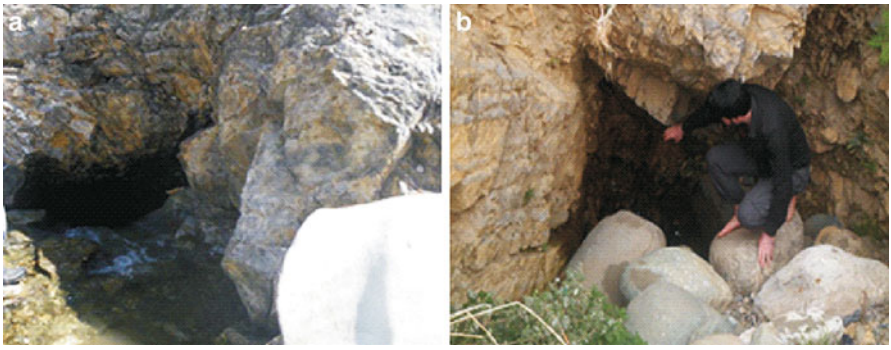

Fig. 17.9 Field photograph of the conduits identified along the course of the stream: (**a**) Photograph taken during higher streamflow and (**b**) under lean flow

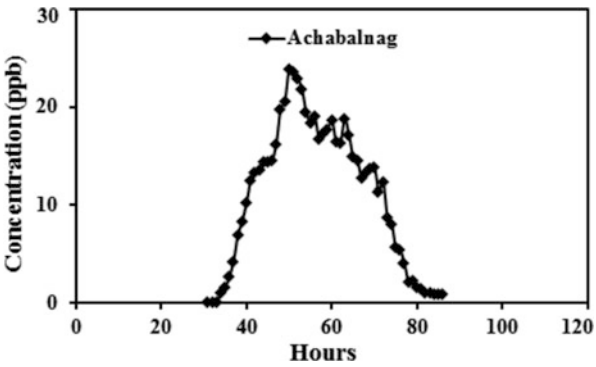

Fig. 17.10 Dye test for Achabalnag karst spring

4 Conclusions

The study was carried out in Bringi watershed, one of the mountainous catchments of the Kashmir Valley. The highly fluctuating discharge of the perennial karst spring indicates well developed subsurface karst. The analysis of spring and stream hydrographs showed that there is a hydrological connection between the streams and springs, which is also corroborated by the hydrogeochemical and isotopic data. The study suggests that snow melt is the dominant contributor to stream and spring flow. The mean recharge altitude of 1900–2200 m amsl was estimated for the Achabalnag karst spring using the vertical isotopic gradient of precipitations. Field investigation followed by tracer tests have confirmed the point sources of recharge at Dewalgam and Adigam. The less travel time and rapid flow suggested that spring is vulnerable to contaminants. Therefore, the recharge area of the spring must be protected, restricted and conserved from human activities.

Acknowledgement The authors are thankful to scientists from IAS, IAD, BARC, Mumbai and Dr. R.D. Deshpande from PRL, Ahmedabad for the isotope analysis.

References

Araguas-Araguas, L., Froehlich, K. and Rozanski, K. (2000). Deuterium and oxygen-18 isotope composition of precipitation and atmospheric moisture. *Hydrol. Process.*, **14:** 1341–1355.

Bakalowicz, M. (2005). Karst groundwater: A challenge for new resources. *Hydrogeol. Jour.*, **13:** 148–160.

Bloom, A.L. (1998). Karst and Speleology. *In:* Bloom, A.L., Geomorphology: A Systematic Analysis of Late Cenozoic Landforms. Prentice Hall, New Jersey.

Bohlke, J.K. (2002). Groundwater recharge and agricultural contamination. *Hydrogeol. Jour.*, **10:** 153–179.

Bonacci, O. (2004). Hazards caused by natural and anthropogenic changes of catchment area in karst. *Natural Hazards and Earth Sys. Sci.*, **4:** 655–661.

Bretz, J.H. (1942). Vadose and phreatic features of limestone caverns. *The Jour. of Geol.*, **50:** 675–811.

Brinkmann, R. and Parise, M. (2012). Karst environments: Problems, management, human impacts, and sustainability – An introduction to the special issue. *J. Cave Karst Stud.*, **74(2):** 135–136.

Brinkmann, R., Wilson, K., Elko, N., Seale, L., Florea, L.J. and Vacher, H.L. (2007). Sinkhole distribution based on pre-development mapping in urbanized Pinellas County, Florida, USA. *In:* Parise, M. and Gunn, J. (eds), Natural and Anthropogenic Hazards in Karst Areas. Geol. Soc. of Lond.

Clark, I.D. and Fritz, P. (1997). Environmental Isotopes in Hydrogeology. Lewis Publishers, Boca Raton.

Cooper, A.H., Farrant, A.R. and Price, S.J. (2011). The use of karst geomorphology for planning, hazard avoidance and development in Great Britain. *Geomorphology*, **134:** 118–131.

COST action 65 (1995). Hydrogeological aspects of groundwater protection in karstic areas. Final COST action 65 report. Report EUR 16547, Directorate General of Research and Development, European Commission Office. Publication of European Communities, Luxembourg.

Coward, J.M., Waltham, A.C. and Bowser, R.J. (1972). Karst springs in the valley of Kashmir. *Jour. of Hydrol.*, **16:** 213–223.

Culver, D.C. and White, W.B. (2005). Encyclopedia of Caves. Elsevier Academic Press, Amsterdam.

Dansgaard, W. (1964). Stable Isotopes in precipitation. *Tellus*, **16:** 436–467.

De Waele, J. and Follesa, R. (2004). Human impact on karst: The example of Lusaka (Zambia). *International Jour. of Speleol.*, **32:** 71–84.

Delle Rose, M., Parise, M. and Andriani, G.F. (2007). Evaluating the impact of quarrying on karst aquifers of Salento (southern Italy). *In:* Natural and anthropogenic Hazard in Karst Areas, Parise, M. and Gunn, J. (eds).

Drew, D. and Hötzl, H. (1999). Karst Hydrogeology and Human Activities. Impacts, Consequences and Implications. Inter. Contri. to Hydrogeol. A.A. Balkeman.

Epstein, S. and Mayeda, T. (1953). Variation of δ18O content in waters from natural sources. *Geochem. Cosmochem. Acta.*, **4:** 213–224.

Fleitmann, D., Burns, S.J., Neff, U., Mudelsee, M., Mangini, A. and Matter, A. (2004). Palaeoclimatic interpretation of high-resolution oxygen isotope profiles derived from annually laminated speleothems from Southern Oman. *Quatern. Sci. Rev.*, **23:** 935–945.

Ford, D. and Williams, P. (2007). Karst hydrogeology and geomorphology. Wiley, Chichester.

Friedman, I., Smith, G.I., Gleason, J.D., Warden, A. and Harris, J.M. (1992). Stable isotope composition of waters in southeastern California, Part 1. Modern precipitation. *J. Geophys. Res.*, **97:** 5795–5812.

Frumkin, A. (1999). Interaction between karst, water and agriculture over the climatic gradient of Israel. *Int. J. Speleol.*, **26B(1/4):** 99–110.

Gat, J.R. (2010). Isotopes Hydrology: A case study of the water cycle. Vol. 6. Imperial College Press.

Giné, S.A. (1999). Agriculture, grazing and land use changes at the Serra de Tramuntana karstic mountains. *Inter. Jour. of Speleol.*, **28B:** 5–14.

Gunn, J. (1993a). The geomorphological impacts of limestone quarrying. *In:* Williams, P.W. (ed.), Karst terrains: Environmental changes and human impacts. Cremlingen-Destedt, Catena Verlag.

Gunn, J. (2004). Encyclopedia of caves and karst science. Fitzroy Dearborn, New York.

Gunn, J. (2007). Contributory zone definition for groundwater source protection and hazard mitigation in carbonate aquifers. *In:* Natural and anthropogenic hazard in karst areas. Parise, M. and Gunn, J. (eds). Geol. Soc. Lond., 279, 97–109.

Gunn, J. (1993b). The geomorphic impacts of limestone quarrying. *In:* Williams, P.W. (ed.), Karst terrains—Environmental changes and human impact. Catena Supplement 25, Catena Verlag, Cremlingen.

IAEA (1967). Tritium and other environmental isotopes in the hydrological cycle. IAEA, Vienna. Tech. rep., 73.

IAEA/WMO (1999). Global Network for Isotopes in Precipitation. The GNIP Database. <http://www-naweb.iaea.org/napc/ih/IHS_resources_gnip.html.

Jeelani, G. (2005). Chemical quality of the spring waters of Anantnag, Kashmir. *Jour. Geol. Soc. India*, **66:** 453–462.

Jeelani, G. (2008). Aquifer response to regional climate variability in a part of Kashmir Himalaya in India. *Hydrogeol. Jour.*, **16:** 1625–1633.

Jennings, J.N. (1985). Karst geomorphology. Basil Blackwell, Oxford.

Johnson, K.S. and Neal, J.T. (2003). Evaporite Karst and Engineering/Environmental Problems in the United States. *Oklahoma Geol. Sur. Circular*. 109.

Kacaroglu, F. (1999). Review of groundwater pollution and protection in karst areas. *Water Air Soil Pollution*, **113:** 337–356.

Käss, W. (1998). Tracing Technique in Geohydrology. Balkema, Rotterdam.

Kendall, C. and McDonnell, J.J. (1998). Isotope Tracers in Catchment Hydrology. Science, B.V. (ed.). Elsevier, Amsterdam.

Klimchouk, A. (2002). Subsidence Hazards in different Types of Karst: Evolutionary and speleogenetic Approach. *Int. J. Speleol.*, **31(1/4):** 5–18.

Klimchouk, A.B., Ford, D.C., Palmer, A.N. and Dreybrodt, W. (2000). Speleogenesis: Evolution of Karst Aquifers, Huntsville, A.L. National Speleological Society, Inc.

Kovačič, G. and Ravbar, N. (2005). A review of the potential and actual sources of pollution to groundwater in selected karst areas in Slovenia. *Natural Hazards and Earth Sys. Sci.*, **5/2:** 225–233.

Kozary, M.T., Dunlap, J.C. and Humphrey, W.E. (1968). Incidence of saline deposits in geologic time. *Geol. Soc. of Amer.*, **88:** 43–57.

Lachniet, M.S. and Patterson, W.P. (2009). Oxygen isotope values of precipitation and surface waters in northern Central America (Belize and Guatemala) are dominated by temperature and amount effects. *Earth Planet. Sc. Lett.*, **284:** 435–446.

Langelier, Wilfred F., and Harvey F. Ludwig. "Graphical methods for indicating the mineral character of natural waters." Journal (American Water Works Association) 34.3 (1942): 335–352.

Lamoreaux, P., Assad, F. and McCarley, A. (1993). Annoted bibliography of karst terraines. Vol. 5. Inter. Contri. to Hydrogeol. (IAH) Hanover Heise.

Lerch, R.N. (2011). Contaminant transport in two central Missouri karst recharge areas. *Jour. of Cave and Karst Stud.*, **73(2):** 99–113.

Middlemiss, C.S. (1910). Revision of Silurian-Trias sequence of Kashmir. *Rec. Geol. Surv. India*, **40:** 206–260.

Middlemiss, C.S. (1911). Sections in the Pir Panjal range and Sindh Valley, Kashmir. *Rec. Geol. Surv. India*, **1:** 115–144.

Mijatović, B. (1987). Catastrophic flood in the polje of Cetinje in February 1986: A typical example of the environmental impact of karst, Proceed. of the sec. multidisciplinary conf. on sinkholes and the environm. Impacts of karst, Orlando. Balkema, Rotterdam.

Mook, W.G. (2000). Environmental isotopes in the hydrological cycle. *In:* Vol. I. Introduction. Mook, W.G. (ed.). Inter. Atomic Energy Agency, Groningen.

Nicod, J. (1972). Pays et paysages du calcaire, Presses Universitaires de France, Paris, 242 pp.

North, L.A., VanBeynen, P.E. and Parise, M. (2009). Interregional comparison of karst disturbance: West-central Florida and southeast Italy. *Jour. of Environ. Management*, **90(5):** 1770–1781.

Palmer, A.N. (1991). Origin and morphology of caves. *Geol. Soc. of Amer. Bullet.*, **103:** 1–21.

Palmer, A.N. (2007). Cave geology. Cave Books, Dayton, OH.

Parise, M. (2010). Hazards in karst. *In:* Bonacci, O. (ed.), Proc. Int. Interdisc. Conf. "Sustainability of the karst environment", Plitvice Lakes (Croatia), 23–26 Sept. 2009, IHPUnesco, Series on Groundwater, 2, 155–162.

Parise M. (2012). Management of water resources in karst environments, and negative effects of land use changes in the Murge area (Apulia, Italy). Karst Development. Vol 2(1).

Parise, M. and Gunn, J. (2007). Natural and anthropogenic hazards in karst areas: Recognition, Analysis and Mitigation. Geol. Soc. Lond., 279.

Parise, M. and Pascali, V. (2003). Surface and subsurface environmental degradation in the karst of Apulia (southern Italy). *Environ. Geol*., **44:** 247–256.

Piper, A. M. (1944), A graphic procedure in the geochemical interpretation of water-analyses, Eos Trans. AGU, 25(6), 914–928, doi:10.1029/TR025i006p00914.

Rajmohan, N., Elango, L., Ramachandran, S. and Natarajan, M. (2000). Major ion correlation in groundwater of Kancheepuram region, south India. *Indian J. Environ. Protection*, **20(3):** 188–193.

Rozanski, K., Aruguas-Aruguas, L. and Ganfiantini, R. (1993). Isotopic patterns in modern global precipitation. *Geophys. Monogr*., **78:** 1–36.

Sauro, U. (1993). Human impact on the karst of the Venetian Fore-Alps, Italy. *Environ. Geol*., **21:** 115–121.

Sauro, U. (2006). Changes in the use of natural resources and human impact in the karst environment of the Venetian prealps (Italy). *Jour. of Acta Carso*., **35(2):** 57–63.

Schmitz, R. and Schroeder C. (2006). Urban site investigation in the Belgian karst belt. The Geol. Soc. of Lond.

Schnegg, P.A. (2002). An inexpensive field Fluorometer for hydrogeological tracer tests with three tracers and turbidity measurement. Paper presented at the XXXII IAH and VI ALHSUD Congress "Groundwater and Human Development", Mar del Plata, Argentina, 21–25.

Schnegg, P.A. (2003). A new field fluorometer for multi-tracer tests and turbidity measurement applied to hydrogeological problems. Paper presented at the 8th Congress of International da Sociedade Brasileira de Geofísica, Rio de Janeiro, R J, Brasil.

Schnegg, P.A. and Flynn, R.M. (2002). Online field fluorometers for hydrogeological tracer tests. *In:* Isotope und Tracer in der Wasserforschung, Technische Universität Bergakademie Freiberg, Wissenschaftliche Mitteilungen, Institut für Geologie., **19:** 29–36.

Smart, P.L. and Laidlaw, I.M.S. (1977). An evaluation of some fluorescent dyes for water tracing. *Wat. Resour. Res*., **13:** 15–33.

Spizzico, M., Lopez, N. and Sciannamblo, D. (2005). Analysis of the potential contamination risk of groundwater resources circulating in areas with anthropogenic activities. *Nat. Haz. Eart. Sys Sci*., **5:** 109–116.

Sweeting, M.M. (1981). Karst Geomorphology. *In:* Rhodes, W. and Fairbridge, C.U. (eds), Benchmark papers in geology, 59. Hutchinson Ross Publishing Company, Stroudsburg.

UNESCO (2000). Groundwater pollution. International Hydrological Programme.

Urich, P.B. (2002) Land use in karst terrain: Review of impacts of primary activities on temperate karst ecosystems. *Sci. for Conser*., **198:** 60.

Vesper, D.J., Loop, C.M. and White, W.B. (2001). Contaminant transport in karst aquifers: Speleogenesis and Evolution of Karst Aquifers. *Theor. and Appl. Karstol*., **13–14:** 101–111.

Wadia, D.N. (1975). Geology of India. Tata McGraw Hill, New Delhi.

White, W.B. (1988). Geomorphology and hydrogeology of karst terrains. Oxford University Press, Oxford.

Williams, P.W. (1993). Karst terrains: Environmental changes and human impact. *In:* NFZFG (eds). Catena Supplement 25, Catena Verlag, Cremlingen-Destedt.

Chapter 18
Identify the Major Reasons to Cause Vulnerability to Mekong Delta Under the Impacts of Drought and Climate Change

Bui Viet Hung

1 Mekong Delta

The Mekong Delta lies within the humid tropics, characterized by consistently high mean monthly temperatures (25–29 °C) and high but seasonal rainfall (1200–2300 mm). Discharge of the Mekong River exhibits strong seasonal variation in corresponding rainfalls. The low flow period (December to May) occurs during the dry season and the earliest stages of the wet season. The low rainfall and high evaporation during the annual dry season place constraints on human habitation and activity in the Mekong Delta. Such conditions also give rise to other problems such as salinity intrusion in coastal areas and acidification in ASS (Acid Sulfate Soil) areas. Shorter periods of dryness, which occur during the onset, or toward the end, of the wet season in some years, may also be extremely damaging to newly planted crops (Thuan 2006).

The topography of Mekong Delta is flat with a dense canal network, which is strongly influenced by the annual floods of the Mekong River. Due to its favourable climatic features, the Mekong Delta has a year-round crop regime. However, Mekong floods arriving late or ending early can lead to large scale drought problems in the Delta. In addition, the main water flow of the Mekong River in the dry season is rather small and its water level is low. Seawater intrudes deeply inland, sometimes as far as 40–50 km from the sea, which has serious adverse effects on rice and fruit trees (White 2002; Long 2014).

The Mekong Delta (MD) is the main agricultural production region in Viet Nam due to fertile soils and abundant water sources. MD has about four million ha of rice area, and more than 18 million tons of rice produced annually—half of the total

B.V. Hung (✉)
Environmental Department, University of Sciences, 227 Nguyen Van Cu Str. District 5, Ho Chi Minh City, Viet Nam
e-mail: bvhung@hcmus.edu.vn

F. Kurisu et al. (eds.), *Trends in Asian Water Environmental Science and Technology*, DOI 10.1007/978-3-319-39259-2_18

amount of paddy rice in Viet Nam. It has also a large fruit production with cultivating area more than 252 million ha and annual production about three million tons. The MD had high economic growth in the 1996–2004 periods with an annual growth rate of 11.2 % (compared with the national growth rate of 7.0 %). In the MD, rice is still the most important crop. In 2004, the total rice area of the MD was 3.8 million ha, accounting for 86 % of total crop area. The average rice yield was 4.9 t/ha and total paddy rice production was 18.5 million tons. In the period of 2000–2004, rice area decreased by 0.8 % annually whereas the yield and output increased by 3.3 and 2.4 % per annum, respectively. With the regional economic development, the fresh water demand for living and production is increasing higher to cause pressure to support the fresh water of Mekong River. MD is sub-area 10 V (Fig. 18.1) (MRC-FMMP 2010).

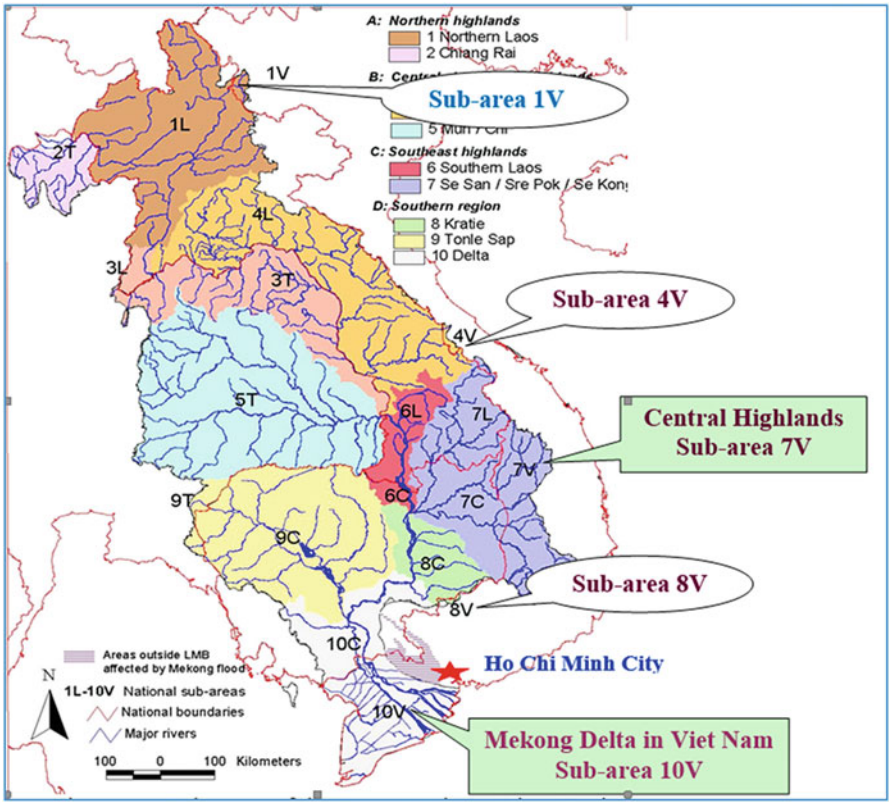

Fig. 18.1 Sub-areas of the Lower Mekong River Basin

The Drought Phenomena in MD Historically, serious drought ravaged the region from April to June of 1983, 1992, 1998, and from October to December of 1958 and 1992. Drought during these years affected 4000 ha to nearly 230,000 ha of farmland, and entirely destroyed 1000 ha to 390,000 ha. The winter-spring and summer-autumn drought in 1998 caused shortage of water for 1.1 million people, affected nearly 274,850 ha of summer-autumn crop area and destroyed over 320,000 ha. Therefore, an effective and comprehensive hydro-meteorological disaster management plan is required in this region, as one of the key economic zones of the nation, to preserve and sustain its resources and richness (Nuoi 2007; SCFSC 2014).

Based on the summaries of Department of Cultivation (MARD), there was about 300,000 ha rice areas in Mekong Delta impacted by the drought-salinity situation in the dry-season 2013. There were more than 100,000 ha rice areas impacted directly, affected seriously to capacity.

The Increasing of Drought on Climate Change – Sea Level Rises Condition Based on the climate change and sea level rises scenarios for Viet Nam published in 2011, the average temperature will increase about 1.5 °C and the average annual rainfall will decrease about 10–15 % (see Fig. 18.2). Thus, the status of lack of water or limited water supply will occur and become serious. These are the initial conditions for drought happened. And if the status remains longer, the impacts of drought on regional socio-economy will be larger and remain longer (IMHEN 2011).

The climate change Scenarios for Mekong Delta of Viet Nam have higher annual average temperature in dry season, which increase the ability of drought occurence

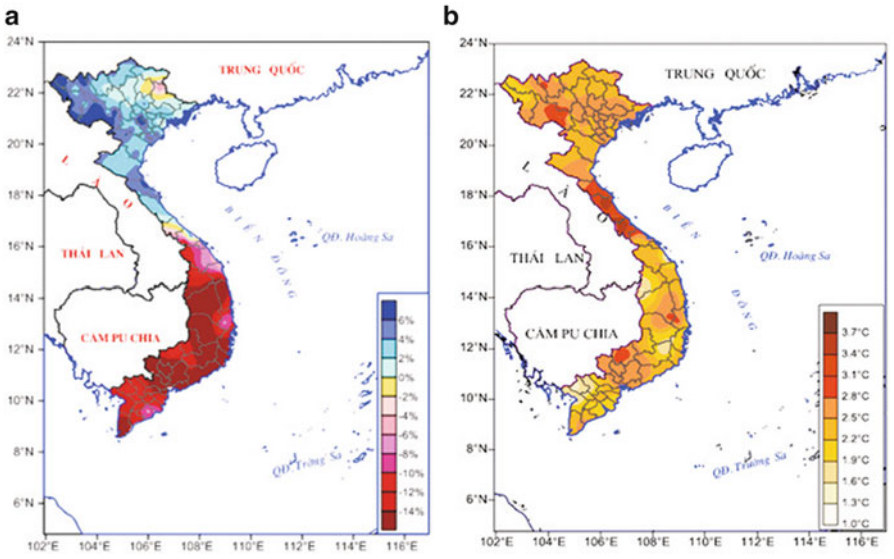

Fig. 18.2 The changing levels (%) of (**a**) annual rainfall and (**b**) temperature in dry season, during last twentieth century under middle emission scenario

and longer drought period. The sea level rise and low flow in river are main factors to lead the salinity water from sea to intrude deeply into Mekong Delta. The salinity water intrusion into inland is deep and a long time to cause the adverse effects to the water supply for living as well as production in region. In case, it is named the agricultural drought, which is a last step of drought's classification. The initial assesment identifies the drought impacts but does not identify the underlying reasons for these impacts (NHMFC 2010).

Therefore, the impacts by drought to Mekong Delta are very clear and really serious. Drought impacts caused a lot of losses for Mekong Delta's production and livings of local community. It caused losses to especially economic, environment and social sectors. Or, it caused vulnerability to Mekong Delta.

2 Assessment Method of Drought Impacts to Eco-social Sectors

Impact assessment examines the consequences of a given event or change. For example, drought is typically associated with a number of outcomes. Drought impact assessments begin by identifying direct consequences of the drought, such as reduced crop yields, livestock losses, and reservoir depletion. These direct outcomes can then be traced to secondary consequences (often social effects), such as the forced sale of household assets or land, dislocation, or physical and emotional stress. This initial assessment identifies the drought impacts but does not identify the underlying reasons for these impacts (NHMFC 2010).

Drought impacts can be classified as economic, environmental, or social, although many impacts may span more than one sector. By using the checklist of drought impacts, they can be identified/known in the region. Recent drought impacts, especially if they are associated with severe to extreme drought, are identified more heavily than the impacts of historical drought. Recent events more accurately reflect current vulnerabilities. Attention should also be given to specific impacts that are expected to emerge in the future (Sam 2007).

Impact assessment also provides a framework for identifying the social, economic, and environmental causes of drought impacts. It bridges the gap between impact assessment and policy formulation by directing policy attention to underlying causes of drought impact types rather than the result i.e. the negative impacts, which follow triggering events such as drought. For example, the direct impact of precipitation deficiency may be a reduction of crop yields. Quick approaching community method may have different ways, such as rapid assessment or rural community participatory assessment (Participatory/Rapid Rural Appraisal – PRA/RRA), by questionnaires combined with the direct interviewing. The impact assessments caused by drought are implemented by using questionnaire combined with direct interviewing each stakeholder or groups of stakeholders. The approach has strong points which enable to get all different cases and opinions of many

stakeholders. It has a weak point that the interviewers have to explain carefully to all stakeholders before interviewing (Hung 2014).

For impact types assessment caused by the drought in Mekong Delta, consultant has to follow the methodology shown below:

- Review the national/regional activity/response programme/strategy related to the natural calamity prevention and other relevant documents of Viet Nam to identify directions and priorities of the IWRM practices required in the agriculture and irrigation developments in Mekong Delta.
- Meeting with all relevant stakeholders to assess all drought impact types and impact levels in the Mekong Delta of Viet Nam which is officially identified as one of the most drought prone areas of Viet Nam. They will have to find out all methodologies which have been applied in their province in response to each specific impact and map out the advantages and disadvantages of those applications. In Mekong Delta province like Tien Giang, Kien Giang, An Giang, HauGiang, TraVinh, Bac Lieu, Ben Tre, Soc Trang, Long An, Vinh Long, Dong Thap, Ca Mau provinces and Can Tho city will be under direct impacts of drought and climate change.
- Collect and bind all provincial data from all national consultation meetings on types of basal drought impact types and causes assessment.
- Compilation, analysis, and report writing. Analysis is based on the matrix tables about the economic, environmental and social sectors impacted by drought and the root causes of drought impact types. We count the number of stakeholders agree or not about sectors impacted by drought and what the root causes of drought impact types are at stakeholder's locations.
- The total number of questionnaire used in vulnerability assessment is 76 which covered three sectors (economic, society and environment). Each question has three selection/choices (history, current and potential) in impact identification by drought. Each question has six options (cost, distribution, growing, priority, recovery and rank).

While assessing the vulnerability caused by drought impacts in Mekong Delta, the climate change impacts will be evaluated and identify clearly the relationship between them through the increasing impact ability and level of drought to the production and living of regional people.

3 Identification of Drought Impact Types and Causes

Drought impacts to economic, environmental and social sectors awarded by local community in Mekong Delta can be grouped into three different types: (1) historical drought, (2) current drought, and (3) potential drought. Historical drought impacts that occurred in the past and likely or unlikely to happen in recent years. Current drought impacts are that happened in last years (1–5 years) and they are like or unlike the types of impacts in the past. The recent drought impacts, especially if

they are associated with severe to extreme drought, should be weighted more heavily than the impacts of historical drought, in most cases. And potential drought impact is the major impact which can cause significant damages to agricultural product or main households' income in future (Hung 2014).

3.1 The Identification of Drought Impact Types to Each Sector in Mekong Delta

The Drought Impacts to Mekong Delta's Economic Sector Based on the discussions and choices of provincial representers in drought impacts assessment meeting, we can see that most of type drought impacts to economic sector appeared in the past, at present and potentially in future. All provincial representers, 12/12, have agreed with this identification (see Fig. 18.3).

The Drought Impacts to Mekong Delta's Environment Sector Based on the discussions and choices of provincial representers in drought impacts assessment meeting, we can also see that most of kinds of drought impacts to environment sector appeared in the past, at present and potentially in future. Number of agreement's options is more than 10/12 (see Fig. 18.4).

The Drought Impacts to Mekong Delta's Social Sector We can also see that most of type of drought impacts to social sector appeared in the past, at present and potentially in future like economic and environment sectors. Number of agreement's options is more than 7/12 (see Fig. 18.5).

Firstly, we can primarily conclude about the occurrence of drought impacts in Mekong Delta such as: it has happened but uneven in the past and present. It is

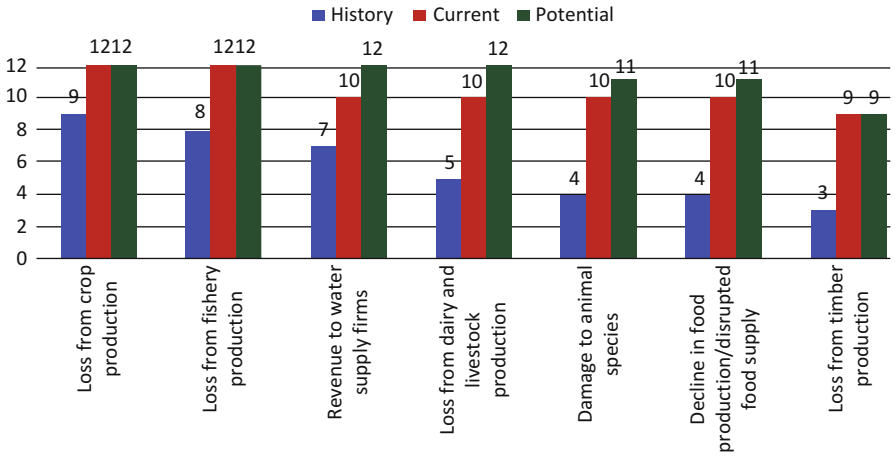

Fig. 18.3 The agreement's levels about types of drought impact to economic sector

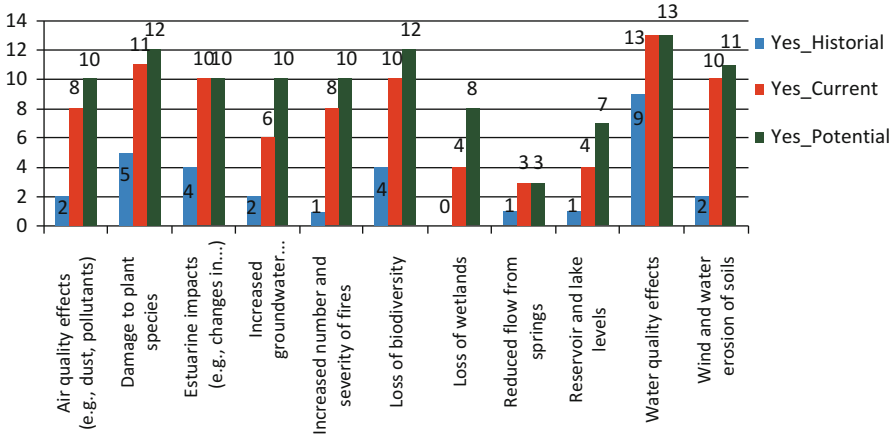

Fig. 18.4 The agreement's levels about types of drought impact to environmental sector

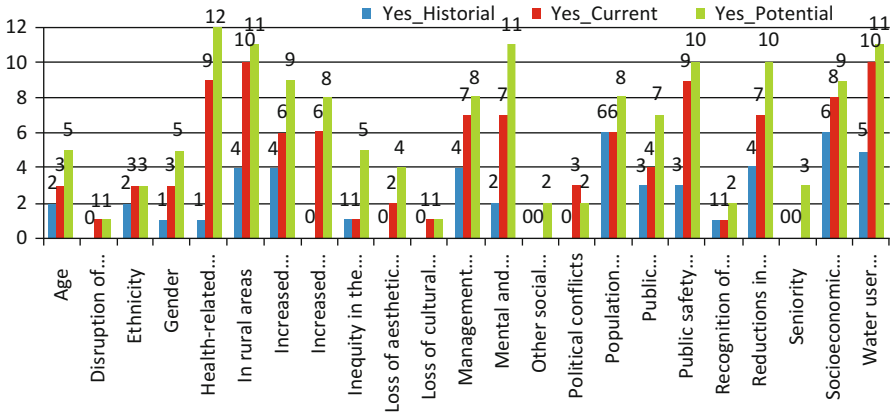

Fig. 18.5 The agreement's levels about types of drought impact to social sector

potential to occur in future. Most of the Mekong Delta provinces, which have representers attending at the vulnerability assessment meeting (over 10/12) have agreed with these identifications.

3.2 Major Drought Impacts to Each Sector in Mekong Delta

Based on above results about the identification of drought impacts types to economic, environment and social sectors in Mekong Delta, we can analyse to find the

major drought impact types to these sectors. The analysis and foundation of major drought impact types were through three criteria such as (Hung 2014):

Cost From list of drought impact types occurring in the past, at present and potentially in future, which types to cause damage to economic, environment and social sectors; it is the highest number of selection.

Distribution From list of drought impact types happened in the past, at present and potentially in future, which types are equally distributed or considered at most of the areas in Mekong Delta; it is the highest number of selection.

Growing From list of drought impact types happened in the past, at present and potentially in future, which types continuously grew in next periods; it is the highest number of selection.

Publish Priority From list of drought impact types happened in the past, at present and potentially in future, which types are known and cared a lot by local community.

Recovery From list of drought impact types happened in the past, at present and potentially in future, which branches were impacted by drought considered that could be recovered after drought gone and selected with the highest number of selection.

The priority levels of all major drought impact types mentions the impacted levels or their serious levels to people (economic and society) and nature (environment). They are not generally like other. Based on the arrangement of priority levels got in the vulnerability assessment meeting, the priority levels of all major drought impact types are shown in Fig. 18.6. Therefore, the most priority issues of participators belonged to the economic sector as annual and perennial crop, crop quality, fish habitat, income or energy supported living.

Therefore, after assessment, we can consider some major drought impact types to economic, environment and social sectors in Mekong Delta, such as:

Economic Sector (i) Annual and perennial crop losses; (ii) Costs to energy industry and consumers associated with substituting more expensive fuels (oil) for hydroelectric power; (iii) Damage to crop quality; (iv) Damage to fish habitat; (v) Income loss for farmers and others directly affected; (vi) Increased energy demand and reduced supply because of drought-related power curtailments; (vii) Insect infestation; (viii) Loss of farmers through bankruptcy; (ix) Loss of young fish due to decreased flows; (x) Loss to industries directly dependent on agricultural production (e.g., machinery and fertilizer manufacturers, food processors, etc.); (xi) Plant disease; (xii) Reduced productivity of cropland; (xiii) Unemployment from drought-related production declines; and (xiv) Wildlife damage to crops.

Environment Sector (i) Water quality effects and (ii) Loss of biodiversity.

Social Sector (i) Population migrations; (ii) Rural areas and (iii) Increased poverty in general.

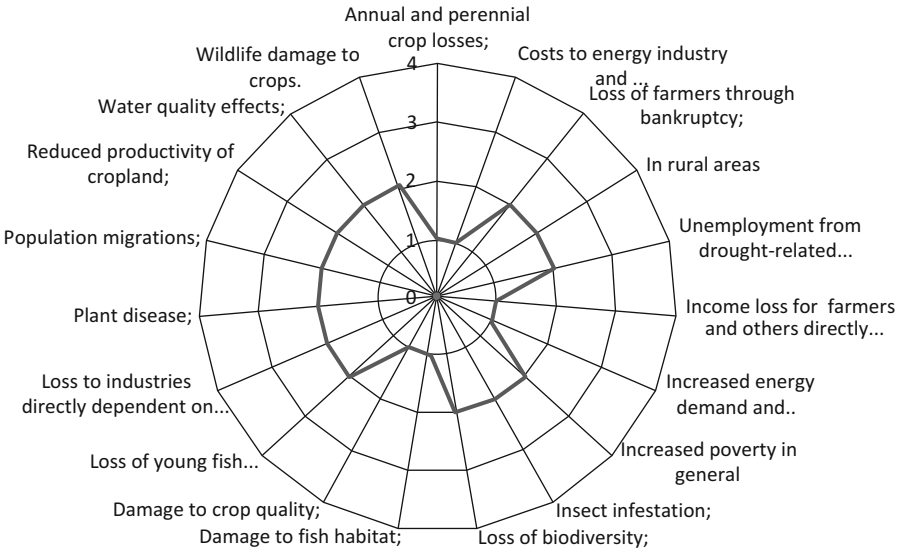

Fig. 18.6 The priority rank of major drought impact types to sectors in Mekong Delta

3.3 The Causes of Major Drought Impact Types

In the vulnerability assessment meeting, besides the identification of major drought impacts to economic, environmental and social sectors, it also focussed on the identification of their causes. We have used the drought risks reduction matrix table in vulnerability assessment meeting to find the basic causes through the discussion and interviews (Hung 2014).

The basic causes of drought impact types of the economic, environmental and social sectors were related to the drought's origins as well as its results such as:

The Natural Changes (the water resources, the land resources, hydro-meteorology): The basic causes of drought impact types are identified as the salinity intrusion from sea; the lack of fresh water for livings and production; the current weather variations (rain reduced and non-rule; rain is less and occurred late; the temperature increases high, the time lag of fresh water is more lengthened etc.).

The Economic Activities The non-conformity with breed crops about type, planting methods; cropping schedule; fertilizer for crops; lack of fund as well as lack of technology for production. The risks of production weren't interested (production insurance), it is especially in the agriculture and aquaculture where their products were depended on the natural conditions very much. Additionally, the causes were from the weakness of irrigation system which had the functions by keeping fresh water and preventing salinity intrusion. The causes were also from the O&M.

The Community's Awareness The using resources was untrue, wasted and non-scientific; the awareness about the drought and climate change as well as the adaptation/responding activities were limited and low.

3.4 The Sectors Vulnerable Caused by Drought Impacts in Mekong Delta

Vulnerability may be defined as "the conditions determined by physical, social, economic and environmental factors or processes, which increase the susceptibility of a community to the impact of hazards" (Balica 2007). Further vulnerability assessment provides a framework for identifying the social, economic, and environmental causes of drought impacts. It bridges the gap between impact assessment and policy formulation by directing policy attention to underlying causes of vulnerability rather than the result, the negative impacts, which follow triggering events such as drought.

Based on previous discussions, it is evident that agriculture and aquaculture is going to get affected mostly due to drought and climate change. While agriculture sector will suffer economic loss due to reduction in annual crop production and associated deteriorated farmer's condition, similarly in aquaculture production is going to decrease and livelihood of farmers will be affected (Hung 2014).

3.5 Importance of Identification of Major Drought Impact Types and Vulnerable Sector

It is very important issue to assess the vulnerability caused by drought impacts and also climate change affected (Factor causes the increasing drought disaster in future). The vulnerability identified as the property, resources, systems, and cultural, economic, environmental, and social activity is susceptible to harm, degradation, or destruction on being exposed to hostile agents or factors. The hostile agent or factor researched here is drought calamity which is considered in increasing sense of climate change. Also in the climate change impacts assessment, climate change is the natural calamity with many affects/impacts to wide sectors and many factors of regions. The major impact type's identification as drought impacts help us understand clearly, enough and correctly its causes and consequences for economic and social development.

The major drought impact type's identification is the foundation to assess the vulnerability, consequence of all natural calamities impacting/affecting to regional economic, environment and social sectors.

4 Conclusion

The low rainfall and high evaporation during the annual dry season make the pressures on human habitation and activity in the Mekong Delta. The dry season was prolonged to become cause of drought. Economic, environment and social sectors are impacted by drought and sea level rises when the climate change happens in Mekong Delta. Through discussion of local participants in vulnerability assessment meeting, the main sectors impacted by drought are agriculture, aquaculture, water supply, water quality and life quality in Mekong delta.

Causes of drought impacts types to these sectors are identified such as salinity intrusion, lack of fresh water for living and production, O&M hydraulic works system weakness. Through discussion, all participants agreed that application and implementation of the mitigation and response activities help to reduce drought impacts.

Drought is an extreme weather condition where there is lack of upstream flow in Mekong Delta due to less or no rainfall. Most drought researches are based on the equal water resources as upstream flow, groundwater or water stored in canal system with demands from production and living. However, causes of drought impacts types include salinity intrusion, ineffective O&M hydraulic works system as well as production as cropping schedule, breeds of crop and community's awareness. Therefore, it needs to have special and professional researches about drought impacts which contribute in climate change situation.

References

Balica, S.F. (2007). Development and Application of Flood Vulnerability Indices for Various Spatial Scales. UNESCO-IHE, MSc Thesis (WSE – HERBD – 07.01).

Hung, B.V. (2014). Vulnerability assessment due to drought impacts and climate change in Mekong Delta part of Viet Nam. Drought Management Programme, and MRC, Phnom Penh, Cambodia, 2014.

Ian, White (2002). Water management in the Mekong Delta: Changes, Conflicts and Opportunities. Centre for Resource and Environmental Studies, the Australian National University Canberra ACT 0200 Australia, Australia.

IMHEN (2011). Scenarios of climate change and sea level rises for Viet Nam. Ministry of Natural Resources and Environments, Hanoi.

Long, B.D. (2014). Collected Data and Information on the 2013 Flood. National Center of Meteorology and Hydrology Forecasting, Ministry of Nature Science and Environment, Ha Noi.

MRC-FMMP (2010). Seasonal Flood Situation Report for the Lower Mekong River Basin, Flood Mitigated Management Program, MRC, Phnom Penh, Cambodia.

NHMFC (2010). Particulars of Hydrology Meteorology of Viet Nam in 2011. Ministry of Nature Science and Environment, Ha Noi.

Nuoi, N.S. (2007). National Strategy for protection and Mitigation of Disaster up to 2020. Ministry of Nature Science and Environment, Ha Noi, 2007, page 8–9

Sam, L. (2007). Research salinity intrusion to support the social-economic Development in the coastal zones of the Mekong Delta, The KC.08-18 subject of the Environmental protection and

Disaster prevention program. Southern Institute of Water Resource Researches, Ministry of Agriculture and Rural Development, Hanoi.

SCFSC (2014). The flood report of Mekong Delta in 2013. Ministry of Nature Science and Environment, Ha Noi.

Thuan, N.T. (2006). The dry season flow in the Mekong Delta: The report collection of the Science Technology conference. *The Institute of Hydrology Technology and Environments*, **10:** 55–57.

Chapter 19
Multi-pathway Risk Assessment of Trihalomethanes Exposure in Drinking Water Supplies

Minashree Kumari and S.K. Gupta

1 Introduction

Disinfection is the last step in the water treatment processes for the protection of public health. In India, chlorine is used as the primary disinfectant because of its low cost and convenience for application in water purification. However, chlorination results in formation of trihalomethanes (THMs) in drinking water which can pose severe health threat due to their potential carcinogenicity. In recent decades, various epidemiological studies have been conducted to determine the relationship between THMs and different health outcomes e.g., cancers and reproductive outcomes (Hrudey 2009). Llopis-González et al. (2011) suggested that exposure to THMs increase the risk of bladder, colon, rectum, leukemia, stomach and rectal cancers. The results of animal studies have demonstrated that liver, kidney and intestinal tumorigenesis are associated with chronic ingestion of THMs (Yang et al. 2000). Since THMs are the most prevalent and well documented disinfection by product (DBP) compounds in drinking water, they are generally considered as indicators of DBP exposure in epidemiological investigations.

Recent studies have attempted to improve exposure assessment by considering individual exposure durations, concentration levels and water intake per day. However, only a few studies accounted for spatial and temporal fluctuations in THM levels across the distribution system. Furthermore, seeking to improve the exposure assessment, studies have begun to incorporate behavioural determinants of different routes of exposure to DBPs such as dermal absorption and inhalation

M. Kumari (✉) • S.K. Gupta
Department of Environmental Science and Engineering, Indian School of Mines, Dhanbad, Jharkhand 826004, India
e-mail: minashreekumari2501@gmail.com

F. Kurisu et al. (eds.), *Trends in Asian Water Environmental Science and Technology*, DOI 10.1007/978-3-319-39259-2_19

during bathing and showering, and ingestion of drinking water but the contribution of these was unclear (Hoffman et al. 2008). Lee et al. (2004) calculated cancer risks and hazard index of THMs through different exposure routes for tap water in Hong Kong, and reported that exposure through oral ingestion had higher risk than through dermal absorption and inhalation. Similar results were reported by Tokmak et al. (2004) and Amjad et al. (2013), who concluded that the highest risk comes from exposure to chloroform through oral ingestion. It has also been reported that THMs are generally well absorbed, metabolized and rapidly eliminated by mammals after oral or inhalation exposure (IPCS 2009). The discrepancy that the importance of the three exposure pathways ranked differently in the studies may be attributed to different concentration and speciation of THMs present in the water.

Traditional risk assessment of water often consider only ingestion exposure to toxic chemicals, but studies showed that inhalation and dermal absorption be considered in the risk assessment studies since 1990 (Jo et al. 1990). Therefore, the objective of this study is to conduct multi-pathway risk assessment of THMs based on their concentrations within the distribution systems of five water treatment plants (WTPs) in Jharkhand and West Bengal. The THM concentrations in drinking water samples were first analysed. Further, cancer and non-cancer risk associated with these THMs were estimated using prediction models for both males and females, respectively. Till date no such study has been carried out in this region of India.

2 Materials and Methods

Drinking water samples were collected from five selected water treatment plants (WTPs) situated in the Eastern region of India as shown in Fig. 19.1. Among sampling locations, Kolkata and Raniganj are situated in West Bengal, whereas the rest three are in Jharkhand, India (Table 19.1). Two main rivers (i.e. Ganga and Damodar) were the source of raw waters to these WTPs. All these water treatment plants (WTPs) follow the conventional method of treatment comprising coagulation-flocculation, sedimentation, filtration and chlorination or disinfection.

For monitoring of THMs, 25 samples were collected at each sampling location. The samples were collected in 40-ml clean glass vials with polypropylene cap and PTFE-faced rubber septa and it was added with sodium sulphite (0.010 g) as a de-chlorinating agent to eliminate any residual chlorine to stop further THM formation. The samples were stored in dark at temperature <4 °C for further analysis.

Fig. 19.1 Map of study area showing locations of WTPs

Table 19.1 Details of water treatment plants selected for the study

Name of the WTPs	Location	Latitude & longitude	Capacity (MGD)
Mineral Area Development Authority (MADA)	Jamadoba, Dhanbad, Jharkhand	23°42′25.09″ N	21
		86°25′07.93″ E	
Asansol-Durgapur Development Authority (ADDA) WTP	Durgapur, West Bengal	23°37′16.57″ N	5
		87°07′56.51″ E	
Indira Gandhi Water Treatment Plant (IGWTP)	Kolkata, West Bengal	22°46′40.52″ N	260
		88°20′39.84″ E	
Maithon WTP (MWTP)	Maithon, Jharkhand	23°46′47.13″ N	14.5
		86°48′42.11″ E	
Swarnrekha Water Treatment Plant (SWTP)	Ranchi, Jharkhand	23°26′30.60″ N	37.5
		85°28′48.23″ E	

2.1 Analysis of THMs

The samples were subjected to liquid-liquid extraction using pentane as a solvent. The vials were then shaken vigorously for 1 min and allowed to stand for 3 min to facilitate phase separation. The pentane phase was removed and placed in 2 ml auto-sampler vials. 1 µl extract was then analyzed using nitrogen as a carrier gas at a flow rate of 1.2 ml/min. THMs were analyzed as per USEPA method 551.1 (USEPA 1995). A Chemito CERES 800 Plus gas chromatograph (Thermo Fischer) equipped with an electron capture detector (ECD) was used for the determination and quantification of THMs. The column used for analysis

was fused silica DB-5, 30 m × 0.32 mm I.D. × 0.30 μm film thicknesses. Analytical grade calibration standards with a purity of >99.5 % were procured from Sigma Aldrich (Germany). The mean recovery of four THM species ranged between 86.9 % and 102.3 %.

2.2 Cancer Risk Estimation

The method developed by the USEPA (1999, 2002, 2005a, b) and recently adopted by Lee et al. (2004) in Hong Kong and Tokmark et al. (2004) in Ankara, Turkey was used for the estimation of lifetime cancer risk of THMs. The cancer risks for exposure through oral ingestion, dermal absorption and inhalation exposure were considered. The reference dose (R_fD) of individual THMs were as per the USEPA guidelines for assessment of cumulative risk over multiple routes of exposure (USEPA 2005a). Equations (19.1) and (19.2) were used for the estimation of total lifetime cancer risk and hazard index due to THMs through different pathways.

$$R_T = \sum_{m=1}^{n} \left\{ \frac{C_m \times EF \times ED}{BW \times AT} \times \left[\begin{array}{l} (SF_{oral} \times IR_w) + \left(SF_{dermal} \times SA \times K_p \times ET\right) \\ +(SF_{inhalation} \times K \times IR_a \times ET) \end{array} \right] \right\} \tag{19.1}$$

$$HI_T = \sum_{m=1}^{n} \left\{ \frac{C_m \times EF \times ED}{BW \times AT} \times \left[\begin{array}{l} \left(\frac{IR_w}{R_fD_{oral}} \right) + \left(\frac{SA \times K_p \times ET}{R_fD_{dermal}} \right) \\ +\left(\frac{K \times IR_a \times ET}{R_fD_{inhalation}} \right) \end{array} \right] \right\} \tag{19.2}$$

where RT is Total lifetime cancer risk (unitless), m – Number of different chemical (unitless), I – Oral, dermal and inhalation expressed as the exposure route is oral, dermal and inhalation exposure, respectively, C_m – Concentration of chemical m in water (mg/L), EF – Exposure frequency (days/year), ED – Exposure duration (year), ET – Exposure time (h/day), IR_a – Daily indoor inhalation rate (m^3/day), IR_w – Daily water ingestion rate (L/day), K – Volatilization factor (unitless), SA – Skin-surface area available for contact (cm^2), K_p – Chemical-specific dermal permeability constant (cm/h), BW – Body weight (kg), AT – Average time (days), HI_T –Total lifetime hazard index (unitless), and R_fD_i is Chronic reference dose from the specified exposure route i (mg/kg × day); i = oral, dermal and inhalation expressed as the exposure route is oral, dermal and inhalation exposure, respectively.

However, in the estimations, body weight was taken as 70 and 60 kg for males and females, respectively and average water ingestion rate of 4.0 L/day, was assumed as per the Indian conditions (ICMR 2009). In inhalation risk calculations,

the daily dose was calculated by assuming 20 m^3 aspirated air per day (Lee et al. 2004). The concentration of THMs in air used for the estimation of risk through inhalation was calculated using a volatilization factor of 0.0005 × 1000 L/m^3 as suggested by USEPA (1991). The cancer slope factor and the reference dose for THMs were provided in the integrated risk information system (IRIS) on the web site of the United States Environmental Protection Agency (USEPA 2005a). The values of other parameters were adopted according to the default values represented by USEPA (1999, 2002).

3 Results and Discussion

3.1 Concentration Range of THMs in Drinking Water Supplies

The concentration of THMs in different WTPs is given in Table 19.2. THMs concentrations varied from plant to plant and was found to be in the range of 274–511 μg/l, which is much higher than the prescribed USEPA standards of 80 μg/l. The values were also higher to those reported in countries like Pakistan, Turkey, Istanbul and Iran (Amjad et al. 2013; Pardakhti et al. 2011; Legay et al. 2011; Chowdhury et al. 2011). Higher values of THMs found in Indian conditions may be attributed to the variation in the surface water quality and the treatment systems adopted (IS, 10500, 2012). Amongst various THMs, chloroform was the predominant contributing more than 97.2 % to the total THM. Its value ranged from 236 to 503 μg/l. BDCM and DBCM made a trivial contribution of 0.02–2 % and 0.03–4 %, respectively. Many researchers also reported major contribution of chloroform in drinking water supplies (Hasan et al. 2010; Karim et al. 2011). However, Charrois et al. (2004) reported that bromoform was the major contributor to total THMs, which was due to the presence of bromide in raw water. However, in our study, bromoform was found below detection limit (0.01 μg/L) which may be attributed to the absence of bromide in raw water. This result is consistent with the results observed for other countries (Pardakhti et al. 2011; Summerhayes et al. 2011). The

Table 19.2 Concentration of THMs in selected WTPs alongwith their standard deviations

	Concentration of THMs (μg/L)					Standards	
THMs	MADA	IGWTP	SWTP	ADDA	Maithon	USEPA (2011)	IS 10500 (2012)
$CHCl_3$	503 ± 5	466 ± 3	255 ± 2.1	236 ± 3.5	501 ± 4.3	80	200
$CHClBr_2$	2 ± 0.2	2 ± 0.3	11 ± 0.2	31 ± 0.1	2 ± 0.02	80	100
$CHCl_2Br$	4 ± 0.1	12 ± 1.2	8 ± 0.2	14 ± 0.4	8 ± 0.2	80	60
$CHBr_3$	–	–	–	–	–	80	100
TTHMs	509 ± 5.3	480 ± 4.5	274 ± 2.5	281 ± 3.9	511 ± 4.52	–	–

contribution sequence followed by THMs was in the order of chloroform > BDCM > DBCM > Bromoform. Similar findings have been reported in the literature (Uyak 2006; Legay et al. 2011; Karim et al. 2011; Pardakhti et al. 2011).

3.2 *Risk Assessment*

3.2.1 Cancer Risk Through Oral Ingestion

Cancer risk from exposures to THMs was estimated based on its concentrations in the drinking water supplies. Cancer risk through oral ingestion was calculated for both males and females and are shown in Table 19.3. Chloroform exhibited the highest cancer risk of 7.78×10^{-4} for females and 6.65×10^{-4} for males in MADA WTP, which is 665–778 times higher than the acceptable risk level (10^{-6}). DBCM imparted the lowest cancer risk for both males and females, respectively which is about 8.4 times higher in females and 7.14 times in males than the acceptable risk level. The average cancer risk of THMs for both males and females was in the order of chloroform > DCBM > DBCM.

Exposure to multiple toxicants results in additive and/or synergistic effects. Hence these compounds, if not individually, together can result in significant cancer risk. Lifetime cancer risk for total THMs was found highest in the Maithon WTP (8.09×10^{-4}) whereas the lowest cancer risk of 4.65×10^{-4} was reported in ADDA WTP. Analysis of data also shows that females are more prone to cancer risk compared to males. Chloroform made the highest percentage contribution (97.3 %) to total cancer risk followed by BDCM (1.5 %) and DBCM (1.2 %). These results are comparable with the previous studies (Uyak 2006; Wang et al. 2007; Viana et al. 2009). Chloroform was found to be the main contributor to cancer risk due to its predominance over other THMs in the studied water.

Table 19.3 Lifetime cancer risk of THMs through oral route

	Chloroform		DBCM		DCBM		TTHMs	
	Female	Male	Female	Male	Female	Male	Female	Male
MADA	7.78E-04	6.65E-04	8.40E-06	7.14E-06	1.24E-05	1.06E-05	7.99E-04	6.83E-04
Maithon	7.75E-04	6.63E-04	8.40E-06	7.14E-06	2.48E-05	2.12E-05	8.08E-04	6.92E-04
IGWTP	7.22E-04	6.17E-04	8.40E-06	7.14E-06	3.72E-05	3.19E-05	7.68E-04	6.56E-04
ADDA	3.94E-04	3.38E-04	4.62E-05	3.95E-05	2.48E-05	2.12E-05	4.65E-04	3.99E-04
SWTP	3.66E-04	3.13E-04	1.30E-04	6.68E-05	4.34E-05	3.72E-05	5.39E-04	4.17E-04

3.2.2 Cancer Risk from Dermal Absorption

It has been reported that skin contact with water during showering, bathing and swimming resulted in the penetration of the contaminants into the body (Weisel and Jo 1996). Although activities of washing and handling wet clothing may also cause dermal adsorption. However, the frequency of exposure is very less. Therefore, showering and bathing activities have been primarily considered in evaluation of cancer risk through dermal adsorption. USEPA stated different available skin-surface areas for males and females (male = 1.94 m^2, female = 1.69 m^2) (Gratt 1996).

As shown in Table 19.4, the cancer risk levels of all the THMs were found to be lower than 10^{-9}, which is very less than the prescribed USEPA risk level (10^{-6}). Therefore, dermal absorption does not possess any risk associated with these THMs.

3.2.3 Cancer Risk from Inhalation Route

Inhalation exposure occurs when the air breathed contains compounds volatilized during water usage like bathing, washing, showering and cooking (Lee et al. 2004; Uyak 2006). As shown in Table 19.5, cancer risk for total THMs due to inhalation exposure were less than 10^{-6}, the acceptable cancer risk level recommended by USEPA for both males and females, respectively. Unlike other routes of exposure where chloroform is the major contributor, in this case, DBCM imparted the highest average cancer risk followed by BDCM and chloroform, for both males and females, respectively. This is mainly due to differences in the cancer slope factor (CSF) values, which is very less for chloroform as compared to DBCM and BDCM (USEPA 1999). The total cancer risk was found to be highest in SWTP (6.24×10^{-8}) and lowest in IGWTP (1.79×10^{-9}). Individually, DBCM reported the highest total cancer risk of 6.11×10^{-8} in SWTP. Similar to other routes of exposure, here also females have been found to have higher cancer risk than males. The percentage contribution of average cancer risks demonstrated that DBCM made the highest contribution (81.9 %) to total risk followed by BDCM (16.2 %) and chloroform (1.9 %).

3.2.4 Non-cancer Risk Assessment

The hazard indices of THMs were also calculated to determine their noncarcinogenic risks. Figures 19.2 and 19.3 show the hazard index of THMs through oral ingestion and dermal absorption for males and females, respectively. The total hazard index was calculated for each compound by summing up the individual index for males and females, respectively. As shown in Fig. 19.2, the total hazard index of chloroform is highest followed by BDCM and DCBM for oral

Table 19.4 Lifetime cancer risk through dermal absorption

	Chloroform		DBCM		DCBM		TTHMs	
WTPs	Female	Male	Female	Male	Female	Male	Female	Male
MADA	6.01E-09	5.90E-09	2.72E-11	2.68E-11	5.60E-11	5.53E-11	6.10E-09	5.98E-09
Maithon	5.98E-09	5.86E-09	2.72E-11	2.68E-11	1.12E-10	1.10E-10	6.12E-09	6.00E-09
IGWTP	5.55E-09	5.47E-09	2.72E-11	2.68E-11	1.67E-10	1.65E-10	5.74E-09	5.66E-09
ADDA	3.04E-09	2.99E-09	1.44E-10	1.48E-10	1.12E-10	1.10E-10	3.30E-09	3.25E-09
SWTP	2.81E-09	2.77E-09	4.22E-10	4.12E-10	1.98E-10	1.93E-10	3.43E-09	3.37E-09

Table 19.5 Lifetime cancer risk due to inhalation exposure

	Chloroform		DBCM		DCBM		TTHMs	
WTPs	Female	Male	Female	Male	Female	Male	Female	Male
MADA	8.33E-06	7.14E-07	1.77E-07	1.52E-07	7.54E-08	6.46E-08	8.58E-06	9.31E-07
Maithon	8.16E-09	7.05E-09	1.77E-07	1.52E-07	1.56E-07	1.33E-07	3.41E-07	2.92E-07
IGWTP	7.76E-09	6.65E-09	1.77E-07	1.52E-07	2.21E-07	1.98E-07	4.06E-07	3.57E-07
ADDA	4.25E-09	3.64E-09	9.78E-08	8.36E-08	1.56E-07	1.33E-07	2.58E-07	2.20E-07
SWTP	3.94E-09	3.37E-09	1.26E-09	2.22E-07	1.27E-07	1.34E-07	1.32E-07	3.59E-07

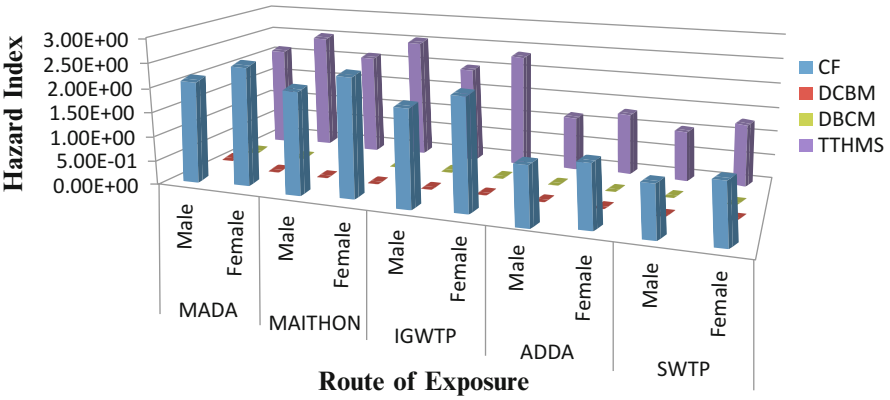

Fig. 19.2 Hazard index through oral ingestion

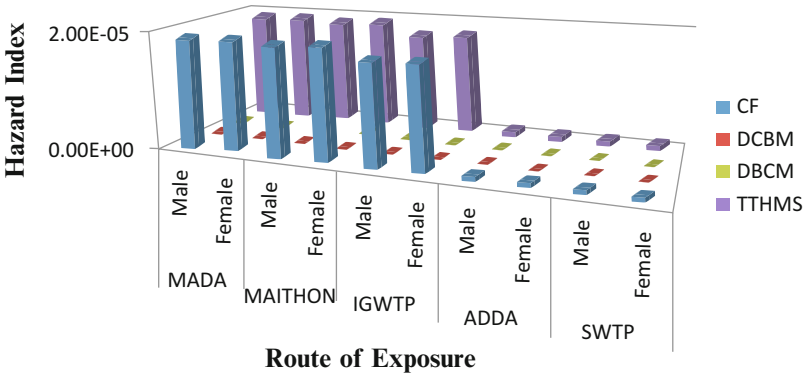

Fig. 19.3 Hazard index through dermal absorption

ingestion. The highest total hazard index for the TTHMs was found in MADA WTP (2.17, 2.63) and lowest in SWTP WTP (1.06, 1.29) for both males and females, respectively. Similarly, for dermal absorption as shown in Fig. 19.3, the average hazard index of chloroform was found to be highest for both males and females respectively. Chloroform exhibited the highest total hazard index of 2.32×10^{-5} followed by BDCM (2.06×10^{-7}) and DCBM (1.537×10^{-8}). MADA WTP reported the highest hazard index values followed by Maithon WTP whereas the hazard index was lowest in ADDA WTP. In previous studies (Lee et al. 2004; Uyak 2006), chloroform was found to have the highest hazard index through oral and dermal routes, which is similar to our study. When the hazard index is more than 1, concern exists over potential toxicity (USEPA 2000). Thus, non-cancer effects due to THMs exposure may cause diseases like jaundice, neuro-behavioural effects, subjective central nervous system effect, and enlarged livers (Viana et al. 2009). For oral ingestion, hazard index is found to exceed 1, whereas for dermal absorption

hazard index it was lower than unity. This implies that oral ingestion is mainly responsible for the non-carcinogenic risk while the risk was negligible for dermal absorption.

4 Conclusions

This study emphasized on establishing the concentration range of THMs and evaluation of their potential carcinogenic and non-carcinogenic risk in drinking water supplies. THM in drinking water supplies ranged from 274 to 511 μg/L which exceeded the permissible USEPA and IS 10500 standards. The study depicted that amongst various THMs, chloroform constituted the major fraction (>97.2 %) followed by $CHBrCl_2$ and $CHBr_2Cl$ (0.02–4 %). The risk assessment of THMs revealed that the highest cancer risk comes from oral ingestion followed by inhalation. However, the risk due to dermal adsorption was found to be insignificant. This may be attributed to low absorption coefficient and less exposure frequency. Chloroform imparted the highest cancer risk. The average total cancer risk was found to be 316 times higher for males and 379 times for females, respectively indicating females are more prone to cancer risk. Non-carcinogenic risk analysis revealed that the risk is mainly through oral ingestion whereas dermal adsorption poses almost negligible risk. The regulatory issue of the THMs should be reviewed carefully based on the results of the health risks calculated from the specific THM species.

Acknowledgement The author acknowledges the Ministry of Drinking Water and Sanitation (GOI), New Delhi for providing financial grant for carrying out the research work.

References

Amjad, H., Imran, H., Rehman, M.S.U., Awan, M.A., Ghaffar, S. and Khan, Z. (2013). Cancer and non-cancer risk assessment of trihalomethanes in urban drinking water supplies in Pakistan. *Ecotox Environ Safe*, **91:** 25–31.

Charrois, J.W.A., Graham, D., Hrudey, S.E. and Froese, K.L. (2004). Disinfection By-Products in small Alberta community drinking-water supplies. *J Toxicol Environ Health Part A*, **67:** 1797–1803.

Chowdhury, S., Rodriguez, M. and Sadiq, R. (2011). Disinfection byproducts in Canadian provinces: Associated cancer risks and associated medical expenses. *J Hazard Mater*, **187:** 574–584.

Gratt, L.B. (1996). Air Toxic Risk Assessment and Management. Van Nostrand Reinhold, New York, NY.

Hasan, A., Thacker, N.P. and Bassin, J. (2010). Trihalomethane formation potential in treated water supplies in urban metro city. *Environ Monit Assess*, **168(1–40):** 489–497.

Hoffman, C.S., Mendola, P., Savitz, D.A., Herring, A.H., Loomis, D., Hartmann, K.E., Singer, P. C., Weinberg, H.S. and Olshan, A.F. (2008). Drinking water disinfection by-product exposure and fetal growth. *Epidemiology*, **19:** 729–737.

Hrudey, S.E. (2009). Chlorination disinfection by-products, public health risk tradeoffs and me. *Water Res*., **43:** 2057–2092.

ICMR (2009). Nutrient requirements and recommended dietary allowances for Indians. A Report of the Expert Group of the Indian Council of Medical Research.

IPCS (2009). Disinfectants and disinfectant by-products. International programme on chemical safety. Environmental Health Criteria Geneva: World Health Organization.

IS 10500 (2012). Indian Standard Drinking Water Specification, Second Revision. ICS 13.060.20.

Jo, W.K., Weisel, C.P. and Lioy, P.J. (1990). Routes of chloroform exposures and body burden from showering with chlorinated tap water. *Risk Anal*., **10:** 575–580.

Karim, Z., Mumtaz, M. and Kamal, T. (2011). Health risk assessment of trihalomethanes of tap water in Karachi, Pakistan. *J Chem Society*, **33:** 215–219.

Lee, S.C., Guo, H., Lam, S.M.J. and Lau, S.L.A. (2004). Multi-pathway risk assessment on disinfection by-products of drinking water in Hong Kong. *Environ Res*., **94:** 47–56.

Legay, C., Rodriguez, M.J., Sadiq, R., Serodes, J.B., Levallois, P. and Proulx, F. (2011). Spatial variations of human health risk associated with exposure to chlorination by-products occurring in drinking water. *J Environ Manage*., **92:** 892–901.

Llopis-González, A., Sagrado-Vives, S., Gimeno-Clemente, N., Yusà-Pelecha, V., Martí-Requena, P., Monforte-Monleón, L. and Morales-Suárez-Varela, M. (2011). Ecological Study on Digestive and Bladder Cancer in Relation to the Level of Trihalomethanes in Drinking Water. *Int J Environ Res*., **5(3):** 613–620.

Pardakhti, A.R., Bidhendi, G.R.N., Torabian, A., Karbassi, A. and Yunesian, M. (2011). Comparative cancer risk assessment of THMs in drinking water from well water sources and surface water sources. *Environ Monit Assess*., **179:** 499–507.

Summerhayes, R.J., Morgan, G.C., Lincoln, D., Edwards, H.P., Earnest, A., Rahman, M.B., Byleveld, P., Cowie, C.T. and Beard, J.R. (2011). Spatio-temporal variation in trihalomethanes in New South Wales. *Water Res*., **45:** 5719–5726.

Tokmak, B., Capar, G., Dilek, F.B. and Yetis, U. (2004). Trihalomethanes and associated potential cancer risks in the water supply in Ankara, Turkey. *Environ Res*., **96:** 345–352.

USEPA (1991). Risk assessment guidance for superfund, Vol. I, Part B. Environmental Protection Agency, Washington, DC, US. EPA/540/R-92/003.

USEPA (1995). Method 551. Determination of chlorinated disinfection by-products and chlorinated solvents in drinking water by liquid-liquid extraction and gas chromatography with electron-capture detection. Environmental monitoring Systems Laboratory, Office of Research and Development, US Environmental Protection Agency, Cincinnati, Ohio.

USEPA (1999). Guidelines for Carcinogen Risk Assessment. Risk Assessment Forum, U.S. Environmental Protection Agency, Washington DC. NCEA-F-0644 (Revised draft).

USEPA (2000). Supplementary guidance for conducting health risk assessment of chemical mixtures. United States Environmental Protection Agency. EPA/630/R-00/002.

USEPA (2002). Integrated Risk Information System (Electronic data base). U.S. Environmental Protection Agency, Washington DC. Retrived October, 2013, from http://www.epa.gov/iris.

USEPA (2005a). Integrated Risk Information System (IRIS). Online. National Center for Environmental Assessment, Washington, DC.

USEPA (2005b). Guidelines for carcinogen risk assessment, risk assessment forum. U.S. Environmental Protection Agency, Washington, DC. EPA/630/P-03/001 F.

USEPA (2011). US Environmental Protection Agency, Edition of the Drinking Water Standards and Health Advisories. Office of Water U.S. Environmental Protection Agency, Washington, DC.

Uyak, V. (2006). Multipathway risk assessment of trihalomethanes exposure in Istanbul drinking water supplies. *Environ Int*., **32:** 12–21.

Viana, R.B., Cavalcante, R.M., Braga, F.M.G., Viana, A.B., Araujo, J.C., Nascimento, R.F. and Pimentel, A.S. (2009). Risk assessment of trihalomethanes from tap water in Fortaleza, Brazil. *Environ Monit Assess*., **151:** 317–325.

Wang, G-S., Deng, Y-C. and Lin, T-F. (2007). Cancer risk assessment from trihalomethanes in drinking water. *Sci Total Environ*., **387:** 86–95.

Weisel, C.P. and Jo, W.-K., 1996. Ingestion, inhalation and dermal exposure to chloroform and trichloroethene from tap water. Environ. Health Perspect. 104, 48–51.

Yang, C.Y., Cheng, B.H., Tsai, S.S., Wu, T.N., Lin, M.C. and Lin, K.C. (2000). Association between chlorination of drinking water and adverse pregnancy outcome in Taiwan. *Environ Health Persp*., **108(8):** 765–768.

Chapter 20
The Study of Water Losses Using Knowledge Based System Approach

Nassereldeen A. Kabbashi, Mohd A. Hasif, and Mohammed E. Saeed

1 Water—Issues and Objectives

Water represents about 70 % of the whole earth surface yet it is limited in its availability as a freshwater to human benefits. The importance is on freshwater assets since it is freshwater resources that are used for daily usage, agricultural and industrial intentions. According to Hu (2006); Lambert and Taylor (2010), freshwater represents about 2.76 % of the total water available on earth. And even with this, it is only less than 1 % which is readily available to be accessed and used by human. About 20 % of the world's population lack access to safe drinking water and about eighty countries, which inhabitat 40 % of the world's population are in severe water crisis situation. Non-revenue water (NRW) can be defined as the amount or quantity of lost water starting from the water treatment plant to the consumers (Farley and Liemberger 2004). In other words, it occurs within the distribution systems added with amount of water that is authorized to use but not billed (De Bonis et al. 2002).

The rapid growth of population, economic development, urbanization and unpredictable climate change have affected the water demand (Cosgrove and Rijsberman 2000). This often creates difficulties to identify water conditions and pollution sources, which is necessary to control effectively pollution in addition to construct successful strategies for minimizing wasting of the resources. The potential responses to this increasing demand are either meeting the new demand with new resources (supply-side) or managing the consumptive demand to avoid the need of developing new resources (demand-side) (Butler and Memon 2006).

Water management must not be taken for granted. There are five major components of the water demand management: (1) Reducing the quantity or quality of

N.A. Kabbashi (✉) • M.A. Hasif • M.E. Saeed
Department of Biotechnology Engineering, International Islamic University Malaysia, Gombak 50728, Malaysia
e-mail: nasreldin@iium.edu.my

F. Kurisu et al. (eds.), *Trends in Asian Water Environmental Science and Technology*, DOI 10.1007/978-3-319-39259-2_20

water required to accomplish specific task, (2) Adjusting the nature of the task so it can be accomplished with less or low water quality, (3) Reducing losses in movement from source through use to disposal, (4) Shifting tie of use to off-peak periods, and (5) Increasing the ability of the system to operate during drought seasons (Trow and Pearson 2010). Reducing the water loss is an objective contained in the water demand management and the aim is to reduce the losses and improve the distribution efficiency of water distribution systems. The other parts of the objectives are to investigate the factors which lead to the increasing of Non-Revenue water around the world especially in Malaysia.

1.1 The Study Area

Approximate area of Kuala Terengganu is 60,528 ha which covers about 4.67 % of the state itself. Based on the report from the Population and Housing of Census Malaysia, the population in Kuala Terengganu in 2012 was 343,284. Syarikat Air Terengganu Sdn. Bhd. (SATU) originally belonged to a government department known as Jabatan Air Terengganu (JBAT) that was responsible to provide potable water to people (Terengganu Water Corporation 2010). There are six plants which are introduced in every district around the state of Terengganu with management, operation and water treatment process. As shown in Fig. 20.1, they are:

- Kuala Terengganu/Marang district
- Dungun/Ketengah district
- Hulu Terengganu district
- Kemaman district
- Besut district
- Setiu district

The piped water supplies in Kuala Terengganu district was started in 1956. The department of water supplies in Kuala Terengganu and Marang district has the largest area for water supply. Water supplies in Terengganu had been operated separately with Jabatan Kerja Raya Terengganu since early 1985 with 170 workers. The department of water supplies had a mission to give a clear water supply facility and enough to support all consumers and population in Terengganu.

There are several reasons for the high level of NRW in the country. These include age of pipe network where it is estimated that about 40 % or 50,900 km of the pipe network was laid 40–60 years ago or earlier; poor maintenance of pipe network and lack of funding for asset replacement and poor construction which resulted in increased leakage in the system; and illegal connections contributing significantly to commercial losses and revenue loss to the utilities. Absence of coherent implementation for Active Leakage Control has allowed NRW to hover at its present level of 36 % for some time now.

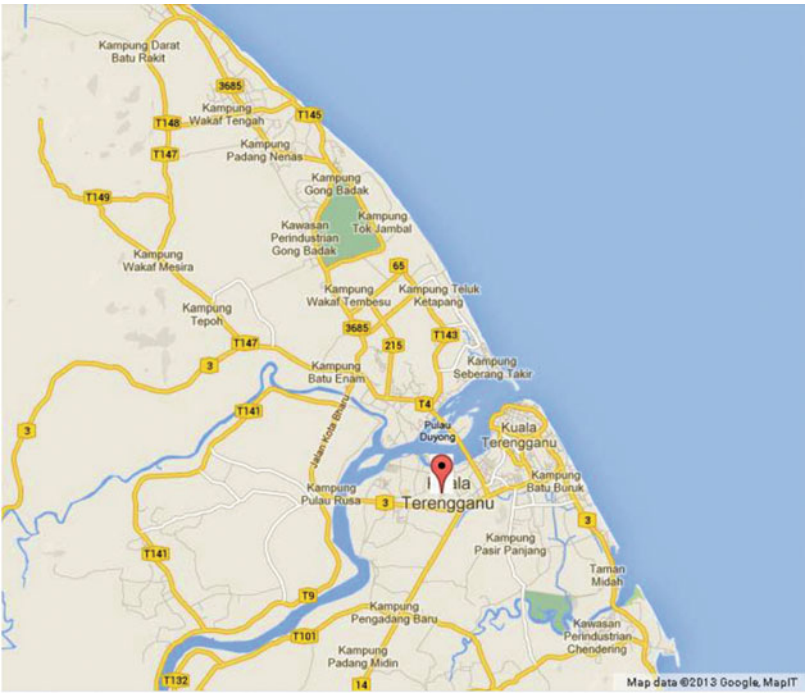

Fig. 20.1 Map of Kuala Terengganu district

1.2 Water Balance

The use of the term "Unaccounted Water" should be discontinued according to International Water Association (IWA), because of widely varying interpretations of the term worldwide on one hand and for that all components of the water balance should be accounted for on the other hand (Koelbl and Gschleiner 2009). Instead, IWA has recommended a new international standard water balance for water losses using the term "Non-Revenue Water".

Two main components of water loss are commercial losses and physical losses where physical losses occur within the distribution system and commercial losses occur during meter reading and billing. Commercial losses can occur due to unauthorized consumption and customers metering inaccuracies added with data handling errors. Example of unauthorized consumption are illegal connections, meter by-passing and poor billing collection systems. Three components of physical loss are

- Leakage from transmission, distribution and reticulation mains
- Leakage and overflow from the utility's reservoirs/storage tank
- Leakage on service connections up to customer's meter.

There are two components for commercial loss which are

- Unauthorized consumption
- Customers meter inaccuracies and data handling errors.

2 Materials and Methods

For this non-revenue water assessment, the focus goes to quantitative data collection as it represents a quantity of some sort. How much the loss of water? How big the leakage problem? How much the volume input? These kind of questions normally give numerical answers (Farley and Trow 2003; Skinner 2003). In addition, there also is a need to have qualitative data since it can give more understanding about the current and previous situation, emphasizing the problem and interpreting the actions. It can be said that qualitative methods seek to understand people's worlds and the reason of the problem. This secondary data collection focuses more on the population of people in the district—previously, currently and then in the future. If the population is known, many other aspects can be managed such as the availability of the potable water. Analyzing the map also can help in part of how the networking of the water distribution system can affect the amount of the NRW or the progress of the NRW reduction programme.

2.1 Visual Basic Development

Expert system was developed to measure current NRW level and therefore prediction of the NRW level in the future can be predicted approximately. Generally, building an expert system is a highly iterative process.

3 Results and Discussion

3.1 Knowledge Base

Knowledge base in expert system is represented as sets of rules that are checked against the collection of facts or knowledge about current situation, which includes NRW composition, Treatment facilities, Transportation, Amount of NRW, Frequency of billing, Public awareness, Maintenance and Rules & Regulations. For developing the NRW expert system, it is important to identify the knowledge base content which represents the purpose of system (Hassan 1997; Suciu 2008).

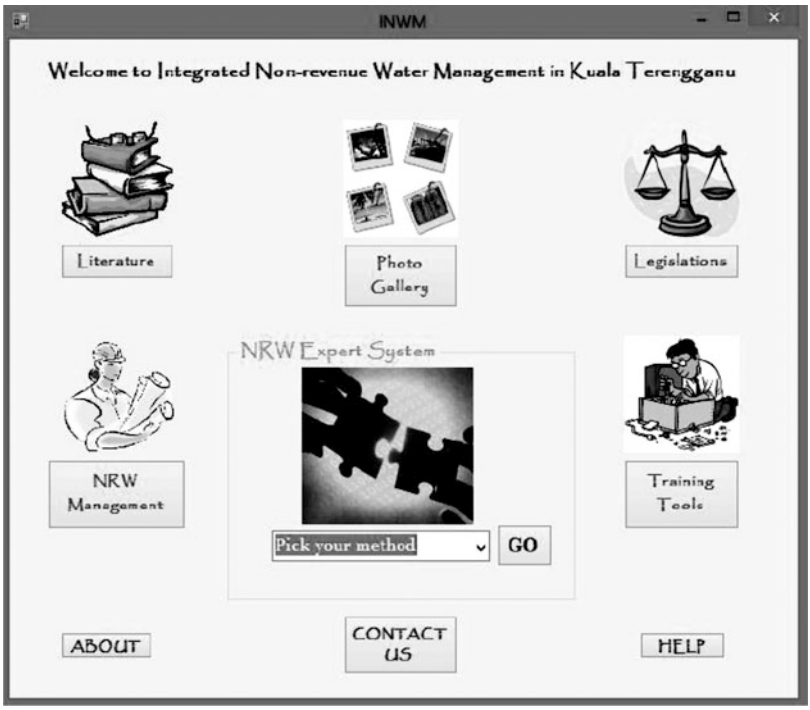

Fig. 20.2 Main user interface

3.2 User Interface

User interface is part of the expert system where the system can interact with the user. The user interface controls the way in which the user interacts and performs tasks with the expert system. It also provides varying opportunities for the user to follow the inference process and to provide explanation features. The interface that is designed by using visual basic is called Form. The main user interface includes Knowledge, NRW composition, Treatment facilities, Rules & Regulations, Maintenance, Public awareness, Frequency of billing, Transportation, Amount of NRW. Figure 20.2 shows knowledge base content.

3.3 Non-revenue Water Expert System (NRWES)

A unique feature of Non-revenue Water Expert System is that it contains several sub forms by which the user can obtain a comprehensive background understanding regarding current non-revenue water management in selected area which is Kuala Terengganu. The sub forms were named as literature, photo gallery, legislations,

training tools, NRW, and finally the non-revenue water expert system itself. Non-revenue water expert system also enables user to browse the concept of expert system by clicking the 'About' button. 'Help' button is also provided for the user to get an overview content of each button so that they can easily understand the function of each button. In addition, for further information, user can find the authors' contacts at About Us button. A rule that is entered in knowledge base will be applied in the development of non-revenue water expert system using Visual Basic programming language. The rule applied is in the form of IF THEN and the NRW expert system that has been developed consists of: (1) NRW components, (2) NRW problems, (3) NRW reduction strategy, (4) Data comparison, and (5) NRW estimation.

The interface for NRW form is illustrated in Fig. 20.3. It consists of choosing different components that contribute to the particular amount of non-revenue water production and the result will show the description for selected option. Then, the user can select any types of recommendation if the consumers face common situation of water leakage or other consumers doing illegal connection. It will give information regarding the "how consumers can help to reduce the amount of non-revenue water". Picture of the common situation that has been selected is also provided in order to get a clear view of the system. The next form is related to the NRW management problem which is mostly faced by the user. There is a rule for choices of NRW problem.

3.4 NRW Detections

This form contains problems associated with NRW and also problem solution. On the other part, there will be also the methods of NRW detection and some explanations about it. User needs to choose the method and then select any solution proposed by the expertise. The solution provided act as a recommendation to that kind of situation faced by the user. A comprehensive explanation for the solution is given where the user would get a better understanding as shown in Fig. 20.4.

3.5 Non-revenue Water Estimation

The NRW estimation form consists of data taken from the literature review and Syrikat Air Trengganu (SATU). This is very important knowledge where the user enables to know the amount of NRW generation in the future. The amount of NRW that is predicted until year 2020 is shown in Table 20.1 where user can make a comparison with the previous data. The prediction of total NRW generation in Kuala Terengganu is by taking assumption that the rate of population increase is 1.6 % per year and the percentage of allowable NRW is 38 % based on the scheme from SATU. If no proper management is conducted for the next few years, the % of

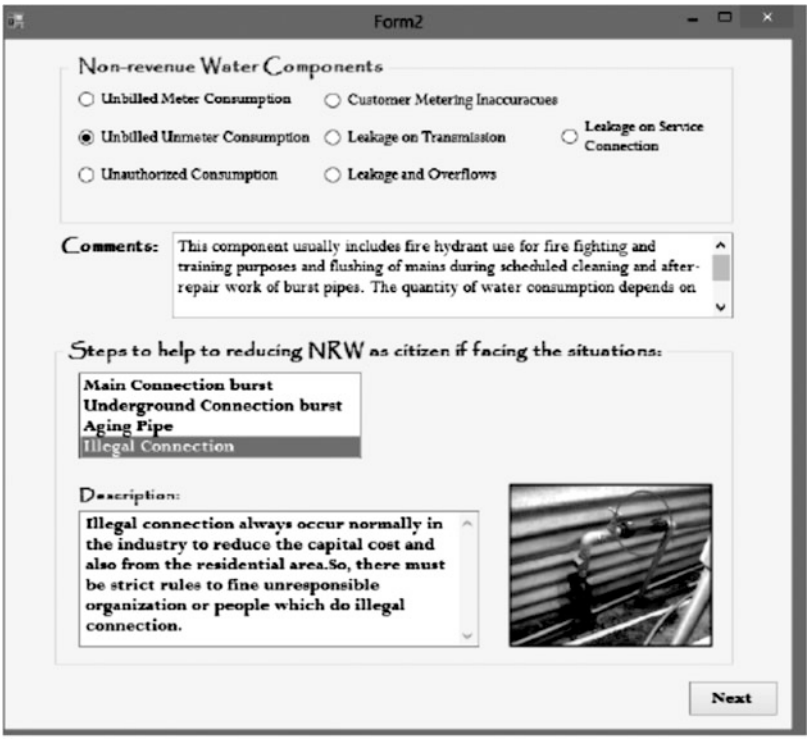

Fig. 20.3 NRW components form

the NRW in Kuala Terengganu will have potential to increase more than 40 %. Assume that the user wants to know the amount of NRW generated in year 2015; IF he/she selects 2015 which is case 4, THEN the population, amount of water production per year (m^3/year), NRW amount per year (m^3/year) and cost of NRW per year (RM/year) are displayed. Similar rule is applied for other choices.

3.6 System Validation

The forecasting for NRW estimation in NRW Expert System (NRWES) is done by comparing it with the data from SATU. The amount of NRW (per year) that is estimated for year 2012, 2013, 2014, 2015, 2016, 2017, 2018, 2019 and 2020 is allowable to the rate of NRW limit set by SATU. For instance, if the current NRW generation trends continue increasing at 38 % rate per year and 1.6 % rate increase in the population, the NRW generation will follow the same trends as previous data. These trends are used to predict the future tendency and also help with the design of the maintenance and management strategy to avoid further increase of NRW.

Fig. 20.4 Illustrations of rule into NRW detection form

Table 20.1 NRW data from SATU

Year	Population of K. Terengganu (Thousands)	Water production per year (m^3/year)	NRW amount per year (m^3/year)	Cost of NRW per year (RM/year)
2014	348,411	67,420,884	25,619,936	10,760,373
2015	354,016	68,499,607	26,029,850	10,932,537
2016	359,680	69,544,751	26,427,005	11,099,342
2017	365,435	70,657,490	26,849,468	11,276,935
2018	371,281	71,787,842	27,279,372	11,457,336
2019	377,221	72,936,351	27,715,813	11,640,641
2020	383,257	74,103,422	28,159,300	11,826,906

3.7 System Maintenance

When the expert system has been successfully developed, it will not remain static. As the world changes and our knowledge changes, so the knowledge base must change (Forsyth 1989). It becomes necessary when additional knowledge will need to be added to a knowledge base or existing knowledge deleted or changed at a later stage. The rules in the knowledge base can be added, changed or deleted without worrying about how the changes will affect the overall system.

4 Conclusions

In this project, the expert system tool in developing the NRW-ES is using Visual Basic Express Edition 2010. It is an ideal programing language for developing sophisticated professional applications for Microsoft Windows. The overall development of expert system has been carried out in several phases, including problem definition, knowledge acquisition, knowledge base, prototype development, prototype validation and implementation.

Although the expert system at this stage is useful among the potential users such as local authorities, consulting firms, researchers and students, it can be improved for the choices of proper management of non-revenue water for more efficient expertise. The expert system can be improved by adding an assessment tool with technical details such as terminology, calculations and examples. A related website regarding NRW management and power point presentation also could be included in the future study.

Acknowledgement Financial support provided by any IIUM, KOE, BTE Department is highly appreciated and acknowledged.

References

Butler, David and Memon, Fayyaz (eds) (2006). Water Demand Management. IWA, London, UK.

Cosgrove, W. and Rijsberman, F. (2000). World Water Vision Making Water Everybodies Business (1st ed.). Earthscan Publications, London.

De Bonis, P., Fattoruso, G., Pagano, A. and Pasanisi, F. (2002). Transport of pollutants in coastal areas: A comparison among different mathematical models. *In:* Appropriate Environmental and Solid Waste Management and Technologies for Developing Countries. G. Kocasoy, T. Atabarut and I. Nuhoglu (eds), vol. 5. Bogaziçi University Press, Istanbul.

Farley, M. and Liemberger, R. (2004). Developing a Non-Revenue Water Reduction Strategy. Part 2: Planning and Implementing the Strategy. Conference Proceedings, IWA World Water Congress, 19–24 September, 2004, Marrakech.

Farley, Malcom and Trow, Stuart (2003). Losses in Water Distribution Networks. A Practitioner's Guide to Assessment, Monitoring and Control. IWA London, UK.

Frederick Forsyth. (1989). Expert Systems: Principles and Case Studies. 2nd Ed. Chapman & Hall, Ltd. London, UK

Hassan, H. (1997). Water Quantity and Quality Assessment for Suwa Lake and Tenryu River Basin Regarding the Impact of Future Climate Change. PhD thesis, Department of Urban Engineering, The University of Tokyo.

Hu, Desheng (2006). Water Rights: An International and Comparative study. IWA, London, UK.

Koelbl, J. and Gschleiner, R. (2009). Austria's new guideline for water losses. *Water*, **21:** 55–56.

Lambert, A. and Taylor, R. (2010). Water loss guidelines. Water New Zealand, New Zealand Water and Wastes Association, Wairoa, New Zealand.

Otaki, M., Yano, K. and Ohgaki, S. (1998). Virus removal in a membrane separation process. *Wat. Sci. Tech.*, **37(10):** 107–116.

Skinner Brian (2003). Individual project. A WEDC Postgraduate Module. Loughborough University: Loughborough, UK
Suciu CR, Tartiu VE (2008). Knowledge applied in the municipal waste. Econ. Inform. 4: 65–67.
Terengganu Water Corporation (2010). Water Tariff, Syarikat Air Terengganu Sdn. Bhd (SATU) Commercial Department, Kuala Terengganu.
Trow, S. and Pearson, D. (2010). Setting targets for non-revenue water reduction. *Water*, **21:** 40–43.

Index

F. Kurisu et al. (eds.), *Trends in Asian Water Environmental Science and Technology*, DOI 10.1007/978-3-319-39259-2